

## University of Southampton Research Repository ePrints Soton

Copyright © and Moral Rights for this thesis are retained by the author and/or other copyright owners. A copy can be downloaded for personal non-commercial research or study, without prior permission or charge. This thesis cannot be reproduced or quoted extensively from without first obtaining permission in writing from the copyright holder/s. The content must not be changed in any way or sold commercially in any format or medium without the formal permission of the copyright holders.

When referring to this work, full bibliographic details including the author, title, awarding institution and date of the thesis must be given e.g.

AUTHOR (year of submission) "Full thesis title", University of Southampton, name of the University School or Department, PhD Thesis, pagination

**University of Southampton**

Faculty of Engineering, Science and Mathematics  
School of Ocean and Earth Science

THE PHOTOPHYSIOLOGY AND PRIMARY  
PRODUCTIVITY OF PHYTOPLANKTON WITHIN THE  
DEEP CHLOROPHYLL MAXIMUM.

By

Anna Elizabeth Hickman

This Thesis is Submitted for  
Doctor of Philosophy

April 2007

UNIVERSITY OF SOUTHAMPTON

ABSTRACT

FACULTY OF ENGINEERING, SCIENCE AND MATHEMATICS

SCHOOL OF OCEAN AND EARTH SCIENCE

Doctor of Philosophy

THE PHOTOPHYSIOLOGY AND PRIMARY PRODUCTIVITY OF  
PHYTOPLANKTON WITHIN THE DEEP CHLOROPHYLL MAXIMUM

By Anna Elizabeth Hickman

In temperate shelf seas, a deep chlorophyll maximum (DCM) persists within the thermocline during summer stratification. This study explores the significance of primary production (PP) within the DCM and provides a detailed investigation into the mechanisms of phytoplankton adaptation to this tidally dynamic and dimly-lit environment. Comparison is drawn to the DCM in a range of hydrographic regimes in the open ocean.

Data are presented from two cruises in the Celtic Sea during summer (2003 and 2005) and one from the Atlantic Ocean (AMT15, 2004). Phytoplankton physiological measurements were obtained from  $^{14}\text{C}$  Photosynthesis vs. Irradiance (P vs. E) experiments and a bench-top Fast Repetition Rate Fluorometer (FRRF). Water-column profiles of PP were empirically modelled using P vs. E parameters and measurements of spectral *in situ* irradiance.

Across the Celtic Sea shelf the DCM was located towards the base of the thermocline and was tightly coupled to the nitracline. The thermocline is presented as a 3-layer system, the top and bottom layers dominated by physical mixing and a mid-layer which is relatively stable and occurs at the top of the nitracline. Nitrate flux into the thermocline from the BML was maximal at spring tides and could support almost all the PP in the thermocline. It appears that nitrate supply and utilisation is roughly balanced over spring - neap timescales.

Within the shelf sea thermocline, layering of phytoplankton taxonomy was observed, with the maxima of cell concentrations decoupled from those of cellular pigment concentrations. The FRRF-derived effective absorption cross section of photosystem II ( $\sigma_{\text{PSII}}$ ) and photosynthetic efficiency (Fv/Fm) co-varied with pigment composition, and did not appear to contribute to photo-acclimation. Data indicated that the mechanism of photo-acclimation was by the number, rather than size, of PSII reaction centres.

In contrast to the surface mixed layer, phytoplankton at the DCM remained light limited and PP in the thermocline was more sensitive to incident irradiance than in the surface. In the Celtic Sea, the potential range in water-column integrated PP between a cloudy and sunny day was greater than the spatial range in PP across the region. PP within the thermocline contributed 28 – 84 % of vertically-integrated daily PP.

The mechanism of photoacclimation appeared to be consistent between the shelf sea and open ocean environments. Throughout the Atlantic Ocean PP in the DCM contributed between 15 – 80 % of total water column production.

It is shown that physical – biological coupling is a major determinant on phytoplankton taxonomy, physiology and productivity in the DCM.

## THESIS CONTENTS

<b>1</b>	<b>INTRODUCTION</b>	<b>1 - 27</b>
<b>1.1</b>	<b>Photosynthesis</b>	<b>1</b>
1.2.1	Light Reactions	2
1.2.2	Dark Reactions	4
1.2.3	Respiration	4
1.2.4	Nutrient Utilisation	5
1.2.5	Terminology	6
<b>1.2</b>	<b>Growth Conditions and Photophysiology of Marine Phytoplankton</b>	<b>6</b>
1.2.1	Light	7
1.2.2	Nutrients	8
1.2.3	Adaptation and Acclimation	8
<b>1.3</b>	<b>Physical-Biological Coupling in the Ocean</b>	<b>10</b>
1.3.1	The Temperate Shelf Seas	10
1.3.2	The Open Ocean	16
<b>1.4</b>	<b>Measurement of Phytoplankton Physiology</b>	<b>19</b>
1.4.1	P vs. E Experiments	19
1.4.2	Fast Repetition Rate Fluorometer	22
1.4.3	<sup>14</sup> C vs. FRRF-derived Physiological Parameters	25
<b>1.5</b>	<b>Thesis Objectives</b>	<b>26</b>
<b>1.6</b>	<b>Presentation of Thesis</b>	<b>27</b>
<b>2</b>	<b>METHODS</b>	<b>28 - 64</b>
<b>2.1</b>	<b>Sampling Procedure</b>	<b>29</b>
<b>2.2</b>	<b>Measurements of Primary Production</b>	<b>30</b>
2.2.1	Incubation Experiments	30
2.2.2	Caveats of Sample Incubation	36
<b>2.3</b>	<b>Fast Repetition Rate Fluorometer (FRRF)</b>	<b>37</b>
<b>2.4</b>	<b>Additional Measurements</b>	<b>39</b>
2.4.1	CTD Measurements	39
2.4.2	Biological Samples	41
<b>2.5</b>	<b>Methods of Data Analysis</b>	<b>50</b>
2.5.1	Spectral Corrections	50
2.5.2	Modelling <i>in situ</i> Water Column Optics	52
2.5.3	Estimations of <i>in situ</i> Primary Production	58
<b>2.6</b>	<b>Statistical Methods</b>	<b>64</b>
<b>3</b>	<b>PHOTOPHYSIOLOGY OF PHYTOPLANKTON IN THE CELTIC SEA</b>	<b>65-101</b>
<b>3.1</b>	<b>Study Area</b>	<b>65</b>
<b>3.2</b>	<b>Optical Properties of Phytoplankton</b>	<b>66</b>
3.2.1	Particle Absorption	66
3.2.2	Pigment Packaging	69
3.2.3	Absorption by Non-Photosynthetic Carotenoids	72
3.2.4	Chromatic Adaptation	73
<b>3.3</b>	<b>Directly Measured Physiological Parameters</b>	<b>76</b>
3.3.1	The effect of Spectral Correction	77

3.3.2	Coherence between $^{14}\text{C}$ and FRRF Techniques	78
3.3.3	Diel Variability	80
3.3.4	Depth Variability	81
<b>3.4</b>	<b>Light Harvesting Parameters</b>	<b>82</b>
3.4.1	$\sigma_{\text{PSII}}$	82
3.4.2	$\alpha^*$ and $\Phi_m$	86
<b>3.5</b>	<b>Electron Transfer Parameters</b>	<b>89</b>
3.5.1	$P_m^*$ and $E_{K_{14C}}$	89
3.5.2	$1/\tau_{Q_a}$ and $E_{K_{\text{ETR},478}}$	89
<b>3.6</b>	<b><math>E_{K_{14C}}</math> and <i>in situ</i> Irradiance</b>	<b>92</b>
3.6.1	Ek-independent Variability	93
<b>3.7</b>	<b>Photoacclimation and Adaptation</b>	<b>96</b>
3.7.1	Adaptation	96
3.7.2	Photoacclimation	96
<b>3.8</b>	<b>Summary of Main Points</b>	<b>101</b>
<b>4</b>	<b>PRIMARY PRODUCTION IN THE CELTIC SEA</b>	<b>102 - 135</b>
<b>4.1</b>	<b>Study Area</b>	<b>102</b>
<b>4.2</b>	<b>Hydrography, Chl-a and Nitrate Distribution</b>	<b>104</b>
4.2.1	Chlorophyll-a Distribution within the Thermocline	111
4.2.2	Phytoplankton Taxonomy	115
<b>4.3</b>	<b>Primary Productivity through the Water Column</b>	<b>118</b>
4.3.1	<i>In situ</i> Spectral Irradiance	118
4.3.2	<i>In situ</i> Primary Production	121
4.3.3	Controls on Primary Production	127
4.3.4	Temporal Variability in Primary Production	130
4.3.5	The Significance of Primary Production in the Thermocline	133
<b>4.4</b>	<b>Summary of Main Points</b>	<b>134</b>
<b>5</b>	<b>NEW PRODUCTION IN THE CELTIC SEA</b>	<b>136 - 162</b>
<b>5.1</b>	<b>Study Area</b>	<b>136</b>
5.1.1	Vertical Distribution of $\text{NO}_3^-$ and Dissolved $\text{O}_2$	136
<b>5.2</b>	<b>Light-response of <math>\text{NO}_3^-</math> uptake and <math>\text{O}_2</math> evolution at the DCM</b>	<b>138</b>
5.2.1	Nitrate Uptake at the DCM	138
5.2.2	Oxygen Evolution at the DCM	142
<b>5.3</b>	<b>Nitrate Flux into the Thermocline</b>	<b>144</b>
<b>5.4</b>	<b>Distributions of Chl-a, <math>\text{NO}_3^-</math>, <math>\text{O}_2</math> and PP in the Thermocline</b>	<b>148</b>
5.4.1	Distributions of Chl-a and Dissolved $\text{O}_2$ on the Nitracline	148
5.4.2	Physical-Biological Interaction and Implications for New Production in the Thermocline	153
<b>5.5</b>	<b>Summary of Main Points</b>	<b>161</b>
<b>6</b>	<b>PHYTOPLANKTON PHOTOPHYSIOLOGY AND PRIMARY PRODUCTION IN THE ATLANTIC OCEAN</b>	<b>163 - 199</b>
<b>6.1</b>	<b>Study Area</b>	<b>163</b>
<b>6.2</b>	<b>Hydrography and Phytoplankton Distribution</b>	<b>164</b>
<b>6.3</b>	<b>Phytoplankton Photophysiology</b>	<b>171</b>
6.3.1	Optical Properties of Phytoplankton	171
6.3.2	Directly Measured Physiological Parameters	173

6.3.3	Light Harvesting Parameters	176
6.3.4	Electron Transfer Parameters	181
6.3.5	Light Saturation Index, Ek	184
6.3.6	Adaptation and Photoacclimation	187
<b>6.4</b>	<b>Chl-a and Primary Productivity through the Water Column</b>	<b>189</b>
6.4.1	Chl-a Distribution	189
6.4.2	<i>In situ</i> Primary Production	191
6.4.3	Controls on Primary Production	195
6.4.4	The Significance of Primary Production in the DCML	196
<b>6.5</b>	<b>Summary of Main Points</b>	<b>198</b>
<b>7</b>	<b>SYNTHESIS AND DISCUSSION</b>	<b>200 - 225</b>
<b>7.1</b>	<b>Phytoplankton Physiology in the DCM</b>	<b>200</b>
7.1.1	Adaptation	201
7.1.2	Photoacclimation	204
<b>7.2</b>	<b>The DCM of the Celtic Sea Shelf</b>	<b>209</b>
7.2.1	Primary Production in the Thermocline	209
7.2.2	The Physical and Biological Structure of the Thermocline	210
<b>7.3</b>	<b>The DCM of the Atlantic Ocean</b>	<b>215</b>
<b>7.4</b>	<b>Temporal and Regional Significance of the DCM</b>	<b>218</b>
7.4.1	Total and New Production in the Celtic Sea	218
7.4.2	Total Production in the Atlantic Ocean	221
<b>7.5</b>	<b>Methodological Considerations</b>	<b>223</b>
<b>7.6</b>	<b>Concluding Remarks</b>	<b>224</b>
<b>8</b>	<b>REFERENCES</b>	<b>226 - 237</b>

## LIST OF FIGURES

Figure	Figure Title	Page
1.1	The ‘Z-Scheme’ of photosynthesis	3
1.2	Schematic of vertical section of a shelf sea	12
1.3	Schematic of Photosynthesis verses Irradiance (P vs. E) curve	19
1.4	Schematic of saturation and relaxation of photosystem II (PSII) by FRRF	23
2.1	Photograph of P vs. E incubator	31
2.2	Photograph of bench-top FRRF set-up	37
2.3	The relationship between CTD chl-a and sample chl-a, CS03	44
2.4	The relationship between CTD chl-a : sample chl-a and <i>in situ</i> PAR, CS05	45
2.5	Assumed <i>in vivo</i> weight-specific absorption spectra	49
2.6	Example excitation, phytoplankton absorption and <i>in situ</i> irradiance spectra	51
2.7	The wavelength composition of surface irradiance	55
2.8	Relationship between $K_d(\lambda)$ and chl-a at five wavelengths, CS05	56
2.9	Relationship between $K_d(\lambda)$ and chl-a at five wavelengths, AMT15	57
2.10	Daily PP from $^{14}\text{C}$ P vs. E parameters compared to SIS incubations, CS03	63
3.1	Map of physiological sample locations in the Celtic Sea	65
3.2	Examples of phytoplankton absorption spectra ( $a(\lambda)^*_{\text{meas}}$ )	67
3.3	Ratios of $a(\lambda)^*_{\text{meas}}$ for selected wavelengths against depth, CS05	68
3.4	Example phytoplankton absorption spectra measured by the filter technique compared to the pigment reconstruction technique	69
3.5	Packaging Index against depth, CS05	72
3.6	Example of absorbance spectra before and after the removal of NPC	73
3.7	The difference in normalised spectral composition between the DCM and the surface for <i>in situ</i> irradiance, $a^*_{\text{ps}}$ and $a^*_{\text{pspig}}$ , CS05	74
3.8	Variability of wavelength ratios of $a(\lambda)^*_{\text{pspig}}$ and <i>in situ</i> irradiance, CS05	75
3.9	Variability in physiological parameters against optical depth, CS05	76
3.10	Comparison of P vs. E and FRRF parameters, CS05	79
3.11	Diel variability of physiological parameters, CS03	80
3.12	Relationship between $\sigma_{\text{PSII}}$ and measurements of PSC:chl-a and $a^*_{\text{meas}}$ , CS05	83
3.13	Relationship between $\sigma_{\text{PSII}}$ and the main pigment ratios, CS03	84
3.14	Relationship between $\sigma_{\text{PSII}}$ and the main pigment ratios, CS05	84
3.15	Relationship between $\sigma_{\text{PSII}}$ and Fv/Fm, CS05	85
3.16	Relationship between $\Phi_m$ and NPC:PSC and $\alpha^*_{^{14}\text{C}}$ and POC:PON, CS05	87
3.17	Relationship between $\alpha^*$ and the Tidal Amplitude Index (TAI), CS05	88
3.18	Relationship between $E_k$ , $P^*_m$ and electron transfer rates, CS05	90
3.19	Comparison of $E_{k_{\text{in situ}}}$ and <i>in situ</i> growth irradiance, CS05	92
3.20	Relationship between $P^*_m$ and $\alpha^*$ , CS05	94
3.21	Relationship between $P^*_m$ and $1/\tau_{\text{Qa}}$ in the SML and thermocline, CS05	95
3.22	Vertical gradients of picoeukaryote and <i>Synechococcus</i> characteristics at an example shelf site, CS05	97
3.23	Relationship between $E_{k_{^{14}\text{C}}}$ and <i>Synechococcus</i> and picoeukaryote cellular pigment concentrations, CS05	98
3.24	Variability in $P^c_m$ and $\alpha^c$ with optical depth, CS05	99
4.1	Map of all sampling stations in the Celtic Sea	103
4.2	Satellite images of chl-a and SST in the Celtic Sea region	104
4.3	Seasoar section from the shelf edge to the Irish Sea front, CS03	105
4.4	Temporal variability in chl-a and density structure at example sites	106
4.5	Relationship between integrated chl-a and layer thickness for SURF, THERM and WC	111
4.6	BML nitrate concentration in the Celtic Sea	112
4.7	Distribution of chl-a and nitrate through the thermocline at the main stations	113
4.8	Relationship between chl-a and nitrate for two example stations	114
4.9	Cross-shelf edge sections of <i>Synechococcus</i> , <i>Prochlorococcus</i> and picoeukaryote cellular abundance, CS05	116

## **LIST OF FIGURES (cont.)**

<b>4.10</b>	Vertical gradients of picoeukaryote and <i>Synechococcus</i> cellular abundance and pigment ratios at an example shelf site, CS05	117
<b>4.11</b>	PAR during the sunniest and cloudiest days of each cruise, CS03 and CS05	119
<b>4.12</b>	Example of <i>in situ</i> light field characteristics for an example shelf station	120
<b>4.13</b>	Example of the light absorbed by phytoplankton an example shelf station	121
<b>4.14</b>	Vertical profiles of chl-a and estimated daily PP, CS03 and CS05	123
<b>4.15</b>	Relationship between $P_{WC}$ and integrated chl-a for cloudy and sunny conditions, CS05	128
<b>4.16</b>	Relationships between $P_{SURF}$ , $P_{THERM}$ and $P_{WC}$ compared to chl-a and irradiance, CS05	129
<b>4.17</b>	The percentage contribution of daily $P_{THERM}$ to $P_{WC}$ for cloudy and sunny conditions, CS03 and CS05	133
<b>5.1</b>	Vertical profiles of chl-a, PP, nitrate and %O <sub>2</sub> for selected locations	137
<b>5.2</b>	<sup>14</sup> C, <sup>13</sup> C and <sup>15</sup> N uptake vs. irradiance curves at the DCM at CS1 and CS3	139
<b>5.3</b>	<sup>14</sup> C: <sup>15</sup> N and <sup>13</sup> C: <sup>15</sup> N uptake ratios vs. irradiance at the DCM at CS1 and CS3	140
<b>5.4</b>	<sup>14</sup> C uptake and O <sub>2</sub> evolution vs. irradiance curves at the DCM at CS1 and X7	142
<b>5.5</b>	Distribution of chl-a and AOU on the nitracline at each location, CS03 and CS05	149
<b>5.6</b>	Distribution of chl-a and AOU on the nitracline at all locations, CS05	151
<b>5.7</b>	Relationship between chl-a maximum and %O <sub>2</sub> maximum, CS05	152
<b>5.8</b>	Schematic of oxygen evolution compared to a simple linear mixing model	154
<b>5.9</b>	Schematic of 3-layer and 2-layer thermocline models	158
<b>5.10</b>	Profiles of chl-a, nitrate and %O <sub>2</sub> at selected sites	159
<b>6.1</b>	AMT15 cruise track and sample locations	164
<b>6.2</b>	Section of chl-a compared to temperature, depth of 1μM nitrate and depth of 1% surface irradiance, AMT15	165
<b>6.3</b>	Profiles of chl-a, temperature and nitrate for three example casts, AMT15	166
<b>6.4</b>	Sections of <i>Synechococcus</i> , <i>Prochlorococcus</i> and picoeukaryote cellular abundance, AMT15	167
<b>6.5</b>	Sections of selected pigment concentrations (per chl-a), AMT15	168
<b>6.6</b>	Sections of NPC:chl-a, PSC:chl-a and chl-a:Tpig, AMT15	170
<b>6.7</b>	The difference in normalised spectral composition between the DCM and the surface for <i>in situ</i> irradiance, $a(\lambda)^*_{ps}$ and $a(\lambda)^*_{pspig}$ , AMT15	172
<b>6.8</b>	Sections of P vs. E and FRRF parameters, AMT15	175
<b>6.9</b>	Relationship between $\sigma_{PSII}$ and Hex+But:chl-a with other pigments highlighted, AMT15	177
<b>6.10</b>	Relationship between $\sigma_{PSII}$ and Fv/Fm with major pigments highlighted, AMT15	178
<b>6.11</b>	Relationship between $\Phi_m$ and selected variables, AMT15	180
<b>6.12</b>	Relationship between $1/\tau_{Qa}$ and Hex+But:chl-a with other pigments highlighted, AMT15	182
<b>6.13</b>	Relationship between electron transfer rates and $P^*_m$ , AMT15	183
<b>6.14</b>	Relationship between <sup>14</sup> C-derived and FRRF-derived $E_k$ , AMT15	185
<b>6.15</b>	Relationship between $\sigma_{PSII}$ and ratio of picoeukaryotes to cyanobacteria, AMT15	186
<b>6.16</b>	Comparison of $E_{k,insitu}$ and <i>in situ</i> growth irradiance, AMT15	187
<b>6.17</b>	Vertical gradients of picoeukaryote, <i>Prochlorococcus</i> and <i>Synechococcus</i> characteristics at an example oligotrophic site, AMT15	188
<b>6.18</b>	Relationship between integrated chl-a and DCM peak depth for SML, DCML and WC	191
<b>6.19</b>	Vertical profiles of chl-a and estimated daily PP, AMT15	192
<b>6.20</b>	Relationships between $P_{SURF}$ , $P_{DCML}$ and $P_{WC}$ and selected variables, AMT15	195
<b>6.21</b>	The percentage contribution of daily $P_{DCML}$ to $P_{WC}$ , AMT15	197
<b>7.1</b>	Estimated daily PP within the DCML and water-column, CS05 and AMT15	222

## LIST OF TABLES

<b>Table</b>	<b>Table Title</b>	<b>Page</b>
2.1	Persons responsible for data collection	29
3.1	The significance test (ANOVA) between means of physiological parameters at each of four sample depths, CS05	81
4.1	Chl-a concentrations and thermocline boundary depths at the main stations, CS03 and CS05	108
4.2	Estimated daily PP in the SML, THERM and WC, CS03 and CS05	125
4.3	Co-variance of layer thickness, PP and chl-a in the SML, THERM and WC, CS03 and CS05	131
5.1	Nitrate flux into the thermocline at available locations, CS03 and CS05	145
5.2	Excess %O <sub>2</sub> saturation and estimated timescales for accumulation in the thermocline, CS05	155
6.1	Chl-a concentrations and DCML boundary depths at representative stations, AMT15	190
6.2	Estimated daily PP in the SML, DCML and WC, AMT15	193
7.1	Estimated annual new and total PP in the Celtic Sea	220

## LIST OF PUBLICATIONS

Publications produced during the course of this thesis are as follows:

- Moore, C.M., Suggett, D.J., **Hickman, A.E.**, Kim, Y.N., Tweddle, J.F., Sharples, J., Geider, R.J. and Holligan, P.M. (2006). Phytoplankton photoacclimation and photoadaptation in response to environmental gradients in a shelf sea. *Limnology and Oceanography* 52 (2) 936-949.
- Poulton, A.J., Holligan, P.M, **Hickman, A.E.**, Kim, Y.N., Stinchcombe, M.C., Adey, T.R., Holeton, C., Root, S.E., Chamberlain, K., Woodward, E.M.S. (2006) Size-fractionated carbon fixation, chlorophyll-biomass and diagnostic pigments in the Atlantic Ocean. *Deep Sea Research II* 53 1593-1610.
- Moore, C.M., Seeyave, S, **Hickman, A.E.**, Allen, J.T., Lucas, M.I., Planquette, H., Pollard, R.T., Poulton, A.J. (*Submitted*). Iron-light interactions during the CROZet natural iron bloom and EXport experiment (CROZEX) I: phytoplankton growth and photophysiology. *Deep Sea Research II*.
- Moore, C.M., **Hickman, A.E.**, Poulton, A.J., Seeyave, S., Lucas, M.I. (*Submitted*). Iron-light interactions during the CROZet natural iron bloom and EXport experiment (CROZEX) II: taxonomic responses and elemental stoichiometry. *Deep Sea Research II*.
- Rippeth, T.P., Palmer, M.R., Tweddle, J.F., Sharples, J., Inall, M., Fisher, N., **Hickman, A.E.**, Holligan, P.M., Kim, Y.N., Moore, C.M., Simpson, J. (*Submitted*). Diapycnal nutrient fluxes in seasonally stratified shelf seas. *Limnology and Oceanography*.
- Sharples, J., Tweddle, J.F., Green, M., Palmer, M., Kim, Y.N., **Hickman, A.E.**, Holligan, P.M., Moore, C.M., Rippeth, T.P., Simpson, J.H., Kristov, V. (*Submitted*). Spring-neap modulation of internal tide mixing and vertical nitrate fluxes at the shelf edge in summer. *Limnology and Oceanography*.

Some of the data and ideas contained within Moore et al. (2006) are included in Chapter 3 of this thesis. While the paper presents data obtained during one of the research cruises (Celtic Sea, 2003) this thesis emphasises results from the subsequent cruise (Celtic Sea, 2005) which both supports and considerably expands upon the work already published. The paper is referenced where appropriate.

**DECLARATION OF AUTHORSHIP**

I, ....., [please print name]

declare that the thesis entitled [enter title]

.....

.....

and the work presented in the thesis are both my own, and have been generated by me as the result of my own original research. I confirm that:

- this work was done wholly or mainly while in candidature for a research degree at this University;
- where any part of this thesis has previously been submitted for a degree or any other qualification at this University or any other institution, this has been clearly stated;
- where I have consulted the published work of others, this is always clearly attributed;
- where I have quoted from the work of others, the source is always given. With the exception of such quotations, this thesis is entirely my own work;
- I have acknowledged all main sources of help;
- where the thesis is based on work done by myself jointly with others, I have made clear exactly what was done by others and what I have contributed myself;
- none of this work has been published before submission, **or** [delete as appropriate] parts of this work have been published as: [please list references]

Moore, C.M., Suggett, D.J., **Hickman, A.E.**, Kim, Y.N., Tweddle, J.F., Sharples, J., Geider, R.J. and Holligan, P.M. (2006). Phytoplankton photoacclimation and photoadaptation in response to environmental gradients in a shelf sea. *Limnology and Oceanography* 52 (2) 936-949.

**Signed:** .....

**Date:** .....

## ACKNOWLEDGEMENTS

I have received support from many people during the course of my PhD. Thanks must first go to my supervisors, Patrick Holligan and Jonathan Sharples for unequalled guidance and encouragement over the past four years. There are numerous other people to whom I am particularly grateful: Mike Lucas, Duncan Purdie and Alex Poulton for setting me on my way in the lab and for all-round advice and discussion; Mark Moore and Dave Suggett for putting up with my endless questions about phytoplankton physiology and guiding me around the world of active fluorescence; Gavin Tilstone, Gerald Moore, Vladimir Kristov and Sam Lavender for various contributions and discussions regarding marine optics; Phil Warwick for assistance with the radioisotope. Thanks also to Ian Robinson, Duncan (again) and Debora Iglesias-Rodriguez for attendance and useful suggestions in panel meetings, and to the people behind all the other doors in NOC I have knocked on over the years.

I am also grateful to all those amongst the AMT and CROZEX communities for having me on board, and particularly to Andy Rees for helping me conquer AMT15! Thanks to the officers and crew of the *RRS* Discovery, *RRS* James Clark Ross and *RRS* Charles Darwin, and to the UKORS staff who have helped me fix various bits of kit in those few nervous moments.

This work was funded by NERC (Studentship NER/S/A/2002/10398) and was in association with NERC Grant NER/A/S/2001/00449.

Of course no acknowledgement would be complete without thanks to the inhabitants of the Platform on a Friday night; to Alex, Jo, Steph and Jacqui for all the dancin'; to Young for all the photos; to my family for unwavering support and Mark, thank you.

## LIST OF COMMONLY USED ABBREVIATIONS

<b>Abbreviation</b> → Subscript	<b>Abbreviation Definition</b> → Subscript Definition	<b>Units</b>
<b>Physiological Parameters</b>		
a*	Chl-a specific phytoplankton absorption summed over wavelengths 400-700 nm	m <sup>2</sup> (mg chl-a) <sup>-1</sup>
a(λ)*	Shape of chl-a specific phytoplankton absorption (i.e. wavelength resolved)	m <sup>2</sup> (mg chl-a) <sup>-1</sup>
meas	Measured by filter technique	
ps	Measured by filter technique with absorption by non-photosynthetic carotenoids (NPC) removed	
pig	Measured by pigment reconstruction technique	
pspig	Measured by pigment reconstruction technique, NPC removed	
P* <sub>m</sub>	Chl-a specific maximum photosynthetic rate	mg C (mg chl-a) <sup>-1</sup> h <sup>-1</sup>
α*	Maximum light utilisation coefficient	mg C (mg chl-a) <sup>-1</sup> h <sup>-1</sup> (μE m <sup>-2</sup> s <sup>-1</sup> ) <sup>-1</sup>
14C	Directly measured	
478	Corrected to FRRF excitation spectrum	
insitu	Corrected to <i>in situ</i> irradiance spectrum	
Φ <sub>m</sub>	Maximum quantum yield of photosynthesis	mol C (mol photons) <sup>-1</sup>
Ek	Light saturation parameter	μE m <sup>-2</sup> s <sup>-1</sup>
14C	Directly measured from <sup>14</sup> C	
478	Corrected to FRRF excitation spectrum	
insitu	Corrected to <i>in situ</i> irradiance spectrum	
ETR,478	Obtained from FRRF	
1/τ	Rate of electron transport	s <sup>-1</sup>
Qa	Transport from Qa to PQ pool	
PSII	Transport through whole chain	
σ <sub>PSII</sub>	Functional absorption cross section of PSII	x10 <sup>-20</sup> m <sup>2</sup> quanta <sup>-1</sup>
Fv/Fm	Quantum efficiency of photochemistry	Dimensionless
<b>Optical Measurements</b>		
λ	Wavelength	nm
E(λ,z)	Irradiance for wavelength λ (nm) and depth z (m). Irradiance is expressed in units of μEinstein m <sup>-2</sup> s <sup>-2</sup> (or μE m <sup>-2</sup> s <sup>-1</sup> ) where an Einstein is equal to one mole of photons	μE m <sup>-2</sup> s <sup>-1</sup>
PAR	Photosynthetically Available Radiation (400-700 nm)	μE m <sup>-2</sup> s <sup>-1</sup>
Kd(λ)	Diffuse attenuation coefficient of downwelling irradiance for wavelength λ	m <sup>-1</sup>
Ē(λ,0)	Wavelength resolved irradiance spectrum just below the surface, scaled to PAR = 1 μE m <sup>-2</sup> s <sup>-1</sup>	μE m <sup>-2</sup> s <sup>-1</sup>

## LIST OF COMMONLY USED ABBREVIATIONS (cont.)

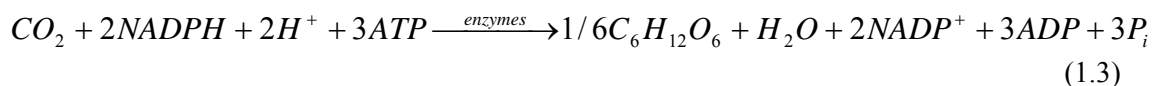
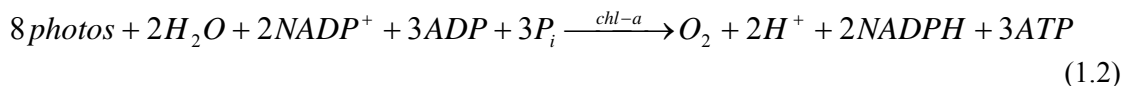
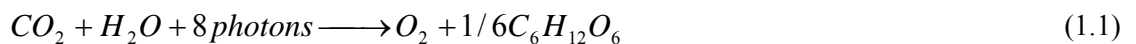
<b>Abbreviation</b> → Subscript	<b>Abbreviation Definition</b> → Subscript Definition	<b>Units</b>
OD	Optical Depth (depth (m) x $K_d$ ( $m^{-1}$ ))	Dimensionless
Percentage Irradiance	Irradiance as a percentage of that just below the surface	%
Light Depth	Depth associated with a given irradiance as a percentage of that just below the surface	m
Mean Growth Irradiance	Mean irradiance to which phytoplankton are exposed over a 24 hour period	$\mu E\ m^{-2}\ s^{-1}$
<b>Primary Production Estimates</b>		
P	Vertically integrated primary production	$mg\ C\ m^{-2}\ d^{-1}$
SURF	within the surface mixed layer	
THERM	within the thermocline	
DCML	within the deep chlorophyll maximum layer	
WC	within the productive region of the water column	
<b>Abbreviations in Text</b>		
CS03	Celtic Sea cruise, 2003	
CS05	Celtic Sea cruise, 2005	
AMT15	Atlantic Meridional Transect cruise 15	
JD	Julian Day. The day of the year where January 1 <sup>st</sup> is day 1.	
PP	Primary Production	
FRRF	Fast Repetition Rate Fluorometer	
PSI	Photosystem I	
PSII	Photosystem II	
ETR	Electron Transfer Rate	
SML	Surface Mixed Layer	
BML	Bottom Mixed Layer	
THERM	Thermocline Layer	
DCM	Deep Chlorophyll Maximum	
DCML	Deep Chlorophyll Maximum Layer	
chl-a	Chlorophyll-a	
Fuc	Fucoxanthin	
Hex	19'-hexanoyloxyfucoxanthin	
But	19'-butanoyloxyfucoxanthin	
NPC	Non photosynthetically active carotenoids	
PSC	Photosynthetically active carotenoids	
%O <sub>2</sub>	Dissolved oxygen as percentage saturation	%
AOU	Apparent Oxygen Utilisation	$mg\ l^{-1}$

## CHAPTER 1: INTRODUCTION

This introduction provides background and context for the work presented. The chapter is divided into three parts. The first summarises the process of photosynthesis and the factors important for algal growth in the ocean. The second part introduces the hydrographic environments that are the focus of this study, namely the Celtic Sea and Atlantic Ocean and includes a short literature review of current understanding of the biological-physical coupling in these regions. The final part deals with the principles of the techniques used to measure algal photosynthesis and photophysiology.

### 1.1 Photosynthesis

Primary production in the surface ocean refers to the formation of organic carbon by planktonic autotrophs using solar energy. By harnessing light to provide the chemical energy, phytoplankton form organic matter (carbohydrate) by the reduction of inorganic carbon. A detailed account of the processes involved in photosynthesis by marine algae can be found in Falkowski and Raven (1997), here the key reactions are summarised. Photosynthesis (Eqn. 1.1) can broadly be described in terms of two reactions. The first are the ‘light’ reactions, which use energy from absorbed photons for the splitting of water. The light reactions also generate NADPH from the reduction of  $\text{NADP}^+$  and ATP from the combination of ADP and inorganic phosphate ( $\text{P}_i$ ) (Eqn. 1.2). The second set of reactions, the ‘dark’ reactions, does not require energy from light and utilises the NADPH and ATP from the light reactions to reduce  $\text{CO}_2$  to carbohydrate (Eqn 1.3).



In eukaryotic algae, the photosynthetic apparatus required for these reactions is contained in chloroplasts within the cytoplasm which contain a stacked formation of thylakoid membranes. Aqueous liquid is contained within the thylakoids (the lumen) and occurs between them (the stroma) (e.g. Prezelin 1981). In contrast, in prokaryotic cyanobacteria (and photosynthetic bacteria) the thylakoid membranes occur in sheet-like formation in the cell wall rather than in separate chloroplasts. Regardless of the organisation of the apparatus, the light reactions take place in the thylakoid membranes and the dark reactions within the stroma. A brief description of the light and dark reactions are given in the following sections and follows more detailed accounts provided in Falkowski and Raven (1997), Kirk (1994) and Geider and MacIntyre (2002).

### 1.2.1 Light Reactions

The first stage of the photosynthetic process is light capture. The light-harvesting apparatus of the cell is composed of a number of 'photosystems', each containing a reaction centre and a light-capturing antenna. Light is initially absorbed by the antennae which is a bed of pigments unique in composition to different algal taxa. From the antennae, excitation energy is passed to the reaction centre, where the photochemical reaction occurs.

There are two types of photosystem in marine algae, Photosystem I (PSI) (containing the chlorophyll molecule P680 in associated reaction centre, RCI) and Photosystem II (containing P700 in associated reaction centre, RCII). Light energy is absorbed preferentially into the lower energy P680 of PSII, where it raises the energy level of an electron. The excited electron, is liberated by a charge separation, and begins its route along the electron transport chain to PSI following the 'Z-scheme' (Fig. 1.1). Once an electron has left P680 a replacement electron is drawn ultimately from H<sub>2</sub>O (via amino acid tyrosine and Mn atoms) (Figure 1.1, Eqn. 1.2).

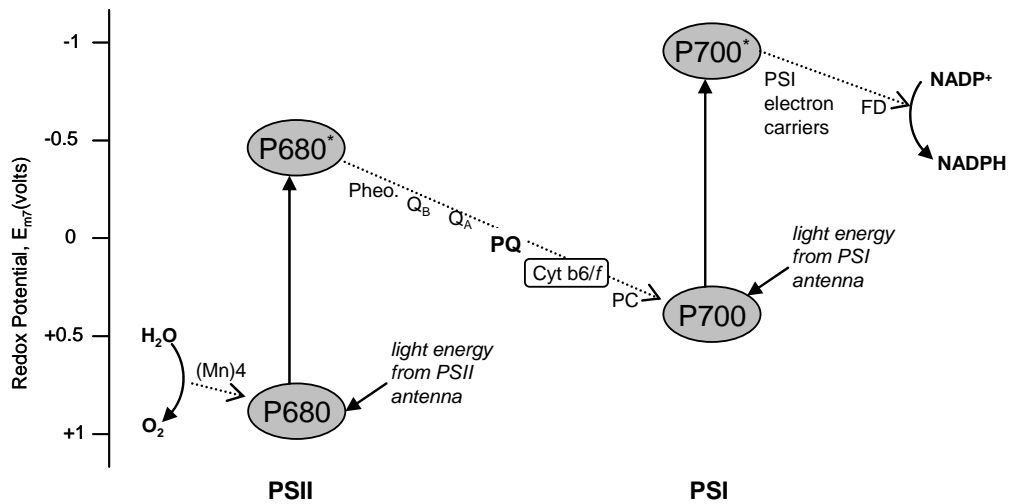


Figure 1.1. The ‘Z-Scheme’ of photosynthesis. Details are described in the text.

The electron progresses from its excited state in P680 by reducing the primary acceptor (Qa) which is a quinone bound to a protein. Electrons are passed along the electron transport chain (ETC) from PSII via electron carriers (phaeophytin – quinone Qa – quinone Qb – plastoquinone (PQ)) travelling by diffusion through the thylakoid membrane until they reach cytochrome complex bf (ctd  $b_6/f$ ). The cytochrome complex bf delivers electrons to P700 (of PSI) by diffusion through the thylakoid lumen via plastocyanine (PC). In PSI, absorption of a second photon at P700 causes a further charge separation. A final series of electron carriers pass the electron to ferredoxin (FD) where NADPH is formed from reduction of  $\text{NADP}^+$ . P700 draws a replacement electron from cytochrome bf. Eight protons are transported across the thylakoid membrane for each molecule of oxygen liberated, causing a potential difference across the membrane as well as a pH gradient. This proton gradient is reversed by ATP synthesis in the stroma via photophosphorylation.

The oxidation of the plastoquinol is typically the slowest reaction in the photosynthetic electron pathway (Falkowski and Raven 1997). It is therefore possible for cytochrome bf to be oxidized whilst the PQ pool remains reduced, i.e. PSI cannot obtain an electron from PSII. In this instance electrons may begin cycling around PSI, passed from ferredoxin back to cytochrome bf complex; thus producing ATP (but not NADPH) without the oxidation of water or the reduction of carbon dioxide. This cyclic electron flow is poorly quantified but is thought to be an important source of ATP in nitrogen-fixing cyanobacteria and important in nutrient-limited eukaryotic cells (Falkowski and Raven 1997).

The elements key to the investigation of photosynthesis and physiology are light capture and rates of electron transport along the ETC. The redox state of Qa is significant to considering the rate-limiting processes of the light reactions of photosynthesis. In an oxidized state Qa is ready to receive an electron, the rate of donation of electrons is less than that of electron departure. In this state of oxidized Qa reaction centres are referred to as 'open'. Hence the rate-limiting photosynthetic processes are those associated with light-capture and the rate of photosynthesis is regarded as light-limited. Conversely, Qa is reduced if the rate of electron donation to Qa exceeds the rate of removal. Reaction centres are referred to as 'closed'. The rate of removal of electrons from Qa could be limited by a number of possible rate-limiting steps in the processes downstream of Qa, and reactions centres are likely to be closed if photosynthesis is light saturated.

### 1.2.2 Dark Reactions

The dark reactions are responsible for the conversion of CO<sub>2</sub> to organic matter and are fuelled by the high energy products (ATP and NADPH) of the light reactions. Carbon dioxide is reduced within the stroma, by a series of enzyme-catalyzed reactions known as the Calvin – Benson cycle (Falkowski and Raven 1997). A key enzyme in this process is ribulose-1,5-bisphosphate carboxylase/oxygenase (Rubisco).

In addition to the light and dark reactions, many other complex reactions occur within the cell. These include those associated with respiration and nutrient utilisation and are briefly described below.

### 1.2.3 Respiration

Two types of respiration occur in marine alga; 'dark respiration' and 'photorespiration' (Geider 1992). Dark respiration occurs continuously via the oxidation of organic carbon. There are four components of dark respiration, glycolysis, the oxidative pentose phosphate pathway, the Krebs cycle and respiratory electron transport. Dark respiration can decrease the apparent net photosynthetic rate since it appears to reduce the amount of oxygen evolved per unit light absorbed.

Other pathways for oxygen consumption can occur in the light including photorespiration and the Mehler reaction. In the case of photorespiration the yield of photosynthesis is reduced as Rubisco accepts O<sub>2</sub> in place of CO<sub>2</sub> and generates no ATP, a process which may account as much as 15% of gross O<sub>2</sub> evolution in phytoplankton (Geider

1992). In the Mehler Reaction, O<sub>2</sub> produced by the oxidation of water in PSII is reduced by electrons carried by PSI, producing ATP and ultimately leading to the production of H<sub>2</sub>O. About 20% of photons absorbed in low light may be used in the Mehler reaction (Falkowski and Raven 1997).

#### 1.2.4 Nutrient Utilisation

Many elements including nitrogen, phosphorus, silicon and trace metals (including iron, zinc, copper) are required for phytoplankton growth. Requirements for nutrients include the production of enzymes, porphyrins and chlorins required for the synthesis of phytoplankton pigments and electron carriers with nitrogen a principle nutrient in most biosynthetic reactions (Falkowski and Raven 1997).

The concentration of nitrogen and phosphorus in marine particulate organic matter is close to that in seawater and occurs along with carbon in concentrations roughly conforming to the ration 106C:16N:1P (by atoms) known as the Redfield ratio (Redfield 1934, Redfield et al. 1963). This represents the mean over time and space scales but is known to vary with taxonomic composition and light availability (Geider et al. 1998, Geider and La Roche 2002, Klausmeier et al. 2003) as well as varying over timescales of hours in both the uptake stoichiometry and cellular composition of marine algae (Sambrotto et al. 1993, Banse 1994b).

Nitrogen is assimilated by phytoplankton in organic (urea) and inorganic (nitrate, nitrite, ammonium) forms and atmospheric N<sub>2</sub> may be 'fixed' by a small proportion of specialised phytoplankton. The oxidised form of nitrogen (nitrate) must be reduced for use in the cell using electrons generated in photosynthesis (Falkowski and Raven 1997). Phytoplankton growth fuelled by (typically) ammonium and urea is termed *Regenerated Production*, whilst *New Production* is used to describe production based on a source of nitrogen (normally nitrate) from outside the immediate environment (Dugdale and Goering 1967). The latter is often from the deep ocean where remineralisation of organic nitrogen to nitrate (ammonification and nitrification) occurs as part of the 'microbial loop' (e.g. Azam et al. 1983). The ratio of new to total production is termed the *f-ratio* (e.g. Harrison et al. 1987) and is traditionally used to infer the amount of carbon export since utilisation of new nitrate from below the euphotic zone may be assumed to balance export of carbon to depth (Dugdale and Goering 1967). Estimations of the f-ratio based on measurement of nitrate uptake has recently been brought into question as nitrification (as a source of nitrate) is seen to be significant in surface waters (Yool et al. 2007).

### 1.2.5 Terminology

Following definitions of Williams (1993) and Sakshaug et. al (1997) the term *gross photosynthesis* refers to the amount of oxygen evolved from the photochemical oxidation of water, whilst *net photosynthesis* refers to that corrected for respiratory losses by the phytoplankton. The *gross carbon fixation* includes all carbon fixed in photosynthesis regardless of whether or not it ultimately becomes part of the organism (Williams 1993). *Net carbon fixation* refers to the carbon uptake following losses of CO<sub>2</sub> from the oxidation of organic carbon in the light.

Phytoplankton carbon fixation rates are typically normalised to chlorophyll-a (chl-a) as a convenient indicator of phytoplankton biomass *in situ*. However, since the amount of chl-a per unit phytoplankton carbon biomass (C) (i.e. the ratio chl-a:C) is known to vary, a chl-a-specific carbon fixation rate is not a direct measure of phytoplankton population growth (Eppley 1972, Geider 1987, Cullen and Lewis 1988, Sakshaug et al. 1997). Following Eppley (1980) the phytoplankton growth rate ( $\mu$ ) is obtained from:

$$\mu = P^* \cdot \text{chl-a:C} \quad (1.4)$$

where P\* is the steady-state chl-a specific carbon fixation rate.

Since not all photochemical energy is utilised for the fixation of carbon, gross carbon fixation is always less than oxygen evolved. The ratio of moles of oxygen evolved to carbon fixed is termed the *Photosynthetic Quotient* (Laws 1991). Typical values are in the range 1.1 - 1.4 (Laws 1991) with the absolute value reflecting the relative amounts of protein, lipid and nucleic acid as well as carbohydrate synthesized within the cell (Laws 1991). The photosynthetic quotient is generally increased when nitrate is the main source of nitrogen due to the photochemical energy demands of nitrate reduction (Laws 1991).

## **1.2 Growth Conditions and Photophysiology of Marine Phytoplankton**

This section provides a summary of the key factors important in determining phytoplankton photosynthesis and therefore growth in the marine environment. The effect of the physical environment on phytoplankton distribution is described with emphasis on the ability of phytoplankton to adapt to changing environmental conditions.

Through the processes of photosynthesis, photoautotrophs require water, light and nutrients in order to grow. Temperature also influences the rate of photosynthesis due to the

temperature-dependent biochemical reactions (e.g. the dark reactions) (Geider 1987, Davison 1991). Phytoplankton growth and distribution in the ocean is driven, in part, by the co-availability of light and nutrients and is subsequently influenced by the physical processes which govern the availability of these resources (e.g. Sverdrup 1953, Dugdale 1967).

### 1.2.1 Light

Light, or irradiance ( $E$ ), in the marine environment comes from sunlight and is defined as the radiant flux of light energy incident on an area of surface. Irradiance is expressed in units of  $\mu\text{Einstein m}^{-2} \text{ s}^{-2}$  (or  $\mu\text{E m}^{-2} \text{ s}^{-1}$ ) where an Einstein is equal to one mole of photons. Irradiance that is useable by phytoplankton lies within the range of wavelengths 400-700 nm and is referred to as Photosynthetically Available Radiation (PAR). The wavelength of light is denoted  $\lambda$  (nm). Light diminishes exponentially through the water column (Eqn. 1.5), at a rate that is dependent on the wavelength:

$$E(z, \lambda) = E(0, \lambda)e^{-Kd(\lambda) \cdot z} \quad (1.5)$$

Where  $E(z, \lambda)$  and  $E(0, \lambda)$  represent the irradiance of wavelength,  $\lambda$ , at depth  $z$  and 0 meters respectively.  $Kd(\lambda)$  is the vertical attenuation coefficient ( $\text{m}^{-1}$ ) of downwelling irradiance at wavelength  $\lambda$ . Light is attenuated by water as well as by scattering or absorbing particles suspended within in it, including phytoplankton (Kirk 1994). These processes are both dependent on, as well as affect, the spectral composition of light within the water column (Kirk 1994). In general, red light (~600 – 700 nm) is attenuated strongly by pure water and is typically extinguished at shallower depths compared to photons of lower wavelengths (Kirk 1994). The depth to which solar irradiance penetrates the water column is typically defined by the depth at which PAR declines to 1% of the value just below the surface (Kirk 1994) and this region of the surface ocean is referred to as the *euphotic zone*.

The time-averaged light available for any given phytoplankton cell depends on the depth of the phytoplankton cell and subsequently on the physical mixing of the cell within the light gradient. It follows that the depth through which a phytoplankton cell is mixed is critical in determining the amount of light available and therefore the potential for growth. Hereafter the term *growth irradiance* is used to indicate the irradiance (PAR) the phytoplankton are exposed and *mean growth irradiance* refers to that averaged over a 24 hour period.

Following the conceptual model of Sverdrup (1953), the depth at which photosynthesis of a given phytoplankton cell equals its respiration is termed the *compensation depth* whilst the depth at which the water-column integrated photosynthesis equals the integrated respiration is termed the *critical depth*. It follows from this simplistic model that if mixing of phytoplankton cells is restricted to a depth shallower than the critical depth then net photosynthesis will occur (Sverdrup 1953). The model provides a useful reference for the concept of mixing and phytoplankton growth, however real scenarios do not necessarily conform to the model's simplicity. For example, if mixing rates are slower than a critical value phytoplankton growth rates may exceed rates of mixing and net growth occurs regardless of the mixing depth (Huisman et al. 1999). Smetacek and Passow (1990) also note the uncertainties regarding whether the model refers to net community respiration or only that associated with the phytoplankton.

### 1.2.2 Nutrients

As outlined above, phytoplankton require nutrients for photosynthesis. Nutrient availability in the marine environment results from both physical pathways of supply and removal by mixing and nutrient cycling by biological processes. Phytoplankton growth is limited if any of the required nutrients are unavailable (von Liebig 1840) and, in contrast, phytoplankton flourish in regions where nutrient supply exceeds the demand (Dugdale 1967).

The requirement for nutrients is dependent on phytoplankton species. For example, diatoms require silicate to build frustules and can exhibit rapid rates of nitrate uptake such that they are suited to regions where rapid influxes of new nutrients occur. In comparison, small celled picoplankton (particularly cyanobacteria) can take up nutrients at lower concentrations owing to their large surface-area to volume ratio (Chisholm 1992, Veldhuis and Kraay 1993).

### 1.2.3 Adaptation and Acclimation

Following Falkowski and LaRoche (1991) *adaptation* refers to the evolutionary processes that result in species specific (genotypic) traits in phytoplankton. Adaptation leads to differences in phytoplankton physiology (and other factors) between species. Changes in phytoplankton community structure may subsequently result from variations in the physical, chemical or biological environment. For example, dominant phytoplankton groups prevail as they out-compete others in the community of genotypes, due to the suitability of their species-specific traits to the environment. In contrast, *acclimation* describes the intra-species (phenotypic)

response of algae to changes in growth conditions at the organism level (Falkowski and LaRoche 1991). The terms *photoacclimation* and *photoadaptation* refer to adaptation and acclimation in response to change in the light environment specifically.

Photoacclimation results from changes of the photosynthetic apparatus within the cell and occurs on timescales shorter than, or comparable to, the lifetime of the cell (i.e. a few days) (e.g. reviews by Falkowski et al. 1980, Falkowski and LaRoche 1991, MacIntyre et al. 2002). Exposure to low light conditions results in an increase in photosynthetic pigments within the light harvesting antennae, the trade off to this process is cellular self-shading as pigment density increases, known as the *package effect* (Duysens 1956, Morel and Bricaud 1981, Berner et al. 1989). There are two main strategies of photoacclimation: the first is via an increase in the 'size' of the light harvesting antennae associated with the each reaction centre, whilst the second is by increasing the number of photosynthetic units (Falkowski and Owens 1980, Perry et al. 1981). Both of these strategies lead to an increase in the amount of chl-a within the cell relative to carbon biomass, i.e. an increase in chl-a:C (e.g. Geider 1987).

The increase in photosynthetic accessory pigments may or may not occur in constant proportion to chl-a (Falkowski and LaRoche 1991). A change in the ratio of the numbers of pigments that do not transfer light energy to chl-a (non-photosynthetic carotenoids) (e.g. Bidigare et al. 1990b) compared to photosynthetic carotenoids may also occur in response to a change in irradiance (Falkowski and LaRoche 1991). Variation in the ratio of PSI to PSII reaction centres, redistribution of excitation energy between PSII and PSI (for example, via the state transitions described by Falkowski et al. 1986) and electron cycling around PSI (Falkowski and Raven 1997) are also processes which may act to balance cycling of electrons between the two photosystems in response to changing light conditions (Falkowski and Raven 1997). Electron cycling (around PSI and PSII) and the state transitions (Falkowski et al. 1986, Falkowski and Raven 1997) are thought to manage the relative flow of electrons between the two photosystems in conditions of rapidly fluctuating irradiance, such as in response to periodic cloud cover or rapid mixing (Falkowski and Raven 1997).

There are many taxonomic traits relevant to light capture of which the type and number of pigments associated with the light harvesting antennae, the structure of the photosynthetic apparatus and the maximum capacity for carbon fixation are examples (Falkowski and Raven 1997). The potential acclimation responses are further traits of phytoplankton species.

Since nutrients, in particular nitrogen, are required for the synthesis and repair of light harvesting apparatus, nutrient limitation potentially affects the ability of the cell to acclimate to changing light conditions (Falkowski and Raven 1997).

The timescales of adaptation and acclimation compared to physical processes are fundamental in defining the phytoplankton distribution and species composition in the marine environment (Denman and Gargett 1983, Cullen and Lewis 1988), for example, uniformity in phytoplankton taxonomy and physiology may occur in mixed layers where the mixing timescales are shorter than those of photoacclimation or photoadaptation.

### **1.3 Physical-Biological Coupling in the Ocean**

The following section provides an overview of the physical marine environments relevant to this study, in particular the seasonally stratified temperate shelf sea and, more briefly, the stratified open ocean. The focus is on the influence of the physical environment on the distribution and growth of phytoplankton in the various hydrographic regimes.

#### **1.3.1 The Temperate Shelf Seas**

The shelf seas are relatively shallow (typically < 200 m) regions of the world's oceans located on the continental shelves. The focus for this study is the Celtic Sea, part of the NW European shelf (Sharples and Holligan 2006). The Celtic Sea is broadly similar in physical characteristics to the other shelf seas in this region, namely, the Northern North Sea (Rodhe et al. 2006) and the Bay of Biscay (Lavin et al. 2006) and similar to temperate shelf seas elsewhere (e.g. the New Zealand Shelf (Sharples et al. 2001a)).

The shelf seas are strongly influenced by the tides (owing to their relatively shallow water depth) and coupled with the seasonality experienced in temperate regions this results in the physical environment changing over seasonal, tidal and turbulent mixing timescales.

The following section summarises the seasonal variability in shelf sea environments, before focussing on the hydrographic regimes present in shelf seas during the summer months. The physical processes governing the water column structure are generally representative of many temperate shelf sea environments, however the phytoplankton distribution and growth are summarised according to relevant studies in the Celtic and North Seas. An overview of the physical and biological processes in the Celtic Sea can be found in Sharples and Holligan (2006), what follows is a brief introduction to the important concepts.

A fundamental physical process in the tidally dynamic shelf seas is the competition between mixing (caused by tidally generated turbulence at the seabed and that generated by wind mixing at the surface) and buoyancy input from solar heating (Simpson and Hunter 1974, Simpson and Bowers 1981). During the winter months, the lack of heat input to a temperate

shelf sea means that wind and tidal mixing fully mix the water column to depth (Sharples and Holligan 2006). The increase in solar heating during spring provides enough heat input (and therefore buoyancy) to the surface waters such that buoyancy may overcome mixing and the water column becomes thermally stratified. The temperature gradient between the warm surface waters and cool bottom waters is known as the *thermocline* and when established this acts as a barrier to vertical diapycnal transport (Sharples et al. 2001b). In some areas of the shelf, the tidal mixing continues to overcome the buoyancy input and the water column remains mixed. The boundary between regions of stratified and mixed water is known as a *tidal mixing front*.

During the winter, phytoplankton growth and biomass is relatively low (e.g.  $0.25 - 0.4 \text{ mg m}^{-3}$ ) (Joint et al. 1986) owing to the low irradiance of winter sunlight and the fact that the phytoplankton are mixed through the entire water column. Increased solar irradiance and the onset of seasonal stratification confines phytoplankton to the well-lit surface waters (above the critical depth) and a spring bloom occurs (e.g. Sverdrup 1953). In the Celtic Sea, a chl-a concentration of  $\sim 12 \text{ mg m}^{-3}$  has been recorded in the surface during a spring bloom (Joint et al. 1986). Nutrient depletion leads to the collapse of the spring bloom and the surface waters remain nutrient depleted until the breakdown of stratification in autumn (Pingree et al. 1976, Sharples et al. 2001b).

During the summer the nitrogen to phosphorous ratio (N:P) usually decreases such that nitrate (rather than phosphorous) is the limiting nutrient to phytoplankton growth (Pingree et al. 1977). Figure 1.2 illustrates the physical structure of a typical shelf sea during the summer months and illustrates that four distinct hydrographic regimes are present. The physical and biological processes associated with each of the mixed, frontal, shelf edge and stratified regions during summer are provided below.

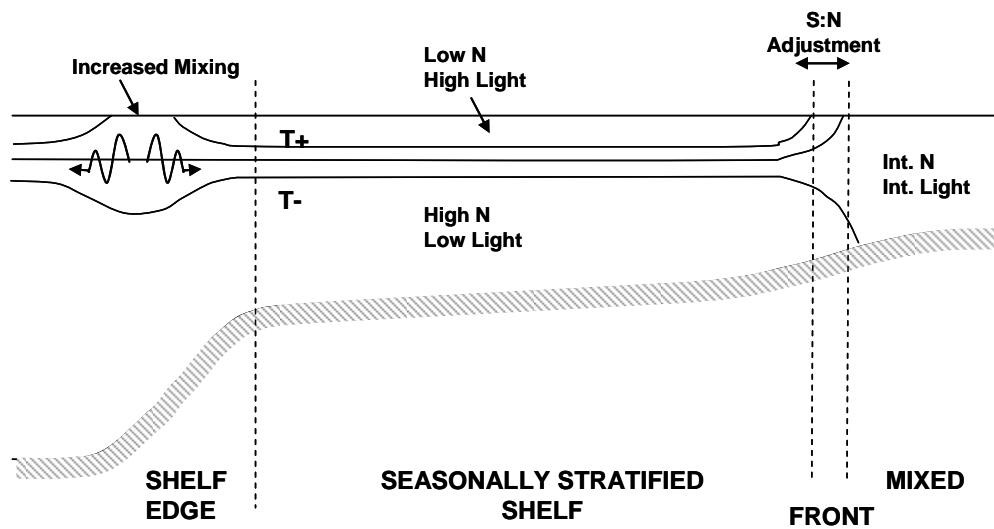


Figure 1.2. Schematic representation of vertical section of a shelf sea. Solid lines represent temperature contours. The shelf edge is characterised by a broad thermocline and the development of internal waves. The stratified shelf is characterised by a narrow thermocline with warm ( $T^+$ ) water low in nutrients (N) overlying cool ( $T^-$ ) nutrient rich water. Tidal mixing fronts bound the region between the stratified and mixed water, which are susceptible to horizontal migration due to tidal mixing (as described in text). The mixed water column is typically characterised by intermediate levels of light and nutrients (as described in text). Adapted from Simpson (1998).

### *Mixed Water*

Since mixed regions are those where tidal and wind mixing overcomes buoyancy inputs they are typically regions of shallow water (Fig. 1.2) and / or locally high tidal current speeds such that turbulence generated at the seabed is strong enough to mix the buoyancy input at the surface (Sharples and Holligan 2006). The amount of phytoplankton growth in a mixed water column depends on the water depth and the mixing rates that dictate the mean irradiance for phytoplankton (Sverdrup 1953) as well as nutrient availability (Holligan et al. 1984b). Chl-a concentration in the mixed region of the Western English Channel (off N. W. France), where typical water depth is  $\sim 100$  m, was  $1-2 \text{ mg m}^{-3}$  with integrated productivity around  $\sim 15 \text{ mg C m}^{-2} \text{ h}^{-1}$  (Holligan et al. 1984c). Diatoms dominated the phytoplankton community but other species were also present (Holligan et al. 1984b).

### *Tidal Mixing Fronts*

As the boundary between tidally mixed and stratified water columns fronts define the region where forces of tidal mixing and stratification are in balance (Simpson and Hunter 1974). Fronts

are identified as the location at which mixing causes the thermocline to reach the surface (Fig. 1.2), thus causing both horizontal as well as vertical gradients in physical properties. Assuming constant wind stress and buoyancy input, Simpson and Hunter (1974) defined the position of tidal mixing fronts to be located at a critical value of  $h/U^3$  where  $h$  is the depth of the water column (in meters), and  $U$  is the depth mean tidal current speed ( $\text{m s}^{-1}$ ). However other factors such as wind mixing are also important to determining the exact position of these fronts (e.g. Simpson and Sharples, 1994). Due to the dependence of frontal location on tidal current speed, frontal position is known to migrate (by order few kilometres) with tidal current strength over the spring – neap cycles (Pingree et al. 1975, Richardson and Pedersen 1998, Moore et al. 2003).

Fronts typically have greater surface chl-a than in stratified or mixed waters (Richardson et al. 1985). Chl-a at the surface of the Ushant Front (off NW France) has been observed to reach  $34 - 54 \text{ mg m}^{-3}$  (Holligan et al. 1984c) whilst daily integrated primary production ranged from  $900 - 1300 \text{ mg C m}^{-2} \text{ d}^{-1}$  over spring – neap timescales (Moore et al. 2003). The cause of high biomass and primary production at fronts is thought to be largely due to nutrient supply during spring-neap migration (Pingree et al. 1975, Richardson et al. 1998, Moore et al. 2003). In the North Sea, frontal excursions over the spring-neap cycle and the associated trapping of nitrate in the SML is estimated to fuel new production of  $24 - 48 \text{ g C m}^{-2}$  annually (Richardson et al. 2000). Dinoflagellates formed a significant fraction of the phytoplankton population at the Ushant front (Holligan et al. 1984c).

### *The Shelf Edge*

The shelf edge is a front marking the boundary between the stratified shelf sea and the stratified open ocean (Fig. 1.2). The steep bathymetry of the continental shelf slope induces mixing that causes the thermocline to reach the surface, again forming horizontal as well as vertical gradient in physical properties as in the case of tidal mixing fronts (Pingree and Mardell 1981, Joint et al. 2001, Sharples and Holligan 2006). Tidal mixing at the shelf edge may also lead to the formation of internal tides (Pingree and Mardell 1981, Huthnance 1989) and associated internal waves and solitons (Holligan et al. 1985), providing a route for the exchange of water mass properties between oceanic and shelf waters, including nutrients and carbon (Holligan et al. 1985, Huthnance 1989, Sharples et al. 2001b). Increased mixing at the shelf edge supplies nutrients to the euphotic zone and is normally associated with increased chl-a at the surface compared to the neighbouring strongly stratified waters (Pingree and Mardell 1981). At the Celtic Sea shelf break, depth-integrated chl-a in the order of  $10-20 \text{ mg m}^{-3}$  accounted for

primary production of  $400 - 1400 \text{ mg C m}^{-2} \text{ d}^{-1}$  (Joint et al. 2001). Phytoplankton assemblages at the Celtic Sea shelf edge are generally mixed and may contain small diatoms (Pingree et al. 1982), with cells  $> 5 \mu\text{m}$  in diameter accounting for around half the primary production (Joint et al. 2001).

### *The Stratified Shelf*

The seasonally stratified shelf region is characterised by warm, buoyant nutrient depleted surface mixed layer (SML) overlaying cool, dense, nutrient rich waters in the bottom mixed layer (BML), with the two layers divided by a thermocline (Fig. 1.2). Although referring specifically to the temperature gradient, the thermocline typically also reflects the density gradient (Sharples and Holligan 2006).

The physical processes acting on the thermocline across the stratified shelf are complex. Turbulent energy generated by wind stress at the surface and friction caused by tidal currents at the seabed is dissipated at the top and bottom boundaries of the thermocline respectively (e.g. Sharples et al. 2001b, Simpson 2000). The thermocline itself is a region of minimum turbulent dissipation and is therefore the location of high stability (Sharples et al. 2001b). Other physical processes acting on the thermocline include the propagation of internal waves, internal tides and solitons formed at the shelf edge (Pingree and Mardell 1981, Holligan et al. 1985) which lead to vertical movement of the thermocline over periods of hours to days (Sharples et al. 2001b).

The turbulent dissipation at the base of the thermocline is responsible for mixing nutrients (including nitrate) into the thermocline from the BML (Richardson et al. 1998). The nutrient flux is dependent on the nitrate gradient and the energy dissipated at the base of the thermocline and subsequently varies with tidal periodicity (Sharples et al. 2001b). The flux of nitrate across a range of locations in the NW European Shelf was estimated to be between  $1.5 - 11 \text{ mmol m}^{-2} \text{ d}^{-1}$ , measured via a variety of methods (Pingree and Pennycuik 1975, Holligan et al. 1984c, Horne et al. 1996, Sharples et al. 2001b).

The depth of the thermocline is of paramount importance in defining the phytoplankton growth conditions, with enough light for phytoplankton growth (both in the SML and thermocline itself) if the thermocline is shallower than the compensation depth (following Sverdrup (1953)). Despite high nutrient concentrations in the BML, there is generally not enough light for significant phytoplankton growth whilst phytoplankton growth in the SML is nutrient-limited and considered to be mostly sustained by regenerated production (Pingree et al. 1976, Holligan et al. 1984c). Chl-a concentration in the SML of the Celtic Sea region throughout summer (after the spring bloom) is typically  $< 1 \text{ mg m}^{-3}$  with recorded primary production of  $\sim 2$

mg C m<sup>-3</sup> h<sup>-1</sup> (Holligan et al. 1984c). The phytoplankton community consists of small phytoplankton (< 5 µm) typically dominated by nanoflagellates (Holligan et al. 1984c, Joint and Pomroy 1986).

Increased concentrations of chl-a are routinely observed in the thermocline region of the water column, forming a deep chlorophyll maximum (DCM) (e.g. Sharples and Holligan 2006). The suggested mechanisms for the formation of chlorophyll maxima include the passive sinking of phytoplankton cells (e.g. Steel and Yench 1960), reduced zooplankton grazing (Kononen et al. 1998), aggregation of motile phytoplankton (Cullen and Eppley 1981), the increase in phytoplankton cellular pigment concentration (chl-a:C) in response to low light conditions (Steele 1964) and net growth of phytoplankton *in situ* potentially fuelled by nitrate supply up the nitracline (Pingree and Pennycuik 1975, Sharples and Tett 1994, Sharples et al. 2001b).

In the Celtic Sea Sharples et al (2001b) demonstrated that the thermocline is located above the compensation depth at light levels > 1% of surface irradiance and that nitrate flux from the BML could support, at least in part, net growth of phytoplankton within the thermocline. An increase in chl-a:C at the thermocline compared to at the surface also indicates the contribution of cellular pigment concentration to the magnitude of the chl-a maxima (Steele 1964, Holligan et al. 1984b).

Holligan et al. (1984b) recorded chl-a concentration in the thermocline of the Celtic Sea of ~3 mg m<sup>-3</sup> and primary production in the thermocline of ~2 - 6 mg C m<sup>-3</sup> h<sup>-1</sup>, though values of > 30 mg C m<sup>-3</sup> h<sup>-1</sup> were observed by Pingree et al. (1976). Chl-a concentration and primary productivity are seen to vary considerably within the thermocline (with chl-a concentrations up to ~80 mg m<sup>-3</sup> (Sharples et al. 2001b)) with horizontal and temporal patchiness of phytoplankton considered to reflect of the dynamic nature of the physical environment (Sharples and Holligan 2006). The phytoplankton community in the thermocline is typically dominated by small (< 5 µm) cells, however at certain times larger dinoflagellates and some diatoms may dominate the community (Holligan and Harbour 1977, Holligan et al. 1984b, Joint et al. 1986).

The proportion of production within the thermocline that is considered new is that which is fuelled by nitrate supplied from the BML (after Dugdale and Goering 1967). Since nitrate remains depleted in the SML the thermocline is considered to be the main site of new production in the stratified regions of shelf seas (Sharples and Holligan 2006). The stocks of nitrate in the BML are those remaining from winter nitrate concentrations as well as from regeneration processes in the BML (e.g. Maguer et al. 1999) and bottom sediments (Trimmer et al. 1999). Subsequently the definition of new production is somewhat questionable in temperate shelf sea systems (away from the influence of the shelf edge) where a fraction of the nitrate

supplied from the BML during summer results from nitrate regenerated since the onset of stratification, as well as that regenerated over seasonal timescales (reviewed by Sharples and Holligan (2006)).

In order to maintain an accumulation of biomass, phytoplankton carbon fixation must exceed losses including grazing, mortality and sinking from the euphotic zone. In the case of the thermocline a major sink for phytoplankton is mixing of cells to the BML by the same turbulent mixing processes that supply nitrate (Sharples et al. 2001b). Other phytoplankton loss mechanisms include grazing, sinking of cells into the BML and cell death and subsequent lysis (e.g. Allen et al. 2004). Despite numerous independent studies, relatively little is known about processes influencing the autotrophic community either directly (grazing) or indirectly (biogeochemical cycling) in shelf environments (Sharples et al. 2001b), although large zooplankton may be associated with the DCM (Holligan et al. 1984b, Richardson et al. 1998). Timescales of regeneration of nutrients by the benthos remain largely unknown in these systems (Sharples and Holligan 2006).

### 1.3.2 The Open Ocean

The potential mechanisms of formation and maintenance of the DCM in the open ocean include those mentioned for shelf sea environments above with the same considerations regarding the maintenance of the DCM above phytoplankton loss terms. In the open ocean the form of the DCM and the functioning of the phytoplankton within it varies widely, largely depending on the physical processes acting in the region (Cullen and Eppley 1981, Cullen 1982, Cullen et al. 1982). As with the shelf sea environment, the co-availability of light and nutrients is fundamental in determining phytoplankton growth at the DCM (Letelier et al. 2004). Across a range of hydrographic regimes the DCM may be associated with the depth of the pycnocline (Goering et al. 1970, Herbland and Voituriez 1979) or that of the nitracline (Maranon et al. 2000, Letelier et al. 2004) and typically (although not always) associated at the depth of 1% surface irradiance (Poulton 2002, Letelier et al. 2004).

The DCM often reflects a cellular pigment (chl-a:C) maximum (Steele and Yentsch 1960, McManus and Dawson 1994, Chavez et al. 1996) and may be associated with a change in phytoplankton composition and / or size structure compared to in the surface (McManus and Dawson 1994, Revelante and Gilmartin 1995). The DCM may also represent a primary productivity maximum and / or a phytoplankton biomass maximum (Herbland and Voituriez 1979, Furuya 1990).

In order to provide a summary of the DCM characteristics in hydrographic regimes relevant to this study, the following paragraphs summarise previous observations in the Atlantic Ocean. A summary of the hydrographic regimes of the Atlantic Ocean is included in Robinson et al. (2006) whilst a detailed review of the form and functioning of the DCM in the Atlantic Ocean is documented by Poulton (2002). Phytoplankton community structure and primary production estimates through the Atlantic Ocean are well documented (e.g. Maranon and Holligan 1999, Maranon et al. 2000, 2001, Perez et al. 2006) though only Perez et al. (2006) focuses on the DCM.

The high latitude regions of the Atlantic Ocean are characterised by a seasonal thermocline and are associated with a spring bloom and summer stratified conditions with a nutrient limited SML (e.g. Longhurst 1998, Robinson et al. 2006). Chl-a concentration during spring bloom conditions were around  $\sim 1 \text{ mg m}^{-3}$  (Maranon and Holligan 1999). Water column primary productivity of  $> 500 \text{ mg C m}^{-2} \text{ d}^{-1}$  in the high latitude regions was observed during local spring (Maranon et al. 2000). A DCM of around  $0.2 - 0.4 \text{ mg m}^{-3}$  (compared to SML chl-a  $< 0.2 \text{ mg m}^{-3}$ ) was also a biomass maximum and sometimes also a primary production maximum (Maranon et al. 2000).

The tropical and subtropical Atlantic Ocean is characterised by a deep thermocline which is deepest in the central oligotrophic gyres (e.g. Longhurst 1998, Robinson et al. 2006). Above the thermocline, nitrate concentrations remain low ( $< 0.1 \mu\text{M}$ ) throughout the year (e.g. Maranon et al. 2000). In the oligotrophic gyres the nitracline may be deeper than the thermocline with the DCM located at the top of the nitrate gradient (Perez et al. 2006). The surface waters of the oligotrophic gyres are characterised by very low chl-a concentrations ( $< 0.2 \text{ mg m}^{-3}$ ) with a DCM of  $\sim 0.2 - 0.4 \text{ mg m}^{-3}$ . In general, the DCM is a pigment (chl-a:C) maximum and not a biomass or productivity maximum (Maranon et al. 2000, Perez et al. 2006). Primary production at the DCM in the gyres is typically  $< 1 \text{ mg C m}^{-3} \text{ d}^{-1}$  (Poulton et al. 2006a). The gyres are dominated by cyanobacteria (*Synechococcus* and *Prochlorococcus*) and small flagellates  $< 5 \mu\text{m}$  (Maranon et al. 2000).

Upwelling regions include the equator (due to diverging water masses to the North and South) and regions along the West African continental boundary (wind induced upwelling). Shoaling of the nitracline in these regions causes (nanomolar) increases in nitrate concentrations recorded in the surface of both equatorial and NW African upwelling waters (Planas et al. 1999, Maranon et al. 2000). The upwelling region off NW Africa is an area of increased chl-a, biomass and productivity with increased contribution of larger size classes of phytoplankton and increased presence of diatoms (Maranon et al. 2000, Maranon et al. 2001). In contrast, the

upwelling of the equatorial Atlantic is a region of increased biomass and productivity but without such a significant change in size structure of phytoplankton (Maranon et al. 2001). In both the equatorial and NW African upwelling regions the DCM is often associated with a biomass as well as productivity maximum (Maranon et al. 2000).

Mixed water of the South Subtropical Convergence (SSTC), a water mass beyond the southern boundary of the South Atlantic gyre (e.g. Robinson et al. 2006), is associated with surface nitrate concentrations in excess of  $> 10 \mu\text{M}$  and primary production  $> 500 \text{ mg C m}^{-2} \text{ d}^{-1}$  during austral spring (Maranon et al. 2000).

In general, the physical processes determining nutrient supply in the open ocean are still poorly understood. Nitrate flux from below the euphotic zone is thought to be an important factor determining phytoplankton growth rates in the open ocean (Planas et al. 1999, Maranon et al. 2000). However numerous studies show that nitrate uptake rates far exceeded the flux from the BML and highlight the significance of other external sources of nitrate into these regions (Lewis et al. 1986, Planas et al. 1999). Measurements of nitrate uptake and new production are limited (e.g. Lewis et al. 1986, Planas, et al, 1999) largely due to the difficulties in obtaining accurate measurement of ambient nutrient concentrations (Planas et al. 1999). Generally, the highest *f*-ratios are found in equatorial regions ( $\sim 0.4$ ) with low *f*-ratios in the oligotrophic gyres ( $< 0.2$ ) (reviewed by Planas, et al. (1999)). Estimates of the *f*-ratio (particularly those calculated by measurements of nutrient uptake) in the open ocean should be considered with caution as (for example) nitrogen fixation and near-surface nitrification may be significant in these regions but remain poorly understood (e.g. Yool et al. 2007).

The variability in DCM form and functioning in response to the physical processes is true of both open ocean and shelf sea environments (Cullen 1982, Sharples and Holligan 2006). The stratified shelf seas represent an extreme case where physical processes dominate the water column structure mainly due to their shallow water depth and tidal mixing (Sharples and Holligan 2006). The DCM in the stratified Celtic Sea is strictly restricted to the thermocline and maintained at light levels well in excess of the 1% surface irradiance. In contrast, in the oligotrophic gyres the weak influence of mixing may allow the DCM to be maintained below the thermocline with its depth only restricted to that of light availability (Cullen 1982). The shelf sea case is similar to the open ocean high latitude regions by the occurrence of winter mixing and seasonal stratification, and similar to the upwelling regions by the elevated light conditions at the DCM and the upward nitrate flux (Cullen 1982, Poulton 2002).

## 1.4 Measurement of Phytoplankton Physiology

This section describes two methods for quantifying the functioning of phytoplankton cells in field populations, by measuring the phytoplankton response to light. The first method is the traditional measurement of  $^{14}\text{C}$ -labelled carbon fixation of a phytoplankton sample across a range of light conditions, the Photosynthesis vs. Irradiance (P vs. E) method. A detailed discussion of the physiological information gained by this method is described by MacIntyre et al. (2002) as well as Sakshaug et al. (1997) and Laws (2002).

A more recent technique is the use of active fluorescence here described in terms of the Fast Repetition Rate Fluorometer (FRRF). The measurement of the fluorescent response of phytoplankton to a sequence of excitation flashlets provides information on part of the photosynthesis process (Falkowski and Raven 1997). Detailed discussion of this theory behind the technique is given by Kraus and Weiss (1991), Kolber and Falkowski (1993), Kolber et al. (1998) and reviewed by Falkowski and Raven (1997).

### 1.4.1 P vs. E Experiments

Measurement of photosynthetic rates for a phytoplankton sample over a range of light conditions provides a description of the inherent light-dependency of photosynthesis and photoacclimation state of the phytoplankton (Fig 1.3). This approach can be employed to measure the light-response of any variable, for example,  $^{15}\text{N}$  uptake, although focus here is on the measurement of photosynthetic rates by  $^{14}\text{C}$ -fixation or  $\text{O}_2$ - evolution over the time course of the incubation (Williams 1993). Photosynthetic rates are typically normalised to chl-a.

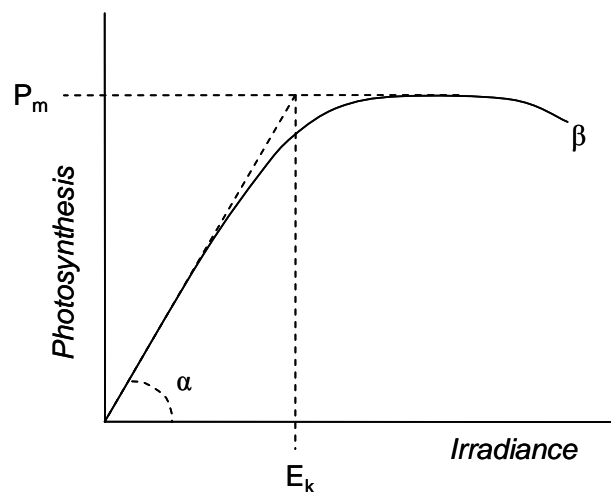


Figure 1.3. Schematic of Photosynthesis versus Irradiance (P vs. E) curve. Parameters indicated are described in text.

The shape of the P vs. E curve varies with the photo-acclimation state of phytoplankton and can vary both within and between species (Sakshaug et al. 1997). The shape of the P vs. E curve is described by the parameters indicated in Figure 1.3, the ecological relevance of these parameters is described below.

The intercept of the P vs. E curve is typically non-zero. In the case of oxygen evolution, the intercept is typically less than zero due to net community respiration and in the case of carbon fixation it is always positive resulting from light-independent processes and / or systematic experimental artefacts (Sakshaug et al. 1997).

### *Physiological Parameters*

**$\alpha$  (and  $\Phi_M$ )** - The initial slope of the P vs. E curve is close to linear and represents the increase in the amount of photosynthesis per unit incident light. It is known as the *maximum light utilization coefficient* (Mauzerall and Herron 1970, Sakshaug et al. 1997) denoted  $\alpha$  and has units of (mg O<sub>2</sub> evolved or CO<sub>2</sub> fixed m<sup>-3</sup> h<sup>-1</sup>) (μE m<sup>-2</sup> s<sup>-1</sup>)<sup>-1</sup>. In this linear region of the curve the rate-limiting process is the absorption of photons by the light harvesting antennae, and photosynthesis is light-limited.

The value of  $\alpha$  is dependent on the spectral quality of the light in the incubator relative to the spectra of light absorbed by the phytoplankton. Although relative trends are informative, the absolute value has no ecological significance unless a correction is applied to account for the difference between the spectral light field in the P vs. E incubator compared to *in situ*. When the photosynthetic rate is normalised to chl-a,  $\alpha$  is denoted  $\alpha^*$  and has units (mol O<sub>2</sub> evolved or CO<sub>2</sub> fixed h<sup>-1</sup>) (mg chl-a)<sup>-1</sup> (μE m<sup>-2</sup> s<sup>-1</sup>)<sup>-1</sup>.

The *maximum quantum yield* ( $\Phi_m$ ) is the amount of carbon fixed per unit light absorbed (Mauzerall and Herron 1970, Sakshaug et al. 1997). It is related to  $\alpha^*$  by the ratio of incident light to light absorbed (Falkowski et al. 1985) and is calculated from Equation 1.6:

$$\phi_m = \alpha^* \cdot \frac{1}{a^*} \cdot 0.0231 \quad (1.6)$$

where  $a^*$  is the spectral light absorption by phytoplankton normalised to chl-a (m<sup>2</sup> (mg chl-a)<sup>-1</sup>) and the 0.0231 factor converts milligrams of C to moles, μmoles of photons (or μE) to moles

and hours to seconds. Thus  $\Phi_m$  is independent of both chlorophyll-a and unit area and has units of (mol O<sub>2</sub> evolved or CO<sub>2</sub> fixed (mol absorbed photons)<sup>-1</sup>). Since 8 photons are required to derive one molecule of O<sub>2</sub>, it follows that  $\Phi_m$  has a theoretical maximum of 0.125 (Kok 1948).

Variability in  $\alpha^*$  is theoretically largely genotypic as a result of changes in  $\alpha^*$  due to the pigment composition and pigment packaging (Geider et al. 1993a, Babin et al. 1996, MacIntyre et al. 2002). Significant decrease in the maximum quantum yield ( $\Phi_m$ ) may occur in surface phytoplankton with increased proportions of photoprotecting pigments that absorb light but do not transfer energy to photochemistry (Marra et al. 2000). However, quantum efficiency is also seen to decline under nutrient stress (Welschmeyer and Lorenzen 1981, Geider et al. 1993b) but the role of light and nutrients in phenotypic variability of this parameter remains unclear (MacIntyre et al. 2002).

**P<sub>m</sub>** - The *light-saturated photosynthetic rate*, P<sub>m</sub>, is the maximum rate of photosynthesis and has units of (mg O<sub>2</sub> evolved or CO<sub>2</sub> fixed m<sup>-3</sup> h<sup>-1</sup>). At this maximal photosynthetic rate a further increase in irradiance will not cause an increase in photosynthesis. As such, it is the processes downstream of light capture (such as electron transfer or carbon fixation) that limit the rate of photosynthesis (Sakshaug et al. 1997). P<sub>m</sub> is independent of the light capture processes, including the absorption cross-section of the photosynthetic apparatus, and is therefore not spectrally dependant.

P<sub>m</sub> is typically normalised to chl-a, and is denoted P\*<sub>m</sub> with units (mg O<sub>2</sub> evolved or CO<sub>2</sub> fixed (mg chl-a)<sup>-1</sup> h<sup>-1</sup>). In order to obtain a measure of phytoplankton growth rates, P<sub>m</sub> would require normalisation to carbon biomass, however, due to the difficulties in measuring carbon biomass (or chl-a:C) in the field photosynthesis is typically normalised to chl-a.

In contrast to the light-limited quantum efficiency, variability in light-saturated growth is typically observed to be largely governed by irradiance rather than between species (Geider et al. 1993a). However, a variety of phenotypic responses in P\*<sub>m</sub> is also evident in nutrient stressed cultures, as well as some variability observed between species (Cullen et al. 1992, Geider et al. 1993b).

**Ek** - The *light saturation parameter*, Ek, is a theoretical point on the P vs. E curve representing the incident light at which the rate limiting processes of light capture and photochemical energy conversion and reductant utilization are balanced (Talling 1957, Escoubas et al. 1995, Sakshaug et al. 1997). Ek has units of light (μE m<sup>-2</sup> s<sup>-1</sup>) and is calculated by Equation 1.7.

$$E_k = \frac{P_m^*}{\alpha^*} \quad (1.7)$$

$E_k$  is independent of the variable used to normalise photosynthesis (typically chl-a). Like  $\alpha^*$ ,  $E_k$  is spectrally dependant and as such its absolute value has no ecological relevance unless spectral differences between the light source used in the incubator and *in situ* irradiance are accounted for. Resulting from processes controlling  $P_m^*$  and  $\alpha^*$ ,  $E_k$  occurs at an irradiance just below that of maximal photosynthesis and represents the balance between maximising growth rates and limiting the potential of photo-damage under very high irradiances (Geider et al. 1998, Laws et al. 2002).

**$\beta$**  - Increasing irradiance beyond the level of saturation, eventually leads to a decline in photosynthetic rate. Quantified by parameter  $\beta^*$  this is known as *photoinhibition*. Photoinhibition reflects photo-damage in the phytoplankton antennae and is dependant on both the level of irradiance and the duration of exposure (Falkowski and Raven 1997).

#### 1.4.2 Fast Repetition Rate Fluorometer

The Fast Repetition Rate Fluorometer (FRRF) is used to investigate photosynthetic rates via measurement of the fluorescence response to a prescribed series of stimulating flashes (Falkowski and Raven, 1997). In contrast to  $^{14}\text{C}$ -uptake or  $\text{O}_2$ -evolution photosynthetic rate measurements described above, the FRRF measures processes associated with PSII only rather than the entire photosynthesis process. The following is a brief overview of the relevant photosynthetic processes described more fully by Falkowski and Raven (1997).

As mentioned above, on capturing a photon of light at PSII (and subsequent excitation of an electron at the associated reaction centre) the first electron acceptor (Qa) of the electron transport chain between PSII and PSI becomes reduced, but only if the reaction centre is initially 'open' (i.e. Qa is initially oxidized). When the reaction centre is 'closed' (Qa is already reduced) there is a high probability that the absorbed light energy will be re-released as fluorescence.

At room temperature algae fluoresce at about 685 nm (Falkowski and Raven 1997). The stimulating flashes given by the FRRF induce a change in the ratio of fluorescence emitted to light absorbed at PSII, a parameter known as the fluorescence yield (F) (Kolber and Falkowski 1993). Figure 1.4 illustrates the change in fluorescence yield of phytoplankton given a sequence of flashlets by the FRRF over time.

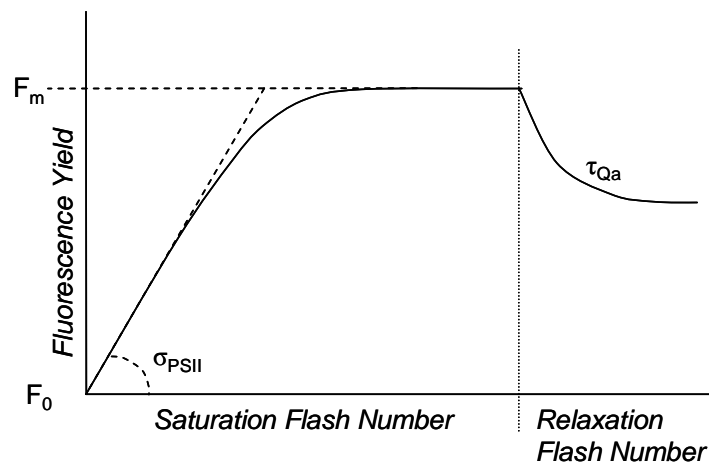


Figure 1.4. Schematic of the fluorescence yield resulting from a sequence of saturation and relaxation flashlets given by the FRRF. A full description of this process (and identification of the parameters indicated) is described in text.

Under low illumination algae fluoresce at a constant low level, denoted  $F_0$ . With increased light, as reaction centres become closed, fluorescence increases until it reaches a maximum level,  $F_m$ . The difference between the maximum and minimum levels of fluorescence ( $F_m - F_0$ ) is called the *variable fluorescence*  $F_v$ . It follows that fluorescence is closely related to the oxidation state of Qa as this affects the rate at which electrons are transferred from PSII. The excitation flashes from the FRRF are of equal intensity but are delivered in close repetition designed to progressively close reaction centres and raise fluorescence from  $F_0$  to  $F_m$ .

At the plateau of the fluorescence yield at  $F_m$  and the achievement of the closure of all RCII, PSII is light-saturated. Under conditions of PSII light-saturation the rate of light absorption of PSII is equal to or exceeds that of steady-state electron transport away from Qa, i.e. the rate limiting process for the turnover of electrons through PSII when PSII are light saturated is this oxidation rate of Qa. In order to measure the fluorescence yield as reaction centres become open a series of sub-saturating ‘relaxation flashes’ are given. The decrease in fluorescence yield illustrates the re-opening of reaction centres as electrons are passed from Qa to PQ, the timescales of which relates to the rate of electron transfer ( $1/\tau$ ).

### *Physiological Parameters*

**$F_v/F_m$**  - The variable fluorescence yield,  $F_v$ , is commonly normalized by  $F_m$  to give an expression,  $F_v/F_m$ , known as the *quantum efficiency of photochemistry*.  $F_v/F_m$  represents the amount of energy absorbed by PSII to that which is emitted (as fluorescence), and is therefore a

quantitative measure of photochemical energy conversion efficiency of PSII. Following a series of culture experiments a maximum value of 0.65 for  $F_v/F_m$  has been suggested (Kolber et al. 1988, Kolber et al. 1998).

Variability of  $F_v/F_m$  results from the functional organization of the photosynthetic apparatus (e.g. Kolber and Falkowski 1993, Falkowski and Kolber 1995, Kolber et al. 1998), and is seen to be reduced in conditions of nutrient stress (e.g. Greene et al. 1991, 1994).

$\sigma_{PSII}$  - The *effective absorption cross section*,  $\sigma_{PSII}$ , represents the rate of light saturation of PSII (i.e. the rate of increase in fluorescence yield from  $F_0$  to  $F_m$ ). This parameter is a measure of the efficiency of light capture by the light harvesting antennae relative to the number of RCIIIs, or the “size” of the photosynthetic unit (Falkowski and Raven 1997). Technically,  $\sigma_{PSII}$  is a quantification of the probability of a photon of light being absorbed and utilized for photochemistry rather than a measure of the physical size of the antennae (Falkowski and Raven 1997).

$\sigma_{PSII}$  is dependent on the spectral composition of the incident light and is related to the spectral absorption cross section by Equation 1.8 (Sakshaug et al. 1997):

$$\alpha^*(\lambda) = n\sigma(\lambda)_{PSII} \quad (1.8)$$

where  $n$  represents the number of PSII reaction centres per unit chl-a, PSII:chl-a. The value of  $\sigma_{PSII}$  is therefore sensitive to changes in the structure and pigment composition of PSII (Falkowski and Raven, 1997).

Variation in  $\sigma_{PSII}$  is seen across phytoplankton taxa, primarily due to phytoplankton pigment composition and the presence of non-photosynthetic pigments, but photoacclimation and nutrient stress are also seen to affect this parameter (Kolber et al. 1990, Geider et al. 1993b, Suggett et al. 2004).

$1/\tau_{Qa}$  (and  $1/\tau_{PSII}$ ) – The *rate of electron transport* ( $1/\tau$ ) away from PSII (ie. from  $Q_a$  to the PQ pool) is denoted  $1/\tau_{Qa}$ , and may be measured directly by the FRRF if, by flash sequence design, the FRRF does not change the redox state of the PQ pool so allowing electrons to be passed to PSI and the dark reactions unhindered (Falkowski and Raven 1997, Moore et al. 2006).

Calculation of the rate of whole chain electron transport ( $1/\tau_{PSII}$ ) is possible from the relation shown in Equation 1.9, assuming  $^{14}C$ -derived  $E_k$  ( $E_{k14C}$ ) represents the light level at

which the rates of photochemistry and whole chain electron transport are balanced (Falkowski and Raven 1997):

$$1 / \tau_{PSII} = Ek_{14C}(\lambda) \sigma_{PSII}(\lambda) \quad (1.9)$$

**Ek<sub>ETR</sub>**—The light saturation parameter obtained from FRRF parameters via Equation 1.10 (Ek<sub>ETR</sub>) represents the light level at which PSII becomes saturated (Moore et al. 2006).

$$Ek_{ETR} = \frac{166030}{\sigma_{PSII} \cdot \tau_{Qa}} \quad (1.10)$$

where  $\sigma_{PSII}$  and  $\tau_{Qa}$  are measured from FRRF and 166030 converts units to provide the light saturation parameter Ek with units ( $\mu\text{E m}^{-2} \text{s}^{-1}$ ).

### 1.4.3 <sup>14</sup>C vs. FRRF-derived Physiological Parameters

In order to obtain carbon fixation rates from FRRF-derived measurements, or for direct comparison of FRRF-derived parameters and those of the <sup>14</sup>C P vs. E curve, a number of factors must be known. These factors largely arise from the fact that carbon fixation measures something between net and gross photosynthesis and are typically normalised to chl-a whilst the FRRF technique estimates gross electron turnover by PSII. The following theoretical relationships provide the basis for comparison of FRRF and <sup>14</sup>C derived parameters (Kolber and Falkowski 1993, Suggett et al. 2004):

$$P^*_m = C \cdot f \cdot (PSII : chla) \cdot 1 / \tau_{PSII} \cdot P_{Quot}^{-1} \quad (1.11)$$

$$\alpha^* = C \cdot f \cdot (PSII : chla) \cdot \sigma_{PSII} \cdot P_{Quot}^{-1} \quad (1.12)$$

Where  $P^*_m$  and  $\alpha^*$  are <sup>14</sup>C parameters which roughly correspond to the FRRF parameters  $1/\tau_{PSII}$  and  $\sigma_{PSII}$  by the consideration of the photosynthetic quotient ( $P_{Quot}$ ),  $f$ , which is a measure of the fraction of the PSII reaction centres which are functional and PSII:chl-a which represents the number of PSII reaction centres per unit chl-a. C is a constant required for unit conversions, and includes a factor of 0.25 which is an assumed value for the quantum efficiency of electron

transport through PSII (i.e. 4 photons are required to evolve 1 mol O<sub>2</sub> within PSII). In application of these equations, the unknown variables are also assigned assumed values, with  $f$  typically assigned the value  $(F_v/F_m)/0.65$  where 0.65 is the suggested maximum of  $F_v/F_m$  (Geider et al. 1993a, Kolber and Falkowski 1993) and PSII:chl-a is assumed equal to 1/500 with 500 an assumed value of the chl-a per PSII (Kolber and Falkowski 1993). There are many uncertainties in estimation of these variables (see discussions by Suggett et al. (2001, 2004), Moore et al. (2003)). Processes such as cyclic electron flow around PSII, photorespiration and the Mehler reaction (affecting measurement of net compared to gross photosynthesis) act to ‘decouple’ <sup>14</sup>C measured physiological parameters from their FRRF-derived equivalents (Suggett et al. 2004). Also notable are the ratios of PSI:PSII and PSI:chl-a which affect the overall chl-a concentration and therefore the value of PSII:chl-a, but are not easily measurable in the field and are known to vary between species and growth conditions in a manner which remains poorly understood (Falkowski et al. 1981).

## 1.5 Thesis Objectives

The principle aim of this thesis is to investigate the coupling between the biological and physical processes that govern the primary productivity of phytoplankton within the deep chlorophyll maximum (DCM). The main focus for this study is a seasonally stratified (tidally active) shelf sea, although comparisons are also made with open ocean environments.

The main research themes of the thesis are to:

- Assess how phytoplankton community composition and physiology within the DCM are determined by the physical environment.
- Quantify the primary production of phytoplankton within the DCM and establish its significance to water-column production.
- Investigate how primary production in the DCM is influenced by temporal and spatial changes in the physical environment.
- Define the relationship between new nutrient availability and primary production in the DCM.

## 1.6 Presentation of Thesis

Data collected within a temperate shelf sea form the main focus of the study, and are therefore collated into the following chapters:

The photophysiology of phytoplankton within the DCM is addressed in **Chapter 3** using a combination of physiological measurements made by FRRF and  $^{14}\text{C}$ -uptake P vs. E experiments. **Chapter 4** establishes the hydrographic context of the shelf sea DCM and quantifies the primary production within the DCM across a range of locations using a novel empirical modelling approach. This chapter also addresses the influence of variability in the physical environment on productivity of the DCM. Specific attention is given to the role of nutrient availability in **Chapter 5**. The principles governing the primary production of the DCM within the shelf sea thermocline are compared to these in a range of hydrographic conditions in the Atlantic Ocean. The analysis concerning the open ocean environments is self-contained in **Chapter 6**. A discussion of the results from all chapters is given in **Chapter 7**.

## CHAPTER 2: METHODS

Data were collected during two cruises in the Celtic Sea during 25<sup>th</sup> July – 14<sup>th</sup> August 2003 (CS03) and 15<sup>th</sup> July – 6<sup>th</sup> August 2005 (CS05) and one transect through the Atlantic open ocean 17<sup>th</sup> September – 29<sup>th</sup> October 2004 (AMT15). Cruises were carried out on board the *RRS* James Clark Ross (CS03), the *RRS* Charles Darwin (CS05) and the *RRS* Discovery (AMT15).

A list of measurements made during each cruise is given in Table 2.1. Where supplied by other contributors, data processing and calibration was overseen by the author and in some cases re-calibrated to suit the specific needs of this study. On all three cruises, <sup>14</sup>C P vs. E experiments were carried out by the author. During AMT15, all FRRF and many <sup>14</sup>C-Simulated-In-Situ (SIS) incubation experiments were also carried out by the author. Laboratory analysis of particle absorption measurements were made by the author for cruises CS05 and AMT15 as well as some laboratory analysis of HPLC samples from CS05.

Table 2.1. Persons responsible for data collection during CS03, CS05 and AMT15. Names in parenthesis indicate persons involved with post-cruise analysis and /or data processing. n/a indicates samples not obtained or included in this analysis, (a) indicates the author.

Measurement	CS03	CS05	AMT15
<sup>14</sup> C P vs. E Experiments	A. Hickman (a)	A. Hickman (a)	A. Hickman (a)
<sup>14</sup> C SIS Experiments	P. Carmeno V. Perez	n/a	A. Hickman (a) T. Adey
<sup>15</sup> N and <sup>13</sup> C P vs. E Experiments	M. Lucas (S. Painter)	n/a	n/a
O <sub>2</sub> P vs. E Experiments	T. Adey	n/a	n/a
%O <sub>2</sub> Saturation	T. Adey (D. Purdie)	D. Purdie	n/a
FRRF Measurements	C.M. Moore J. Tweddle Y.N. Kim	C.M. Moore J. Tweddle Y.N. Kim	A. Hickman (a)
CTD Initial Calibrations (including <i>in vivo</i> chl-a)	J. Sharples	J. Sharples	(BODC)
Nutrients	D. Hydes	Y.N. Kim M. Qurban	K. Chamberlain M. Woodward
Chl-a	P. Holligan	P. Holligan Y.N. Kim (A. Hickman (a))	A. Pattenden
HPLC Pigments	P. Holligan Y.N. Kim	P. Holligan Y.N. Kim (A. Hickman (a))	A. Pattenden (C. Holeton)
Analytical Flow Cytometry	P. Holligan (M. Zubkov)	P. Holligan (C.M. Moore)	J. Heywood
Phytoplankton Identification	P. Holligan Y.N. Kim (A. Poulton)	P. Holligan Y.N. Kim (A. Poulton)	n/a
Particle Absorption	P. Holligan (D. Suggett)	P. Holligan (A. Hickman (a))	A. Pattenden (A. Hickman (a))
POC/N	P. Holligan (A. Poulton) (R. Harris) (P. Head)	P. Holligan (A. Poulton) (R. Harris) (P. Head)	A. Pattenden (A. Poulton) (R. Harris) (P. Head)
<i>In situ</i> Optics	G. Tilstone	V. Kristov	L. Hay G. Moore (S. Lavender)

## 2.1 Sampling Procedure

During CS03, the full suite of biological measurements were obtained at two depths, one in the surface mixed layer (SML) and one at the peak of the deep chlorophyll maximum (DCM).

Sampling locations included the Celtic Sea shelf edge, multiple stations on the stratified region

of the shelf (hereafter referred to as *stratified shelf*), close to the Irish Sea front and in the mixed waters of the Irish Sea. Sampling was normally carried out during the night, but some samples were collected during the day. Water column optics measurements were obtained at a limited number of stations.

During CS05, four depths were routinely sampled for biological measurements. Two samples were from the SML, the first close to the surface (typically 2 m) and the second close to the base of the SML before the increase in chl-a associated with the DCM. The other two samples depths were within the thermocline, the first on the up-slope of the DCM and the second at the DCM peak. Locations included the Celtic Sea shelf edge, multiple stations on the stratified shelf, including stations located close to and over a bank and oceanic stations just beyond the shelf edge. All biological sampling was carried out at night, usually just before dawn. Multiple optics casts were carried out at a number of locations.

During both cruises depths were selected based on the CTD fluorescence profile at the time of sampling. For each cruise some locations were occupied for 25 hour period with sampling for biological measurements generally carried out twice. A limited number of these stations were re-visited at two periods in the spring-neap tidal cycle.

AMT15 was a six-week passage from the UK to South Africa. Biological samples were collected just before dawn, with further chl-a and optics data obtained just before (local) midday. Six depths were routinely sampled for most biological samples representing the depths at which irradiance was 97%, 55%, 33%, 14%, 1%, 0.1% of surface irradiance (i.e. light depths), as assigned from the optics data obtained the previous day. However, sample depths were adapted to fit the chl-a profile such that the “1%” sample was always at the peak of the DCM.  $^{14}\text{C}$  P vs. E curves were obtained from one depth in the SML and at the peak of the DCM (the 55% and 1% light depths).

Opaque sampling tubes and carboys were used for all transfer and storage of water to prevent exposing samples to the light.

## 2.2 Measurements of Primary Production

### 2.2.1 Incubation Experiments

#### *$^{14}\text{C}$ P vs. E experiments*

Rates of primary production were obtained using the  $^{14}\text{C}$ -uptake method first established by Steeman-Nielsen (1952). This method is used due to its high sensitivity (Williams et al 1993), particularly during short incubations. It has been critiqued throughout its use due to uncertainties

and inconsistencies between experimental protocols (Bender et al. 1987, Laws et al. 2002, Marra 2002).

For all three cruises, water samples from each depth were sub-sampled into 15 x 73 ml clear polycarbonate bottles and 3 opaque bottles. All bottles were spiked with  $^{14}\text{C}$  in the form of buffered sodium bicarbonate ( $\text{NaH}^{14}\text{CO}_3$ ) (Amersham Biosciences, UK), with a spike of 10  $\mu\text{Ci}$  used in the Celtic Sea and 20  $\mu\text{Ci}$  in the Atlantic Ocean.

The light bottles and dark bottles were incubated in a P vs. E incubator with a gradational light field for two hours (or 2 - 4 hours during CS03) (Fig. 2.1). Samples were maintained at sea surface and mid-thermocline temperatures throughout incubation. The light field was produced by tungsten halogen lamps behind blue light filters. The resulting emission spectrum was measured after each cruise. The irradiance inside each bottle was monitored periodically throughout the cruises using a Biospherical Instruments QSL-2000  $4\pi$  PAR sensor.



Fig. 2.1. P vs. E Incubator in the laboratory. Heat generated by the tungsten halogen lamps was dispersed using a bench-top fan and an independent water tank circulating seawater. Two incubation channels were cooled by surface water and two channels to the mid-thermocline temperature using a chiller.

After incubation, samples were filtered through 2.5 mm diameter 0.2  $\mu\text{m}$  polycarbonate filters (47 mm diameter 0.2  $\mu\text{m}$  for AMT15), and subsequently fumed over 1M HCl for 30-60 minutes in an airtight container. 5 ml of scintillation cocktail (Optiphase Hi-Safe 3) was added to filters prior to scintillation counting. Handling time of samples, particularly after spiking, was kept to a minimum. All work was carried out in dimmed red lights to minimise  $^{14}\text{C}$ -uptake during handling of samples.

Standards were taken to check the activity of the  $^{14}\text{C}$  spike. 9.9 ml carbon dioxide absorber (Carbo-sorb E) was spiked with 10  $\mu\text{Ci}$  of  $^{14}\text{C}$  (in 100  $\mu\text{l}$ ) at the same time as the sample bottles. 10 x 100  $\mu\text{l}$  replicate sub-samples were removed from this mixture and added to scintillation vials along with 5 ml of scintillation cocktail (Permafluor E+) for counting. All

counting was carried out on a TriCarb 3900TR liquid scintillation counter on board at least 24 hours after sample preparation.

Carbon fixation rates were calculated by Equation 2.1, adapted from Joint and Pomroy (1986):

$$P = \frac{DPM \times TCO_2 \times 1.05}{DPM_{add} \times h} \quad (2.1)$$

where P is the carbon fixed ( $\text{mg C m}^{-3} \text{ h}^{-1}$ ), DPM is the disintegrations per minute or activity of the sample,  $DPM_{add}$  is the activity of the spike and h is the length of the incubation (in hours). The factor 1.05 accounts for the preferential uptake of  $^{12}\text{C}$  over  $^{14}\text{C}$  (Strickland and Parsons 1968).  $TCO_2$  is the total weight of carbon dioxide present ( $\text{mg C m}^{-3}$ ) and was calculated via Equation 2.2 (Parsons et al. 1984):

$$TCO_2 = ((salinity \times 0.067) - 0.05) \times 0.96 \times 12010 \quad (2.2)$$

where 0.067 converts salinity to total alkalinity ( $\text{meq l}^{-1}$ ), subtracting 0.05 gives carbonate alkalinity, multiplication of 0.96 gives total carbon dioxide and the multiplication factor 12010 converts  $\text{meq l}^{-1}$  to  $\text{mg C m}^{-3}$ . Calculation of  $TCO_2$  was carried out using *in situ* salinity values measured by the CTD.

Data were fitted to the model of Jassby and Platt (1976) in order to quantify the physiological parameters  $\alpha^*$  and  $P^*_m$  (Equation 2.3), with the modification of an intercept parameter (C). An intercept parameter is an alternative to subtracting dark uptake values and forcing through the origin (following Suggett et al. (2001)), to provide a good fit through the linear part of the P vs. E curve.

$$P^* = P^*_m \cdot \tanh(E\alpha^* / P^*_m) + C \quad (2.3)$$

In general, incubation light levels were not high enough to cause photoinhibition in surface samples. For consistency within the dataset, Equation 2.3 was fitted to just beyond saturation ( $P^*_m$ ) for all P vs. E curves (MacIntyre et al. 2002).

Normalisation to chl-a was performed using HPLC-measured chl-a values (see below). Where no HPLC values were available, fluorometer chl-a values (via acetone extraction, see

below) were multiplied by a weighting factor. The weighting factor was the regression between fluorometric chl-a and HPLC chl-a for the subset of samples acquired for  $^{14}\text{C}$  P vs. E experiments. Weighting factors for the three cruises were 0.77 (CS03), 0.95 (CS05) and 0.92 (AMT15).

**Methodological Considerations** – P vs. E curves are assumed to represent instantaneous physiology. This is likely to be the case in short (< ~4 h) incubations where phytoplankton have not had a chance to adjust their physiology over the course of the incubation and have not been affected by handling and removal from field conditions (Sakshaug et al. 1997). Reports of photoacclimation of phytoplankton occurring over the time of the incubation include Falkowski (1980). Samples must also be maintained as close as possible to *in situ* temperature to avoid temperature-induced changes in the photosynthetic rates (Davison 1991).

Important considerations include the treatment of the results from the dark bottles (Peterson 1980), since the dark bottle does not represent respiration (it is always positive). Dark uptake is thought to be due to a combination of non-photosynthetic  $^{14}\text{C}$ -uptake (for example by bacteria) or by inactive fixation (Legendre et al. 1983, Li et al. 1993) and these processes are assumed to remain constant in the light. This assumption is not necessarily the case, for example, non-photosynthetic carbon uptake is known to be different in the light than in the dark (Legendre et al. 1983, Li et al. 1993).

Another key shortcoming of the  $^{14}\text{C}$ -uptake method is in the release of labelled  $^{14}\text{C}$  as dissolved organic carbon (DOC), which acts to artificially reduce measured  $^{14}\text{C}$  uptake. This occurs due to excretion in photorespiration, exudation through the plasmalemma (Raven 1993), cell lysis (spontaneous or following viral attack (van Boekel et al. 1992, Cottrell and Suttle 1995)) or sloppy feeding by zooplankton grazers (Roy et al. 1989). DOC production and its affect on  $^{14}\text{C}$ -uptake measurements has been documented by Maranon et al. (2004, 2006) and in general the effect is thought to be minimized by short incubations, < 12 h (Laws 1984). During CS03 DOC uptake was ~20% of total primary production (particulate and dissolved organic carbon production) and was observed to remain constant across a wide range of irradiances (Maranon et al. 2006).

It is generally agreed that  $^{14}\text{C}$  uptake represents something between net and gross photosynthesis, depending mainly on the growth rate of the phytoplankton compared to the duration of the incubation, and whether or not the incubation spans a day night cycle (Sakshaug et al. 1997, Laws et al. 2002, Marra 2002). Short incubations are assumed to provide closer to gross photosynthesis. Consequently, although the accuracy and sensitivity of measuring the  $^{14}\text{C}$

fixed over a short incubation period is high, the major errors arise in the assumption of what the measurement represents (Marra 2002). For the remainder of this thesis, the amount of carbon fixed is assumed to represent gross primary production as defined by Sakshaug (1997) and is therefore an underestimate by the amount the carbon fixation represents net, rather than gross, photosynthesis.

Errors associated with the curve fitting (MacIntyre et al. 2002) in obtaining parameters  $\alpha^*$  and  $P^*_m$  are considered minimal compared to the experimental errors and assumptions. All curves were fitted with  $r^2 > 0.99$ ,  $r^2 > 0.98$  and  $r^2 > 0.87$  for CS03, CS05 and AMT15 respectively. Intercept values (C) (Eqn. 2.3) compared to the average dark bottle values (Dk) for each curve were in good agreement for all cruises, and results of model II regression were:

CS03:	$C = 0.96.Dk - 0.17$	$n = 40, r^2 = 0.88$
CS05:	$C = 0.90.Dk - 0.06$	$n = 48, r^2 = 0.68$
AMT15:	$C = 1.13.Dk - 0.14$	$n = 32, r^2 = 0.93$

**SIS incubations** – Simulated-In-Situ (SIS) incubations were carried out during CS03, following protocols outlined in Maranon et al. (2006). Samples were collected before dawn and incubated on deck in light and temperature conditions similar to those *in situ*. Incubations for both cruises were from dawn to dusk, typically ~12-16 hours. All on-deck incubators were held at temperatures matching the surface (for samples from SML) or chlorophyll maximum (for samples from within the thermocline). Combinations of blue light filters were used to provide a light environment closely resembling that of *in situ* irradiance.

During AMT15, incubation was carried out in 125 ml polycarbonate bottles with 3 clear samples and 3 darks from each depth. Each sample was spiked with 20  $\mu\text{Ci}$  before incubation. Samples were then filtered through 40 mm diameter 0.2  $\mu\text{m}$  polycarbonate filters, and filters fumed and counted following the same methods as used for P vs. E experiments during CS03 and CS05.

### *O<sub>2</sub> P vs. E experiments*

During CS03 and CS05 the light-response of dissolved oxygen evolution by phytoplankton was determined for DCM samples using a Winkler assay and an automated titration system (Williams et al. 1979, Williams and Jenkinson 1982). The same P vs. E incubator was used as for <sup>14</sup>C P vs. E experiments (Fig. 2.1).

Water samples were separated into a number of 50 ml glass bottles and 4-5 were randomly selected and fixed with Winkler reagents at the beginning of the incubation. 4-5 bottles were incubated in the dark to determine respiration rates. Remaining (< 40) bottles were incubated for 3-4 hours. Light and dark bottles were fixed with Winkler reagents at the end of the incubation. Photosynthesis was estimated following the light-dark method where respiratory losses of oxygen in the dark were subtracted from oxygen evolution in the light (Williams et al. 1979). P vs. E curves were fitted following the same methods as for  $^{14}\text{C}$ -uptake (Eqn. 2.3), although no intercept parameter was used such that curves were forced through the origin.

Oxygen evolved during the light incubations represents net community production and following dark correction yields gross photosynthesis (Laws et al. 2002). The crucial assumption is that respiration in the dark is equal to that in the light (Laws et al. 2002). The oxygen evolution method is less sensitive than the  $^{14}\text{C}$ -uptake technique due to the fact that background levels of dissolved oxygen are large compared to the relatively small changes in concentration over periods of a few hours (Williams 1993). In this study  $\text{O}_2$  P vs. E experiments were extended to ~4 hours, with only a limited number of DCM samples providing good responses.

Uncertainties surrounding the oxygen light-dark method lie primarily in the assumptions regarding respiration although, as with the  $^{14}\text{C}$  method, these problems are minimised by the use of short (or at least consistent) incubation periods (Laws et al. 2002, Marra 2002). Dissolved oxygen measurements were also obtained for discrete bottle samples in order to calibrate the CTD  $\text{O}_2$  probe (see below). Precision of the dissolved oxygen measurements was excellent, for example routinely  $\pm 1 \mu\text{mol l}^{-1}$  (0.3%) during CS05.

### $^{15}\text{N}$ P vs. E experiments

During CS03 and CS05 the light response of nitrate uptake at the DCM was estimated via stable isotope ( $^{15}\text{N}$ ) labelling technique (Dugdale and Goering 1967) and stable isotope mass spectroscopy (Fiedler and Proksch 1975).

Water from the DCM (during CS03) was separated into 13 x 1 litre polycarbonate bottles. Samples were spiked with stable isotopes in the form  $\text{K}^{15}\text{NO}_3$  (98%  $^{15}\text{N}$ ) and  $\text{Na}^{13}\text{CO}_3$  (99%  $^{13}\text{C}$ ) respectively. In order to limit alteration of the ambient nitrate pool the spike additions were made within ~10% *in situ* concentration, which required analysis of ambient nutrient concentration prior to spiking. Samples were placed in a dedicated P vs. E incubator, cooled to *in situ* temperature, and incubated for 3.5 – 4.5 h. After incubation samples were filtered through ash-dried GF/F filters, supported on a glass filter holder, and afterwards rinsed several times

with fresh filtered sea water. The filters were stored in Petri dishes and frozen to  $-20\text{ }^{\circ}\text{C}$  until return to the lab.

Samples were ‘pelleted’ into combustible tin cups for analysis on a GV Isoprime Mass Spectrometer coupled to a Eurovector elemental analyser, which included the use of standards as a check on instrument performance. The instrument was adjusted for optimal measurement of both  $^{13}\text{C}$  and  $^{15}\text{N}$ . Uptake rates were estimated based on calculations of Dugdale and Wilkerson (1986). Nitrate-uptake vs. irradiance curves were fitted in the same way as for  $^{14}\text{C}$ , with an intercept parameter included (as in equation 2.3).

In a similar manner to  $^{14}\text{C}$  uptake estimates, both  $^{13}\text{C}$  and  $^{15}\text{NO}_3^-$  uptake may be underestimated due to subsequent losses of labelled nitrate from cells during the time course of the incubation, but this can be minimised by using short incubations. For dual labelled samples, the mass spectroscopy proved problematic, with manual adjustment of instrument setup required to measure the two isotopes. The instrument setup was tuned to obtain accurate measurements of  $^{15}\text{NO}_3^-$  uptake rates in preference to  $^{13}\text{C}$  uptake such that the latter measurements should be considered with caution.

Full discussion of errors associated with the  $^{15}\text{NO}_3^-$  uptake technique is provided in Dugdale and Wilkerson (1989). Issues surrounding comparison of  $^{14}\text{C}$  and  $^{15}\text{N}$  bottle incubations are described in detail by Bouteiller (1993). Major limitations of the  $^{15}\text{NO}_3^-$  method result from the inability to accurately measure ambient nutrient concentrations in low nutrient waters, and the potential for changing the nutrient availability (and subsequently the uptake rate) due to the nitrate spike (Dugdale and Wilkerson 1986). The inability to accurately measure the ambient nitrate concentrations meant that the  $^{15}\text{NO}_3^-$  uptake technique was only considered for samples where nitrate concentrations were relatively high (at least  $1\text{ }\mu\text{M}$ ).

### 2.2.2 Caveats of Sample Incubation

Incubation experiments are generally assumed to represent processes that would be occurring in the field. In all incubation experiments, handling and containment of samples and removal from the natural environment act against this principle. Such issues have long been debated (e.g. Dugdale and Wilkerson 1989, Laws et al. 2002, Marra 2002) and some examples of particular concerns are given below.

Bottle size is an important consideration in incubation techniques, with problems such as collision and confinement damage of cells and lack of nutrient cycling dependent on bottle size and type (Gieskes et al. 1979, Laws 1991). However, these issues are largely relieved in

short incubations (< 2 h) and the use of polycarbonate bottles (Laws et al. 1987, Laws 1991). Another consideration is the inhomogeneous distribution and/or settling of cells which could potentially influence the light environment to which the cells are exposed.

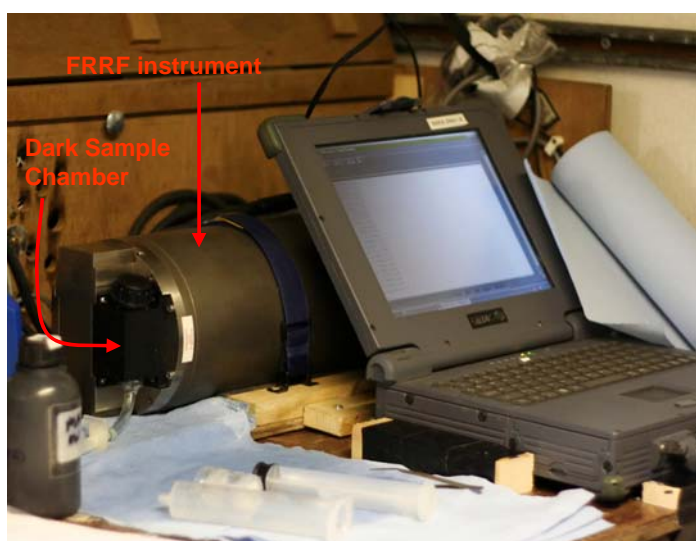
Bottle samples are co-inhabited by phytoplankton, bacteria and zooplankton, leading to the possibility of selective population changes and zooplankton grazing within the bottle (Banse 1994a). This is most problematic for small bottle samples and/or samples from regions associated with small scale patchiness which increase the likelihood of variability in the components of the mixed population contained within samples. Gas and nutrient exchange within and between organisms confined in the bottle is virtually impossible to quantify, and typically results in a reduction of the measured photosynthetic (or nutrient uptake) rates measured (Dugdale and Wilkerson 1986, Laws et al. 2002, Marra 2002).

Incubated samples are removed from the turbulence or mixing environments that they would normally be exposed to *in situ* and are therefore isolated from any associated nutrient inputs. Further, samples held at light levels assumed to represent those in the field may not be representative if samples are in fact mixed within a light gradient over the period of the duration of the incubation.

### 2.3 Fast Repetition Rate Fluorometer (FRRF)

Discrete water samples were analysed using a lab-based Chelsea Scientific Instruments Fasttracka™ Fast Repetition Rate fluorometer (FRRF) (Figure 2.2). Samples were allowed to dark-acclimate for > 30 minutes in the constant temperature lab (held at 14°C (CS05), 17°C (AMT15) and *in situ* temperature +/- 2 °C (CS03)).

Figure 2.2. FRRF setup in the lab. Samples were dark acclimated in cool, dark conditions for ~ 30 min before sampling. Samples were placed into the dark sample chamber and the flash sequence was run a number of times (see text). An additional sub-sample was then filtered (through GFF then 0.2 µm) and run as a sea water blank.



Variable chlorophyll fluorescence was stimulated by sequences of 100 1.1  $\mu\text{s}$  saturation flashes at 2.3  $\mu\text{s}$  intervals followed by 20 1.1  $\mu\text{s}$  relaxation flashes at 98.8  $\mu\text{s}$  intervals. Relaxation flashlets were timed to provide maximal resolution of Qa relaxation kinetics (Moore et al., 2006). Blank water samples were obtained by filtering a sub-sample through a GF/F and then a 0.2  $\mu\text{m}$  polycarbonate filter, and running the filtrate through the sample procedure (Cullen and Davis 2003). Samples were run on the highest gain setting that did not saturate the sample, with blanks run on matching gain settings to the associated sample. For samples of very high biomass dilution was carried out using filtered seawater (through a GF/F and then 0.2  $\mu\text{m}$  polycarbonate filter) from the associated sample.

The fluorescence transient ( $f$ ) at time  $t$  was fitted to the bio-physical model of Kolber et al. (1998) to derive minimal ( $F_0$ ), maximal ( $F_m$ ) fluorescence yields using Equation 2.4:

$$f(t) = F_0 + (F_m - F_0) \left( C(t) \frac{1-p}{1-C(t)p} \right) \quad (2.4)$$

where  $p$  is the connectivity parameter. The fraction of closed reaction centres ( $C(t)$ ) was determined iteratively using Equation 2.5:

$$\frac{dC(t)}{dt} = i(t) \sigma_{PSII} \frac{1-C(t)}{1-C(t)p} - \frac{C(t)}{\tau_{Qa}} \quad (2.5)$$

where  $i(t)$  is the flash intensity (Kolber et al. 1998). Equations 2.4 and 2.5 were applied to both the saturation and relaxation parts of the curve. An iterative fit was employed to obtain values for  $\sigma_{PSII}$  and  $\tau_{Qa}$ . Curve fitting was based on original codes provided to the FRRF community by S. Laney (Laney 2003) adjusted so that the asymptotic value reached during relaxation (Fig. 1.4) obtained by the steady-state solution of Eqn. 2.5 provided the value of  $\tau_{Qa}$  (Moore et al. 2006). In order to minimise errors in the curve-fitting process curves were averaged over 160-512 individual sequences (Suggett et al. 2004). A value of  $E_k$  derived from FRRF parameters  $\sigma_{PSII}$  and  $1/\tau_{Qa}$  was estimated from Eqn. 1.10.

The commercial instrument used in this study allowed only constant delay between relaxation flashes. As such, only one component of the rate of Qa reoxidation could be measured. Since the relaxation flash sequence lasted  $\sim 2\text{ms}$  in duration,  $1/\tau_{Qa}$  measured by the

instrument represents the mean value of transport from Qa through the PQ pool (Crofts et al. 1993, Moore et al. 2006).

Benefits of the FRRF measurement include the relatively instantaneous measurements of phytoplankton physiology and reduced bottle effects. Further, the FRRF measures the gross electron transfer rate without necessity of the assumptions surrounding respiration, as in the case of gas exchange or nutrient uptake measurements (Suggett et al. 2001). However, it is not without its limitation, principally the restriction to monitoring of PSII processes only, rather than the complete (PSI+PSII) system. Other parameters, such as PSI:PSII and chl-a:PSII, required to relate FRRF-derived parameters to bulk cellular processes, are not well constrained (Suggett et al. 2004).

The use of a lab based instrument and dark-acclimated samples avoided many of the problems associated with *in situ* profiling instruments, including those associated with non-photochemical quenching, short-term photochemical-activity and state transitions (Falkowski and Raven 1997, Moore et al. 2006). The static environment also allows for quantification of sea water blanks, which is of particular significance in low biomass oligotrophic waters (Cullen and Davis 2003).

## 2.4 Additional Measurements

During all cruises the ships meteorological package recorded incident PAR ( $\mu\text{E m}^{-2} \text{s}^{-1}$ ) and water depth (m). Additional measurements relevant to this study are detailed below.

### 2.4.1 CTD Measurements

On all cruises, vertical profiles of conductivity, temperature and depth (CTD) were obtained using a Seabird 911 CTD profiling system. CTD frames included two temperature and conductivity sensors, a Chelsea Instruments Aquatracka MKIII chlorophyll fluorometer and rosette with 24 x 20 litre Niskin bottles for water collection.

For the Celtic Sea cruises the main stainless steel CTD frame was also equipped with 2 Chelsea Instrument Fastracka FRRFs with PAR sensors and 1 Seabird dissolved oxygen sensor. A titanium CTD frame was used for a minority of casts during CS03, and included all instruments mentioned with the exception of the FRRFs.

During AMT15 the main stainless steel CTD frame was used for pre-dawn biological sampling and included a SBE 43 Oxygen sensor. A titanium CTD was used for Optics (midday) casts and included a SBE 43 Oxygen sensor and two Chelsea downwelling irradiance (PAR) sensors.

Water samples were obtained on the up-cast during the CTD deployment. Inconsistency in the winch speed on *RRS* Charles Darwin during CS05 caused ‘step’ like features in the CTD profiles. These features were largely overcome through post-processing of the profile data by J. Sharples. The resulting post processing may have resulted in CTD temperature and salinity measurements systematically offset from the real *in situ* values.

### **Salinity Calibration:**

During CS03 associated errors on CTD salinity measurements were mostly within rms < 0.01, though nine casts had rms 0.01 – 0.02 and three casts were flagged as unreliable. During CS05 CTD salinity was calibrated to within +/- 0.003, and during AMT15 to within +/- 0.030.

### **PAR Sensor Calibration:**

During CS03 underwater PAR was measured by the two Chelsea Fastracka FRRFs, calibrated by Chelsea Instruments. During CS05 the PAR sensor on the FRRF did not return usable data. For this cruise, all optics data was obtained from a freefall SATLANTIC instrument (see below). During AMT15, the Chelsea Downwelling PAR sensor on the titanium CTD was converted into PAR ( $\mu\text{E m}^{-2} \text{s}^{-1}$ ) from sensor voltages using the following:

$$\text{AMT15:} \quad \text{PAR} = \exp(\text{VOLTS} \times 5.101 - 8.3209) \times 0.04234$$

Optical depths (OD) were calculated from (depth (m) x Kd(PAR)) where Kd(PAR) is the vertical light attenuation of PAR ( $\text{m}^{-1}$ ). For estimation of OD, the Kd(PAR) was obtained from the gradient of the log(E(z)) vs. depth relationship in the surface waters, which was assumed to be linear between 2 m and the base of the SML. During CS03 Kd(PAR) from a representative cast was assumed to hold for each visit to each region. For AMT15 the Kd(PAR) for the pre-dawn casts was assumed to be the same as for the midday cast on that day. Errors in Kd(PAR) estimates (and therefore OD) as a result of these assumptions are acknowledged. Consideration of SML chl-a concentration and Kd(PAR) estimates within (compared to between) regions suggested that but the magnitude of such errors were minimal.

### **Oxygen Probe Calibration:**

During CS03 and CS05 the dissolved oxygen probe on the CTD (DO(CTD)) was calibrated with 50 ml water samples analysed following the Winkler titration method (see above), following:

$$\begin{aligned} \text{CS03: } \text{DO} &= 1.112 \times \text{DO(CTD)} + 0.072 & n = 106, r^2 = 0.975 \\ \text{CS05: } \text{DO} &= 1.03 \times \text{DO(CTD)} + 0.36 & \text{rms error} = \pm 0.13 \text{ mg l}^{-1} \end{aligned}$$

Where DO represents the calibrated CTD value ( $\text{mg l}^{-1}$ ). Percentage oxygen saturation ( $\%O_2$ ) was calculated as the ratio of dissolved oxygen to that of the theoretical saturation limit of seawater at *in situ* temperature and salinity at a pressure of 1 atmosphere, Equation 2.6:

$$\%O_2 = 100 \cdot \text{DO} / \text{SOL} \quad (2.6)$$

where DO is the dissolved oxygen from the (calibrated) oxygen probe ( $\text{mg l}^{-1}$ ), and SOL is the solubility of oxygen in seawater ( $\text{mg l}^{-1}$ ). The solubility of oxygen in seawater represents the amount of dissolved oxygen the parcel of water (with *in situ* temperature and salinity) would have contained at the saturation limit when it was last in contact with the atmosphere, and was obtained following Weiss (1970). The Apparent Oxygen Utilisation (AOU) with units  $\text{mg l}^{-1}$  was estimated following Equation 2.7 (e.g. Boyer et al. 1999):

$$\text{AOU} = \text{SOL} - \text{DO} \quad (2.7)$$

### **Seasoar Acquisitions:**

Conductivity, temperature, fluorescence and depth measurements were also obtained by undulating towed instrument (Seasoar) system during CS03 and CS05. The primary seasoar instrument during CS03 was a Penguin Seasoar, which included a Chelsea Instruments Minipack (CTD and chlorophyll fluorescence) and a Fastracka FRRF connected to the onboard Penguin data acquisition and control computer. Seasoar instruments were calibrated using CTD casts performed immediately prior to or after the seasoar tows. Only data from night-time tows are presented such that correction for quenching of the fluorometer was not required.

## 2.4.2 Biological Samples

### *Phytoplankton, Chlorophyll-a and Pigment Concentration*

#### **Fluorometric Chlorophyll-a:**

Fluorometric analysis of chlorophyll-a samples was carried out following the methods of Welschmeyer (1994) using a Turner Designs digital Fluorometer. Water samples (100-500ml) were filtered through 25 mm diameter Whatman GF/F filters and stored in 90% acetone for > 24 hours in refrigerated, dark conditions before analysis. Size fractionated chlorophyll

concentrations were also analysed in < 2 µm, 2-5 µm, 5-10 µm and > 10 µm fractions. All chl-a measurements were calibrated against a standard where chl-a concentration was determined spectrophotometrically (Cecil 292 Digital Ultraviolet Spectrophotometer) on a chl-a standard solution (Sigma UK) made up in 90% (HPLC Grade) acetone following Jeffrey and Humphrey (1975). A series of dilutions from the chl-a standard was then run on the Turner Fluorometer.

Fluorometric chl-a following Welschmeyer (1994) measures chl-a fluorescence within a variable background of other pigments with similar absorption bands (Trees et al. 1985). This interference generally causes an overestimation of chl-a. Other errors associated with fluorometric chl-a measurements are assumed to be minimal with operator error the most likely source (e.g. sample preparation, fluorometer reading and calibration). During all cruises operator error was kept to a minimum by maintaining consistency in the person/s responsible for sample collection and fluorometer reading.

### **HPLC pigments:**

During CS03 and CS05 duplicate filters from the filtration of 1-2 litres of seawater were frozen in -80 °C for full pigment analysis on return to the lab. Pigment composition was obtained following the methods of Barlow et al. (1997b) using a Thermo Separation Products High Performance Liquid Chromatograph (HPLC).

During AMT15 duplicates of 2-4 litres of water were filtered for these samples, and HPLC analysis followed methods of (Barlow et al. 1997a) to provide identification of divinyl chl-a. Total chl-a was obtained from addition of mono-vinyl and divinyl- chlorophyll-a.

All HPLC estimates were compared to standards of both pure chl-a and a pigment mixture of known concentrations. Errors associated with HPLC are typically associated with poor retrieval of pigment concentrations of minor pigments, particularly in low biomass regions. During AMT15 detection limits on all HPLC-derived pigments were 0.002 mg m<sup>-3</sup> or less (Poulton et al. 2006a).

Following Trees et al. (2000) the relationship between HPLC-derived chl-a and the total accessory pigments (chlorophylls b and c and the carotenoids) was roughly constant within cruises. The slopes of the regressions of the log-log relationship of the total accessory pigments against chl-a were 1.08 for CS03 (n = 51, r<sup>2</sup> = 0.925), 0.98 for CS05 (n = 151, r<sup>2</sup> = 0.963) and 0.874 for AMT15 (n = 176, r<sup>2</sup> = 0.990). The slopes of the regression coefficients correlate well to that of Trees et al. (2000) who observed an average slope of 0.93 over a wide range of oceanographic environments. The difference in slopes between AMT15 and Celtic Sea cruises may occur largely due to the different accessory pigments quantified by the two HPLC analysis

methods used. The similarity of the relationships to those of Trees et al. (2000) give confidence that the pigment ratios (to chl-a) are reliable.

### **Comparison of Fluorometric and HPLC chl-a:**

In contrast to fluorometric analysis, Chl-a derived from HPLC minimises interference from other pigments by physically separating the component pigments. Chl-a from this method was typically 82-92% of that measured by the fluorometric approach, and was assumed to represent a more accurate value for chl-a. All fluorometric samples were weighted by the regression between fluorometric and HPLC-derived chl-a values. The corrections applied to fluorometric values were as follows:

CS03:	Weighted chl-a = Fluorometer chl-a x 0.82	n = 51, r <sup>2</sup> = 0.79
CS05:	Weighted chl-a = Fluorometer chl-a x 0.86	n = 143, r <sup>2</sup> = 0.86
AMT15:	Weighted chl-a = Fluorometer chl-a x 0.92	n = 178, r <sup>2</sup> = 0.93

For AMT15 data all samples with HPLC chl-a > 1 mg m<sup>-3</sup> were removed from the calibration to avoid dominance of a few high values in the regression. Values of chl-a quoted in this study are those after the application of the weighting factor. The only exceptions are HPLC pigment ratios which are referenced to actual HPLC derived chl-a.

### ***In situ* Chl-a:**

Nominal *in vivo* chl-a values were obtained from a fluorometer attached to the CTD (CTD chl-a) after Seabird processing of CTD fluorometer voltages. These nominal CTD chl-a (CTDchl-a<sub>NOM</sub>) values were subsequently depth binned (1 m bins) and calibrated against the chl-a (weighted to HPLC) sample values. Regional differences in the relationship between sample and CTD chl-a were evident (Fig. 2.3).

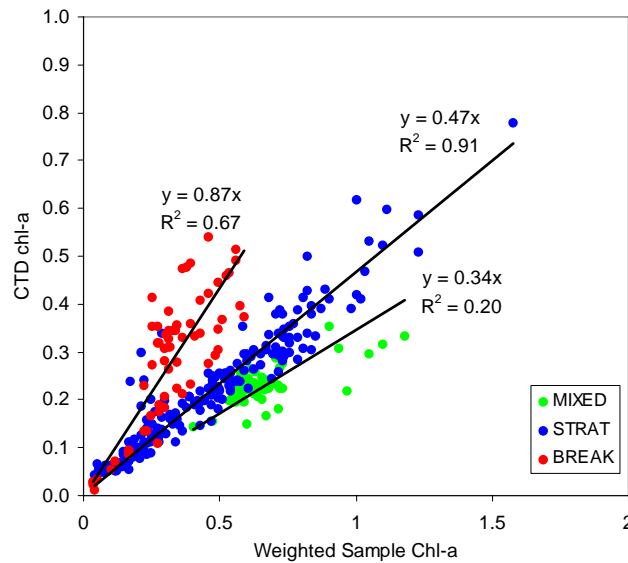


Figure 2.3. The relationship between CTD chl-a and Weighted Sample Chl-a during CS03 in the mixed, stratified and shelf-edge regions. Weighted chl-a was obtained from fluorometric chl-a multiplied by a correction factor to give values closer to chl-a measured by HPLC (see text).

The following regional calibrations were applied to obtain calibrated CTD chl-a (CTDchl-a<sub>CALIB</sub>):

CS03:

Stratified Shelf	$CTDchl-a_{CALIB} = CTDchl-a_{NOM} \times 2.14$	$n = 233, r^2 = 0.91$
Shelf Break and Oceanic	$CTDchl-a_{CALIB} = CTDchl-a_{NOM} \times 1.15$	$n = 63, r^2 = 0.87$
Mixed	$CTDchl-a_{CALIB} = CTDchl-a_{NOM} \times 2.90$	$n = 60, r^2 = 0.20$

CS05:

Stratified Shelf:	$CTDchl-a_{CALIB} = CTDchl-a_{NOM} \times 1.61$	$n = 197, r^2 = 0.89$
Shelf Break and Oceanic	$CTDchl-a_{CALIB} = CTDchl-a_{NOM} \times 0.98$	$n = 94, r^2 = 0.85$

AMT15:  $CTDchl-a_{CALIB} = CTDchl-a_{NOM} \times 1.16$   $n = 142, r^2 = 0.78$

Across the AMT transect the regression between nominal CTD chl-a and weighted chl-a varied between regions, but since the regression fits were not improved greatly on regional segregation ( $r^2$  remained  $< 0.85$ ) a single calibration factor was applied throughout the transect.

For all cruises, data were excluded from the calibrations if chl-a sample concentrations were in excess of  $2 \text{ mg m}^{-3}$  (or  $1 \text{ mg m}^{-3}$  for AMT15), or less than  $0.01 \text{ mg m}^{-3}$ . Values where the gradient between samples at neighbouring depths was less than  $0.05 \text{ mg m}^{-2}$  were ignored as this increased the risk of a mismatch between the CTD fluorometer sensor depth and the Niskin bottle inlet (and therefore between the *in situ* and bottle sample chl-a measurement). CTD chl values were also ignored from daytime casts where *in situ* PAR exceeded  $100 \mu\text{E m}^{-2} \text{ s}^{-1}$  due to quenching of the CTD fluorometer, as described below.

Quenching of the CTD fluorometer caused a decrease in CTD fluorescence compared to sample chl-a near the surface of daytime CTD casts (Fig. 2.4). Quenching was observed to be significant where *in situ* PAR was in excess of  $100 \mu\text{E m}^{-2} \text{ s}^{-1}$ . CTD chl-a values above this threshold were removed. For this purpose, estimation of *in situ* PAR at the sample depths were obtained from the ships PAR averaged over 60 min following CTD deployment, multiplied by the (cruise-specific) constant for transmittance through the sea-surface (see below) and extrapolated to the sample depths using the region-specific  $K_d(\text{PAR})$  (assumed constant through the water column).

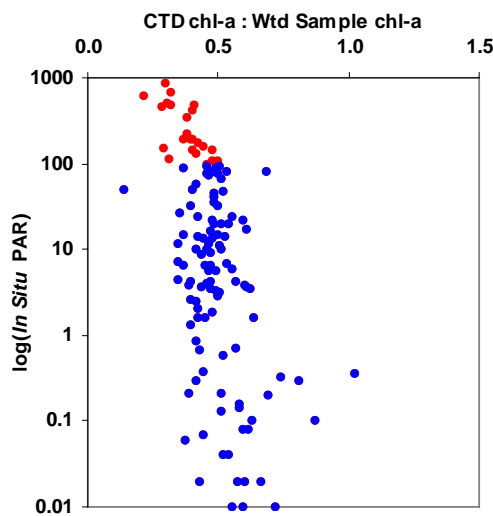


Figure 2.4. The relationship between CTD chl-a : Weighted Sample Chl-a and *in situ* PAR. *In situ* PAR at the sample depth was estimated via reconstruction of the *in situ* light fields (see text) and the ambient irradiance was obtained from the ships PAR sensor and averaged over 60 minutes from the start of each CTD. Weighted chl-a was obtained from fluorometric chl-a multiplied by a weighting factor to give values closer to chl-a measured by HPLC (see text) Data shown are from stratified shelf stations during CS03.

CTD Chl-a profiles were ‘reconstructed’ using a linear extrapolation between the remaining calibrated CTD profile and surface chl-a sample data where available. Casts that could not be corrected for quenching, due to the lack of suitable surface chl-a samples were disregarded. During CS03 a minority of samples were collected using a titanium frame CTD system. Since no chl-a samples were collected from the CTD attached to this frame the fluorescence profiles from this system could not be corrected for quenching and were subsequently disregarded.

### **Phytoplankton Identification and Enumeration:**

Water samples (100 – 250 ml) were collected and fixed with 2 % Lugols iodine and/or formalin for microscope identification of phytoplankton, using a Leiss inverted microscope.

Formaldehyde settling allowed quantification of coccolithophores. Identification techniques followed those of Poulton (*Submitted*). Problems associated with microscope analysis are wide ranging and well documented (e.g. Venrick 1978, 1983), and include chemical preservation (e.g. cell shrinkage), sub-sampling inconsistencies, identification of small or rare cells and subsequently the subjective opinion of the observer.

### *Nutrient concentrations*

During CS03 and CS05 nutrient samples were analysed on board using standard colorimetric techniques using a Skalar AAII-type Autoanalyser following methods of Brewer and Riley (1965). Nitrate concentrations were obtained to a detection limit of ~0.1  $\mu\text{M}$ .

During AMT15 micromolar concentrations of nitrate were obtained colorimetrically using a Bran and Luebbe Autoanalyser III (AAIII) following methods described in Rees et al. (2006) and Woodward and Owens et al. (1990). Total nitrate (from nitrate + nitrite) at nanomolar concentrations was also obtained colorimetrically using a Liquid Waveguide Capillary cell and photo-diode detectors (Woodward and Owens 1990, Rees et al. 2006). The two datasets were subsequently combined to give total nitrate concentrations at maximal accuracy through the water column.

### *POC/N*

Particulate organic carbon and nitrogen was estimated following methods as in Poulton et al. (2006b). 1-4 litres was filtered onto ash dried (> 400 °C for at least 12 hours) GF/F filters. Filters were subsequently stored at -20 °C or -80 °C until return to the lab. Samples were stored at -80°C to allow for use for HPLC pigment analysis if necessary. On return to the lab, filters were acid fumed and analysed using a Thermo Finnegan Flash EA1112 Elemental Analyser.

### *Analytical Flow Cytometry*

The cyanobacteria (*Prochlorococcus* and *Synechococcus*) and other mixed picoeukaryotes (< 2 µm) were identified by Analytical Flow Cytometry (FACSort, Becton Dickinson, Oxford, UK), based on their fluorescence, according to Zubkov et al. (1998) and Heywood et al (2006). Flow rate was calculated by the addition of latex beads as an internal standard. Cell numbers were obtained as well as cellular fluorescence, cell size was inferred from the directly-measured cellular side scatter.

Flow cytometry provides an accurate method for enumeration and measurement of fluorescence characteristics of cyanobacteria and picoeukaryotes. Errors associated with quantification of picoeukaryotes are generally greater than those of the cyanobacteria as these cells are in the outer limit of the size-range of the instrument. A detailed account of flow cytometry techniques may be found in Zubkov et al. (2000).

### *Phytoplankton Absorption by the 'Filter Technique'*

Phytoplankton absorption of intact cells was obtained by the 'filter technique' (Allali et al. 1997, Bricaud et al. 2004) as described by Suggett et al. (2001). 1-4 litres of water were filtered onto Whatman GF/F filters, paying careful attention to achieve even sample distribution on the filter, and stored in -80°C until analysis on return to the lab. Samples were thawed before being measured on a Hitachi U-3000 spectrophotometer fitted with a φ60 integrating sphere following Tassan and Ferrari (1995). Each filter was bleached with 1-2% NaClO for de-pigmentation and re-run as a blank to obtain the phytoplankton absorption isolated from absorption by other detrital components (Tassan and Ferrari 1995). Particle absorption,  $a(\lambda)_{meas}$ , ( $m^{-1}$ ) was calculated by Equation 2.7:

$$a(\lambda)_{meas} = \frac{2.303 \cdot D(\lambda) \cdot S}{\beta(\lambda) \cdot V} \quad (2.7)$$

where S is the particulate retention area of the GF/F filter measured using the spectrophotometer ( $m^2$ ), V is the volume of filtered seawater ( $m^3$ ) and  $D(\lambda)$  is the optical density of all particulate material retained on the filter normalized to that at 750 nm.  $\beta(\lambda)$  is the wavelength-dependent path-length amplification factor, or *beta-factor* after Butler (1962).

For CS03 the beta-factor was measured from absorption of cells in suspension (D. Suggett, *pers. comm.*). However due to the two-year gap between analysis, a more recent amplification factor for the machine setup was used for CS05 and AMT15 samples following Suggett et al. (2006):

$$\beta(\lambda) = 1.63 \cdot D(\lambda)^{-0.22} \quad (2.8)$$

Estimation of  $a(\lambda)_{\text{meas}}$  was then normalised to chl-a and is denoted  $a(\lambda)_{\text{meas}}^*$  (the asterisk denoting normalization by chl-a). The sum of absorption over all wavelengths from 400-700 nm is denoted  $a_{\text{meas}}^*$ . Errors associated with instrument measurements were minimised by running the spectrophotometer three times for triplicate measurements of each sample and each blank. A significant source of error in the measurement of particle absorption by this method is in the choice of the beta-factor. The beta-factor corrects for the scattering of light within the filter, and between the filter and the particles and the (typically wavelength specific) beta-factor inevitably affects the value of  $a_{\text{meas}}^*$  as well as the shape of the absorption spectra (Bricaud and Stramski 1990). A full summary on this topic is given by Allali (1997, their Appendix 8). Using data from CS05, the choice of beta correction varied the magnitude of  $a_{\text{meas}}^*$  by an average of < 5 % (+/- 4%) (by comparing beta correction factor of Eqn. 2.8 and that obtained experimentally for CS03 (Moore et al. 2006)). For CS05 a student's T-test showed that the values of  $a_{\text{meas}}^*$  (all data) using the two beta-corrections were not significantly different (to 95% confidence level) indicating that the difference in  $a_{\text{meas}}^*$  due to the choice of beta-correction was not significant compared to the variability in  $a_{\text{meas}}^*$  between samples.

Magnitudes of  $a_{\text{meas}}^*$  for all three cruises were at the higher end of the range of samples obtained from around the world's oceans by Bricaud et al. (1995, 2004). Further, mean values from CS03 were 80% of the mean for CS05. The choice of beta correction did not account for the offset between cruises. Since no source of measurement or processing error was identified, and the absolute magnitude of the calculated  $a_{\text{meas}}^*$  could not be disqualified when compared to the literature values, the estimates of  $a_{\text{meas}}^*$  were accepted with caution.

### *Phytoplankton Absorption by the 'Pigment Reconstruction Technique'*

Phytoplankton absorption spectra were constructed from the pigment composition of disrupted cells (as measured from HPLC), scaled by the weight-specific absorption spectra of the main pigment groups (Bidigare et al. 1990b, Marra et al. 2000).

Following Marra et al. (2000), pigments were grouped into the photosynthetically active carotenoids (PSC) (including mono- and di- vinyl chl-b, chl-c, peridinin, fucoxanthin, 19'-hexanoyloxyfucoxanthin, 19'-butanoyloxyfucoxanthin and prasinoxanthin) and non-photosynthetically active carotenoids (NPC) (including violaxanthin, diadinoxanthin, alloxanthin, lutein, zeaxanthin and  $\beta$ -carotene). The particular pigments included in these two groups were dependent on the pigments resolved by the HPCL method used (Barlow et al. 1997ab). Assumed weight-specific absorption spectra for chl-a, chl-b, chl-c, PSC and NPC are shown in Figure 2.5 (Bidigare et al. 1990b, Marra et al. 2000).

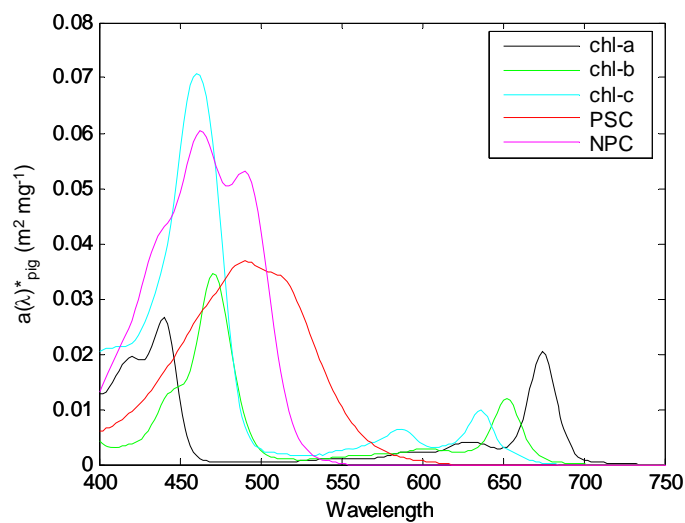


Figure 2.5. Assumed *in vivo* weight-specific absorption spectra of the main pigment groups (Bidigare et al. 1990b, Marra et al. 2000). NPC and PSC are photosynthetically active carotenoids and non-photosynthetically active carotenoids as defined in the text.

The weight-specific pigment spectra were scaled by the contribution of pigments in these groups as measured by HPLC (Bidigare et al. 1990b, Marra et al. 2000). Phytoplankton absorption by this method was subsequently normalised to chl-a and denoted  $a(\lambda)^*_{\text{pig}}$ , with the sum of absorption over 400-700 nm annotated  $a^*_{\text{pig}}$ .

### Absorption by Photosynthetic Carotenoids:

Absorption by photosynthetic pigments only was estimated using the pigment reconstruction technique, by simply ignoring the contribution of NPCs (following Marra et al. 2000, Suggett et al. 2004). The chl-a normalised absorption by photosynthetic carotenoids from HPLC is denoted

$a(\lambda)_{pspig}^*$ . The absorption spectra of intact cells without the contribution of NPC (denoted,  $a(\lambda)_{ps}^*$ ) were estimated from Equation 2.9 (Suggett et al. 2004, Moore et al. 2006):

$$a(\lambda)_{ps}^* = a(\lambda)_{meas}^* \cdot \frac{a(\lambda)_{pspig}^*}{a(\lambda)_{pig}^*} \quad (2.9)$$

The total absorption by PSC is obtained from the sum of  $a(\lambda)_{ps}^*$  from 400-700 nm, and denoted  $a_{ps}^*$ . A summary of limitations of the pigment reconstruction method is given in Bricaud et al. (2004, their Appendix A). It is clear that a major limitation of the pigment reconstruction method lies in the accurate representation of accessory pigments by the generalised spectra of NPC or PSC. Further, the contribution of minor pigments may be underestimated and/or have larger relative errors compared to the more abundant pigments, an issue which is particularly problematic in low biomass waters. Uncertainties in this method are further exacerbated in oligotrophic waters due to the presence of phycobillin-containing cryptophytes and cyanobacteria since the HPLC methods do not quantify the phycobilliproteins (Suggett et al. 2004).

The inadequacies of pigment reconstruction could also affect the quantification of  $a_{ps}^*$ , although the relative proportion of absorption by (PSC + chlorophylls):NPC should be well represented by the ratio of  $a_{pspig}^*$  to  $a_{pig}^*$  such that the magnitude of  $a_{ps}^*$  should be reasonable.

## 2.5 Methods of Data Analysis

### 2.5.1 Spectral Corrections

Excitation spectra for the P vs. E incubator lamp and FRRF are shown in Figure 2.6. The difference between the excitation spectra of the  $^{14}C$  P vs. E incubator and the FRRF mean that a correction must be applied before comparison of spectrally-dependent physiological parameters (Suggett et al. 2001). Further, the ecological relevance of parameter values can only be assessed after correction for the difference between excitation spectrum and that of *in situ* irradiance (Fig. 2.6) (Suggett et al. 2001).

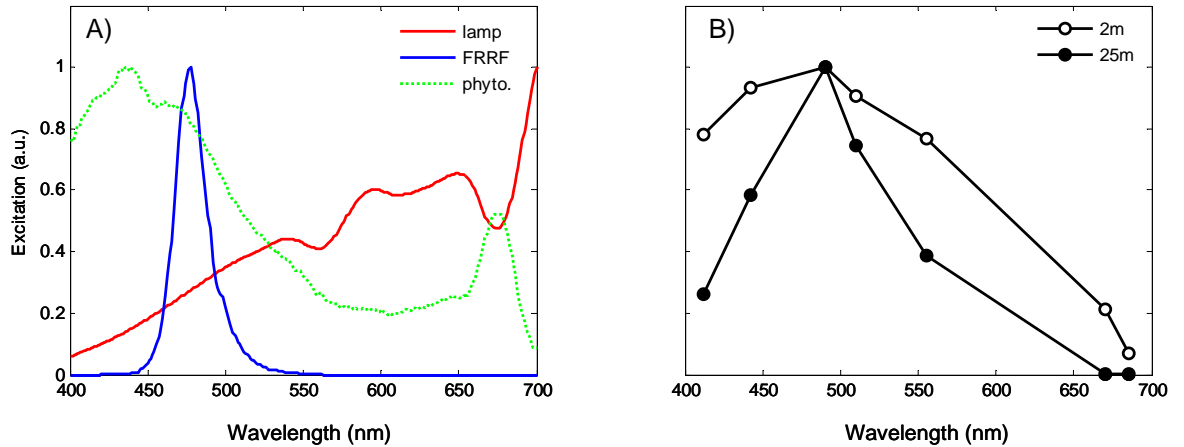


Figure 2.6. A) Example (normalised) phytoplankton absorption spectrum compared to excitation spectrum of the FRRF and P vs. E incubator lamp. B) Example of (normalised) *in situ* light spectrum at 2 m and 25 m (taken from real data collected at CS1, CS03).

The generic equation for adjusting parameter X as measured by excitation spectra ‘x’ into that expressed in terms of spectra ‘y’ is (Suggett et al. 2001, Moore et al. 2006):

$$X_y = X_x \frac{\int_{400-700nm} a(\lambda) \cdot E_y(\lambda) \int_{400-700nm} E_x(\lambda)}{\int_{400-700nm} a(\lambda) \cdot E_x(\lambda) \int_{400-700nm} E_y(\lambda)} \quad (2.10)$$

Where  $E_x(\lambda)$  and  $E_y(\lambda)$  are the irradiance spectra of ‘x’ and ‘y’, and  $a(\lambda)^*$  is the absorption spectrum of phytoplankton. For example for  $^{14}\text{C}$  P vs. E derived parameters to be corrected for the difference in excitation spectra with that of the FRRF,  $E_x(\lambda)$  and  $E_y(\lambda)$  are the irradiance spectra for the P vs. E incubator lamp and FRRF respectively, i.e.  $E_{14\text{C}}(\lambda)$  and  $E_{478}(\lambda)$ , where subscript ‘478’ denotes the expression of the parameter in terms of excitation spectra of the FRRF which is centred on the wavelength 478 nm. Hereafter, the subscripts  $X_{14\text{C}}$ ,  $X_{478}$  and  $X_{\text{insitu}}$  denote parameters weighed to the  $^{14}\text{C}$  incubator lamp, the FRRF and *in situ* irradiance spectra respectively. The light absorption by phytoplankton  $a(\lambda)^*$  may be substituted for any required light absorption coefficient, for example, that measured by the filter technique,  $a(\lambda)^*_{\text{meas}}$ , the pigment reconstruction technique,  $a(\lambda)^*_{\text{pig}}$ , or the equivalents without absorption by NPC ( $a(\lambda)^*_{\text{ps}}$ ,  $a(\lambda)^*_{\text{pspig}}$ ).

### 2.5.2 Modelling *In situ* Water Column Optics

During all cruises the wavelength composition of *in situ* irradiance was measured directly by optical profiling instruments, following methods broadly similar to those of Tilstone et al. (2003) and Lorenzo et al. (2004).

In order to model the absolute irradiance and wavelength composition of *in situ* PAR through the water column under any given ambient above-water irradiance, three factors were obtained. The first was the relationship between the above-water PAR and that recorded just below the surface, namely the ‘transmittance through the sea surface’. The second was the wavelength composition of PAR just below the surface, and the third was the attenuation of light at each wavelength with depth through the water column.

The wavelength composition of PAR just below the surface and the spectral vertical attenuation coefficients also provided the *in situ* irradiance spectra at the depths at which physiological samples were obtained.

During CS03 downwelling irradiance profiles were obtained using a Li-1800 UW spectro-radiometer (Li-Cor) mounted on an independent CTD system. Profiles were only obtained at a limited number of stations. Locations where no optics data were available were CS2 and X7 and for these stations, optics characteristic of CS1 and IS1 (respectively) were assumed (Moore et al. 2006). During CS05 a freefall SATLANTIC downwelling irradiance sensor was deployed at a number of stations across the study area, achieving excellent coverage of hydrographic conditions and times of day.

During AMT15, calibrated data were not available in time for this study. In order to overcome this problem, some data from AMT13 were used, which took place at a similar time of year and followed a nearly identical cruise track. Use of data from AMT13 is clearly stated.

#### *Light penetration through the sea surface*

The transmittance through the sea surface ( $T_{rel}$ ) was calculated from the relationship between PAR just below the surface,  $E(PAR,0)^-$ , and PAR above the surface,  $E(PAR,0)^+$ , at the time of the optics casts (Kirk 1994, Tilstone et al. 1999).

$$T_{rel} = E(PAR,0)^- / E(PAR,0)^+ \quad (2.10)$$

For all cruises  $E(PAR,0)^+$  ( $\mu E m^{-2} s^{-1}$ ) was obtained from the ship’s PAR sensor, as the average irradiance recorded for the 10 min following optics cast deployment.

$E(\text{PAR},0)$  ( $\mu\text{E m}^{-2} \text{s}^{-1}$ ) was obtained from the intercept of the  $\log(E(\text{PAR},z))$  vs. depth relationship as measured by the dedicated optics rig over the surface region (excluding the top 2-10 m depending on the cast). The dedicated optics rig was used in preference to the other PAR sensors for this calculation so that the value of  $T_{\text{rel}}$  inherently accounted for any discrepancies in calibration between the ships PAR sensor and that of the optics profiler. However, since this was not possible for AMT15, this estimation was carried out using the Chelsea PAR sensor on the main titanium CTD frame. Values of  $T_{\text{rel}}$  for the three cruises were as follows:

CS03:	$T_{\text{rel}} = 0.62 \pm 0.13$	$n = 9$
CS05:	$T_{\text{rel}} = 0.66 \pm 0.15$	$n = 43$
AMT15:	$T_{\text{rel}} = 0.61 \pm 0.21$	$n = 28$

As described by Kirk (1994) light penetration through the sea surface varies with solar zenith angle, surface roughness and surface chlorophyll as examples. The variability in this parameter for different wavelengths is often considered to be negligible (Kirk, 1994; Lorenzo, 2004). The relatively small geographical area visited during CS03 and CS05 means that variability of  $T_{\text{rel}}$  is likely to be dominated by variability in the time of optics sampling and surface chl-a. In contrast, AMT15 casts were carried out at around 10:30 – 12:00 h such that variability may not be attributable to the time of day, with much of the variability in  $T_{\text{rel}}$  during AMT15 likely related to changes in solar angle with latitude of the ship. Since most optics casts were carried out in the daylight period away from dawn and dusk, the value of  $T_{\text{rel}}$  is likely to be an upper-bound of the daily range.

For these data, variability in  $T_{\text{rel}}$  was large (standard deviation < 25% of mean for Celtic Sea, < 35% for AMT15) but was not correlated to surface chl-a, time of day or any other measured environmental variable, such that surface roughness and wind speed were likely to be significant factors in the variability (Mobley 1999).

#### *Wavelength composition of the in situ light field*

The surface magnitude of each of the (typically six) measured wavelengths was obtained from the intercept of the linear  $\log(E(\lambda,z))$  vs. depth relationship between 2-10 m and the base of the SML. A simple linear interpolation between wavelengths was used to give complete spectra. The spectra were then scaled by the area under the interpolation (between 400-700 nm) in order to remove the influence of the absolute light condition; subsequently providing the ‘shape’ of the irradiance spectra of PAR equal to 1, hereafter,  $\hat{E}(\lambda,0)$  (with units  $\mu\text{E m}^{-2} \text{s}^{-1}$ ). A wavelength-

specific unit conversion was applied to obtain  $\mu\text{E m}^{-2} \text{s}^{-1}$  from  $\mu\text{Watts cm}^{-2} \text{s}^{-1}$  and a factor of 1.2 used to convert downwelling irradiance into scalar irradiance where necessary (Kirk 1994).

During CS03, the wavelengths measured by the instrument were 412, 442, 490, 510, 555, 670 and 685 nm. Due to the limited number of optics casts that were carried out during CS03 a representative shape,  $\dot{E}(\lambda,0)$ , was used for CS1, CS3 and IS1. The representative shape for CS1 was used for all CS2 and oceanic sites, and IS1 used for X7.

During CS05, the wavelengths measured were 412, 442, 490, 510, 560, 670 and 705 nm. Unfortunately the measurement of irradiance at 705 nm was found to be very variable presumably due to the light at this wavelength being close to the detection limit of the instrument. A cruise-mean value of the ratio of irradiance at 705:490 nm was used to provide the 705 nm contribution for all optics casts. With this correction applied, the contributions of each wavelength to the area varied less than 8% over all optics casts ( $n = 43$ ). Subsequently the average  $\dot{E}(\lambda,0)$  was used throughout the cruise, an assumption supported by other authors (Tilstone et al. 2003, Lorenzo et al. 2004).

Spectral optics data from AMT13 was used to provide the necessary spectral information for AMT15 data analysis. Since AMT13 data were only required to provide the wavelength composition, rather than absolute values, of *in situ* irradiance the substitution of this dataset was deemed acceptable. The wavelengths obtained were 412, 442, 490, 510, 560, 664, 685 nm. The 664 nm wavelength gave spurious results and was disregarded. Typically three casts were deployed at each location, but repeatability between casts was poor. When averaged into regions, error bars on each wavelength within regions were larger than those between regions. However, over the entire cruise the contribution of each wavelength to the area varied < 5%, and so a cruise-mean  $\dot{E}(\lambda,0)$  was assumed for the entire cruise. Example surface spectral shapes,  $\dot{E}(\lambda,0)$ , are illustrated in Figure 2.7.

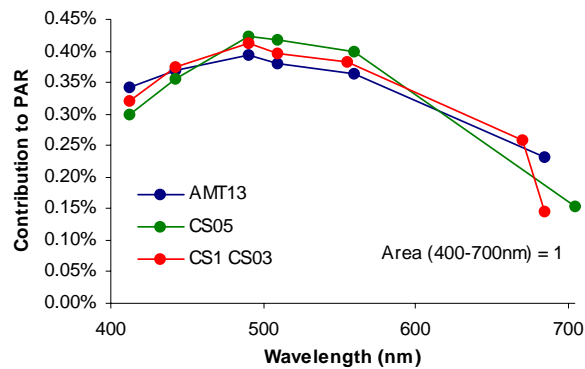


Figure 2.7. Example wavelength composition of in-water surface irradiance normalised to PAR, such that the area of each curve between 400-700 nm is equal to 1 ( $\dot{E}(\lambda,0)$ ).

Spectral underwater irradiance was obtained from:

$$E(\lambda,0)^- = E(\text{PAR},0)^+ \cdot T_{\text{rel}} \cdot \dot{E}(\lambda,0) \quad (2.11)$$

Potential errors on determination of the underwater light field are discussed in Kirk (1994). Major considerations include those which influence the transmittance of light through the air-sea interface (described above). Further, since surface values of spectral irradiance by this method were obtained from fits of the linear  $\log(E(\lambda,z))$  vs. depth relationship, surface water characteristics such as chl-a would also be important. During CS03 and CS05 there was no significant correlation between ratios of  $\dot{E}(\lambda,0) : \dot{E}(490,0)$  and surface chl-a, such that it did not appear that chl-a was a significant influence to the shape of the surface underwater light spectrum. The use of linear interpolation of light between the measured wavelengths may overestimate the contribution of light between  $\sim 560 - 640$  nm compared to typical *in situ* spectra.

#### *Extrapolation of irradiance through the water column*

During CS05 and AMT15 the spectral underwater surface irradiance was extrapolated to depth using  $K_d(\lambda)$  vs. chl-a relationships for available wavelengths (e.g. Moore et al. 2003). Such relationships provided robust quantification of the increased light attenuation associated with the DCM. Chl-a used for these relationships was that scaled to the HPLC chl-a as described above.

During CS05, optics data were matched to chl-a samples obtained from CTD casts taken in the same location and generally within  $\sim 2$  hours of the optics cast.  $K_d(\lambda,z)$  at chl-a sample

depths were obtained over a three metre depth range. The relationships between  $K_d(\lambda, z)$  vs. chl-a for this cruise are illustrated in Figure 2.8.

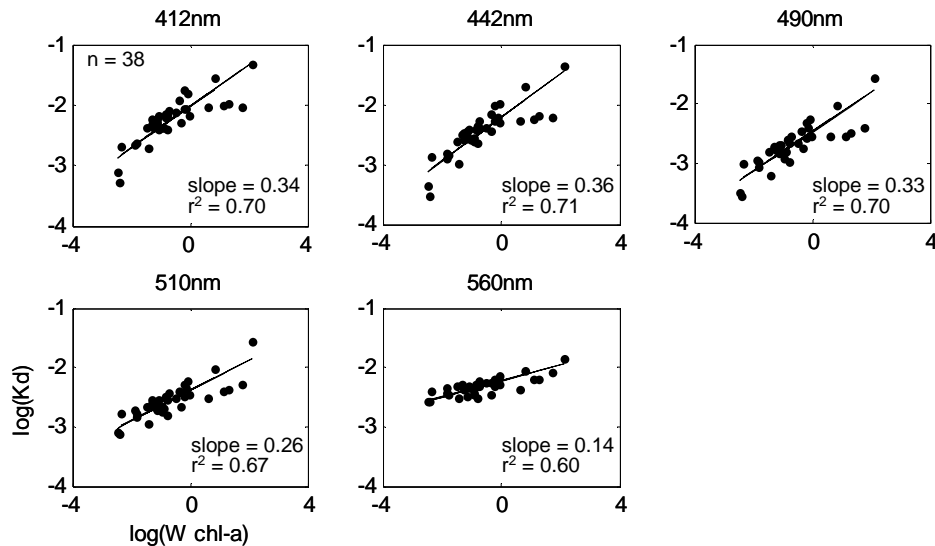


Figure 2.8. Relationship between vertical light attenuation ( $K_d$ ) and chl-a concentration at five wavelengths during CS05. Chl-a is the fluorometric chl-a weighted to the HPLC value as obtained from bottle samples. Statistics shown are the results of model II regression analysis.

A significant correlation existed between chl-a and  $K_d(\lambda)$  for 412, 442, 510, 560 nm. At 705 nm a strong correlation between chl-a and light attenuation would not be expected since light at this wavelength rapidly diminishes to zero and is attenuated most significantly by water, rather than phytoplankton (Kirk 1994). A  $K_d(705)$  vs. chl-a relationship was obtained from the model of Morel and Antoine (1994).

For AMT15,  $K_d(\lambda)$  vs. chl-a relationships (Fig. 2.9) were obtained from CTD chl-a and optics data from the midday optics casts during AMT13, where AMT13 CTD chl-a was calibrated following an identical protocol to that of AMT15. The relationships shown in Figure 2.9 were obtained from surface waters only, due to the depth of the optics profiles not reaching the DCM, but an adequate range of chl-a values was achieved due to the range of hydrographical provinces visited during the cruise. The attenuation at 685 nm was obtained from the model of Morel and Antoine (1994).

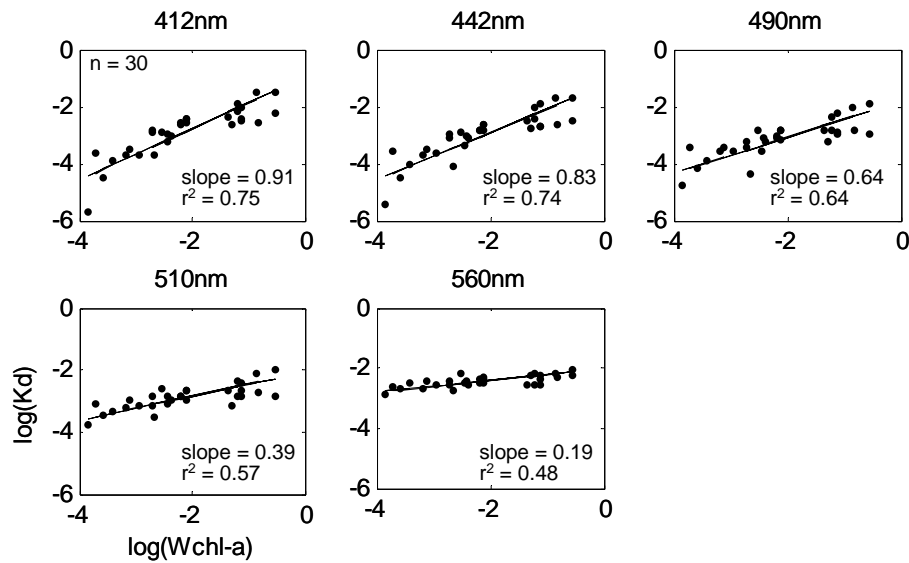


Figure 2.9. Relationship between vertical light attenuation ( $K_d$ ) and chl-a concentration at five wavelengths during AMT15. Chl-a is the fluorometric chl-a weighted to the HPLC value as obtained from bottle samples. Statistics shown are the results of model II regression analysis.

Variability in the coefficients obtained from light attenuation coefficients obtained from these regressions was reasonably well correlated to those obtained by the model of Morel and Antoine (1994) for all wavelengths. In general, the Morel and Antoine (1994) model (MA) tended to overestimate attenuation in low biomass waters and underestimate attenuation in higher biomass waters such as the DCM or Celtic Sea. For example MA-derived  $K_d(\lambda)$ 's were 150% those obtained from AMT13 in the surface of the southern gyre waters, but ~50-60% in the DCM and upwelling regions. In the Celtic Sea MA-derived  $K_d(\lambda)$ 's were typically 90% of those obtained from the data.

The significant correlations between chl-a and wavelength-specific vertical attenuation coefficients suggested that much of the variability in  $K_d(\lambda)$  was with chl-a, such that other absorbing properties, such as yellow substances, were likely to be minimal (Bouman et al. 2000). This is most likely to be true in the Case-1 waters of the Atlantic Ocean, but may cause some of the scatter around the chl-a dependence in the Case-2 waters of the Celtic Sea (Kirk 1994). DOC and other absorbing material may also explain the difference in the slopes of the regressions between AMT15 and CS05 data, particularly at 412, 442 and 490 nm.

During CS03,  $K_d(\lambda)$  vs. chl-a relationships could not be achieved due to the limited optics dataset. Linear fits of the  $\log(E(\lambda, z))$  vs. depth relationship for the SML were used to

obtained constant  $K_d(\lambda)$ .  $K_d(\lambda)$  for CS1, IS1 and CS3 were obtained from the representative casts at these locations, with the representative from CS1 used for all other locations. It follows that for this cruise increased attenuation due to increased chl-a at the DCM was not quantified, leading to potential overestimates of irradiance in the lower part of the DCM.

For a given CTD chl-a profile, the spectral underwater surface irradiance ( $E(\lambda,0^-)$ ) was extrapolated to depth based on the  $K_d(\lambda)$  vs. chl-a relationships. A simple linear interpolation between 400-700 nm provided the complete spectral *in situ* light field at each meter, and a value of PAR. This process could be carried out for any desired incident irradiance at the sea surface.

### 2.5.3 Estimations of *In situ* Primary Production

The amount of carbon fixed at each meter through the water column was estimated under a range of incident irradiances, using knowledge of the light-response of phytoplankton described by the  $^{14}\text{C}$ -derived P vs. E parameters and the reconstructed *in situ* light fields. Methods were broadly similar to those of Tilstone et al. (1999, 2003) and Lorenzo et al. (2004) and originally described by Morel et al. (1996) and Bouman et al. (2000). Methods used in this study most closely resemble those of Tilstone et al. (2003).

Previous models have tended to estimate primary production (PP) at discrete depths, and then interpolate the resulting PP through the water column. However interpolation of the physiological parameters in the first instance (Tilstone et al. 2003) was used in this study leading to full-depth coverage of estimated primary production.

#### *Calculating Primary Production through the water column*

The physiological parameters required for this estimation include the  $^{14}\text{C}$ -derived (chlorophyll normalised) maximum rate of carbon fixation ( $P^*_m$ ), the maximum light utilization coefficient ( $\alpha^*$ ) and the phytoplankton absorption per unit chl-a, which for this analysis is that measured by the filter technique ( $a(\lambda)^*_{\text{meas}}$ ). In order to determine phytoplankton physiological characteristics at each meter through the water column, a simple linear interpolation was applied to these parameters between the discrete sample depths (two depth for AMT15 and CS03, and four sample depths for CS05). In the case of particle absorption ( $a(\lambda)^*_{\text{meas}}$ ) the linear interpolation was carried out on absorption at each wavelength. The surface parameters were assumed constant between the surface and the depth of the SML sample, and the DCM sample parameters assumed constant below the depth of the DCM to the base of the thermocline.

The estimation of primary production for each meter ( $z$ ) through the water column was then achieved by equation 2.12:

$$P(z) = CTDchl(z) \cdot P^*_m(z) \cdot \tanh(E(z)) \cdot \alpha(z)^*_{insitu} / P^*_m(z) \quad (2.12)$$

Where  $P^*_m(z)$  is the maximum photosynthetic rate per unit chl-a ( $\text{mg C (mg chl-a)}^{-1} \text{h}^{-1}$ ) and as determined from the linear interpolation of  $P^*_m$  through the sample depths and  $CTDchl(z)$  represents the chl-a *in situ* as provided by the CTD chl-a profile (used to scale  $P^*_m(z)$ ).  $E(z)$  is the *in situ* irradiance ( $\mu\text{E m}^{-2} \text{s}^{-1}$ ) estimated from the sum of  $E(\lambda, z)$  across 400-700 nm and  $\alpha(z)^*_{insitu}$  is the maximum light utilisation coefficient ( $\text{mg C mg chl-a}^{-1} \text{h}^{-1} (\mu\text{E m}^{-2} \text{s}^{-1})^{-1}$ ) at depth  $z$  (m) spectrally corrected to the *in situ* irradiance via the specific use of Equation 2.10:

$$\alpha(z)^*_{insitu} = \alpha(z)^*_{14C} \frac{\sum_{400-700nm} a(\lambda, z)^* \cdot E(\lambda, z)_{insitu} \sum_{400-700nm} E(\lambda)_{14C}}{\sum_{400-700nm} a(\lambda, z)^* \cdot E(\lambda)_{14C} \sum_{400-700nm} E(\lambda, z)_{insitu}} \quad (2.13)$$

where  $a(\lambda, z)^*$  represents the phytoplankton absorption as obtained from the linear interpolation of  $a(\lambda)^*$  between sample depths.  $E(\lambda)_{14C}$  represents the spectral irradiance of the P vs. E incubator lamp and  $E(\lambda, z)_{insitu}$  indicates the spectral irradiance of *in situ* light at depth  $z$  (m).

The light absorbed by phytoplankton (PUR, Photosynthetically Utilised Radiation) can explicitly be calculated from:

$$PUR(z) = \sum_{400-700} E_{insitu}(\lambda, z) \cdot a(\lambda, z)^* \cdot CTDchl(z) \quad (2.14)$$

Equation 2.12 and 2.13 allowed primary production to be estimated at each meter in the water column for any given suite of physiological and phytoplankton absorption parameters, for any given chl-a profile and under any required incident irradiance.

Estimates of daily PP were obtained by summing hourly PP profiles as constructed for each hour for the irradiance (in hourly bins) recorded by the ships PAR sensor over 24 hours. Physiological parameters and phytoplankton absorption were assumed constant throughout the day. The *in situ* chl-a profile was typically taken as the CTD cast from which the physiological parameters were obtained, and assumed constant throughout the day, although estimates were

also made using all chl-a profiles recorded during 25 hour occupations of some stations, as specified in the relevant sections.

A simple sum of PP estimated at each meter provided integrated-water column production. PP below the base of the DCM (or thermocline) was assumed negligible and photoinhibition in the surface was not considered.

### *Errors on in situ PP profiles*

Detailed error analysis on similar modelling techniques can be found in the literature (e.g. Morel et al. 1996, Tilstone et al. 1999, 2003, Arbones et al. 2000, Lorenzo, et al. 2004). Such discussions focus on relative importance of spectrally-resolved (rather than broadband) models. The potential errors on daily estimates of PP are in addition to those already mentioned for the individual component measurements. In general, the largest errors in the estimates of daily PP are considered not to lie in the measurements themselves, but rather the assumptions required in extrapolating the instantaneous measurements over a 24 hour period. The following section summarises the sources of error that are considered to be most significant in estimating daily PP by the method described above, and quantify the effect on PP estimates where possible.

**Biological considerations:** As described above, the carbon fixed during incubation is net, rather than gross, photosynthesis (Sakshaug et al. 1997). Estimates of daily PP from P vs. E incubations use a relatively short incubation time, which could mean estimated daily PP may be closer to gross primary production than would be achieved from longer (12 – 24 hour) incubations (Morel et al. 1996). However, contrary to longer incubations, diel periodicity in the physiology of the phytoplankton is not accounted for. Physiological measurements from this study (CS03) showed diel periodicity increased the maximum photosynthetic rate ( $P^*_m$ ) by around ~12% (see also Moore et al. 2006) at midday compared to the night-time value, and as such estimation of daily PP from a pre-dawn P vs. E experiment may lead to an underestimation of daily PP by a similar proportion.

Photoinhibition is not accommodated in this method, therefore leading to possible overestimation of daily PP near the surface. Quantifying precisely the effect of photoinhibition is problematic as the observed inhibition in incubation experiments varies depending on the length of time of the incubation (MacIntyre et al. 2002), and this timing is difficult to relate to realistic field conditions due to mixing of cells near the surface *in situ*.

The removal of phytoplankton absorption by non-photosynthetic pigments (NPC) led to decrease in estimates of daily primary production of ~11% +/- 0.3% (CS05 data) in agreement

with Bouman et al. (2000). PP estimates were carried out without consideration of light absorption by these pigments, thus likely lead to an overestimation of daily integrated PP of ~11 % for this reason.

As mentioned above, fitting errors on the estimations of  $\alpha^*$  and  $P^*_m$  are likely to be minimal. However, it is worth noting that errors of estimates on  $\alpha^*$  will be more important when light levels are limiting for photosynthesis, such as at dawn and dusk, with errors on  $P^*_m$  more important during periods of saturated growth. Similarly, errors associated with estimation of phytoplankton absorption spectra and the excitation spectra are likely to be more significant at light limiting irradiance (though will also affect light saturated rates) and have been quantified by Kyewalyanga et al. (1992) and Arbones et al. (2000) to be around ~20%.

Other biological considerations include the linear interpolation of P vs. E parameters between the sample depths, as this may not be representative of true vertical gradients in phytoplankton physiology. This problem is most notable in the case of CS03 and AMT15 where samples were available at only two depths. PP estimates are subsequently likely overestimated in the region between the SML and DCM samples. However, any other interpolation method would not be devoid of problematic assumptions regarding the variability in phytoplankton physiology with depth. A linear interpolation between available sample depths is considered acceptable (e.g. Morel et al. 1996, Tilstone et al. 2003). Increasing the sample resolution to four depths (the top and bottom of the SML and the upslope and peak of the DCM) minimised the errors associated with this assumption for CS05.

Estimation of total water column PP in the shelf seas assumes no production occurs in the BML. In a stratified region of the North Sea Weston et al. (2005) estimated PP below the thermocline to be ~7 % of water column primary production, and as such estimates of daily PP may be underestimated by a similar amount in the Celtic Sea.

Errors on chl-a values (due to calibration of CTD chl-a (section 2.4.2)) would be linearly incorporated into PP estimates.

**Optical considerations:** A major source of error for the reconstruction of the *in situ* light field is likely to be in the estimation of the amount of downwelling irradiance transmitted through the air-sea interface. As mentioned above, variability in this parameter ranged from +/- 25% during CS05 and +/- 35% during AMT15, which would influence the estimated daily PP by a similar magnitude. Applying a cruise-average is considered acceptable (Tilstone et al. 2003, Lorenzo et al. 2004), though this source of variability must be considered when interpreting estimates of PP.

In the measurement of the wavelength composition of in-water surface irradiance, repeatability of measurement of surface irradiance at wavelengths  $> 600$  nm was generally poor and could lead to large differences in the calculated area between 400-700 nm (and subsequently irradiance reaching the deep water). For example, if the measured irradiance at the surface at 705 nm were particularly high, the contribution of all other wavelengths to total PAR would be low, such that the amount of water reaching the deep waters could be underestimated. In this analysis every effort was made to ensure only trustworthy optics data were incorporated, and in the cases of AMT13 and CS05 enough optics casts were made to achieve adequate cruise-averages (Tilstone et al 1999, 2003, Lorenzo et al. 2002, 2004). The variability of daily PP estimated for a range of randomly selected surface spectra at an example site during CS05 (CTD47) was  $< \pm 2\%$  ( $n = 8$ ) from that achieved using the cruise-mean spectral shape. The effect of variance in the wavelength composition of light (for example at dawn and dusk, or due to cloud cover (Kirk 1994)) on daily PP estimated is assumed to be minimal compared to other sources of error (Lorenzo et al. 2002, Tilstone et al. 2003).

In the context of PP estimates, the errors associated with linear interpolation between measured wavebands (expected to overestimate light availability between  $\sim 560$ - $640$  nm compared to typical *in situ* spectra) is considered to be minor, since phytoplankton absorption above  $\sim 550$  nm is low compared to other wavelengths.

Due to the limited number of optics casts carried out during CS03 it is suggested that the estimates of daily integrated PP obtained during CS03 be treated with some caution, particularly at the locations where no optics casts were carried out (CS1 and X7). For all locations during CS03, the total light availability is likely to be overestimated at the DCM due to the use of constant (as opposed to chl-a specific) vertical attenuation coefficients. Irradiance (and therefore PP) at the DCM could be overestimated at the DCM peak by  $\sim 10\%$ , increasing below the DCM (assuming an increase in chl-a at the DCM of  $1 \text{ mg m}^{-3}$  compared to the surface and  $K_d(\lambda)$  vs. chl-a from CS05).

The assumptions regarding optical properties are likely to be most significant for AMT15 where the wide range of hydrographic regimes and seasonal differences contributed to the cruise-averages, and the optics data were routinely obtained close to midday throughout the transect.

The sources of error associated with the use of the optics data mostly lead to uncertainties in the magnitude of underwater irradiance, rather than the shape of the underwater irradiance spectra. Consequently, these errors are likely to be minor in the *in situ* light fields

used for spectral correction of physiological parameters as errors are likely to be minimal compared to the difference between *in situ* spectral shape and that of the laboratory instruments.

The combined errors on daily estimated PP by this method are difficult to quantify. A detailed sensitivity analysis could be carried out, although estimates of errors on each measurement would not be without a considerable degree of uncertainty in most cases. In any case the most significant sources of error are considered to be associated with the assumptions used, rather than errors on the measurements themselves.

### Daily PP estimates compared to SIS measurements

Comparison of estimated daily PP to Simulated-In-Situ (SIS) measurements should be considered a relative comparison as the SIS method is not without uncertainties (Morel et al. 1996, Raateoja et al. 2004). During CS03 daily estimated PP profiles and estimated rates of daily carbon fixation from SIS incubations for available data are shown in figure 2.10. During AMT15, daily estimated PP from the physiological parameters compared to the SIS incubations were well correlated (log:log regression  $n = 41$ ,  $r^2 = 0.826$ ,  $p < 0.001$ ) though PP was generally around ~20% of the SIS value.

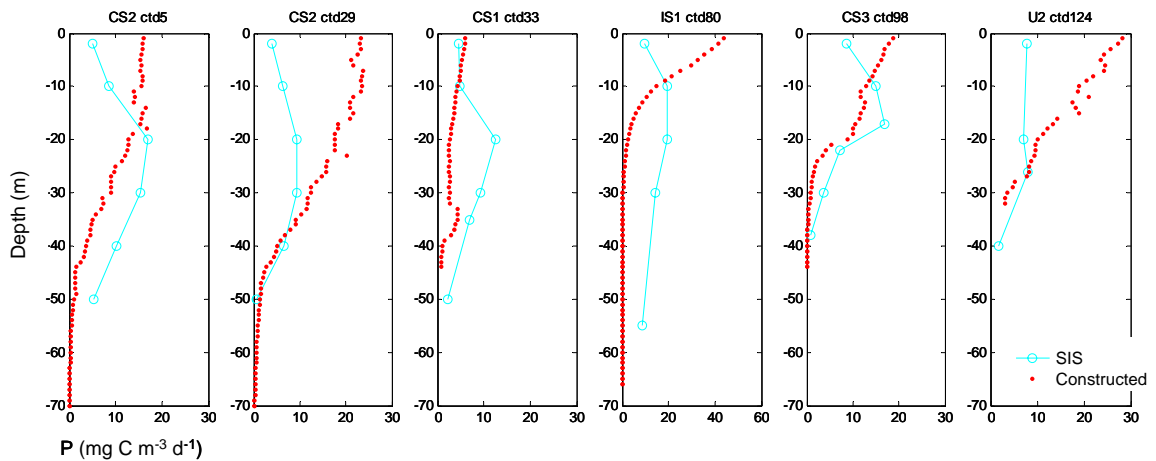


Figure 2.10. Estimated daily primary production as constructed from  $^{14}\text{C}$  P vs. E parameters and the spectral light field (constructed) compared to that derived from 12 hour on deck Simulated-In-Situ (SIS)  $^{14}\text{C}$ -uptake incubations ( $\text{mg C m}^{-3} \text{d}^{-1}$ ). Data are from CS03.

The surface samples for SIS incubations are likely reduced by photoinhibition which is unlikely to be realistic, since phytoplankton doubtfully remain at the surface (SIS incubation irradiance was 97% that of the surface) for the entire day. Other factors leading to offset in the daily estimated PP between these methods include those associated with the different lengths of

incubations and bottle effects, which generally result in lower SIS measurements than estimated PP from P vs. E parameters. SIS measurements in excess of those estimated from P vs. E parameters most likely results from diel changes in the physiology of phytoplankton during the day.

## **2.6 Statistical Methods**

Common statistical analysis techniques were used throughout this analysis. Regression analysis was, where appropriate, a model II type linear regression, allowing errors on both variables. A students t-test was used in data analysis to determine whether two groups of samples of normal distribution have the same mean (with standard deviations unknown but assumed equal), and one-way ANOVA test was used to compare the means of more than two groups of data.

## CHAPTER 3: PHOTOPHYSIOLOGY OF PHYTOPLANKTON IN THE CELTIC SEA

This chapter investigates the differences in phytoplankton physiology within the thermocline compared to the surface, and aims to identify how and why the physiological differences are established. The light absorption properties of the phytoplankton are considered in the first section, followed by a detailed account of the physiological parameters derived from  $^{14}\text{C}$  P vs. E and FRRF methods.

### 3.1 Study Area

Phytoplankton physiological measurements were obtained at the locations shown in Figure 3.1. Sampling at CS2 and U2 was carried out during both cruises. Sampling on two consecutive days was carried out at IS1, CS3, CS1 and CS2 during CS03 and stations that were visited at different times of the spring - neap tidal cycle were CS3, CS2 and B2.

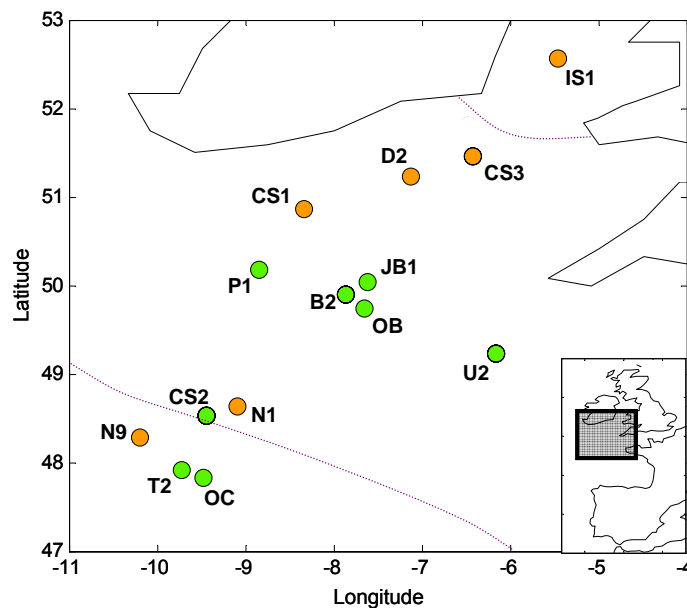


Figure 3.1. Map of sampling locations for physiological measurements in the Celtic Sea during CS03 (orange symbols) and CS05 (green symbols). Dotted lines indicate the location of the Irish Sea front and the Shelf Edge. Station B2 was located on the slope of a bank, with JB1 in the vicinity of the bank but not directly above it. Station OB was not associated with the bank. Stations CS2 and U2 were sampled during both CS03 and CS05.

Water samples for  $^{14}\text{C}$  P vs. E and particle absorbance measurements were obtained from two depths (surface and DCM) during CS03 and at four depths (top and bottom of SML and upslope and peak of DCM) during CS05. At all stations FRRF samples were taken at 2-8 depths through the surface and thermocline.

Unless otherwise stated the results are illustrated for CS05 only, with statistics providing details of results from both CS03 and CS05. Statistics referring to CS03 are provided either for all available data including the mixed water stations or for the stratified stations only (i.e. the shelf, shelf edge and oceanic regions). Statistics for CS03 are quoted as ‘stratified’ where only stratified region were included in the analysis.

## 3.2 Optical Properties of Phytoplankton

### 3.2.1 Particle Absorption

Values of the light absorption parameter measured by the filter technique,  $a^*_{\text{meas}}$ , ( $\text{m}^2 (\text{mg chl-a})^{-1}$ ) fall within the range of the worldwide data reviewed by Bricaud et al (1995, 2004), with  $a^*_{\text{meas}}$  generally decreasing with increased chl-a. Hereafter  $a(\lambda)^*_{\text{meas}}$  refers to wavelength-resolved absorption spectra and  $a^*_{\text{meas}}$  to the sum of the absorption from all wavelengths from 400-700 nm. The asterisk denotes normalisation by chl-a.

Figure 3.2 shows the mean spectral shape of phytoplankton absorption (normalised to 442 nm) in shelf, shelf edge and oceanic waters during CS05. The magnitude of  $a^*_{\text{meas}}$  was generally higher for the oceanic region than for the shelf and shelf edge sites, conforming to trends observed between oligotrophic and mesotrophic conditions (Lazzara et al. 1996). The high absorption at 465 nm relative to 442 nm in the DCM of the oceanic region (Fig. 3.2B) could be attributed to the presence of cyanobacteria, predominantly *Synechococcus* which absorb strongly at these wavelengths (e.g. Bricaud and Stramski 1990). The low absorption between 550-650 nm relative to 442 nm and reduced secondary chl-a peak (at 685 nm) in the oceanic region (Fig. 3.2A and B) are likely to be the result of relatively high absorption at 440 nm rather than particularly low absorption at these wavelengths.

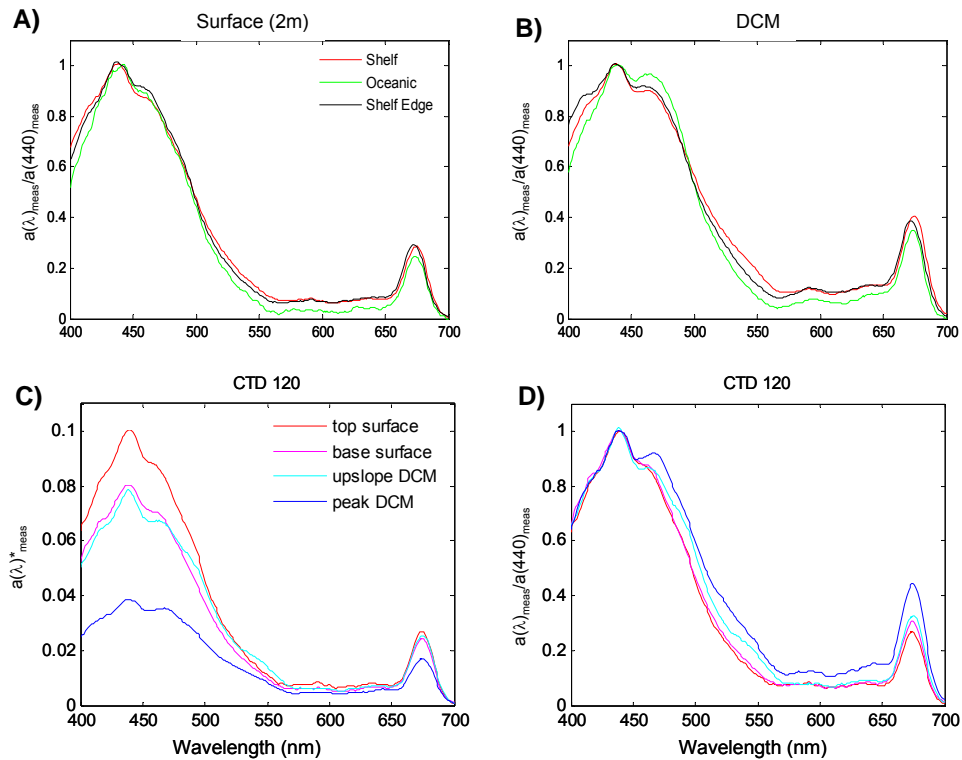


Figure 3.2. Phytoplankton absorption spectra of intact cells as measured by the filter technique,  $a(\lambda)_{\text{meas}}$ . A) Mean  $a(\lambda)_{\text{meas}}$  from the surface (2 m) samples for the main regions visited during CS05 normalised to absorption at 442 nm,  $a(442)_{\text{meas}}$ . B) Mean spectra obtained at the peak of the DCM for the three main regions visited during CS05, normalised to 442 nm. C) Absorption spectra normalised to chl-a ( $\text{m}^2 (\text{mg chl-a})^{-1}$ ) for an example shelf location (JB1, CTD120) visited during CS05,  $a(\lambda)^*_{\text{meas}}$ . D) Absorption spectra as in C, normalised to 442 nm.

During both cruises there was considerably greater variability in  $a^*_{\text{meas}}$  with depth (Fig3.2C, CS03 stratified  $n = 32$ ,  $r^2 = 0.123$ ,  $p = 0.049$ , CS05  $n = 54$ ,  $r^2 = 0.170$ ,  $p = 0.002$ ) than between location, as well as considerable changes in the ‘shape’ of the absorption spectra ( $a(\lambda)^*_{\text{meas}}$ ) with depth (Fig. 3.2B). The change in ‘shape’ of the absorption spectrum occurs for two reasons. The first is due to the pigments associated with the phytoplankton (driven by taxonomic composition) and the second is due to increases in the total photosynthetic pigments within the cells to cope with low light conditions at depth causing self-shading of phytoplankton known as the *package effect* (Duysens 1956), as described in Chapter 1.

The packaging effect occurs across all pigments. Reducing absorption by an amount proportional to the absorption at each wavelength, the package effect leads to a so-called “flattening” of the shape of the absorption spectra. The effect increases with cellular pigment

concentration and, following pigment synthesis in low light conditions, increases with depth (Duysens 1956, Bricaud et al. 1995). Quantifying the contributions of these two mechanisms is problematic as they cannot easily be separated (Morel and Bricaud 1981, Bricaud et al. 1995).

The ratio of absorption at 490:442 nm and 540:442 nm was significantly different between the surface mixed layer (SML) and the thermocline during both cruises (Fig 3.3) (at 95% confidence level for both cruises (CS03 stratified only)). Absorption at 490 nm represents the peak of absorption of photosynthetically active carotenoids (PSC) as well as the secondary peak of non-photosynthetic carotenoids (NPC), while at 540 nm the majority of absorbance is by PSC only (Jeffrey et al. 1997). HPLC analysis also revealed a significant decrease in NPC:chl-a with depth (CS03 stratified  $n = 42$ ,  $r^2 = 0.296$ ,  $p < 0.001$ ; CS05  $n = 11$ ,  $r^2 = 0.200$ ,  $p < 0.001$ ) and as such the increase in 490:442 nm at the DCM was likely to be dominated by variability in NPC. The resulting shift in absorption away from the major peak at 442 nm within the thermocline is likely to be partly due to the pigment content of the phytoplankton cells, with this also contributing to the apparent ‘flattening’ of the shape of the absorption spectra caused by the package effect.

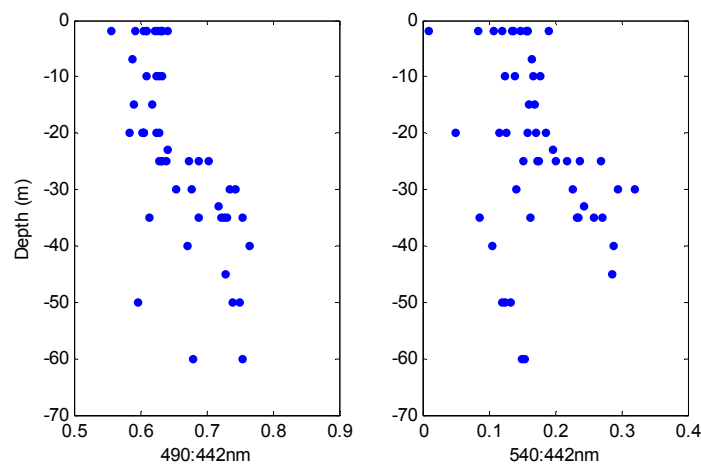


Figure 3.3. Ratios of phytoplankton absorption as measured by the filter technique against depth for all samples collected during CS05.

Both packaging and carotenoid content per unit chlorophyll can be related to cell size; large cells such as diatoms have lower carotenoid content and are strongly affected by packaging, in contrast to smaller cells such as pelagophytes (Ciotti et al. 2002, Bricaud et al. 2004). Changes in absorption characteristics with location and depth cannot easily be separated into those

resulting from changes in pigment compliments and the package effect. Further, both pigment compliment and pigment packaging vary with acclimation to low light as well as phytoplankton taxonomy (e.g. Berner et al. 1989, Suggett et al. 2004).

### 3.2.2 Pigment Packaging

Measurements of phytoplankton light absorption spectra were obtained by two methods (as described in Chapter 2). The first was based on the absorption spectra of intact phytoplankton cells ( $a(\lambda)^*_{\text{meas}}$ ) using the filter technique, and the second was by the pigment reconstruction using pigment concentrations of disrupted cells measured by HPLC ( $a(\lambda)^*_{\text{pig}}$ ) (Bidigare et al. 1990b, Marra et al. 2000).

Until recently it was assumed on theoretical grounds that the chl-a-specific absorption,  $a^*_{\text{meas}}$ , measured on intact cells should be smaller than that derived from HPLC reconstructed pigments  $a^*_{\text{pig}}$ , the difference being due to the (wavelength-dependent) affect of pigment packaging (following Nelson et al. 1993). However, in these data,  $a^*_{\text{meas}}$  was generally greater than  $a^*_{\text{pig}}$ , a finding shared with a number of previous studies (e.g. Bricaud et al. (2004) and references therein). The shape of absorption spectra obtained from the two methods was also dissimilar for surface samples for which the effects of pigment packaging should be minimal (Fig 3.4).

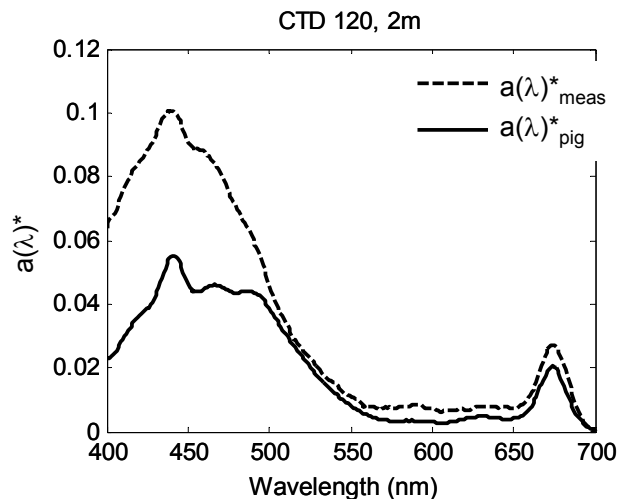


Figure 3.4. Example of an absorption spectrum of intact cells by the filter technique ( $a(\lambda)^*_{\text{meas}}$ ) ( $\text{m}^2 (\text{mg chl-a})^{-1}$ ) compared to by the pigment reconstruction technique ( $a(\lambda)^*_{\text{pig}}$ ) ( $\text{m}^2 (\text{mg chl-a})^{-1}$ ). Reconstruction of absorption spectra from HPLC pigments was carried out following methods explained in Chapter 2.

Suggested reasons for the discrepancy between methods include the presence of carotenoids and phycobiliproteins not measured by HPLC (Nelson et al. 1993, Suggett et al. 2004), or unaccountable differences in absorbance of pigments in solvent compared to that of their in-vivo pigment-protein complexes (Johnsen et al. 1994). In addition, studies involving the deconvolution of the measured absorption spectrum of intact cells into Gaussian bands (giving the weight-specific absorption coefficients of the component pigments) often showed significantly higher band amplitudes than the corresponding pigments in solvent (reviewed by Bricaud et al. (2004), Table A1).

The offset is a systematic bias rather than noise, suggesting experimental artefacts in the two methods are unlikely to solely explain this phenomenon. As also observed by Bricaud et al. (2004) the offset is greatest in low chlorophyll regions, perhaps enhanced by minor pigment concentrations being close to the detection limit of the HPLC technique. Over 20 years of investigation, calculations of pigment packaging have continued to be reported despite the occurrence of this phenomenon in many datasets, and to date this problem remains unresolved. The ‘successful’ illustration of the package effect is likely to be the result of variability in  $a(\lambda)^*_{\text{meas}}$  with depth, compared to the relatively constant  $a(\lambda)^*_{\text{pig}}$ , irrespective of their relative magnitude and was often achieved through ‘scaling’ of absorption spectra to a relative benchmark (e.g. Babin et al. 1993, Bricaud et al. 1995) or through analysis at the secondary chl-a peak at ~675 nm where problems associated with ‘missing’ pigments were assumed to be minimal (Nelson et al. 1993).

Two methods were used to calculate package effect:

#### **Method 1) The Baseline Approach:**

The magnitude of absorbance of the chl-a peak at 675 nm above a theoretical linear baseline from 660-700 nm was calculated, thus removing most of the contribution of chl-b and divinyl chl-b at 675 nm and leaving only the contribution of chl-a at this wavelength (following Nelson et al. 1993). In contrast to  $a(\lambda)^*_{\text{meas}}$ , almost no variability in HPLC reconstructed spectra ( $a(\lambda)^*_{\text{pig}}$ ) was evident at 675 nm with depth. The resulting variation of chl-a-specific absorption at 675 nm should be due solely to pigment packaging at that wavelength. Such that:

$$Q(675)^*_{\text{base}} = a(675)^*_{\text{meas}} / 0.02 \quad (3.1)$$

Where  $a(675)_{\text{meas}}$  is measured from the baseline and 0.02 is the assumed maximal absorption coefficient of chl-a at 675 nm (Bricaud et al. 1983).

### Method 2) The ‘Missing Term’ Approach:

The ‘missing term’ represents the ‘missing’ absorbing pigments not measured by the HPLC method (Bricaud et al. 2004). The missing term was estimated by Bricaud et al. (2004) from the difference in absorption spectra between intact cells on a filter compared to that of the same cells in suspension. The empirical relationship for estimation of the missing term from chl-a of Bricaud et al. (2004) was:

$$a(440)_{\text{miss}} = 0.0525(T\text{chl-a})^{0.855} \quad (3.2)$$

The packaging index (via the missing term) approach,  $Q^*_{\text{miss}}(440)$ , was then calculated by Equation 3.4 and 3.2 (Bricaud et al. 2004):

$$a(440)_{\text{sol}} = a_{\text{pig}}(440) + a(440)_{\text{miss}} \quad (3.3)$$

$$Q(440)^*_{\text{miss}} = a(440)_{\text{meas}} / a(440)_{\text{sol}} \quad (3.4)$$

### Summary:

It is suggested that both  $Q(675)^*_{\text{base}}$  via the baseline approach and  $Q^*_{\text{miss}}(440)$  via the missing term only be considered as qualitative illustrations of pigment packaging. The packaging index for the two methods ranges from 1 (no package effect) to 0 (maximal package effect) (Fig 3.5). Values greater than 1 are due to noise in the data (Bricaud et al. 2004). Both methods show an increase in packaging (decrease in packaging index) with optical depth for CS03 and CS05 though only the relationship for  $Q(440)^*_{\text{miss}}$  was significant (CS03  $n = 21$ ,  $r^2 = 0.433$ ,  $p = 0.001$ ; CS05  $n = 51$ ,  $r^2 = 0.225$ ,  $p < 0.001$ ). Optical depth (OD) was estimated from the sample depth  $\times$   $K_d(\text{PAR})$ .

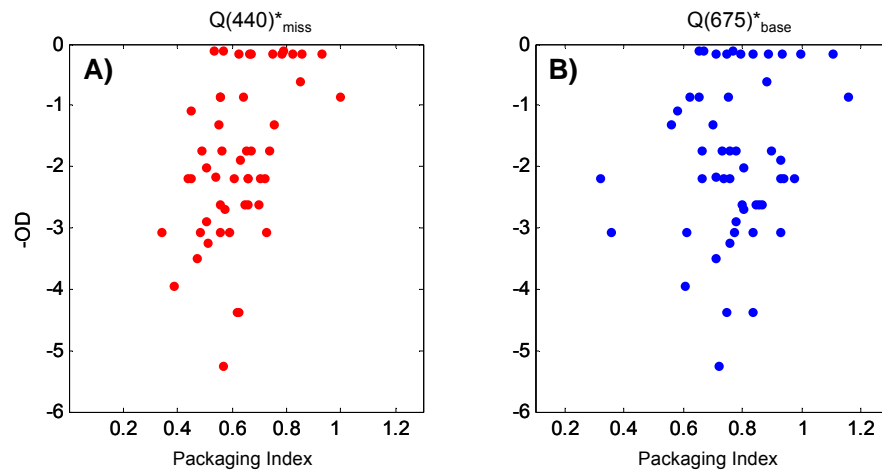


Figure 3.5. Packaging Index (Q) against depth for samples obtained during CS05 as estimated following the A) Missing Term approach and B) Baseline approach. Estimation of Packaging Index by the two methods is described in the text. In both cases packaging index is a relative scale 1 = no packaging, 0 = maximum packaging. Optical depth was estimated from the sample depth (m) x  $K_d(\text{PAR})$  ( $\text{m}^{-1}$ ).

Due to the uncertainties surrounding the HPLC reconstruction and the limited data used to calculate the empirically-derived ‘missing term’ (Bricaud et al. 2004), these results should be considered with caution. Suggestion for the quantification of packaging in future would include cruise-specific estimation of the ‘missing term’. However, comparison of HPLC and filter techniques will always be limited by the accuracy of HPLC measurement of minor pigments and the assumptions surrounding absorption spectra reconstruction (including the grouped pigments into PSC and NPC and uncertainties in weight specific absorption spectra as described in Chapter 2) (Bidigare et al. 1990b, Marra et al. 2000).

### 3.2.3 Absorption by Non-Photosynthetic Carotenoids

The contribution of NPC to phytoplankton absorption spectra were removed following methods in Chapter 2. Since the method involves removing the relative contribution, rather than absolute magnitude of, absorption by NPC, the method should give a reasonable estimate of absorption by photosynthetic pigments only despite the offset between absorption estimated between the pigment reconstruction and filter techniques (as discussed above). An example of the effect of removing absorption by NPC is illustrated in Figure 3.6.

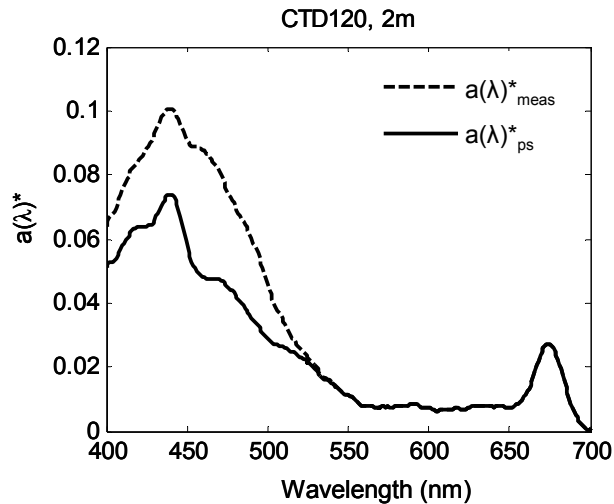


Figure 3.6. Absorbance spectra measured by the filter technique before ( $a(\lambda)^*_{\text{meas}}$ ,  $\text{m}^{-1}$ ) and after ( $a^*_{\text{ps}}$ ,  $\text{m}^{-1}$ ) the removal of non-photosynthetic carotenoids.  $a(\lambda)^*_{\text{ps}}$  was calculated from  $a(\lambda)^*_{\text{meas}} \times (a(\lambda)^*_{\text{pspig}} / a(\lambda)^*_{\text{pig}}$  at each wavelength, explained fully in Chapter 2.

In the surface mixed layer (SML),  $a^*_{\text{ps}}$  was 0.79 (range 0.73 - 0.87 (stratified)) and 0.75 (range 0.54 - 0.82) times that of  $a^*_{\text{meas}}$  during CS03 and CS05 respectively. In the thermocline,  $a^*_{\text{ps}}$  was 0.87 (range 0.83 - 0.90) and 0.83 (range 0.74 - 0.89) times that of  $a^*_{\text{meas}}$  for the respective cruises. The means of both  $a^*_{\text{meas}}$  and  $a^*_{\text{ps}}$  between SML and thermocline samples were significantly different during CS03. In contrast, during CS05 the means of  $a^*_{\text{meas}}$  between surface and thermocline samples were significantly different but means of  $a^*_{\text{ps}}$  were not. This result suggests that absorption by NPC contributed significantly to the vertical gradients in  $a^*_{\text{meas}}$  during CS05 (Allali et al. 1997).

### 3.2.4 Chromatic Adaptation

During both cruises PSC:chl-a was significantly greater within the thermocline compared to in the SML (to 95% confidence via a student's T-test (CS03 stratified only)). Figure 3.7 shows the difference between *in situ* wavelength composition of irradiance at the peak of the DCM compared to that at the surface and the corresponding difference in absorption spectra (with absorption by NPC removed). Similar trends were also observed in data from CS03 (not shown).

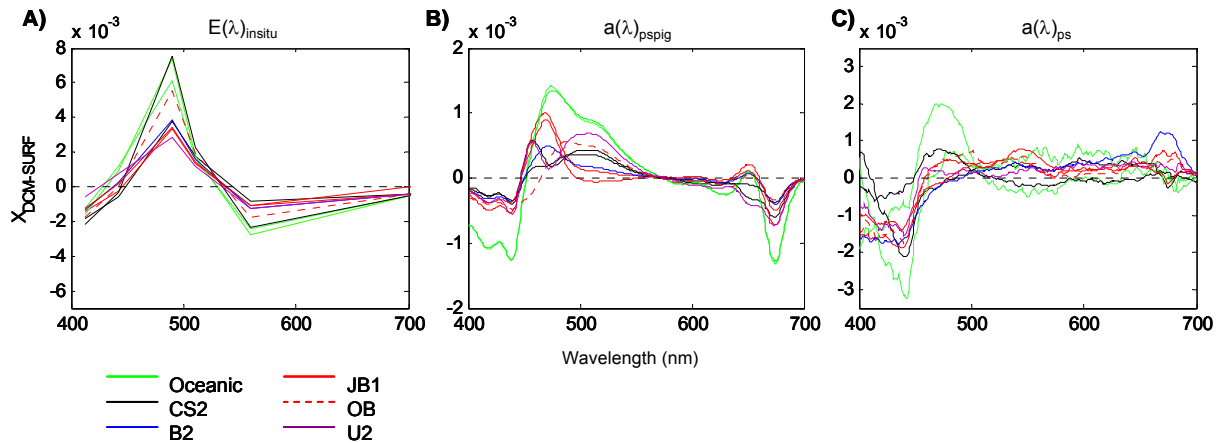


Figure 3.7. The difference in normalised spectral composition between the DCM peak and the surface for A) *in situ* irradiance spectra, B) absorption spectra measured by the pigment reconstruction technique with absorption by non-photosynthetic carotenoids (NPC) removed ( $a(\lambda)_{pspig}$ ), and C) absorption spectra of intact cells measured by the filter technique with absorption by non-photosynthetic carotenoids (NPC) removed ( $a(\lambda)_{ps}$ ). Spectra were normalised to the sum over the range 400-700 nm and then the normalised spectra at the DCM were subtracted from that at the surface (2 m). These figures therefore illustrate the *difference* in the wavelength composition between the surface and DCM. Positive values indicate an increase at the DCM, while negative values indicate a decrease. Coloured lines indicate different locations. Data are presented for CS05 only. Data are to a relative scale with the area under each curve equal to zero.

In each case, spectra were normalised to the total area, and therefore represent the change in the contribution of each wavelength to total PAR, between the surface and DCM. Fig 3.7A illustrates the increase in the contribution of wavelengths 450-520 nm to *in situ* PAR with depth and a decrease in the 400-450 nm contribution. Reconstruction of absorption by photosynthetic pigments ( $a(\lambda)_{pspig}$ ) shows a corresponding increase in absorption of in the range 450-550 nm and decrease between 400-450 nm in the DCM populations compared to those at the surface (Fig. 3.7B). This trend is ubiquitous despite the horizontal and vertical variability in pigment composition and taxonomy across the study area. Absorption by photosynthetic pigments of intact cells ( $a(\lambda)_{ps}$ ) shows a marked decrease in absorption in the range 400-450 nm at the DCM compared to at the surface (Fig. 3.7C), in line with the irradiance spectra, but only a weak increase in absorption between 450-520 nm.

Increased depth resolution of sampling during CS05 allowed investigation of  $a(\lambda)_{pspig}^*$  and  $E(\lambda)_{insitu}$  through the water column (Fig. 3.8). Variability in  $a(\lambda)_{pspig}^*$  wavelength ratio 412:442 nm with depth was significantly correlated with the 412:442 nm ratio of  $E(\lambda)_{insitu}$  ( $n =$

36,  $r^2 = 0.470$ ,  $p < 0.001$ ), This was also true for ratios 490:442 nm ( $n = 36$ ,  $r^2 = 0.405$ ,  $p < 0.001$ ) and 510:442 nm ( $n = 36$ ,  $r^2 = 0.178$ ,  $p = 0.010$ ).

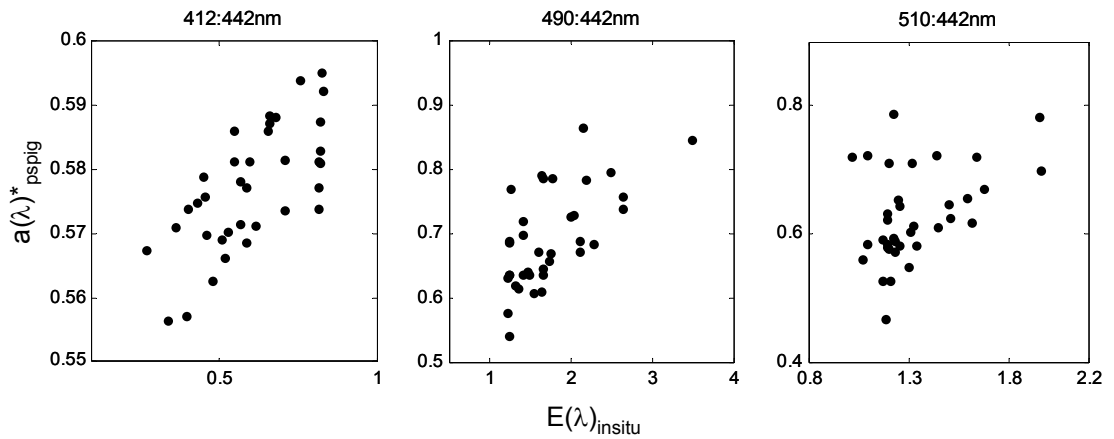


Figure 3.8. Ratios of phytoplankton absorption of photosynthetic pigments as measured by HPLC pigment reconstruction ( $a(\lambda)^*_{pspig}$ ) compared to the variability in the same ratios of *in situ* irradiance ( $E(\lambda)_{insitu}$ ). Data shown for CS05.

Despite the changes in PSC complement of the phytoplankton the absorption of intact cells in the range 450-520 nm was not enhanced at depth (Fig. 3.7C). Following the assumption that the difference in absorption spectra between  $a(\lambda)^*_{pspig}$  and  $a(\lambda)^*_{ps}$  is due to packaging then at the DCM the packaging affect limits the efficiency with which phytoplankton utilise available light at depth. The ‘flattening’ of the absorption spectra by packaging means  $a(\lambda)^*_{ps}$  at the DCM is less similar to  $E(\lambda)_{insitu}$  despite the phytoplankton pigment composition. Importantly, however, the changes in phytoplankton pigment composition would significantly improve the similarity between  $a(\lambda)^*_{meas}$  and  $E(\lambda)_{insitu}$  compared to a situation where there was no change in pigment composition.

At wavelengths  $<600$  nm there was a statistically significant relationship between  $K_d(\lambda)$ , the measured vertical attenuation coefficient, and  $a(\lambda)_{pig}$  for the six wavelengths measured by the optical instrument (not shown) illustrating the impact of phytoplankton absorption on the optical properties of the water column (Kirk 1994). The cause-and-effect of the co-varying phytoplankton absorbance spectra and light penetration is not distinguishable but it is likely that the change in PSC composition of phytoplankton is partly due to the adaptation and/or acclimation of phytoplankton to the change in the total PAR as well as the wavelength distribution of irradiance (e.g. Falkowski and LaRoche 1991).

### 3.3 Directly Measured Physiological Parameters

This section introduces the physiological parameters measured by the  $^{14}\text{C}$  and FRRF methods, with a more thorough investigation and analysis presented in later sections. Some of the ideas and data contained in Moore et al. (2006) are presented in the remainder of this chapter. Moore et al. (2006) presents data from CS03, whilst emphasis here is on the data collected during CS05 in order to support and expand upon the work already published. Moore et al. (2006) is referenced where appropriate.

The  $^{14}\text{C}$  and FRRF-derived physiological values measured during CS05 are shown in Figure 3.9. The definitions of these parameters are provided in Chapter 1.

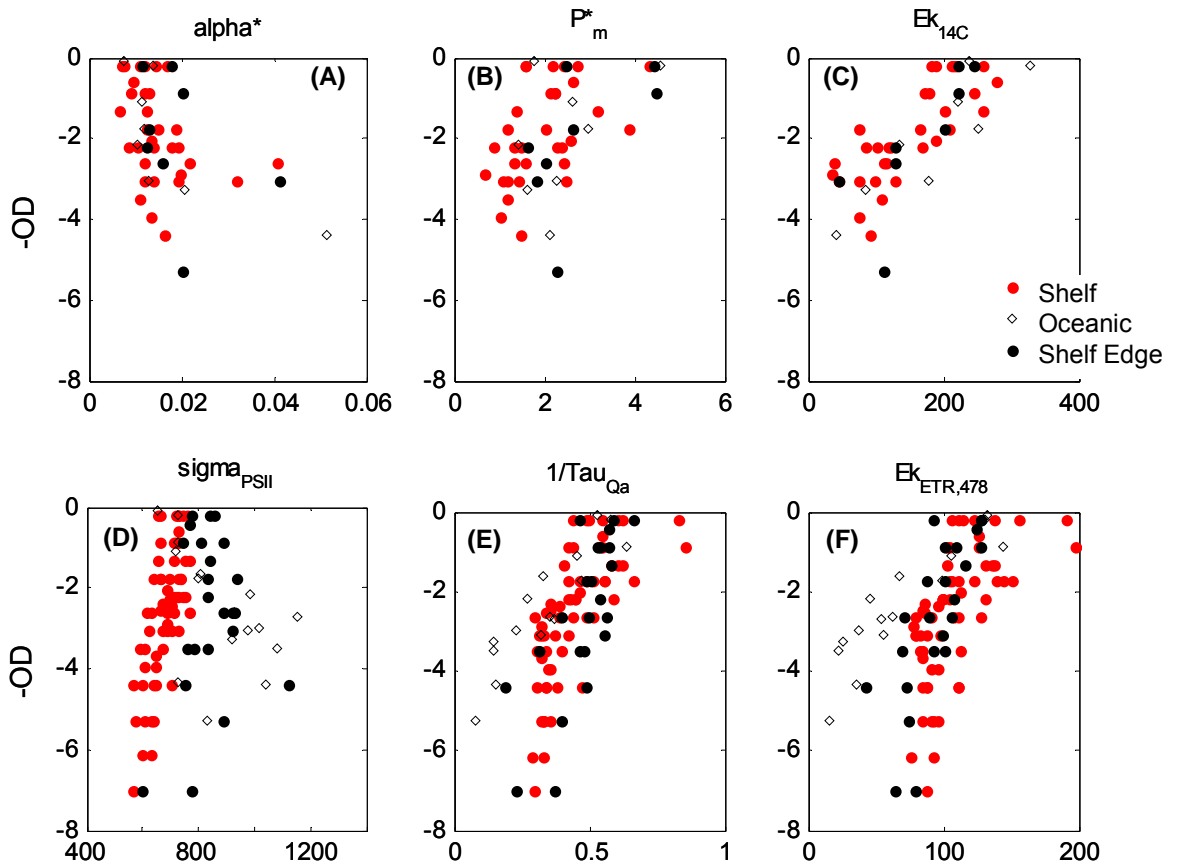


Figure 3.9. Variability in physiological parameters against optical depth. A)  $^{14}\text{C}$ -derived maximum light utilisation coefficient ( $\alpha^*_{14C}$ ), ( $\text{mg C (mg chl-a)}^{-1} \text{ h}^{-1} (\mu\text{E m}^{-2} \text{ s}^{-1})^{-1}$ ). B)  $^{14}\text{C}$ -derived light-saturated photosynthetic rate ( $P_m^*$ ) normalised to chl-a, ( $\text{mg C (mg chl-a)}^{-1} \text{ h}^{-1}$ ), C)  $^{14}\text{C}$ -derived Light saturation parameter ( $E_{k_{14C}}$ ) ( $\mu\text{E m}^{-2} \text{ s}^{-1}$ ), D) FRRF-derived effective absorption cross section  $\sigma_{\text{PSII}}$ , ( $\times 10^{-20} \text{ m}^2 \text{ quanta}^{-1}$ ), E) FRRF-derived electron transport rate from Qa to PQ ( $1/\tau_{\text{Qa}}$ ) ( $\text{s}^{-1}$ ), F) FRRF-derived  $E_{k_{\text{ETR},478}}$  ( $\mu\text{E m}^{-2} \text{ s}^{-1}$ ). Data are presented for CS05 only. Parameters were obtained following methods in Chapter 2. Colours are in legend shown in C). Optical depth was obtained from depth (m)  $\times$   $K_d(\text{PAR}) (\text{m}^{-1})$ .

With the exception of the mixed station (visited during CS03 only) a strong depth dependence was apparent for the  $^{14}\text{C}$ -derived parameters  $P_m^*$  and  $Ek_{14\text{C}}$  and for FRRF-derived  $1/\tau_{\text{Qa}}$  during both cruises.  $^{14}\text{C}$ -derived  $\alpha_{14\text{C}}^*$  remained relatively constant, with a slight increase in the thermocline during CS05 but not CS03 (not shown). There were regional gradients in  $\sigma_{\text{PSII}}$  during both cruises, with some vertical variability during CS05 only.

### 3.3.1 The effect of Spectral Correction

Magnitudes of parameters  $\alpha^*$ ,  $\sigma_{\text{PSII}}$ , and  $Ek$  are dependent on the wavelength of light under which they were measured. Spectral correction was carried out following methods in Chapter 2 and below is a summary of the effect of the spectral correction on the magnitudes of these parameters.

$\alpha_{14\text{C}}^*$  as measured directly from the P vs. E incubator, and  $\alpha_{478}^*$ , (that spectrally-adjusted to the FRRF excitation spectrum), were highly correlated (CS03  $n = 38$ ,  $r^2 = 0.885$ ,  $p < 0.001$ ; CS05  $n = 48$ ,  $r^2 = 0.937$ ,  $p < 0.001$ ) with absolute values of  $\alpha_{478}^*$  factors of 2.3 times (range 2.01- 2.73) and 3.0 times (range 2.5 – 4.0) that of  $\alpha_{14\text{C}}^*$  for CS05 and CS03 respectively.

Values of  $Ek_{478}$  were 0.43 (range 0.37 – 0.57) and 0.34 (range 0.25 - 0.40) times the values of measured  $Ek_{14\text{C}}$  for CS03 and CS05 respectively, while they remained highly correlated (CS03  $n = 38$ ,  $r^2 = 0.933$ ,  $p < 0.001$ ; CS05  $n = 48$ ,  $r^2 = 0.956$ ,  $p < 0.001$ ). However, there was a notable exception at the oceanic stations of CS05 where  $Ek_{478}$  was 0.29 (range 0.25 – 0.31) times that of  $Ek_{14\text{C}}$ . A depth dependence of the relationship between  $Ek_{478}$  and  $Ek_{14\text{C}}$  was evident, particularly during CS03, with  $Ek_{478}:Ek_{14\text{C}}$  reduced in the surface waters (higher  $\alpha_{478}^*:\alpha_{14\text{C}}^*$ ) likely owing to absorption by non-photosynthetic carotenoids in the surface.

Correcting to the *in situ* irradiance spectrum,  $Ek_{\text{insitu}}$ , was a factor of 0.63 (range 0.55 - 0.85) and 0.51 (range 0.36 – 0.60) that of  $Ek_{14\text{C}}$  for CS03 and CS05 respectively, although  $Ek_{14\text{C}}$  and  $Ek_{\text{insitu}}$  were strongly correlated (CS03  $n = 38$ ,  $r^2 = 0.918$ ,  $p < 0.001$ ; CS05  $n = 48$ ,  $r^2 = 0.951$ ,  $p < 0.001$ ).  $\sigma_{\text{PSII}}$  and  $\sigma_{\text{PSII,insitu}}$  were also highly correlated (CS03  $n = 35$ ,  $r^2 = 0.844$ ,  $p < 0.001$ ; CS05  $n = 48$ ,  $r^2 = 0.771$ ,  $p < 0.001$ ). However the difference between  $\sigma_{\text{PSII}}$  and  $\sigma_{\text{insitu}}$  was depth dependent. In the SML,  $\sigma_{\text{insitu}}$  was 0.67 (range 0.62 - 0.75) and 0.62 (range 0.53 - 0.68) times the magnitude of  $\sigma_{\text{PSII}}$  during CS03 and CS05, whilst in the thermocline,  $\sigma_{\text{insitu}}$  was 0.71 (range 0.59 - 0.81) and 0.70 (range 0.63 - 0.77) times  $\sigma_{\text{PSII}}$  for the two cruises. This is due to the FRRF excitation spectrum more closely resembling the *in situ* spectrum at depth compared to at the surface (Moore et al. 2006).

When contributions of non-photosynthetic pigments were removed the quantum yield,  $\Phi_{m,ps}^*$ , was 1.14 (range 1.07 – 1.26) and 1.22 (range 1.09 – 1.51) times that of  $\Phi_m^*$  for CS03 and CS05 respectively, whilst  $E_{k,ps,insitu}$  was a factor of 1.01 (range 1.06 - 1.14) and 1.08 (range 1.05 - 1.13) times  $E_{k,insitu}$  for the two cruises.

### 3.3.2 Coherence between $^{14}C$ and FRRF Techniques

#### *Comparison of $^{14}C$ and FRRF P vs. E curves*

During CS03 samples were held in the light chamber of the bench-top FRRF instrument and exposed to a sequential light gradient. A blue LED cluster was used to provide light ranging from 2-600  $\mu E m^{-2} s^{-1}$  incrementing every five minutes over a total incubation period of one hour. Irradiance was controlled by a microprocessor. The instrument was situated in a constant temperature lab held at *in situ* temperature ( $\pm 2$  °C). Relative light changes were monitored using a CI  $2\pi$  PAR sensor placed beside the sample chamber and the absolute light levels measured within the chamber using a Biospherical Instruments QSL-2000  $4\pi$  PAR sensor. The flash protocol used was the same as that for the *in situ* instrument described by Moore et al. (2006). Sample filtrate was analysed as a blank. The electron transfer rate was plotted against irradiance and the model of Jassby and Platt (1976) fitted to the resulting curve. Subsequently values of  $E_k$ , the light saturation irradiance, via this method were obtained.

The correlation between  $^{14}C$  and FRRF P vs. E derived  $E_k$  is shown in Figure 3.10. The strength of the relative correlation gives confidence in the variability in the techniques. The systematic offset (factor 1.6) discrepancy in the FRRF measurement is likely to be caused by difficulties of accurately measuring the light field in the FRRF instrument sample chamber. Other potential causes of the offset (e.g. small differences in the incubation temperatures, incubation times or bottle (confinement) effects) between incubation types may also contribute to the offset but are unlikely to have caused a large (and relatively systematic) discrepancy.

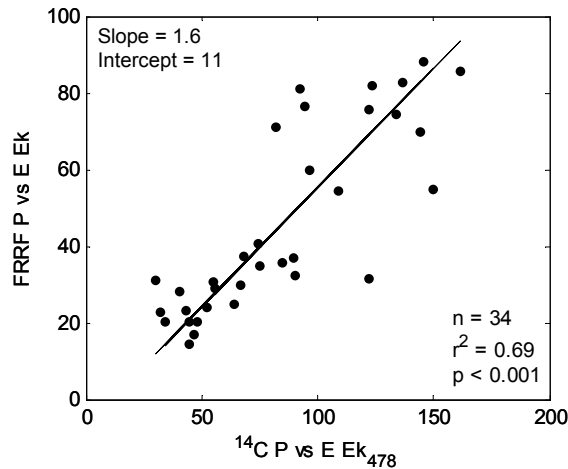


Figure 3.10. Light saturation parameter,  $E_k$  ( $\mu\text{E m}^{-2} \text{s}^{-1}$ ), as derived from  $^{14}\text{C}$  and FRRF light-response curves.  $^{14}\text{C}$ -derived  $E_{k478}$  is corrected for the excitation spectrum of the FRRF. Statistics shown are the result of model II regression analysis.

#### *Independent measurement of RCII:Chl-a*

During CS03 measurement of RCII abundance was carried out following methods of Suggett et al. (2004) and used to obtain an independent estimate of  $\sigma_{\text{PSII}}$  via equation 3.1 (Suggett et al. 2004, Moore et al. 2006):

$$\sigma_{\text{PSII},478\text{calc}} = \frac{a_{ps,478}^* \cdot 0.5F_{730} : a^*}{\text{RCII} : \text{Chla}} \quad (3.5)$$

Where  $a_{ps,478}^*$  refers to the absorption spectra of phytoplankton corrected for the absorbance under an FRRF spectrum,  $0.5F_{730} : a^*$  represents the proportion of light transferred to PSII, estimated by scaling the measured fluorescence excitation spectrum to the absorption spectrum (see Suggett et al. (2004) and references therein). The estimates of  $\sigma_{\text{PSII}}$  by this method and those obtained directly from FRRF measurement were well correlated ( $n = 13$ ,  $r^2 = 0.558$ ,  $p < 0.005$ ) and of similar magnitude, giving confidence in the measurement of  $\sigma_{\text{PSII}}$  from the FRRF (Moore et al. 2006). Measured values of RCII:Chl-a were lowest in the surface at CS3 (527 mol:mol), where high number of *Synechococcus* were present, and were 717 and 703 (mol:mol) at CS1 and the shelf edge respectively (Moore et al. 2006). These values are consistent with laboratory data (Suggett et al. 2004).

### 3.3.3 Diel Variability

All samples during CS05 were collected before dawn. In contrast, during CS03 ~60% of physiological measurements were carried out on samples taken during the day. Figure 3.11 shows the diel variability of the physiological measurements for available locations (Moore et al. 2006).

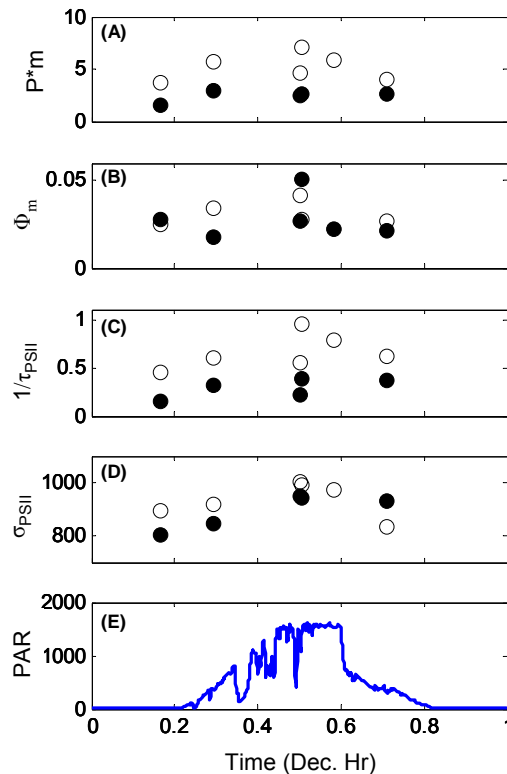


Figure 3.11. Diel variability of physiological parameters at CS3 obtained on JD=217 and JD=222 during CS03. A) light-saturated photosynthetic rate ( $P^*_m$ ) normalised to chl-a, ( $\text{mg C (mg chl-a)}^{-1} \text{ h}^{-1}$ ), B)  $^{14}\text{C}$ -derived maximum quantum yield of photosynthesis ( $\Phi_m$ ) ( $\text{mol C (mol photons)}^{-1}$ ), C) FRRF-derived electron turnover rate from Qa to PQ ( $1/\tau_{Qa}$ ), ( $\text{s}^{-1}$ ), D) FRRF-derived effective absorption cross section  $\sigma_{\text{PSII}}$ , ( $\times 10^{-20} \text{ m}^2 \text{ quanta}^{-1}$ ). E) Incident surface PAR on JD=217 (2003) ( $\mu\text{E m}^{-2} \text{ s}^{-1}$ ). Open circles represent surface samples and closed circles are samples from the thermocline. Parameters were obtained following methods in Chapter 2 (Moore et al. 2006).

Diel variability was evident in parameters relating to electron transfer rates and carbon fixation. In particular, at one instance in the SML at CS3 (when the phytoplankton population was dominated by *Synechococcus*)  $1/\tau_{\text{PSII}}$  at midday was approximately double the pre-dawn value on the 10<sup>th</sup> of August 2003 (JD=222, Fig. 3.11). However, across all available data, daytime

samples only increased the mean of  $P_m^*$  and  $1/\tau_{PSII}$  by 12% and 12.5% respectively with the difference between dawn and midday casts significantly less than the variability in parameter values between and within stations (both parameters exhibiting standard deviations of ~50%) (Moore et al. 2006). Diel variability of  $\Phi_m$  was negligible, with  $\sigma_{PSII}$  exhibiting only a ~10% increase in magnitude at midday. Diel variability was most pronounced in the surface with little evidence of diel variability at the DCM (Moore et al. 2006). Daytime samples have been included in this analysis.

### 3.3.4 Depth Variability

During CS05 physiological parameters were obtained at four depths corresponding to the top and base of the SML and the upslope and peak of the DCM, as defined by the chl-a profile at the time of sampling. The latter two samples were within the thermocline. The results of one-way ANOVA tests, indicating the variability of the physiological parameters between the four depth horizons, are given in Table 3.1.

Table 3.1. The significance test (ANOVA) between means of physiological parameters at each of four sample depths. Sample depths were chosen by the chl-a profile for each CTD cast and are labelled as a = surface (~2 m), b = base of SML, y = upslope of DCM, z = peak of DCM. a and b were within the SML, y and z were within the thermocline. The table groups the depths where parameter means are statistically indistinguishable to the 95% confidence level. For example, for  $\alpha_{14C}^*$ , the means of depths a,b,y are all indistinguishable, but different to z. For  $1/\tau_{Qa}$ , the mean of a is indistinguishable from b but different to y and z, whilst mean of b is indistinguishable from a and y. The table includes all data from CS05.

<b>14C</b>		<b>FRRF</b>	
$\alpha_{14C}^*$	a,b,y z	$\sigma_{PSII}$	a,b,y,z
$P_m^*$	a,b y,z	$1/\tau_{Qa}$	a,b a,b,y b,y,z y,z
$Ek_{14C}$	a,b y z	$Ek_{ETR,478}$	a,b a,b,y b,y,z y,z

The  $^{14}\text{C}$ -derived  $\alpha^*_{14\text{C}}$  was significantly different at the peak of the DCM only, whilst  $P^*_m$  was significantly different between the SML and thermocline, but not within these layers. This resulted in values of  $E_{k_{14\text{C}}}$  that were not significantly different between the top and bottom of the SML but the two depths in the thermocline were each significantly different from all others.

In contrast to the  $^{14}\text{C}$ -derived parameters, those obtained via FRRF showed no distinctly different depth horizons.  $\sigma_{\text{PSII}}$  was not significantly different at between any depths whilst  $E_{k_{\text{ETR},478}}$  and  $1/\tau_{\text{Qa}}$  gradually increased with means generally statistically indistinguishable from those of neighbouring depths.

Insignificant variability in physiological parameters between the top and bottom of the SML indicates that the rate of mixing was greater than that of photoacclimation (Cullen and Lewis 1988), however, a small degree of variability is implied in Figure. 3.9.

### 3.4 Light Harvesting Parameters

This section provides a detailed account of the variability in the physiological parameters related to light capture (namely,  $^{14}\text{C}$ -derived  $\alpha^*$  and  $\Phi_m$ , and FRRF-derived  $\sigma_{\text{PSII}}$ ). A similar account for parameters related to light-saturated rates of photosynthesis ( $P^*_m$ ) and PSII electron transport ( $1/\tau_{\text{Qa}}$  and  $1/\tau_{\text{PSII}}$ ) is given in Section 3.5. The variability in  $E_k$  is addressed in Section 3.6. The chapter concludes with an investigation and discussion into the mechanisms of photoacclimation.

#### 3.4.1 $\sigma_{\text{PSII}}$

By definition, the effective absorption cross section,  $\sigma_{\text{PSII}}$ , is directly proportional to the PSII specific light absorption and the amount of photosynthetic pigment and is inversely correlated to pigment packaging (Falkowski and Raven 1997). Cell size may thus also influence  $\sigma_{\text{PSII}}$  as larger cells typically have lower PSC:chl-a and are more susceptible to packaging compared to small cells (Morel and Bricaud 1981, Moore et al. 2005). However, the importance of taxonomic variability in field conditions on measurement of  $\sigma_{\text{PSII}}$  remains poorly understood (Moore et al. 2006).

As shown in Figure 3.12,  $\sigma_{\text{PSII}}$  was correlated to PSC:chl-a (CS03  $n = 20$ ,  $r^2 = 0.474$ ,  $p < 0.001$ ; CS05  $n = 58$ ,  $r^2 = 0.49$ ,  $p < 0.001$ ) and  $a^*_{\text{pig}}$  (CS03  $n = 24$ ,  $r^2 = 0.215$ ,  $p = 0.023$ ; CS05  $n = 57$ ,  $r^2 = 0.3468$ ,  $p < 0.001$ ). Figure 3.12 also illustrates that variability in PSC:chl-a and  $a^*_{\text{pig}}$  were not dominated by optical depth.

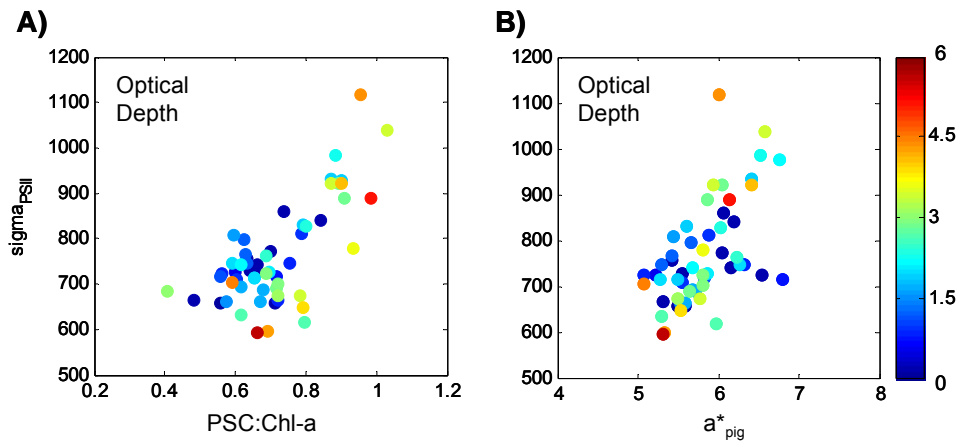


Figure 3.12. Effective absorption cross section,  $\sigma_{\text{PSII}}$ , ( $\times 10^{-20} \text{ m}^2 \text{ quanta}^{-1}$ ) against A) photosynthetic carotenoid (PSC) concentration per unit chl-a (g:g) and B) phytoplankton absorption per unit chl-a,  $a^*_{\text{pig}}$ , ( $\text{m}^2 \text{ (mg chl-a)}^{-1}$ ) for CS05 only. Colour scale is optic depth, estimated from sample depth  $\times K_d(\text{PAR})$ .

Regardless of sample depth, the magnitude of  $\sigma_{\text{PSII}}$  was significantly different between shelf, shelf edge, oceanic and mixed regions (with the exception of between shelf-edge and shelf during CS05) to the 95% confidence level (according to one-way ANOVA).

The variability in  $\sigma_{\text{PSII}}$  with phytoplankton taxonomy is investigated using marker pigments, as obtained by HPLC. Three major pigments were 19'-butanoyloxyfucoxanthin (But), 19'-hexanoyloxyfucoxanthin (Hex), and fucoxanthin (Fuc). These pigments are often considered marker pigments reflecting the presence of pelagophytes, prymnesiophytes and diatoms respectively, although marker pigments are not unique to phytoplankton types, for example, Fuc is also found in prymnesiophytes (Jeffrey et al. 1997).

Detailed description of taxonomic composition across the study area can be found in Chapter 4. In summary, during both cruises phytoplankton assemblage was mixed and contained small pelagophytes and prymnesiophytes. CS03 exhibited similar taxonomic distribution in the surface and the thermocline in contrast to CS05 where taxonomy varied with depth as well as location. In particular, during CS05, the phytoplankton size structure varied with depth in the stratified region, and microscope counts indicated the periodic occurrence of some larger diatoms in the thermocline.

During CS03 variability in  $\sigma_{\text{PSII}}$  was highly correlated to the pigment ratios But:chl-a and Hex:chl-a over the study area (But  $n = 23$ ,  $r^2 = 0.613$ ,  $p < 0.001$ ; Hex  $n = 23$ ,  $r^2 = 0.488$ ,  $p < 0.001$ , Fig. 3.13, also Moore et al. 2006). The horizontal trends in  $\sigma_{\text{PSII}}$  followed the horizontal gradients in these pigment ratios from the oceanic region to the mixed waters.

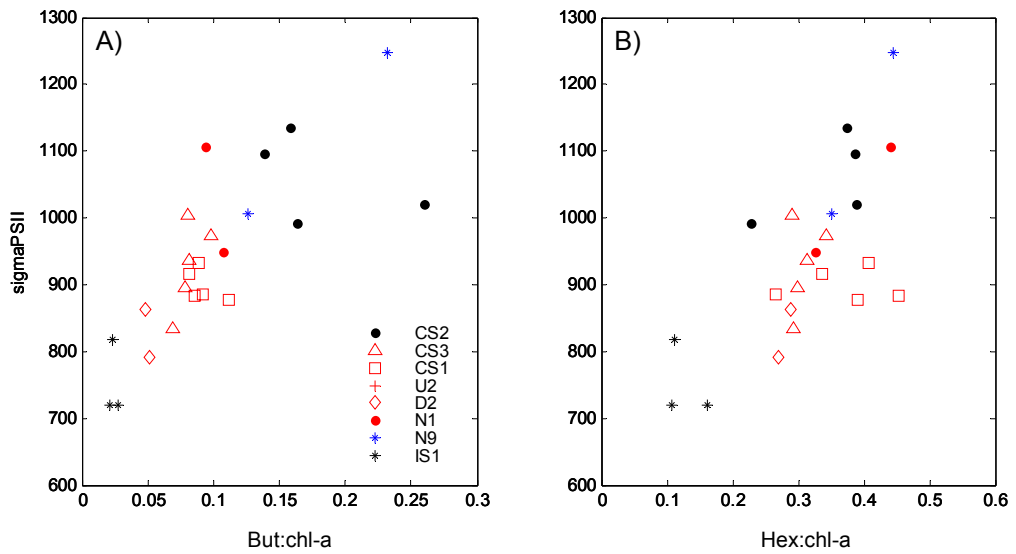


Figure 3.13. Relationship between effective absorption cross section,  $\sigma_{PSII}$ , ( $\times 10^{-20} \text{ m}^2 \text{ quanta}^{-1}$ ) and A) But:Chl-a ratio (g:g), and B) Hex:Chl-a ratio (g:g) during CS03 (Moore et al. 2006).

A significant correlation between  $\sigma_{PSII}$  and the pigment ratios was also observed during CS05 (But  $n = 58$ ,  $r^2 = 0.268$ ,  $p < 0.001$ ; Hex  $n = 58$ ,  $r^2 = 0.112$ ,  $p = 0.010$ , Fig. 3.14), though gradients in taxonomic composition occurred with depth as well as location.

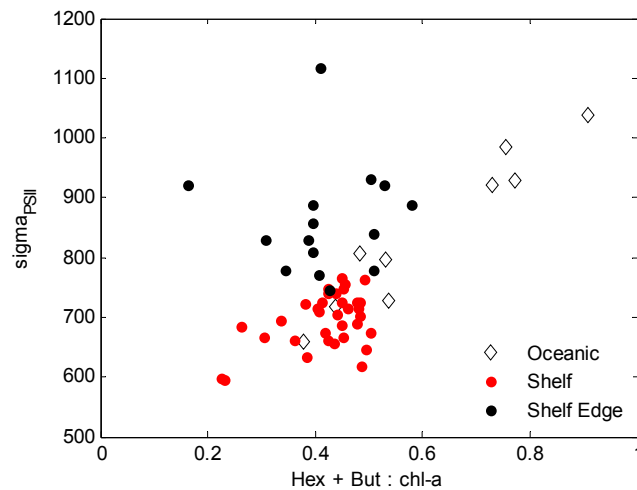


Figure 3.14. Relationship between effective absorption cross section,  $\sigma_{PSII}$ , ( $\times 10^{-20} \text{ m}^2 \text{ quanta}^{-1}$ ) and But+Hex:Chl-a ratio during CS05.

During both cruises the highest values of  $\sigma_{\text{PSII}}$  occurred at the shelf edge and within the DCM in the oceanic region where the concentrations of But:chl-a and Hex:chl-a were greatest. During CS05, in the oceanic region the vertical distribution of But+Hex:chl-a explained 95% of the variability in  $\sigma_{\text{PSII}}$  ( $n = 8$ ,  $r^2 = 0.953$ ,  $p < 0.001$ ). In contrast, during CS05 the relationship between  $\sigma_{\text{PSII}}$  and But+Hex:chl-a was not significant at the shelf edge, where Fuc:chl-a was ~50% greater than on the shelf. These data strongly suggest that the magnitude of  $\sigma_{\text{PSII}}$  is related to phytoplankton community structure, as indicated by the contribution of marker pigments to chl-a. The effect of pigment packaging may further contribute to the variability in  $\sigma_{\text{PSII}}$ , particularly due to the taxonomic dependence of packaging due to both cell size and phytoplankton morphology (Bricaud et al. 2004).

On the shelf during CS05 there was a significant positive correlation between  $\sigma_{\text{PSII}}$  and  $\text{Qa}_{440}$  ( $n = 29$ ,  $r^2 = 0.213$ ,  $p = 0.012$ ) whilst there was no correlation between  $\sigma_{\text{PSII}}$  and  $\text{Qa}(440)$  in the oceanic region potentially reflecting the dependence of  $\sigma_{\text{PSII}}$  on the package effect.

There was no evidence of variability in  $\sigma_{\text{PSII}}$  due to photoacclimation to low light levels in the Celtic Sea region. It is possible that a variation in  $\sigma_{\text{PSII}}$  due to photoacclimation is present in conjunction with taxonomic variability, but it is not distinguishable in these data.

During both cruises  $\sigma_{\text{PSII}}$  and Fv/Fm co-varied across the study region (CS03  $n = 40$ ,  $r^2 = 0.374$ ,  $p < 0.001$  (all data); CS05  $n = 101$ ,  $r^2 = 0.658$ ,  $p < 0.001$ ). It thus follows that variability of Fv/Fm was probably also dominated by phytoplankton taxonomic composition.

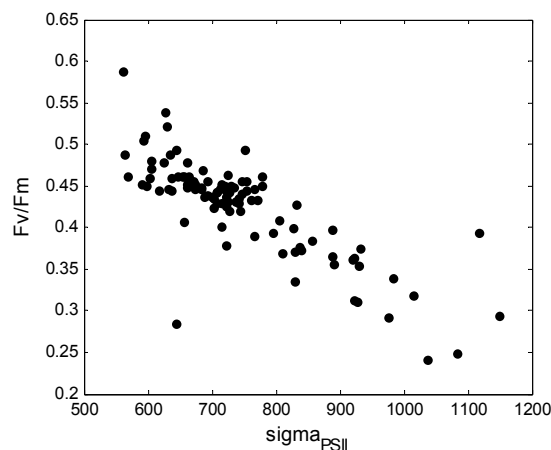


Figure 3.15. Relationship between the effective absorption cross section,  $\sigma_{\text{PSII}}$ , ( $\times 10^{-20} \text{ m}^2 \text{ quanta}^{-1}$ ) and the quantum efficiency of photochemistry, Fv/Fm, as determined from FRRF (Chapter 2). Data are CS05 only.

### 3.4.2 $\alpha^*$ and $\Phi_m$

Values of  $\alpha^*_{\text{insitu}}$  compared well to those measured in the Celtic Sea by Pemberton et al (2004). Values of the maximum quantum yield of photosynthesis,  $\Phi_m$ , ranged from 0.028 $\pm$ 0.011 to 0.049 $\pm$ 0.028 from surface to DCM in the Celtic Sea during 2003 and 0.017 $\pm$ 0.006 to 0.028 $\pm$ 0.015 during 2005. Thus values of  $\Phi_m$  ranged from 22 – 39% and 14 – 22% of the theoretical maximum of 0.125 (mol C (mol photons)<sup>-1</sup>) (Falkowski and Raven 1997) which is in an acceptable range for phytoplankton (Raateoja et al. 2004).

An increase in  $\alpha^*_{14C}$  with optical depth was evident during CS05, with a significant increase at the DCM (Table 3.1) (CS05 n = 48,  $r^2 = 0.219$ ,  $p < 0.001$ , Fig. 3.9). In contrast,  $\alpha^*_{14C}$  did not vary significantly with depth during CS03 (not shown). A significant correlation was evident between  $\alpha^*_{14C}$  and PSC:chl-a during CS05 (CS05 n = 45,  $r^2 = 0.136$ ,  $p = 0.013$ ), though the correlation between  $\alpha^*_{14C}$  and  $a^*_{\text{meas}}$  was not significant during either cruise.

$\alpha^*_{14C}$  and  $\Phi_m$  were significantly correlated (CS03 n = 38,  $r^2 = 0.464$ ,  $p < 0.001$ ; CS05 n = 48,  $r^2 = 0.827$ ,  $p < 0.001$ ), though, in contrast to  $\alpha^*_{14C}$ ,  $\Phi_m$  significantly increased with optical depth during CS03 as well as CS05 (CS03 stratified n = 31,  $r^2 = 0.144$ ,  $p = 0.035$ ; CS05 n = 48,  $r^2 = 0.328$ ,  $p < 0.001$ ). During both cruises high values of  $\alpha^*_{14C}$  and  $\Phi_m$  occurred periodically within the DCM (e.g. Fig 3.9), but it was not possible to determine the cause of these anomalous values.

During CS05 (excepting the periodically high values)  $\alpha^*_{478}$  was significantly (though weakly) correlated to  $\sigma_{\text{PSII}}$  (CS05 n = 42,  $r^2 = 0.117$ ,  $p = 0.027$ ). For all stratified shelf stations there was a significant inverse relationship between  $\Phi_m$  and  $\sigma_{\text{PSII}}$  (CS05 n = 32,  $r^2 = 0.259$ ,  $p = 0.003$ ). Overall the poor correlation between <sup>14</sup>C-derived parameters ( $\alpha^*_{14C}$  and  $\Phi_m$ ) and FRRF-derived  $\sigma_{\text{PSII}}$  potentially indicates that processes influencing light harvesting apparatus of PSII alone compared to PSI+PSII combined were not the same.

Representing the carbon fixed per unit of light absorbed, the magnitude of  $\Phi_m$  differs from  $\alpha^*$  by a factor equivalent to the absorption spectra  $a^*_{\text{meas}}$ . In contrast to  $\alpha^*_{14C}$ , the depth variability in  $\Phi_m$  is therefore sensitive to changes in  $a^*_{\text{meas}}$  and in these data  $\Phi_m$  was significantly (inversely) correlated to  $a^*_{\text{meas}}$  during both cruises (CS03 stratified n = 33,  $r^2 = 0.506$ ,  $p < 0.001$ ; CS05 n = 48,  $r^2 = 0.115$ ,  $p = 0.018$ ), these relationships were weaker when absorption by NPC was not removed.

During CS05,  $\Phi_m$  was inversely correlated to NPC:PSC (CS05 n = 45,  $r^2 = 0.195$ ,  $p = 0.002$ , Figure 3.16) indicating that the carbon fixed per unit light absorbed was reduced when the proportion of non-photosynthetic carotenoids was high (MacIntyre et al. 2002). Further, the relationship between the maximum quantum yield estimated for light absorbed by

photosynthetic carotenoids only ( $\Phi_{m,ps}$ ) and NPS:PSC was not significant. It follows that low quantum yield of photosynthesis may be associated with high phytoplankton absorption, partly due to absorption by NPC near the surface (Babin et al. 1996). However, an increase in  $\Phi_{m,ps}$  with optical depth was still present indicating that the presence of NPS were not the only factor determining the variability in  $\Phi_m$ .

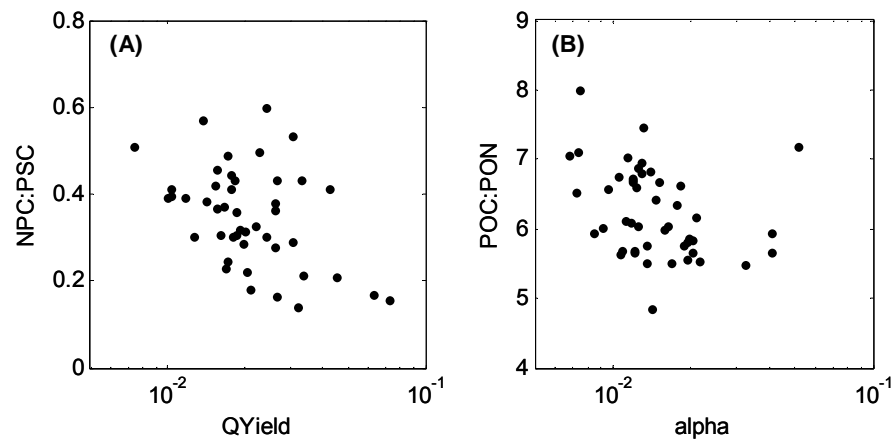


Figure 3.16. A) Relationship between, the maximum quantum yield of photosynthesis, ( $\Phi_m$ ) ( $\text{mol C (mol photons)}^{-1}$ ) and non-photosynthetic carotenoids to photosynthetic carotenoids ratio (NPC:PSC) (g:g) during CS05, pigments composing NPC and PSC are as stated in Chapter 2. B) Relationship between the maximum light utilisation coefficient ( $\alpha^*_{14C}$ ) ( $\text{mg C (mg chl-a)}^{-1} \text{h}^{-1}$  ( $\mu\text{E m}^{-2} \text{s}^{-1}$ ) $^{-1}$ ) and particulate organic carbon to nitrogen (POC:PON) (g:g) ratio during CS05.

Inter-specific differences in  $\Phi_m$  have been observed in culture (e.g. Langdon 1988), but there were no significant relationships between  $\alpha^*_{14C}$  or  $\Phi_m$  and pigment ratios during either cruise. However, the fact that a depth variability in  $\alpha^*_{14C}$  and  $\Phi_m$  was more pronounced during CS05 compared to CS03, when vertical gradients in taxonomy were also observed, suggests that taxonomic variability in  $\alpha^*_{14C}$  or  $\Phi_m$  should not be ruled out.

Excepting the high  $\alpha^*_{14C}$  values, a significant correlation was evident between  $\alpha^*_{14C}$  (and  $\Phi_m$ ) and the POC:PON ratio during CS05 ( $\alpha^*_{14C}$  CS05  $n = 43$ ,  $r^2 = 0.220$ ,  $p = 0.002$ , Fig 3.16B). No POC:PON data were available for CS03. There was also a significant correlation between  $\alpha^*_{14C}$  and nitrate concentration during CS05 ( $n = 44$ ,  $r^2 = 0.248$ ,  $p < 0.001$ ). Such relationships may indicate a dependence of  $\alpha^*_{14C}$  and  $\Phi_m$  on nutrient availability (Babin et al. 1996). However, this evidence is not conclusive since both POC:PON and nitrate concentration vary with depth, and other sources of the depth variability in  $\alpha^*_{14C}$  cannot be excluded. It should

also be noted that phytoplankton typically account for < 10% of total POC in the stratified Celtic Sea shelf (Holligan et al. 1984b).

In order to further investigate the effect of the potential influence of nutrient availability on  $\alpha^*_{14C}$ , a tidal amplitude index (TAI) was assigned for data from CS05. Values of TAI ranged from 0-2 where 0 and 2 represent the occurrence of neap tides, and 1 a spring tide. Figure 3.17 illustrates that  $\alpha^*_{14C}$  in the DCM may be correlated to the spring-neap tidal cycle.

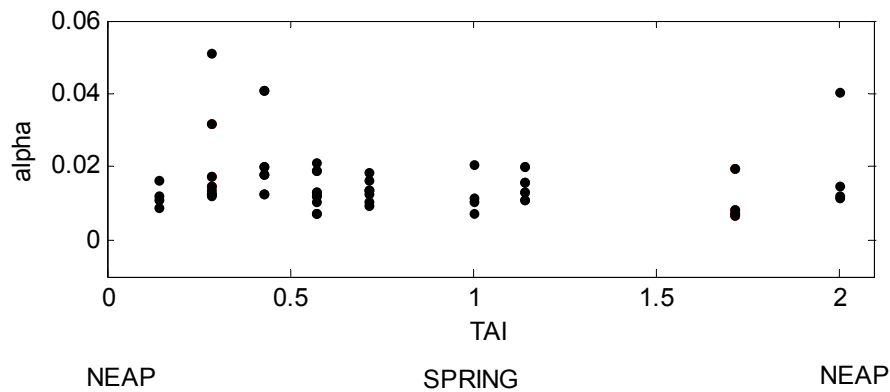


Figure 3.17. Relationship between the maximum light utilisation coefficient ( $\alpha^*_{14C}$ ) ( $\text{mg C (mg chl a)}^{-1} \text{h}^{-1}$  ( $\mu \text{E m}^{-2} \text{s}^{-1}$ ) $^{-1}$ ) and the Tidal Amplitude Index (TAI). TAI is relative scale ranging from 0-2 where 0 and 2 represent the occurrence of neap tides, and 1 a spring tide. Data shown are from CS05 only.

Figure 3.17 suggests that  $\alpha^*_{14C}$  may be higher around neap tides and of particular note the four high  $\alpha^*_{14C}$  and  $\Phi_m$  values (Fig. 3.9) occur close to neap tides. However, the correlation between  $\alpha^*_{14C}$  and TAI was not significant according to correlation analysis, and more data would be required to support this hypothesis.

From these data, it is not possible to determine a dominant factor influencing the variability in  $\alpha^*_{14C}$  and  $\Phi_m$ . Variability in phytoplankton taxonomy, light (and subsequent responses leading to changes in NPC:PSC and pigment packaging) or nutrient availability cannot be identified as individual causal factors, but they cannot be ruled out and may act in combination (Babin et al. 1996, Marra et al. 2000).

### 3.5 Electron Transfer Parameters

#### 3.5.1 $P^*_m$ and $Ek_{14C}$

Magnitudes of  $P^*_m$  were similar to those obtained previously in the Celtic Sea by Pemberton et al. (2004). Variability in the light saturated photosynthetic rates and light saturation parameter,  $Ek_{14C}$ , obtained during CS05 supported the findings of CS03 presented in Moore et al. (2006).

Across the stratified regions the variability in  $P^*_m$  with optical depth was highly significant (CS03 ‘stratified’  $n = 31$ ,  $r^2 = 0.496$ ,  $p < 0.001$ ; CS05  $n = 48$ ,  $r^2 = 0.220$ ,  $p < 0.001$ , Fig. 3.19B). Optical depth also accounted for 69.4 % and 60.7 % of the variability of  $Ek_{14C}$  during CS03 and CS05 respectively (CS03 ‘stratified’  $n = 31$ ,  $r^2 = 0.693$ ,  $p < 0.001$ ; CS05  $n = 48$ ,  $r^2 = 0.607$ ,  $p < 0.001$ ), with a four-fold decrease in  $Ek_{14C}$  from the surface to the DCM (Fig. 3.19C). The variability in  $Ek_{14C}$  was dominated by a change of similar magnitude in  $P^*_m$ , with  $P^*_m$  accounting for 70.1% and 50.0% of the variability in  $Ek_{14C}$  for CS03 and CS05 respectively (CS03 ‘stratified’  $n = 33$ ,  $r^2 = 0.701$ ,  $p < 0.001$ ; CS05  $n = 48$ ,  $r^2 = 0.505$ ,  $p < 0.001$ ).  $P^*_m$  and  $Ek_{14C}$  did not vary significantly between locations during either cruise.

During CS05,  $\alpha^*_{14C}$  contributed 30% to the variability of  $Ek_{14C}$  (CS05  $n = 48$ ,  $r^2 = 0.304$ ,  $p < 0.001$ ), in contrast to only 12% during CS03 (CS03  $n = 38$ ,  $r^2 = 0.124$ ,  $p = 0.030$ ). This was likely to be due, at least in part, to enhanced vertical variability in  $\alpha^*_{14C}$  during CS05 compared to CS03 (described above). There was no correlation between  $P^*_m$  (or  $Ek_{14C}$ ) and PSC:chl-a or nutrient availability that could not conversely be explained by co-variability of these parameters with depth. There was also no correlation between  $P^*_m$  or  $Ek_{14C}$  with POC:PON. As described by Moore et al. (2006), these data indicate that optical depth was the dominant factor in the variability of  $Ek_{14C}$  and that changes in  $Ek_{14C}$  were dominated by  $P^*_m$ , rather than  $\alpha^*_{14C}$ .

#### 3.5.2 $1/\tau_{Qa}$ and $Ek_{ETR,478}$

There was a significant correlation between FRRF-derived  $Ek$  ( $Ek_{ETR,478}$ ) and  $^{14}C$ -derived  $Ek$  corrected to the excitation spectrum of the FRRF ( $Ek_{478}$ ) (Fig. 3.18A) (CS03  $n = 35$ ,  $r^2 = 0.462$ ,  $p < 0.001$  (Moore et al., 2006); CS05  $n = 47$ ,  $r^2 = 0.400$ ,  $p < 0.001$ ).  $Ek_{ETR,478}$  was 2-fold and 1.3-fold greater than  $Ek_{478}$  during CS05 and CS03 respectively.

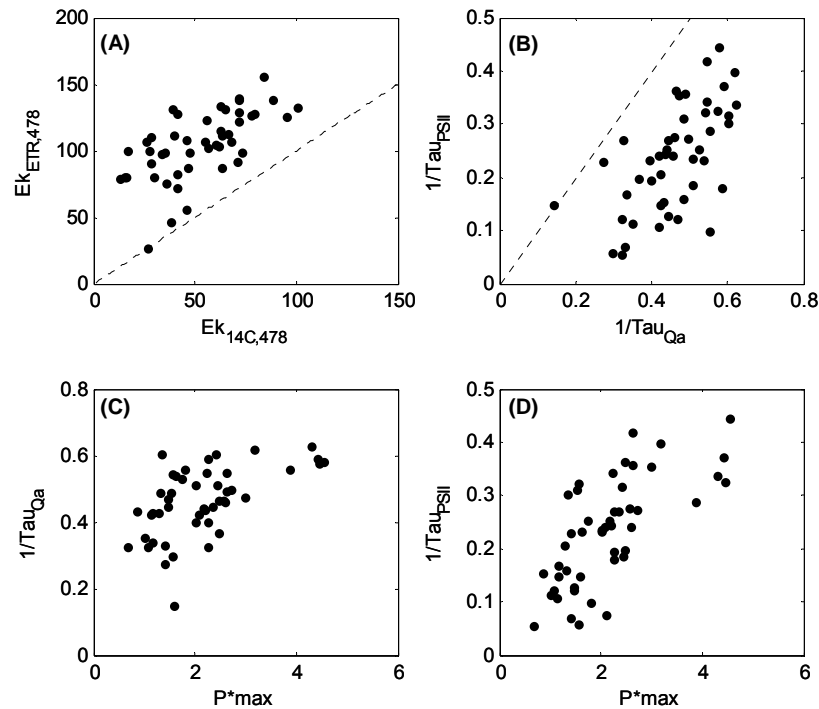


Figure 3.18. A) Relationship between light saturation parameter derived by  $^{14}C$  ( $Ek_{478}$ ) and FRRF ( $Ek_{ETR,478}$ ) ( $\mu E m^{-2} s^{-1}$ ).  $^{14}C$ -derived  $Ek$  is expressed relative to the irradiance excitation spectrum of the FRRF. B) Relationship between electron transport rates from Qa-PQ ( $1/\tau_{Qa}$ ) ( $s^{-1}$ ) and through the whole-chain ( $1/\tau_{PSII}$ ) ( $s^{-1}$ ) estimated from  $166030 \times (\sigma_{PSII} / Ek_{478})$ . C) Relationship between  $1/\tau_{Qa}$  and the light-saturated photosynthetic rate ( $P^*_{m}$ ), ( $mg C (mg chl-a)^{-1} h^{-1}$ ), and D) Relationship between  $1/\tau_{PSII}$  and  $P^*_{m}$ . Data shown from CS05 only. Dotted line indicates 1:1 relationship.

Variability in  $Ek_{ETR,478}$  was significantly correlated to optical depth (CS03 stratified  $n = 28$ ,  $r^2 = 0.391$ ,  $p < 0.001$  (Moore et al., 2006); CS05  $n = 100$ ,  $r^2 = 0.327$ ,  $p < 0.001$ ) and  $1/\tau_{Qa}$  accounted for 73% and 83% of variability in  $Ek_{ETR,478}$  for CS03 and CS05 respectively. In contrast,  $\sigma_{PSII}$  contributed only 52% and 12% of the variability in  $Ek_{ETR,478}$  for the two cruises. The effect of taxonomic influence on  $\sigma_{PSII}$  is reflected in  $Ek_{ETR,478}$  by the (inverse) correlation of this parameter and the pigment ratios during CS03 (But+Hex:chl-a,  $n = 23$ ,  $r^2 = 0.577$ ,  $p < 0.001$ ; Fuc:chl-a,  $n = 23$ ,  $r^2 = 0.206$ ,  $p = 0.030$ ). Variability in  $\sigma_{PSII}$  due to pigment ratios appeared to be offset by  $1/\tau_{Qa}$  such that  $Ek_{ETR,478}$  was acclimated to the light gradient. This is confirmed by the inverse correlation of  $1/\tau_{Qa}$  and pigment ratios (Hex+But:chl-a,  $n = 25$ ,  $r^2 = 0.230$ ,  $p = 0.005$ , Fuc:chl-a  $n = 25$ ,  $r^2 = 0.310$ ,  $p = 0.004$ ). In contrast, during CS05 the vertical gradients in taxonomy and  $\sigma_{PSII}$  varied with location such that no significant correlations between pigment ratios and  $Ek_{ETR,478}$  or  $1/\tau_{Qa}$  were subsequently observed.

In general, variability in  $Ek_{ETR,478}$  was dominated by variability in  $1/\tau_{Qa}$  rather than  $\sigma_{PSII}$  and varied in response to vertical gradients in irradiance (Moore et al. 2006). It follows that the trend in the  $^{14}C$ -derived  $Ek_{14C}$  and  $P^*_m$  was supported by the FRRF measurements.

The vertical gradients in  $P^*_m$  were explained by a significant proportion of the variance of  $1/\tau_{Qa}$  (Fig. 3.18C, CS03  $n = 37$ ,  $r^2 = 0.340$ ,  $p < 0.001$  (Moore et al. 2006), CS05  $n = 47$ ,  $r^2 = 0.315$ ,  $p < 0.001$ ) indicating that the maximal rates of carbon fixation were correlated with the electron transfer rates from Qa to the PQ pool (Sukenik et al. 1987, Moore et al. 2006). Estimation of whole-chain electron transfer rates ( $1/\tau_{PSII}$ ) from  $^{14}C$ -derived  $Ek_{478}$  and  $\sigma_{PSII}$  (Eqn. 1.10) were well correlated to  $1/\tau_{Qa}$  (Fig 3.18B, CS03  $n = 35$ ,  $r^2 = 0.404$ ,  $p < 0.001$  (Moore et al. (2006); CS05  $n = 47$ ,  $r^2 = 0.379$ ,  $p < 0.001$ ). The whole chain electron transfer ( $1/\tau_{PSII}$ ) accounted for 17.5% and 23.6% of the variability in  $Ek_{ETR,478}$  for CS03 and CS05 respectively (CS03  $n = 35$ ,  $r^2 = 0.175$ ,  $p = 0.013$ ; CS05  $n = 47$ ,  $r^2 = 0.237$ ,  $p < 0.001$ ), and was significantly correlated to optical depth (CS03 stratified  $n = 28$ ,  $r^2 = 0.727$ ,  $p < 0.001$ ; CS05  $n = 48$ ,  $r^2 = 0.523$ ,  $p < 0.001$ ).

During CS03 independent measurements of RCII:chl-a (described above) showed only a 1.5-fold variability in RCII:chl-a albeit largely from samples obtained from the DCM (Moore et al. 2006). It follows that, since variability in RCII:chl-a could not explain the 4-fold variability in  $P^*_m$  the maximal carbon fixation capacity ( $P^*_m$ ) should co-vary proportionately with whole-chain electron transfer ( $1/\tau_{PSII}$ ) (refer to Eqn. 1.11, also Moore et al. 2006). In keeping with this argument, the 4-fold variability in  $P^*_m$  was accompanied by a 4-fold variability in  $1/\tau_{PSII}$ , with CS05 data supporting that of CS03 described by Moore et al. (2006). However, the relationship between  $1/\tau_{PSII}$  and  $P^*_m$  is somewhat circular as  $1/\tau_{PSII}$  is calculated from  $Ek_{478}$  so that  $P^*_m$  is inherent in its estimation.

Figure 3.18B illustrates  $1/\tau_{Qa}$  and  $1/\tau_{PSII}$  co-varied which suggests that the factors limiting the electron transfer rates from Qa to PQ ( $1/\tau_{Qa}$ ) were the same as those limiting electron transfer rates though the entire chain ( $1/\tau_{PSII}$ ) (Falkowski and Raven 1997). However, the magnitude of  $1/\tau_{Qa}$  was always greater than  $1/\tau_{PSII}$  (Fig. 3.18B, also Moore et al. 2006) representing faster electron transfer from Qa to PQ than over the entire electron transport chain.

A more detailed discussion of the factors limiting the rates of electron transfer and carbon fixation and are discussed below. These data from the CS03 and CS05 cruises represent the first comparison of  $1/\tau_{Qa}$  measured by FRRF with other independently derived physiological parameters for field populations.

### 3.6 Ek<sub>14C</sub> and *in situ* Irradiance

<sup>14</sup>C-derived Ek<sub>14C</sub>, corrected for the *in situ* light spectrum (Ek<sub>insitu</sub>) was highly correlated to the mean growth irradiance for both cruises (CS03 n = 36, r<sup>2</sup> = 0.177, p = 0.011 (Moore et al. 2006); CS05 n = 48, r<sup>2</sup> = 0.717, p < 0.001, Fig. 3.19). The mean growth irradiance was calculated from the mean PAR experienced by the phytoplankton *in situ* over the 24 hour period prior to sampling, using reconstructed spectral light fields following methods in Chapter 2. For the SML and mixed water columns the irradiance was averaged through the depth of the mixed layer following the assumption that mixing timescales were less than those of acclimation response (Cullen and Lewis 1988, Moore et al. 2003) (see also Table 3.1).

In contrast to the SML, a significant difference in Ek<sub>insitu</sub> was evident between samples taken from the upslope and peak of the DCM (Table 3.1). This suggests that phytoplankton were able to acclimate to light levels associated with their position in the thermocline.

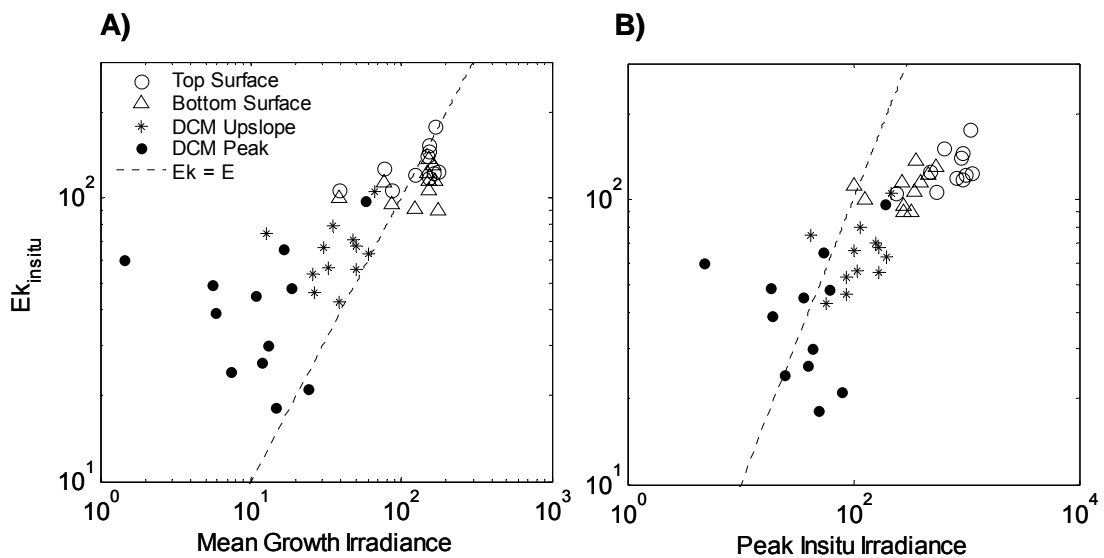


Figure 3.19. The <sup>14</sup>C-derived light saturation parameter, Ek<sub>insitu</sub>, spectrally corrected to the spectra of *in situ* irradiance ( $\mu\text{E m}^{-2} \text{s}^{-1}$ ) against A) mean growth irradiance, and B) peak *in situ* irradiance ( $\mu\text{E m}^{-2} \text{s}^{-1}$ ). The mean growth irradiance was calculated from the mean irradiance experienced over the 24 hour period prior to sampling with spectral composition modelled following methods outlined in Chapter 2. For surface samples irradiance was averaged through the depth of the surface mixed layer (SML). Peak *in situ* irradiance was estimated from mean growth irradiance  $\times$  3.4 (the mean difference between the maximum daily irradiance and the mean daily irradiance). For estimation of peak surface irradiance, the irradiance was not averaged through the SML.

$E_{k_{\text{insitu}}}$  averaged over the SML was 1.7 times the mean growth irradiance for the SML during CS03 (Moore et al. 2006), and 1.0 times during CS05. In contrast, mean  $E_{k_{\text{insitu}}}$  at the peak of the DCM was 9.5 and 2.9 times the mean growth irradiance during CS03 and CS05 respectively (Fig. 3.19A).

On average, the peak irradiances experienced during the day were 3.4 times greater than mean daily irradiance. Peak daily irradiance reflects the maximal irradiance likely to be experienced by the phytoplankton and as such, peak *in situ* irradiances were not averaged through the SML. Mean  $E_{k_{\text{insitu}}}$  in the SML were 0.51 and 0.30 times the peak growth irradiance in the SML for CS03 and CS05 respectively, compared to 2.9 and 0.87 times at the peak of the DCM (Fig. 3.19B, also Moore et al. 2006). It follows from this analysis that the phytoplankton in the SML were close to light-saturation at mean *in situ* irradiance but super-saturated at higher irradiance. In contrast, at the DCM,  $E_{k_{\text{insitu}}}$  remained in excess of  $E_{\text{insitu}}$  even at peak irradiances. Thus phytoplankton photosynthetic rates were sub-optimal at average *in situ* irradiances and closer to light saturation only at peak irradiance (Fig. 3.19 also Moore et al. 2006). DCM populations were possibly light limited for most of the day despite the photo-physiological acclimation evident in the DCM populations (reviewed by Geider et al. (1998) and MacIntyre et al. (2002)).

Figure 3.19B also illustrates that the decrease in irradiance between the upslope and peak of the DCM was the same order of magnitude as the difference between the surface and the base of the SML (~10-fold).

### 3.6.1 Ek-independent Variability

Figure 3.20 illustrates that co-variability of  $\alpha^*_{14C}$  and  $P^*_m$  occurred within the four depth horizons sampled during CS05 (i.e. the top and base of the SML, and the upslope and peak of the DCM). The slope of the regression between  $\alpha^*_{14C}$  and  $P^*_m$  represents the mean  $E_{k_{14C}}$  within the depth horizon.

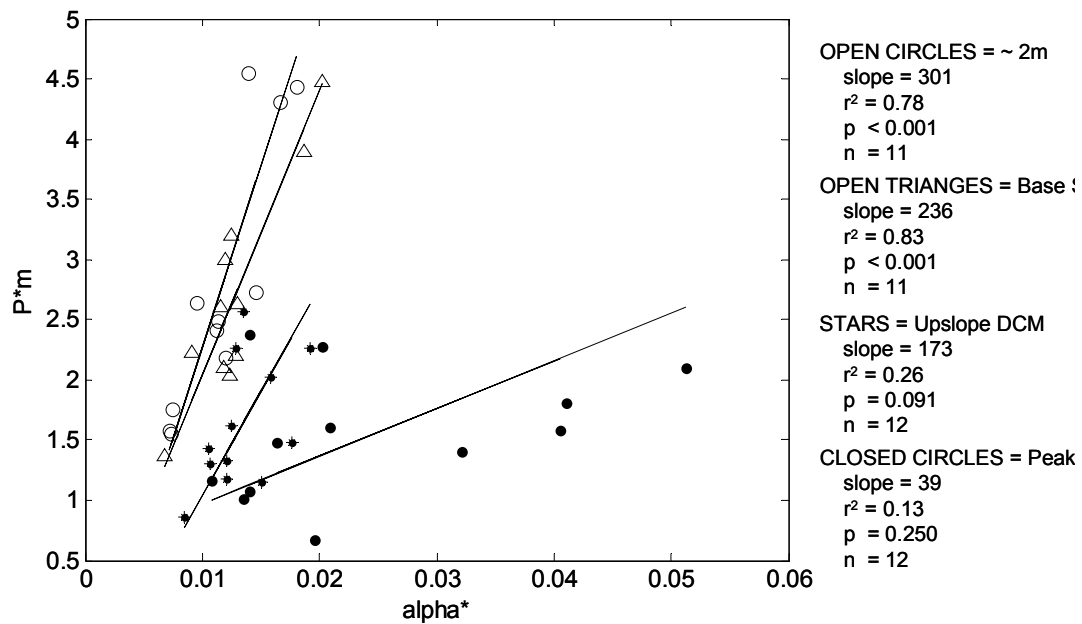


Figure 3.20. Relationship between light utilisation coefficient,  $\alpha^*_{14C}$  ( $\text{mg C (mg chl a)}^{-1} \text{h}^{-1}$  ( $\mu \text{E m}^{-2} \text{s}^{-1}$ ) $^{-1}$ ), and the maximum rate of carbon fixation,  $P^*_m$ , ( $\text{mg C (mg chl-a)}^{-1} \text{h}^{-1}$ ) during CS05. Solid lines indicate the model II regression for each of the depth bins. The slope of each line represents the mean  $Ek_{14C}$  for the depth bins. Results of the regression analysis on each line are given in the legend.

During CS03, co-variance of  $P^*_m$  and  $\alpha^*_{14C}$  within SML and DCM samples was also evident (CS03 SML  $n = 15$ ,  $r^2 = 0.293$ ,  $p = 0.037$ ; DCM  $n = 21$ ,  $r^2 = 0.323$ ,  $p = 0.007$ ). However, a similar trend was not observed in FRRF-derived parameters  $\sigma_{PSII}$  and  $1/\tau_{Qa}$  during either cruise.

Such co-variability of  $\alpha^*_{14C}$  and  $P^*_m$  is termed “Ek-independent” variability and a complete discussion of this phenomenon is included in Behrenfeld et al. (2004). In summary, evidence of Ek-independent variability has been recorded by a number of authors, in one case within SML and BML (see Behrenfeld et al. (2004) and references therein).

All samples (during 2005) were taken at the same time of the day and, as such, co-variability of  $P^*_m$  and  $\alpha^*_{14C}$  in these data cannot be due to diel cycles (Behrenfeld et al. 2004). Variability in temperature may affect rates of enzymatic processes including (potentially) the rates of electron transport (Davison 1991) although the effect of temperature is considered to be of minor significance (Behrenfeld et al. 2004). Cote and Platt (1983) attributed the co-variability of  $\alpha^*_{14C}$  and  $P^*_m$  independently of  $Ek_{14C}$  on the combination of taxonomic composition and nutrient availability, whilst Claustre et al. (1997) suggested taxonomic composition to be the

main cause. Access to nutrients increases the ability of the cell to synthesis chl-a and other pigments (Falkowski and Raven 1997), particularly since the DCM is situated on the nitracline, and may lead to different photoacclimation responses between populations in the DCM compared to in the surface.

Horizontal gradients in  $\alpha^*_{14C}$  along depth horizons may lead to corresponding changes in the degree of variability in  $P^*_m$  through pigment synthesis to achieve the necessary  $Ek_{14C}$ . Since phytoplankton are associated with species-specific pigment compositions and factors such as cell size affect both susceptibility to pigment packaging and nutrient utilisation, it is possible that  $\alpha^*_{14C}$  and  $P^*_m$  co-vary between species in order to obtain a particular  $Ek$ .

Figure 3.21 illustrates that a change in the coupling between  $1/\tau_{Qa}$  and  $P^*_m$  occurs between the SML and the thermocline. Since  $\alpha^*_{14C}$  and  $\sigma_{PSII}$  appear to vary in response to different causal factors it is perhaps not surprising that an offset occurs between  $1/\tau_{Qa}$  and  $P^*_m$  (if  $Ek_{478}$  and  $Ek_{ETR,478}$  co-vary). Vertical gradients in  $1/\tau_{Qa}$  and  $P^*_m$  may accommodate those in  $\sigma_{PSII}$  and  $\alpha^*_{14C}$  respectively, in order to maintain required  $Ek$ .

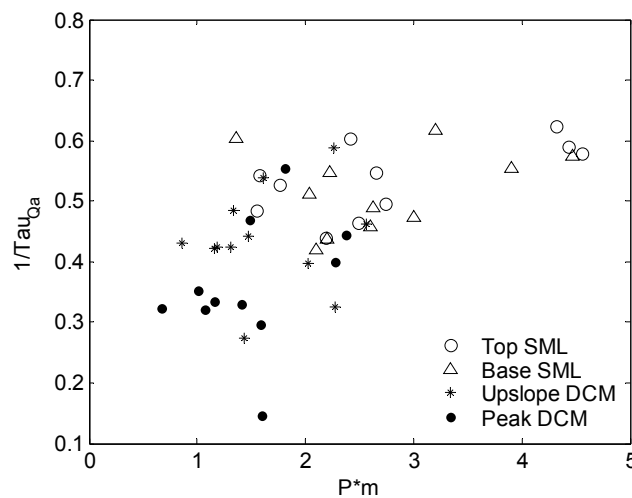


Figure 3.21. Relationship between  $1/\tau_{Qa}$  (s<sup>-1</sup>) and  $P^*_m$  (mg C (mg chl-a)<sup>-1</sup> h<sup>-1</sup>) for surface and thermocline for all data during CS05.

The cause of the observed  $Ek$ -independent variability remains largely unknown, with focus currently on downstream metabolic processes due to the limitation of  $P^*_m$  (Behrenfeld et al. 2004). Given the lack of  $Ek$ -independent variability in FRRF parameters, a key component of the co-variability may stem from factors de-coupling <sup>14</sup>C and FRRF-derived parameters, such as PSI:chl-a or PSII:PSI ratios. This is discussed further in Chapter 7.

### 3.7 Photoacclimation and Adaptation

This section investigates changes in phytoplankton taxonomy and cellular characteristics between the surface and thermocline populations, as well as within the thermocline itself. The potential mechanisms of photoacclimation are briefly discussed as indicated from both the physiological and ecological measurements presented in this chapter.

#### 3.7.1 Adaptation

As described above, phytoplankton taxonomic composition varied across the study region with significant vertical gradients evident during CS05. The vertical gradients in taxonomy were likely (at least in part) a response to the *in situ* irradiance. However, regardless of the taxonomic variability in physiological parameters  $\sigma_{\text{PSII}}$  (and possibly  $\alpha^*_{14\text{C}}$ )  $E_k$  varied in response to the light gradient due to changes in  $P^*_m$  and  $1/\tau_{\text{Qa}}$ .

#### 3.7.2 Photoacclimation

##### *Chl-a:C*

During both cruises Analytical Flow Cytometry (AFC) provided cellular concentrations, cell size and cellular fluorescence measurements for picoeukaryotes (P.euk) and the cyanobacteria *Synechococcus* (Syn). For *Synechococcus*, the measured side scatter (as indicator of cell size) was scaled to represent cellular carbon contents (Bertilsson et al. 2003, Heldal et al. 2003) based on the sizes observed (scaling factor 5). Also for *Synechococcus*, a scaling factor of 0.25 (to obtain chl-a from cell fluorescence) was obtained from the relative contributions of prokaryote and picoeukaryote types enumerated by AFC and the total chl-a concentration of the  $< 2\mu\text{m}$  size fraction (C. M. Moore, *pers. comm.*). No adjustment was made for picoeukaryotes, and the trends in the data were consistent regardless of whether or not this magnitude correction was applied. Depth profiles of *Synechococcus* and picoeukaryote characteristics for an example shelf station (JB1) are shown in Figure 3.22.

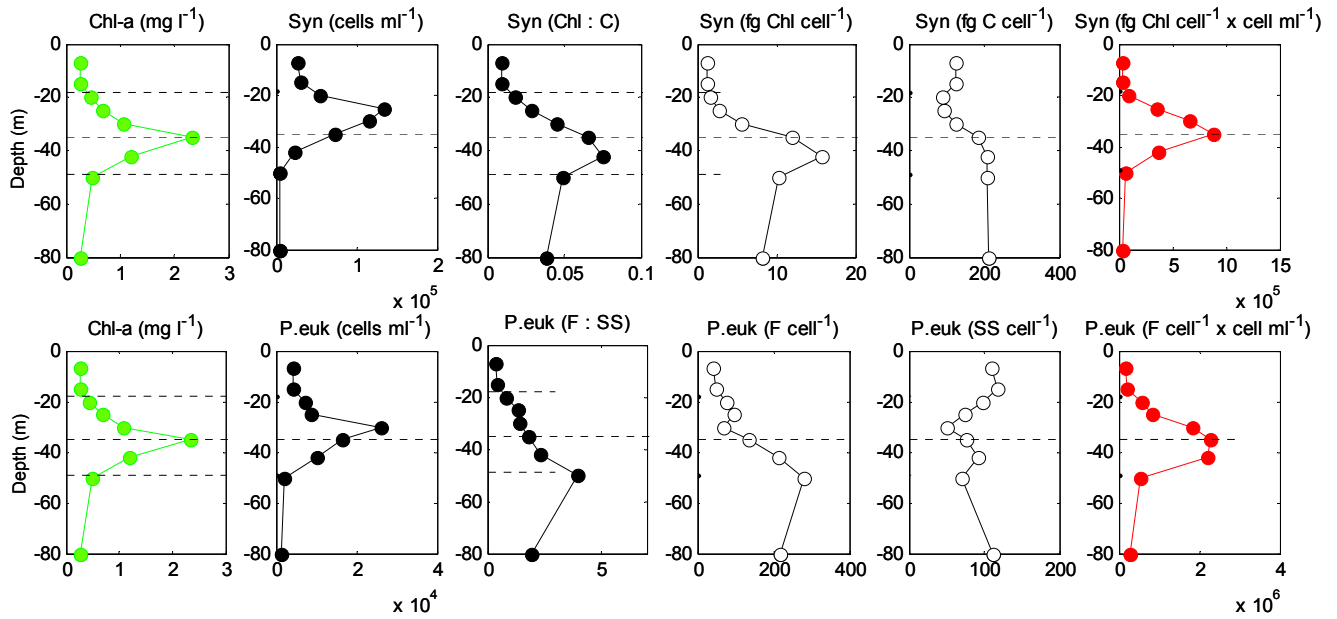


Figure 3.22. Vertical profiles of chlorophyll-a (left hand panel) and characteristics of *Synechococcus* (Syn) and picoeukaryotes (P.euk) obtained from Analytical Flow Cytometry (AFC) against depth, for an example shelf station (JB1) visited during CS05. Cellular fluorescence (F) was adjusted to fg chl-a by a factor ( $\times 0.25$ ) for *Synechococcus* but not picoeukaryotes. Cellular Side Scatter (SS) was adjusted to fg C by a factor ( $\times 5$ ) for *Synechococcus* but not picoeukaryotes. See text for determination of conversion factors. Chl-a:C is in g:g, F:SS is relative scale. Dashed lines in all panels represent the peak of the DCM, with additional (upper and lower) dashed lines in the left hand panels indicating the top and bottom of the thermocline as defined by the density gradient.

Maximal cell concentration ( $\text{cells ml}^{-1}$ ) of *Synechococcus* and picoeukaryotes occurred within the thermocline but above the maximal chl-a concentration of the DCM. In contrast, cellular fluorescence increased consistently throughout the thermocline and was maximal below the peak of the DCM. Figure 3.22 illustrates that the DCM results from the combination of increased cell numbers as well as an increased cellular pigment concentration within the thermocline.

Cellular biomass for both phytoplankton groups (as inferred from side scatter measurements) was lowest at the top of the DCM coinciding with the depth of maximal cell numbers. Hence, cells were smallest when they were most abundant in number. Cellular biomass increased with depth through the thermocline as cellular pigment concentration also increased. These data therefore indicate that cell size may increase in response to increasing cellular pigment content. The increase in cell size also likely relates to increased nitrate concentration at the base of the DCM.

For the stratified shelf and oceanic regions (where the size fraction  $< 2 \mu\text{m}$  accounted for  $\sim 50\%$  of total chl-a) the cellular fluorescence per cellular side scatter (F:SS) increased 4-fold for both *Synechococcus* and picoeukaryotes between the surface (2 m) and peak of the DCM. This change was therefore of the same magnitude as the variability in  $P_m^*$  and  $Ek_{14C}$  between the surface and DCM. Less variability occurred at the shelf edge where the increase was  $< 2$ -fold. However, the shelf edge was typically characterised by larger phytoplankton that were not measured by AFC (chl-a of size fraction  $< 2 \mu\text{m}$  was  $< 40\%$  of total chl-a).

During CS05 there was a significant correlation between  $Ek_{14C}$  and F:SS for *Synechococcus* as well as picoeukaryotes over the entire study region (Syn CS05  $n = 28$ ,  $r^2 = 0.391$ ,  $p < 0.001$ ; P.euk  $n = 28$ ,  $r^2 = 0.356$ ,  $p < 0.001$ , Fig. 3.23), therefore indicating that variability in chl-a:C is a key factor in determining  $Ek_{14C}$  and therefore in photoacclimation (Geider et al. 1998, MacIntyre et al. 2002).

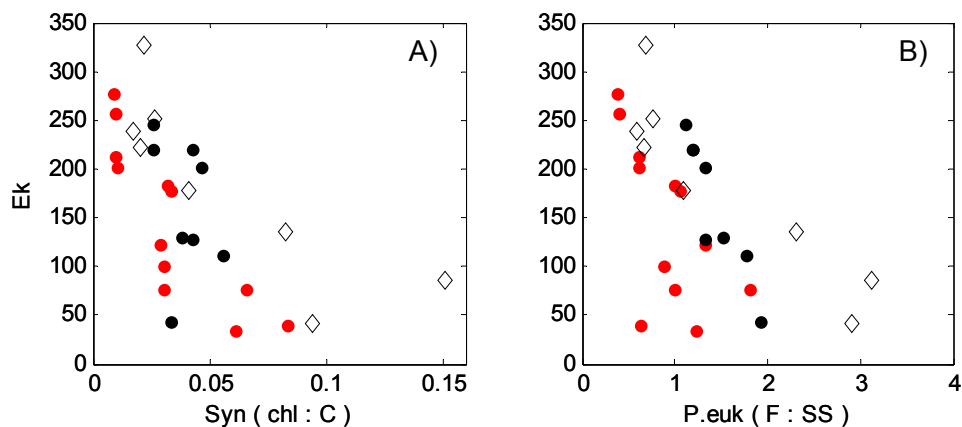


Figure 3.23. Relationship between  $Ek_{14C}$  ( $\mu\text{E m}^{-2} \text{s}^{-1}$ ) and A) *Synechococcus* chl-a:C and B) Picoeukaryote F:SS. Cellular fluorescence (F) was adjusted to chl-a by a factor ( $\times 0.25$ ) for *Synechococcus* but not picoeukaryotes. Cellular Side Scatter (SS) was adjusted to chl-a by a factor ( $\times 0.5$ ) for *Synechococcus* but not Picoeukaryotes. Chl-a:C are g:g, F:SS is relative scale. Black dots = shelf edge, red dots = stratified shelf, open symbols = oceanic.

The carbon specific physiological parameters can be estimated by the specific use of Equation 1.4 (Falkowski and Raven 1997):

$$P_m^C = P_m^* \cdot \text{chl-a:C} \quad (3.6)$$

$$\alpha^C = \alpha^* \cdot \text{chl-a:C} \quad (3.7)$$

where chl-a:C was estimated from the *Synechococcus* chl-a:C as obtained from cellular fluorescence ( $\times 0.25$ ) and side scatter ( $\times 5$ ). A significant increase in  $\alpha^C$  with optical depth was evident across the stratified shelf and oceanic regions (Fig. 3.24) ( $\log(\alpha^C)$  vs. OD  $n = 20$ ,  $r^2 = 0.620$   $p < 0.001$ ) whilst there was no significant difference between  $P_m^C$  at the surface (2 m) and DCM across the stratified shelf. An increase in  $P_m^C$  at the DCM was evident only in the oceanic region (Fig. 3.23).

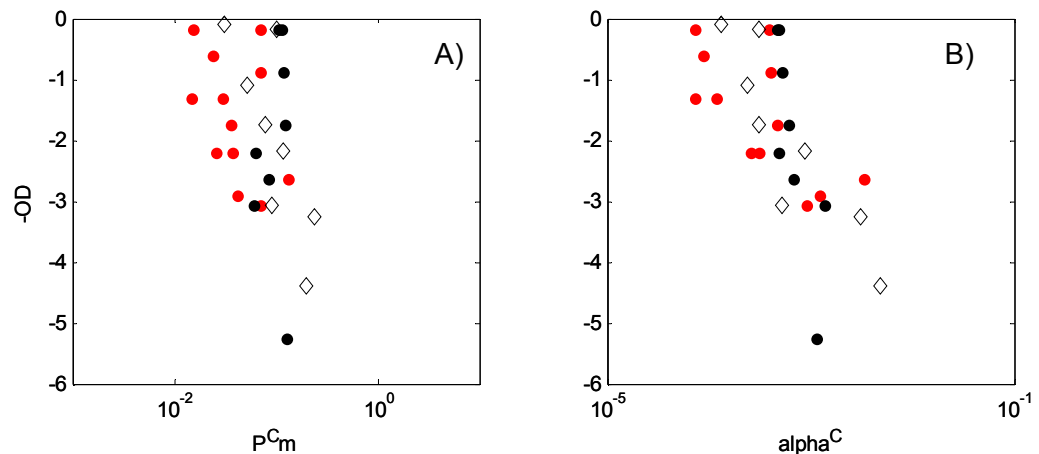


Figure 3.24. A)  $P_m^C$  ( $h^{-1}$ ) against optical depth and B)  $\alpha^C$  ( $h^{-1} (\mu E m^{-2} s^{-1})^{-1}$ ) against optical depth for available data during CS05.  $P_m^C$  and  $\alpha^C$  are as described in text. Black dots = shelf edge, red dots = stratified shelf, open symbols = oceanic.

This analysis indicates that depth variability in  $P_m^*$  was largely attributable to changes in chl-a:C, and that the carbon-specific carbon fixation capacity of the phytoplankton did not vary systematically with depth (Falkowski and Raven 1997, MacIntyre et al. 2002).

Accompanying the increase in *Synechococcus* chl-a:C with depth was a corresponding increase in cellular orange fluorescence which likely represented *Synechococcus* ability to vary the length of the phycobillin-containing distal rods in response to changes in the light environment (Kana and Glibert 1987, MacIntyre et al. 2002).

#### *Mechanism of Photoacclimation*

The data presented in this chapter support the laboratory findings that photoacclimation to low light includes synthesis of cellular chl-a (Falkowski and LaRoche 1991, Geider et al. 1998, MacIntyre et al. 2002). The fact that the variability in  $\sigma_{PSII}$  is not dominated by acclimation to

low light indicates that phytoplankton do not vary the 'size' of the light harvesting antenna servicing individual PSII reaction centres in response to low light (Falkowski and LaRoche 1991, Moore et al. 2006). The synthesis of chl-a must therefore be associated with an increase in the cellular number of PSII reaction centres (Falkowski and LaRoche 1991, Moore et al. 2006), a suggestion which is supported by the (relatively constant) measurement of RCII:chl-a (described above).

It is proposed that the increase in the number of reaction centres per cell resulted in the observed reduction of electron transfer rates of PSII with depth (as each PSII shares a fraction of the cellular carbon fixation capacity) as well as the decrease in  $P_m^*$  that was similar in magnitude to the increase in chl-a:C (Moore et al. 2006). This hypothesis is consistent with recent models (Geider et al. 1998, Moore et al. 2006) and relies upon the assumption that the carbon fixation capacity, or the rate of the Calvin-Benson cycle, is a constant cellular property (Sukenik et al. 1987, Behrenfeld et al. 1998). These data showed that the maximal carbon fixation capacity ( $P_m^C$ ) was constant with optical depth. The significance of the co-variance of the electron transport rates  $1/\tau_{Qa}$  and  $1/\tau_{PSII}$  are discussed below.

Following theory summarised by Falkowski and Raven (1997), co-variance of partial and whole chain electron transport rates ( $1/\tau_{Qa}$  and  $1/\tau_{PSII}$ ) indicates a balance between processes downstream and upstream of the PQ pool. The maximal rate of electron transfer through Qa is  $1.6 \text{ ms}^{-1}$  (the oxidation rate of Qa-) and PQ is  $1 \text{ ms}^{-1}$  (the oxidation rate of PQH<sub>2</sub>) and these maximal rates are not expected to vary with increase of PSII:chl-a (Crofts and Wraight 1983, Falkowski and Raven 1997). As illustrated in Figure 3.18B,  $1/\tau_{Qa}$  is consistently greater than  $1/\tau_{PSII}$  in these data, in line with the magnitudes of the theoretical rates (Falkowski and Raven 1997, Moore et al. 2006). The observed range in magnitudes of  $1/\tau_{Qa}$  and  $1/\tau_{PSII}$  ( $0.1 - 0.9 \text{ m s}^{-1}$ ) were below the theoretical maximum rates during both cruises, and since the rates co-varied, these data suggest that the same process was responsible for limiting the electron transfer rates along the whole chain such that the rate-limiting process is likely to be downstream of PSII. The rate limiting process is typically assumed to be the Calvin Benson cycle, such that the overall capacity for carbon fixation limits the rate of re-oxidation of the PQ pool ( $1/\tau_{PSII}$ ), and subsequently re-oxidation of Qa ( $1/\tau_{Qa}$ ) (Sukenik et al. 1987, Kolber and Falkowski 1993, Cleland 1998, Kana et al. 2002). These observations support the hypothesis of Escoubas et al. (1995) that the cue for photo-acclimation response is in the oxidation state of the PQ pool.

A limitation of this theory is that the current data suggests an apparent faster transfer of electrons through Qa than PQ. Although in line with theoretical maximum rates, (and the fact that  $1/\tau_{Qa}$  should set the upper limit for on the rate of whole chain electron transport ( $1/\tau_{PSII}$ ))

(Moore et al. 2006)) it is not clear that a rate limiting Calvin Benson cycle is causing electrons to be 'backed up' along the transport chain leading to down-chain flow at the same rate through each of the electron carriers. A full mechanistic model for the observed discrepancies between  $1/\tau_{Qa}$  and  $1/\tau_{PSII}$  is currently lacking. Further laboratory and field measurement of the rates of electron transfer through individual electron transport components is probably required before these open questions can be resolved.

### 3.8 Summary of Main Points

The major observations within this chapter were:

- Phytoplankton absorption spectra varied considerably more with depth than horizontally, but pigment packaging proved difficult to quantify.
- Changes in pigment composition and phytoplankton absorption spectra with depth followed the change in the wavelength composition of the *in situ* light field indicating chromatic adaptation of phytoplankton at the DCM.
- Variability in the effective absorption cross section of PSII was determined by pigment composition and not correlated to optical depth.
- Variability in  $\alpha^*_{14C}$  and  $\Phi_m$  could not be attributed to any one environmental variable, but NPC:PSC, and possibly nutrient availability, may be important.
- Flow cytometry revealed increases in chl:C, cell numbers and cell densities within species in the thermocline but at different depths.
- Variability in light saturated photosynthetic rates ( $P^*_m$ ) dominated the variability in  $Ek_{14C}$ . Both parameters were correlated to optical depth.
- Photoacclimation resulted in  $Ek_{insitu}$  close to  $E_{insitu}$ , and DCM populations that were not light saturated.
- Combining FRRF-derived electron transfer rates and  $^{14}C$ -measured  $P^*_m$  and  $Ek_{478}$  indicated that photoacclimation to low light was by increasing the number of PSII reaction centres, and that electron transport from Qa to PQ was apparently limited by the same processes limiting whole chain transport and ultimately carbon fixation.

## **CHAPTER 4: PRIMARY PRODUCTION IN THE CELTIC SEA**

This chapter addresses the implications of the physical environment on the phytoplankton and primary production in the Celtic Sea. Data from all hydrographic regimes visited during the CS03 and CS05 cruises are presented (i.e. oceanic, shelf edge, stratified shelf, frontal and mixed water) although special attention is given to the spatial and temporal variability across the stratified shelf and the implications for primary production within the thermocline.

### **4.1 Study Area**

Figure 4.1 illustrates the sampling locations visited during both cruises (CS03 and CS05). Sampling protocols and methodologies are described in Chapter 2. In order to monitor variability over a semidiurnal tidal cycle, some stations were occupied for a 25 hour period (CS1, CS3a, CS3b, CS2 during CS03 and B2a, B2b, OB, CS2a, and CS2b during CS05). The letters 'a' and 'b' are used to identify the occupation where stations were re-visited at different stages of the spring-neap tidal cycle. During CS05, stations B2 and JB3 were located above the edge of the topographic bank, station JB1 was in the proximity of the bank and OB and P1 were located on a flat shelf location away from the influence of the bank. Stations U2 and CS2 were sampled during both CS03 and CS05.

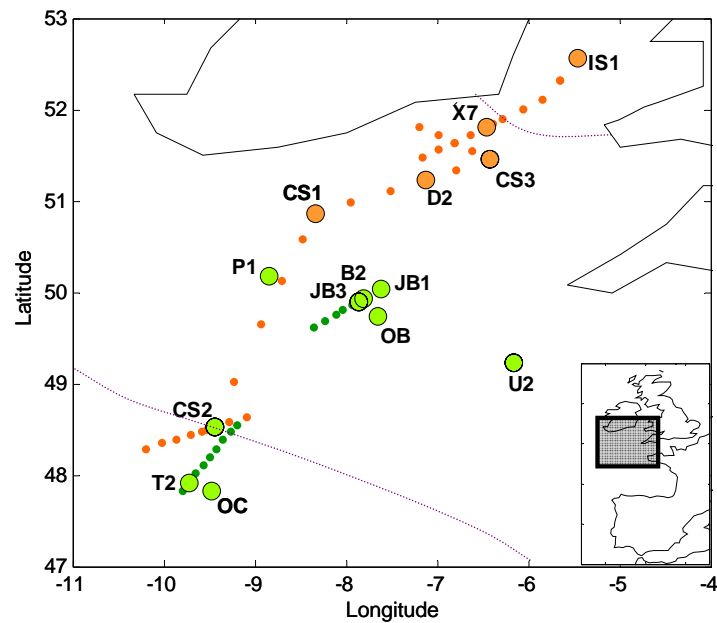


Figure 4.1. Map of sampling locations in the Celtic Sea during CS03 (orange symbols) and CS05 (green symbols). Small symbols indicate the location of all CTD casts and large symbols indicate the main stations where a full suite of biological measurements were obtained. Dotted lines indicate the location of the Irish Sea Front and the Shelf Edge. Station JB3 and B2 were located on the slope of a topographic bank, with JB1 in the vicinity of the bank but not directly above it. Stations CS2 and U2 were sampled during CS03 as well as CS05.

The hydrographic context of the study region is provided in Figure 4.2 showing clearly the location of the Irish Sea front and the extent of the stratified shelf region. The shelf edge is characterised by a decrease in surface temperature and an increase in surface chl-a at the continental shelf slope.

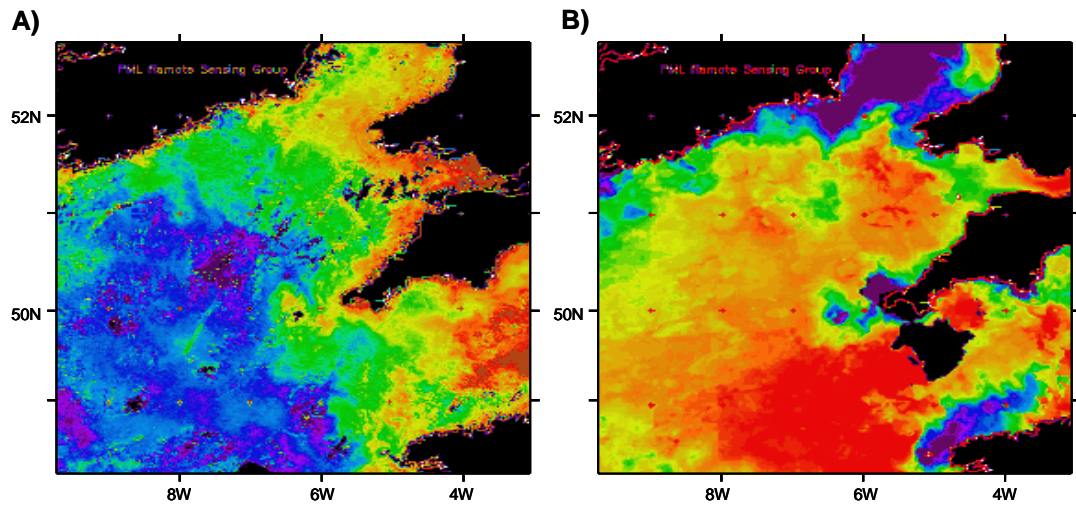


Figure 4.2. Satellite images of the Celtic Sea region. A) SeaWiFS surface chl-a composite July 30<sup>th</sup> to August 5<sup>th</sup> 2003, log scale, purple = 0.01 mg m<sup>-3</sup>, red = 5 mg m<sup>-3</sup>. B) AVHRR Sea Surface Temperature composite August 3<sup>rd</sup> - August 5<sup>th</sup> 2003, purple = 15°C, red = 18°C. Images courtesy of PML Satellite Remote Sensing Group.

The weakly stratified region in the vicinity of the Irish Sea front (and the location of sample site CS3) is associated with increased surface chl-a. Note that the proximity of CS3 to the front varies with the frontal excursion over spring-neap tidal cycles (see Chapter 1).

## 4.2 Hydrography, Chl-a and Nitrate Distribution

This section summarises the hydrographic setting and describes the broad-scale patterns of chl-a distribution across the region. Illustration is given to the variability in the physical environment due to the tidally active nature of the shelf sea. The implications of mixing and nutrient supply on the distribution of chl-a are investigated.

The salinity, temperature and chl-a distributions along a transect from the shelf edge to close the Irish Sea front was obtained from a Seasoar survey during CS03 (Fig. 4.3). Salinity varied horizontally, rather than with depth, across most of the shelf edge and stratified shelf region, ranging from ~35.5 at the shelf edge to ~34.6 in the mixed water on the shelf. Vertical gradients in salinity were only observed close to the Irish Sea front, where salinity ranged from 34.6 at the surface to 35.5 at depth.

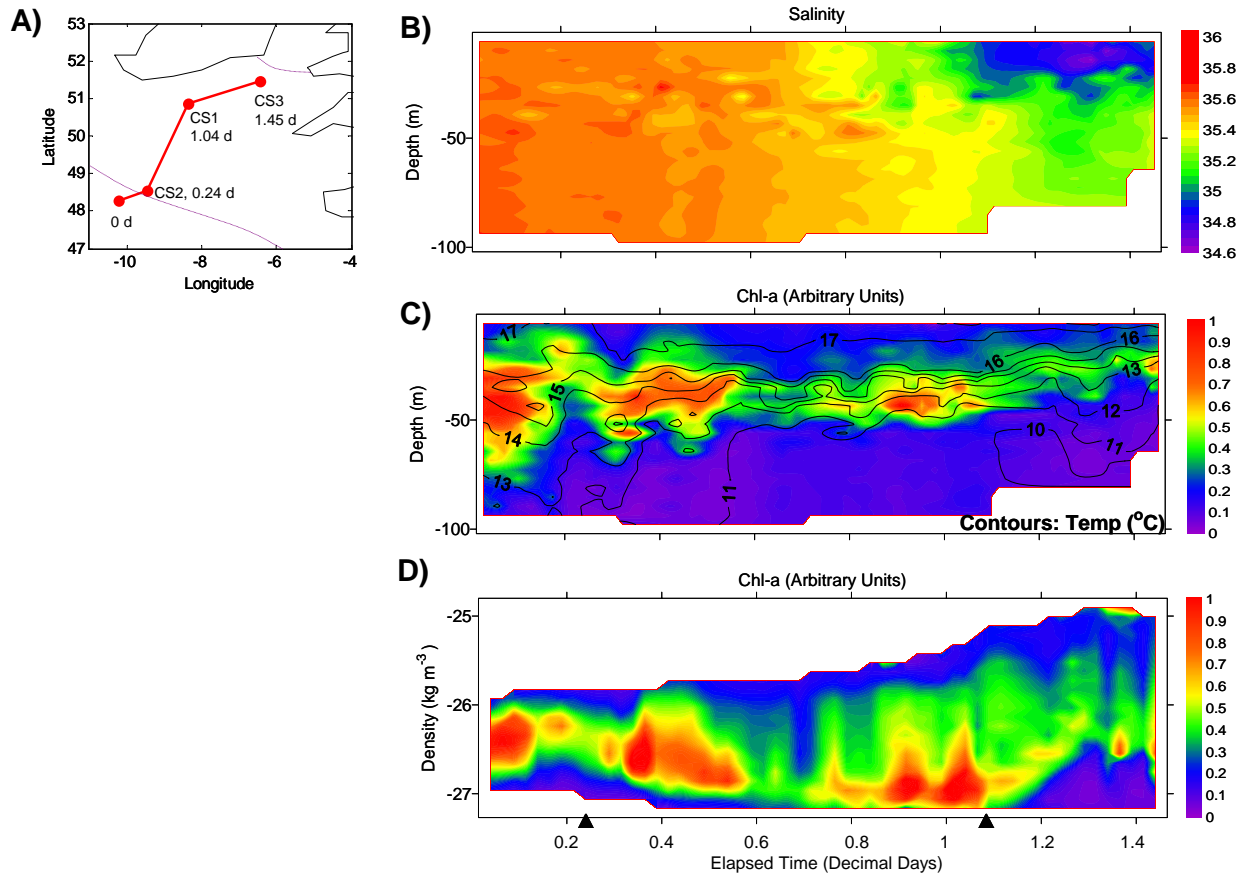


Figure 4.3. Seasoar section during CS03, from the oceanic region (left of panel, JD = 220.61) through CS2 (elapsed time = 0.24 d, JD = 220.85), through CS1 (elapsed time = 1.04 d, JD = 221.65) to CS3 (right of panel, JD = 222.07). Black triangles indicate the location of CS2 and CS1 along the transect. A) Map of transect, B) Salinity against depth, C) chl-a fluorescence (arbitrary units) against depth with temperature contours ( $^{\circ}\text{C}$ ), D) chlorophyll fluorescence against density.

Horizontal gradients in temperature mainly occurred as a result of mixing associated with the shelf edge and Irish Sea fronts. For the stratified shelf region, the vertical gradient in temperature dominated the variability, with temperature ranging from 16 - 19  $^{\circ}\text{C}$  in the surface mixed layer (SML) to 10 - 13.5  $^{\circ}\text{C}$  in the bottom mixed layer (BML). The gradient in temperature occurred over a thermocline region ranging from ~10 - 50 m. In general, as illustrated in Figure 4.3B, the thermocline was broad close to the shelf edge, narrow and relatively deep in the mid-shelf region and shoaled and broadened towards the Irish Sea front where it ultimately reached the surface (not shown).

With the exception of the weakly stratified region close to the Irish Sea front (visited during CS03 only), temperature accounted for 83 % and 97 % of the variability in density during

CS03 and CS05 respectively (CS03  $n = 182$ ,  $r^2 = 0.83$ ,  $p < 0.001$ ; CS05  $n = 454$ ,  $r^2 = 0.97$ ,  $p < 0.001$ ). Hereafter, temperature and density will be used interchangeably to describe the physical structure of the water column.

Across the study area the thermocline was associated with increased concentration of chl-a compared to surface and deep waters (Fig. 4.3B), and was the location of the deep chl-a maxima (DCM). The distribution of chl-a was not homogenous within the thermocline, but instead was patchy both horizontally and vertically (Fig. 4.3C). Figure 4.3C shows that, in generally, chl-a was maximal towards the base of the density gradient (or thermocline). An example of how the water column structure and chl-a distribution varied over time is shown in Figure 4.4.

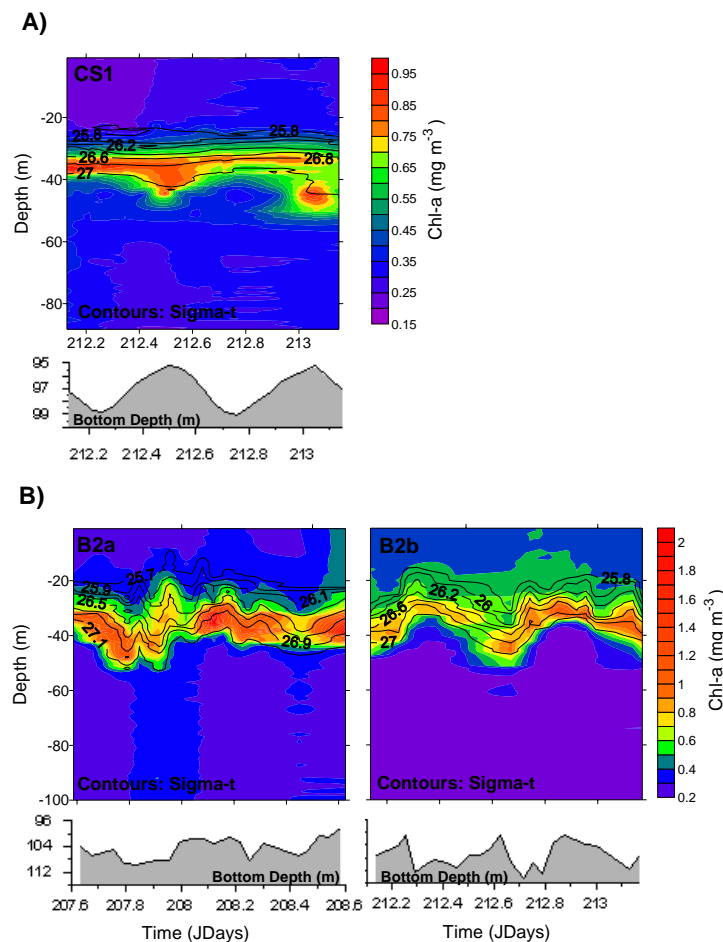


Figure 4.4. Distribution of chl-a (colour scale) and density (contours) ( $\text{kg m}^{-3}$ ) over 25 hour sampling. A) CS1, B) B2 3-days after a spring tide (left panel) and 1-day following neap tide (right panel). Variability of bottom depth at B2 is likely to be due to the ships movement as B2 was on the edge of a topographic bank. Bottom depth was recorded by the ships echosounder. It must be noted that the temporal variability illustrated here was affected by horizontal advection of water past the ship during the period of sampling.

In the shelf sea, temporal variability of the structure of the water column is largely the response to wind and tidal mixing. Tidal mixing varies as a result of changes in the tidal current speeds (and associated turbulent mixing originating from the seabed) and subsequently causes changes in the physical structure of the water column over timescales of hours (semidiurnal tidal cycle) and weeks (spring-neap tidal cycle). Figure 4.4 clearly shows the change in thermocline thickness and/or depth over the 25 hour periods of sampling. Considerable variability over spring-neap cycles was associated with a more variable thermocline structure. It must be noted that the variability illustrated in Figure 4.4 is both the result of temporal variability of water column structure, but also of the horizontal advection of water past the ship during the period of sampling.

The mean thermocline boundary depth and surface- and thermocline- integrated chl-a for the main stations are provided in Table 4.1A and B. The top of the thermocline ( $y$ ) (meters) was defined by the depth ( $y$ ) at base of the SML where the difference in density at  $y-1$  meters and  $y+1$  meters was greater than  $0.04 \text{ kg m}^{-3}$ . The bottom of the thermocline ( $z$ ) (meters) was defined by the depth ( $z$ ) at the top of the BML where the difference in density at  $z$  meters and  $z+5$  meters was greater than  $0.04 \text{ kg m}^{-3}$ . Standard deviations quoted in Table 4.1A and B illustrate the degree of variability over the 25 hour occupations. Repeat occupations are shown separately so that differences between occupations can be identified.

Table 4.1. Chl-a concentration and thermocline boundary depths at the main stations A) during CS03, and B) during CS05. Values are stated as the mean during the occupation of sampling, with number of CTD casts contributing to the mean (n) given in the left hand column. Where  $n > 1$  the standard deviations are given in italics underneath the mean. Stations re-visited for more than one 25 hour occupation are annotated a,b etc. Thermocline boundaries were defined by the density gradient as described in the text. Integrated chl-a concentration was obtained from calibrated CTD fluorescence profiles. The percentage of surface irradiance (percentage irradiance) present at the depth of the DCM peak was calculated from the  $K_d(\lambda)$  vs. chl-a relationships as described in Chapter 2. OCEANIC (in Table 4.1B) refers to oceanic region and includes data collected at T2 and OC.

	Surface Integrated Chl-a ( $\text{mg m}^{-2}$ )	Thermocline Integrated Chl-a ( $\text{mg m}^{-2}$ )	Top of Therm. (m)	Base of Therm. (m)	Thermocline Thickness (m)	DCM Peak Depth (m)	Max chl-a ( $\text{mg m}^{-3}$ )	Percentage Irradiance at the DCM (% surface irradiance)
<b>IS1</b> n = 27	44.7 <i>4.4</i>	- -	- -	- -	- -	- -	0.69 <i>0.2</i>	- -
<b>X7</b> n = 1	46.9 -	- -	- -	25.0 -	- -	7.0 -	3.12 -	- -
<b>CS3a</b> n = 21	4.2 <i>1.5</i>	18.0 <i>3.0</i>	8.0 <i>2.8</i>	35.3 <i>4.8</i>	27.3 <i>4.9</i>	19.1 <i>4.7</i>	1.04 <i>0.3</i>	9.0 <i>6.4</i>
<b>CS3b</b> n = 23	2.9 <i>0.6</i>	19.4 <i>7.6</i>	6.0 <i>1.3</i>	57.2 <i>20.9</i>	51.2 <i>21.3</i>	21.8 <i>5.3</i>	0.92 <i>0.2</i>	7.7 <i>4.0</i>
<b>D2</b> n = 1	3.6 -	17.6 -	11.0 -	65.0 -	54.0 -	36.0 -	0.54 -	1.4 -
<b>CS1</b> n = 17	5.6 <i>1.1</i>	12.3 <i>3.7</i>	23.8 <i>2.8</i>	46.9 <i>5.0</i>	23.1 <i>5.1</i>	39.8 <i>0.4</i>	0.72 <i>0.1</i>	3.2 <i>0.4</i>
<b>CS1</b> n = 1	1.4 -	38.9 -	5.0 -	46.0 -	41.0 -	32.0 -	2.49 -	5.8 -
<b>U2</b> n = 1	4.9 -	9.7 -	13.0 -	32.0 -	19.0 -	27.0 -	0.50 -	8.9 -
<b>CS2</b> n = 25	6.0 <i>3.0</i>	16.4 <i>5.4</i>	15.8 <i>7.6</i>	75.6 <i>13.9</i>	59.8 <i>16.3</i>	30.5 <i>14.5</i>	0.48 <i>0.1</i>	11.1 <i>8.9</i>
<b>CS2</b> n = 1	2.0 -	15.5 -	10.0 -	89.0 -	79.0 -	32.0 -	0.51 -	5.3 -

Table 4.1. B) Refer to caption for Table 4.1A above.

	Surface Integrated Chl-a (mg m <sup>-2</sup> )	Thermocline Integrated Chl-a (mg m <sup>-2</sup> )	Top of Therm. (m)	Base of Therm. (m)	Thermocline Thickness (m)	DCM Peak Depth (m)	Max chl-a (mg m <sup>-3</sup> )	Percentage Irradiance at the DCM (% surface irradiance)
<b>B2</b> n = 1	4.5 -	42.0 -	19.0 -	66.0 -	47.0 -	45 -	2.26 -	2.1 -
<b>B2a</b> n = 18	4.9 1.6	20.8 4.6	15.9 3.5	48.8 5.4	32.9 5.8	39 10	1.10 0.5	4.4 2.5
<b>B2b</b> n = 16	8.9 2.3	15.3 3.2	20.6 4.8	45.1 5.7	24.5 3.8	35 4	0.74 0.2	5.0 1.8
<b>JB3</b> n = 13	9.5 2.2	17.2 4.2	16.8 3.6	43.2 5.3	26.3 6.6	34 4	0.90 0.2	4.5 1.4
<b>JB3</b> n = 1	8.8 -	15.1 -	18.0 -	40.0 -	22.0 -	30 -	1.48 -	6.4 -
<b>OB</b> n = 15	6.6 2.1	15.4 1.8	17.7 4.6	42.9 4.9	25.1 2.2	36 5	0.81 0.2	4.8 2.4
<b>P1</b> n = 3	6.6 2.0	22.4 3.8	18.7 3.5	58.3 3.2	39.7 2.5	38 11	0.97 0.2	4.4 4.2
<b>U2</b> n = 1	1.9 -	29.9 -	5.0 -	34.0 -	29.0 -	24 -	8.36 -	12.2 -
<b>U2</b> n = 1	3.5 -	20.8 -	19.0 -	37.0 -	18.0 -	25 -	5.74 -	16.2 -
<b>U2</b> n = 1	5.2 -	7.4 -	22.0 -	33.0 -	11.0 -	25 -	1.22 -	14.7 -
<b>CS2</b> n = 1	4.1 -	53.5 -	5.0 -	82.0 -	77.0 -	15 -	1.33 -	18.6 -
<b>CS2a</b> n = 6	3.8 1.2	41.5 13.8	7.8 2.6	59.8 12.0	52.0 13.2	23 8	1.45 0.1	12.3 8.9
<b>CS2b</b> n = 8	7.2 6.2	29.3 8.4	15.4 11.9	85.1 10.5	69.8 20.2	32 8	0.85 0.2	6.5 4.1
<b>OCEANIC</b> n = 2	1.7 0.3	22.0 2.4	22.0 1.4	70.0 4.2	48.0 2.8	52.5 3.5	0.5 0.1	3.1 0.4

The thermocline was broadest at the shelf edge (52 – 79 m) and was shallowest towards the Irish Sea front (CS3, 6 – 8 m). On the stratified shelf the thermocline was typically ~20 – 30 m thick and ~11 – 23 m from the surface. The shelf thermocline was narrowest at U2 (11 m at narrowest) and reached a thickness of ~40 m at P1 and at isolated instances at CS1 and B2.

Surface chl-a concentration remained low across the study area, typically in the range 0.2 – 0.8 mg m<sup>-3</sup>. Highest surface chl-a concentrations were recorded at the shelf edge and some high patches were evident over the topographic bank on the shelf (JB3). The magnitude of the DCM was ~0.6 mg m<sup>-3</sup> in the oceanic region and typically ~1 mg m<sup>-3</sup> at the shelf edge and across the stratified shelf. Increased concentrations at the DCM peak were occasionally observed, particularly at the strongly stratified (narrow thermocline) site U2 (maximum observed concentration 8.3 mg m<sup>-3</sup>) and at one occupation of CS1 (maximum observed concentration 2.5 mg m<sup>-3</sup>).

The irradiance at the DCM (as a percentage of that just below the surface, i.e. the *percentage irradiance*) ranged from 2.5 – 20.6 %. Over the majority of the stratified shelf the percentage irradiance at the DCM was 2.5 – 7.5 %. The DCM was at a higher percentage irradiance at the shelf edge, where the thermocline was shallow, as well as at the strongly stratified shelf site (U2) and the oceanic region, where surface chl-a was very low allowing light to penetrate deeper in the water column.

On the shelf, integrated chl-a through the thermocline ranged from 7.4 – 42.0 mg m<sup>-2</sup> and was greater than surface-integrated chl-a at all locations. Both between and within locations, integrated chl-a in the SML, thermocline and productive water-column (defined as the SML + thermocline) was significantly correlated to the layer thickness (as illustrated by the subset of data shown in Figure 4.5) such that the physical structure of the water column largely determined the amount of chl-a present at a location at any one time.

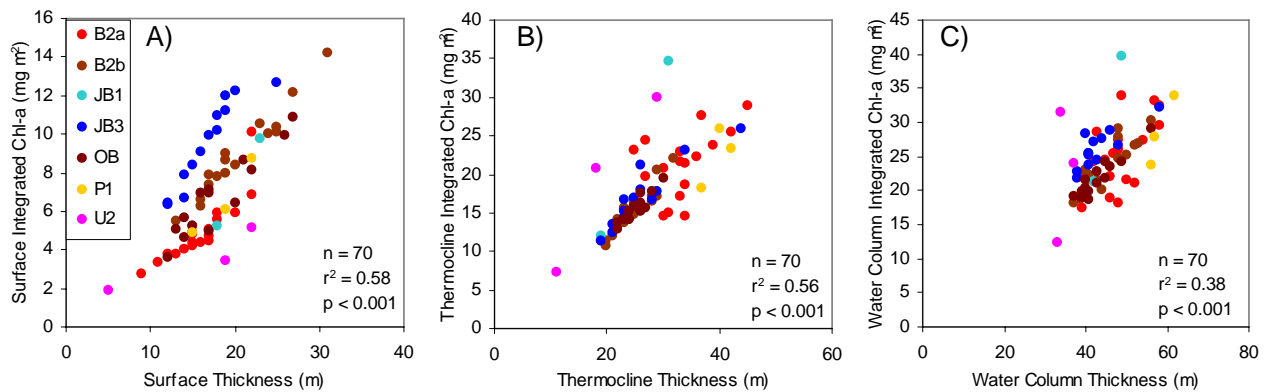


Figure 4.5. Layer-Integrated chl-a ( $\text{mg m}^{-2}$ ) against layer thickness (m) for A) the surface mixed layer, B) the thermocline and C) the productive water-column at the main stratified shelf sites during CS05. The water column thickness was defined as the surface mixed layer + thermocline layer, representing the ‘productive’ region of the water column only. Thermocline boundaries were defined by the density gradient, as explained in the text. Integrated chl-a was obtained from calibrated CTD fluorescence profiles. Statistics quoted are results of model II regression.

#### 4.2.1 Chlorophyll-a Distribution within the Thermocline

The focus of this section is to illustrate the overriding factors governing chl-a distribution within the thermocline, in particular, the significance of nitrate.

##### *Nitrate Concentration*

During both cruises nitrate in the SML on shelf remained below the limit of detection by standard techniques ( $< 0.1 \mu\text{M}$ ). The BML nitrate concentration varied across the study area (Figure 4.6) ranging from  $5.5 - 8 \mu\text{M}$  on the shelf with higher concentrations at the shelf edge and oceanic region ( $> 8 \mu\text{M}$ ).

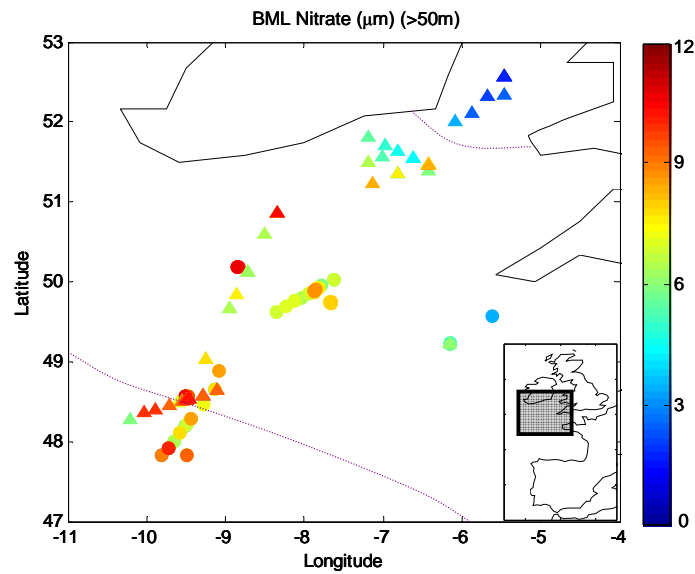


Figure 4.6. Bottom water nitrate concentration across the study area ( $\mu\text{M}$ ), (>50m). Triangles = CS03, Circles = CS05. Dotted lines indicate the location of the Irish Sea front and the Shelf Edge.

The base of the nitrate gradient is determined by physical mixing processes and was subsequently coincident with the base of the thermocline (not shown). The relationship between chl-a and nitrate is described below.

#### *Chl-a and the Nitracline*

The distribution of chl-a and nitrate within the density gradient is shown in Figure 4.7. During 25 hour occupations, the chl-a concentration remained relatively constant despite the changing water column structure caused by the semidiurnal tide. Greater differences in chl-a distribution at a particular location were seen between visits over the spring-neap cycle.

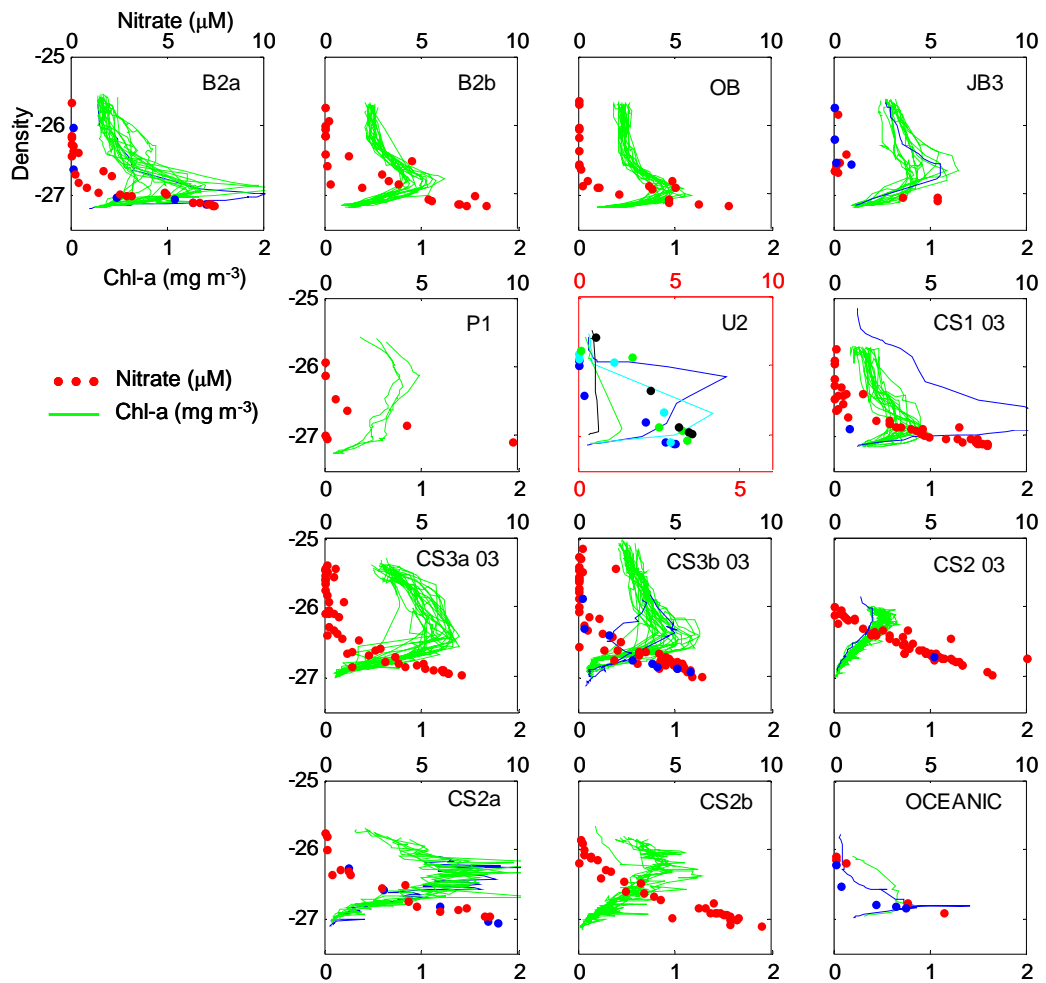


Figure 4.7. Chl-a concentration ( $\text{mg m}^{-3}$ ) (solid lines) and nitrate concentration (symbols) against density ( $\text{sigma-t}$ ,  $\text{kg m}^{-3}$ ) for the main stations. Repeat casts of each occupation are given the same colour. Where stations were revisited for isolated CTD casts, these casts are shown in blue. Where two 25 hour occupations were carried out at the same station, each is shown in a separate panel. U2 was visited three times with only one cast taken at each occupation, each casts is shown in the same panel and identified by a different colour. Scale is highlighted in red to note the different chl-a scale range. Chl-a and density were taken from calibrated CTD profiles. OCEANIC includes data from OC (green and red) and T2 (blue).

At almost all stratified stations away from the shelf edge (including the oceanic stations) the peak of the DCM occurred in the lower part of the thermocline. Further, for the majority of stratified shelf and oceanic sites, the nitrate concentration also typically diminished to  $< \sim 0.1 \mu\text{M}$  below the top of the thermocline.

In contrast, at the shelf edge, the DCM occurred higher up the density gradient and nitrate concentrations remained  $> \sim 0.1 \mu\text{M}$  throughout a greater portion of the density gradient than on the shelf.

Figure 4.8 shows the chl-a distribution on the nitracline for two representative cases for the ‘typical’ shelf and shelf edge scenarios described above. The position of the DCM on the nitracline is generally consistent, regardless of the distribution of these parameters within the density gradient. The DCM is located towards the top of the nitracline where nitrate concentration was  $\sim 1\text{-}2 \mu\text{M}$ . A more detailed analysis on the nitrate and chl-a within the thermocline is given in Chapter 5.

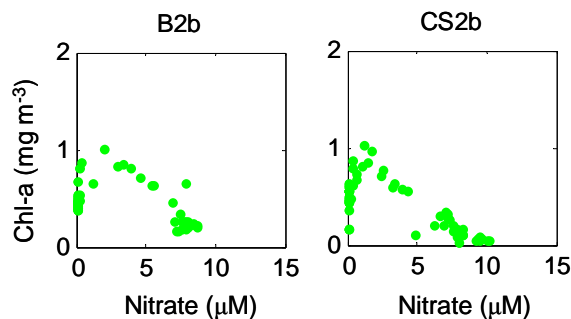


Figure 4.8. Chlorophyll concentration ( $\text{mg m}^{-3}$ ) against nitrate concentration ( $\mu\text{M}$ ) at A) B2a and B) CS2b. Both measurements obtained from bottle samples.

Exceptions to the general trends described above include stations CS1, CS3a and P1. P1 was associated with a broad thermocline ( $\sim 39 \text{ m}$ ) within which the DCM was located in the centre of the density gradient in the region where nitrate concentration was depleted ( $< 0.1 \mu\text{M}$ ). The weakly stratified site, CS3a also exhibited chl-a distribution higher in the density gradient despite diminished nitrate concentrations. Both of these occupations were close to neap tides. One possible explanation may be low tidal mixing and reduced nitrate flux at the time of sampling, with high residual chl-a after a growth period following mixing at spring tides. In contrast to these two stations, the DCM at CS1 occurred in the lower thermocline, but the DCM was at a higher nitrate concentration ( $5 - 6 \mu\text{M}$ ). The base of the thermocline at this site was characterised by a sharp temperature gradient, potentially indicating a mixing boundary that may have allowed the phytoplankton at the DCM to survive further down the nitracline without being mixed into the BML.

The lack of chl-a in the upper-thermocline is probably due to nitrate limitation. The difference in the timescales of the mixing, nitrate utilisation and growth (including chl-a

synthesis) are likely to influence the observed chl-a and nitrate relationship at any one time. Grazing is also an important loss mechanism for chl-a, and the influence of grazers may not be constant through the water column due to the change in phytoplankton cell size (as discussed below and shown in Figure 3.22). Further to the discussion in Chapter 3, the relationship between chl-a and nitrate concentration may indicate that nitrate plays a major role in providing the fuel for chl-a synthesis due to photoacclimation at the DCM, although no relationship was found between the nitrate concentration at the DCM and the DCM magnitude.

Further investigation into nitrate availability and utilisation is given in Chapter 5 and discussed in Chapter 7.

#### 4.2.2 Phytoplankton Taxonomy

During both cruises size fractionated chl-a data indicated that (on average) ~50 % of chl-a was in the < 2 µm size fraction. A relatively constant background community of flagellates accounted for a significant proportion (roughly 80%) of the total estimated phytoplankton carbon biomass across the study area. Larger cells were only significant at the shelf edge where phytoplankton > 10 µm formed a significant fraction of the community composition (typically 25 – 50% of total chl-a was in the > 10 µm size fraction). In general, phytoplankton community structure followed trends previously described (Holligan et al. 1984b, Joint et al. 1986).

Analytical Flow Cytometry (AFC) provided cellular fluorescence, cell number and cell size (from side scatter) of the picophytoplankton (< 2 µm). Cellular fluorescence generally increased with depth in all regions (with the exception of the mixed water column visited during CS03) along with an increase in cell size (as illustrated in Chapter 3).

In the oceanic region, *Prochlorococcus* was evident in the DCM (Fig. 4.9). *Synechococcus* and picoeukaryote cell numbers and estimated biomass (from cell number x cell size) also increased in the DCM though their numbers were low compared to other regions. Concentrations of the phytoplankton pigments 19'-Butanoyloxyfucoxanthin (But) and 19'-Hexanoyloxyfucoxanthin (Hex) (derived from HPLC) dominated in the oceanic region, particularly the oceanic DCM, indicating the presence of pelagophytes and prymesiophytes respectively (data not shown).

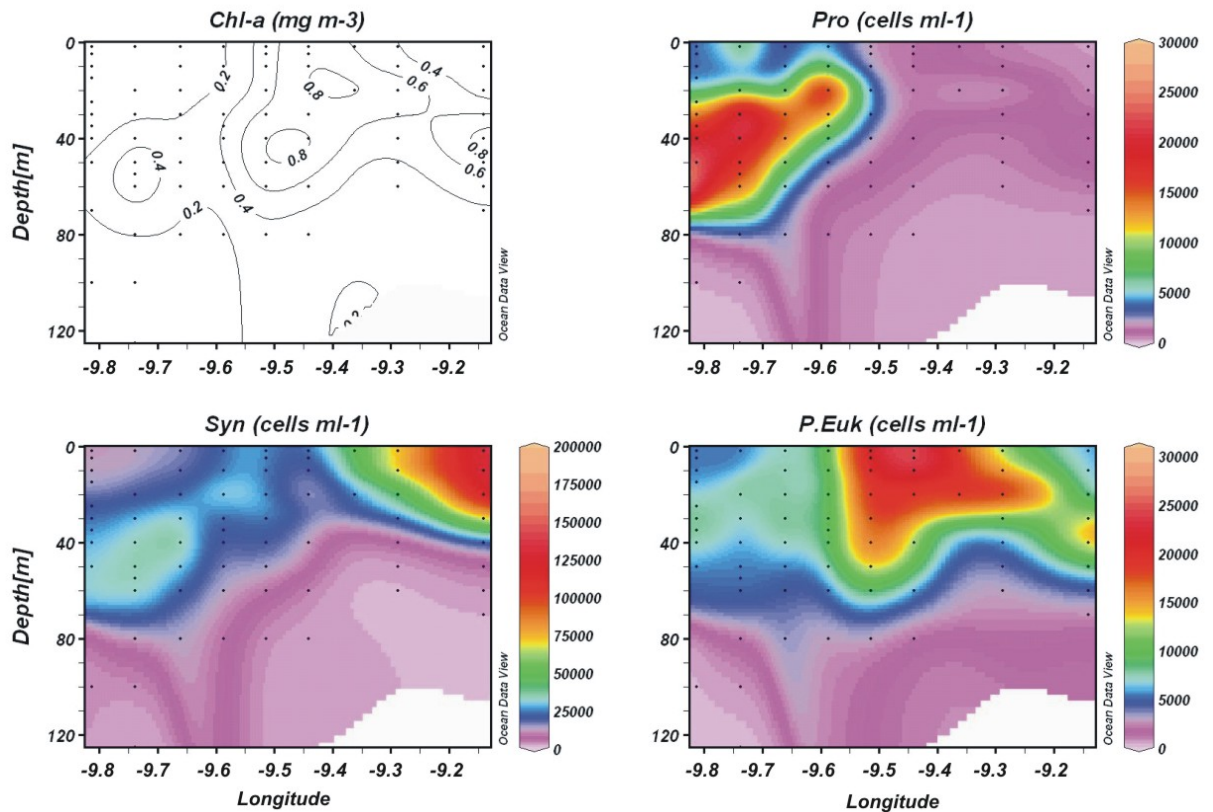


Figure 4.9. Section of concentrations of phytoplankton groups identified by Analytical Flow Cytometry across the shelf break during CS05. Oceanic waters (left of panels), shelf edge (longitude -9.45), stratified shelf (right of panel) (for transect location, see Figure 4.1). Chl-a is from bottle samples, scaled to HPLC-derived chl-a. Syn = *Synechococcus*, Pro = *Prochlorococcus*, P.euk = picoeukaryotes.

The shelf edge was dominated by picoeukaryotes in the surface and the DCM (Fig. 4.9), with diatoms contributing > 25% of estimated community biomass. Picoeukaryote concentrations were about 10 times higher at the shelf edge than in the stratified shelf region. The pigment concentrations of Fucoxanthin (Fuc) were greatest at the shelf edge, particularly at the DCM, probably reflecting the presence of both diatoms and prymnesiophytes (as Hex concentration was also significant). Prymnesiophytes were likely to be coccolithophores in this region (Holligan et al. 1984b, Sharples et al. 2001b).

The surface of the stratified shelf region contained a mixed assemblage of small phytoplankton, including *Synechococcus* (Fig. 4.9). Cell numbers of *Synechococcus* and picoeukaryotes were maximal in the DCM (Fig. 4.9, also see Fig 3.22), which, when combined with the increase in cell size, results in a maxima of estimated biomass (from cell numbers x cell

size). Diatoms were also present periodically in the shelf DCM, but only contributed more than 10% of estimated community biomass on two occasions. During CS05, chl-a within the  $> 2\mu\text{m}$  fraction was often slightly greater in the DCM than in the surface; for example at the shelf site JB1, the proportion of chl-a in the  $> 2\mu\text{m}$  size fraction increased from 50 % in the SML to 54 % at the peak of the DCM. Horizontal and vertical variability in pigment ratios (particularly Fuc:chl-a, But:chl-a and Hex:chl-a) were inconsistent between cruises, with vertical gradients generally more pronounced during CS05 than CS03.

During CS05 the increased depth resolution of sampling allowed the vertical taxonomic structure to be investigated in detail. Figure 4.10 shows the vertical taxonomic structure at a typical shelf site (JB1, CTD16 during CS05), also shown in Figure 3.22, but here focus is on the relative distribution of the phytoplankton types and comparison is made to the HPLC-derived pigment ratios.

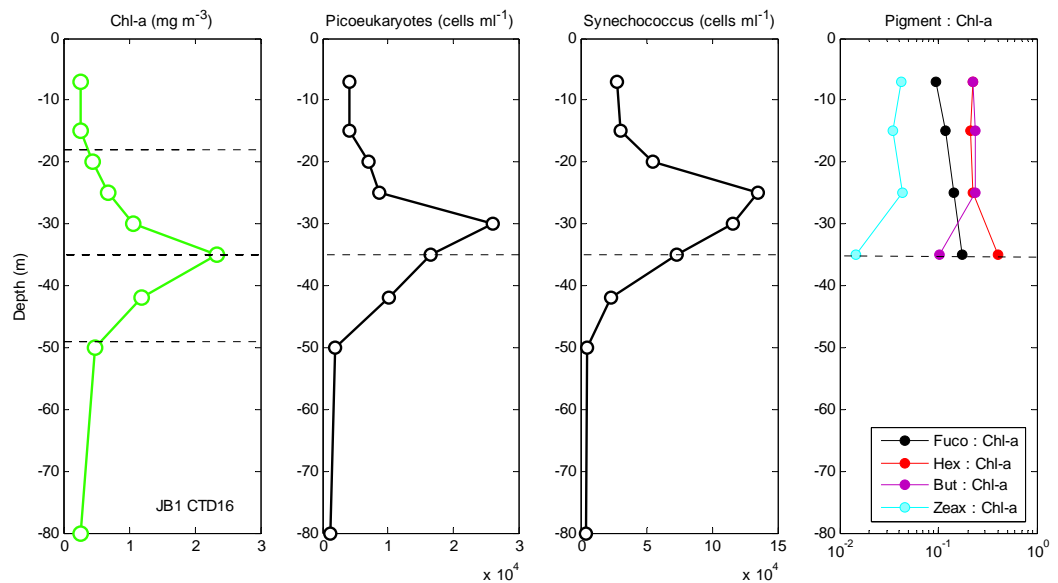


Figure 4.10. Vertical profiles of some phytoplankton groups and pigment for shelf site JB1. Dashed lines in all panels represent the peak of the DCM, with additional (upper and lower) dashed lines in the left hand panel indicating the top and bottom of the thermocline as defined by the density gradient. Chl-a is from bottle samples. Phytoplankton cell numbers from Analytical Flow Cytometry, Pigment ratios obtained from HPLC.

Figure 4.10 (also Fig. 3.22) shows that the maximum cell density of picoeukaryotes occurred deeper than that of *Synechococcus*, thus leading to a layering of these phytoplankton types

within the thermocline. This layered structure was also observed in the relative changes in HPLC-derived pigment ratios (Fig. 4.10). The pigment ratios Zeax:Chl-a and But:Chl-a decreased between the upslope and peak of the DCM. In contrast, the ratios of Fuc:Chl-a and Hex:Chl-a increased at the DCM. The change in pigment ratios supports the AFC data by indicating the assemblage composition shifts from that dominated by *Synechococcus* (Zeax:chl-a) and pelagophytes (But:chl-a) on the upslope of the DCM to that which is dominated by prymnesiophytes (Hex:chl-a and partly Fuc:chl-a) at the DCM peak. This striking feature was evident across the shelf at all locations where data resolution was high enough. This layered structure presumably results from the competition between phytoplankton species in the vertical light and nutrient gradient through the thermocline.

### 4.3 Primary Productivity through the Water Column

This section describes the magnitude and distribution of primary production through the water column, with the aim of quantifying the significance of primary production in the thermocline compared to the SML. Further, the main factors governing the variability in primary production are investigated.

The spectral light field is described in relation to the light available to the phytoplankton, and daily primary production (PP) profiles illustrated for a range of ambient light conditions. The primary production in the water column is divided into the surface mixed layer ( $P_{\text{SURF}}$ ) and thermocline ( $P_{\text{THERM}}$ ) layers in order to ascertain the significance of each layer to the total water column production ( $P_{\text{WC}}$ ). The effect of temporal variability in water-column structure on estimates of PP is discussed.

#### 4.3.1 In situ Spectral Irradiance

Reconstructions of *in situ* light fields were performed as described in Chapter 2. Primary production estimates were obtained for a range of light conditions represented by the sunniest and cloudiest days of each cruise (Fig. 4.11).

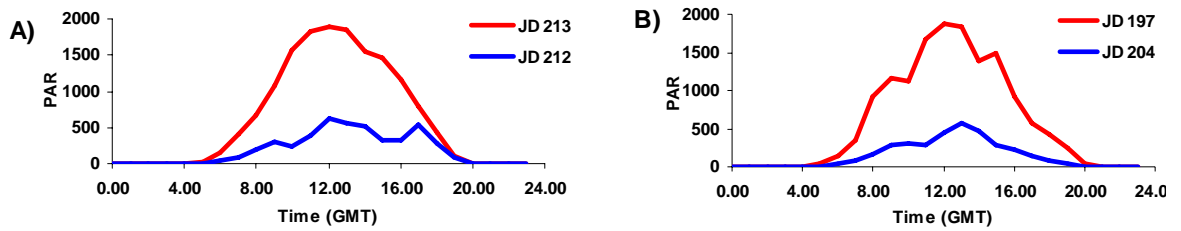


Figure 4.11. Daily variation in Photosynthetically Active Radiation (PAR) recorded by the ships meteorological package ( $\mu\text{E m}^{-2} \text{s}^{-1}$ ). The sunniest (red line) and cloudiest (blue line) days recorded during A) CS03, and B) CS05. Time is in hours (GMT), JD refers to the Julian Day on which the data were recorded. The mean daily irradiance (over 24 hours) for the sunny day was  $625 \mu\text{E m}^{-2} \text{s}^{-1}$  (CS03) and  $591 \mu\text{E m}^{-2} \text{s}^{-1}$  (CS05) and the cloudy day was  $188 \mu\text{E m}^{-2} \text{s}^{-1}$  (CS03) and  $143 \mu\text{E m}^{-2} \text{s}^{-1}$  (CS05).

Figure 4.12C shows the typical spectral composition of light through the water column during CS05. Figure 4.12B illustrates the relative intensity of light ( $E(z)$ ) through the water column at each of the six wavelengths. Wavelength 490 nm had the lowest attenuation and shows an increasing relative contribution to PAR at depth. Wavelengths on the ‘blue’ side of 490 nm (i.e. 410 and 412 nm) attenuate more rapidly than those on the ‘green and yellow’ side (i.e. 510 nm and 560 nm) due largely to the absorption of these wavelengths by phytoplankton and dissolved organic matter (DOM). This results in an increasing relative contribution of ‘green’ light with depth. The rapid attenuation of red light (i.e.  $> 680 \text{ nm}$ ), which typically diminishes by  $\sim 10\text{-}15 \text{ m}$ , is mostly due to attenuation by water (Kirk 1994).

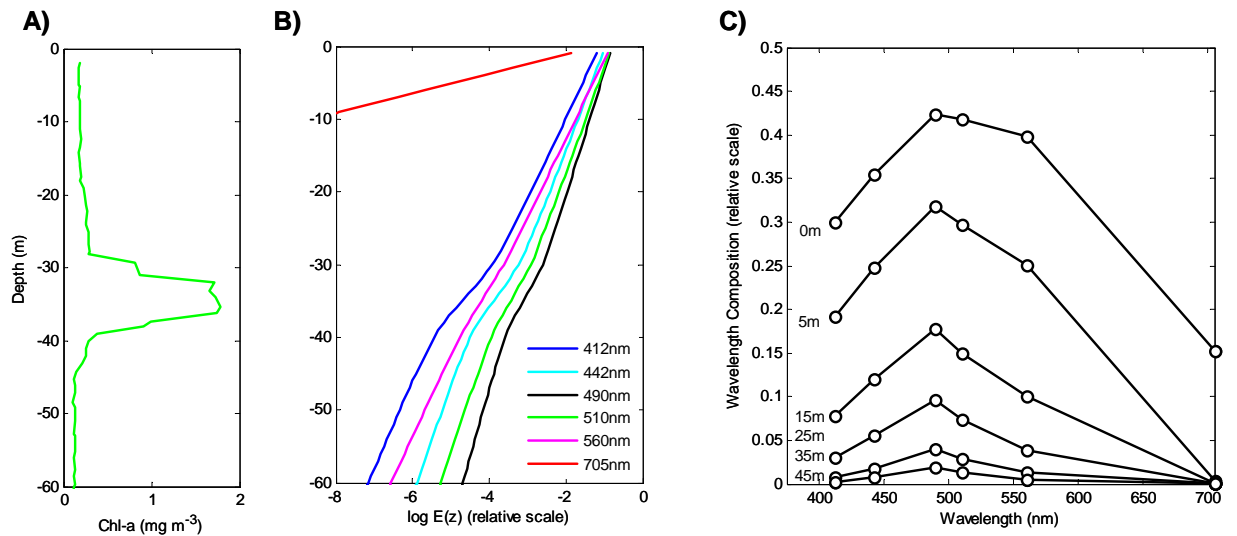


Figure 4.12. An example of reconstructed *in situ* light field characteristics for CS05 using chl-a data from CTD47. A) Chlorophyll-a profile (CTD47), B) normalised irradiance ( $E(z)$ ) through the water column at six wavelengths, C) Magnitude of  $E(z)$  (relative scale) interpolated between six wavelengths at example depths through the water column.

The effect of high chl-a in the DCM on light attenuation is clearly evident in Figure 4.12B, with most wavelengths exhibiting increasing attenuation at the DCM. The relative insensitivity of 560 nm to chl-a is expected as phytoplankton do not absorb light significantly at this wavelength (Kirk 1994).

Light available for phytoplankton depends on the *in situ* light field and the absorption characteristics of the phytoplankton present. The former is partly determined by absorption by phytoplankton in shallower waters (Kirk 1994). Figure 4.13 illustrates an example of the light absorbed by the phytoplankton (Photosynthetically Utilised Radiation, PUR) (as estimated from Eqn 2.14, Chapter 2) for the example light field described above and chl-a and absorption characteristics obtained at JB1 (CTD47, CS05).

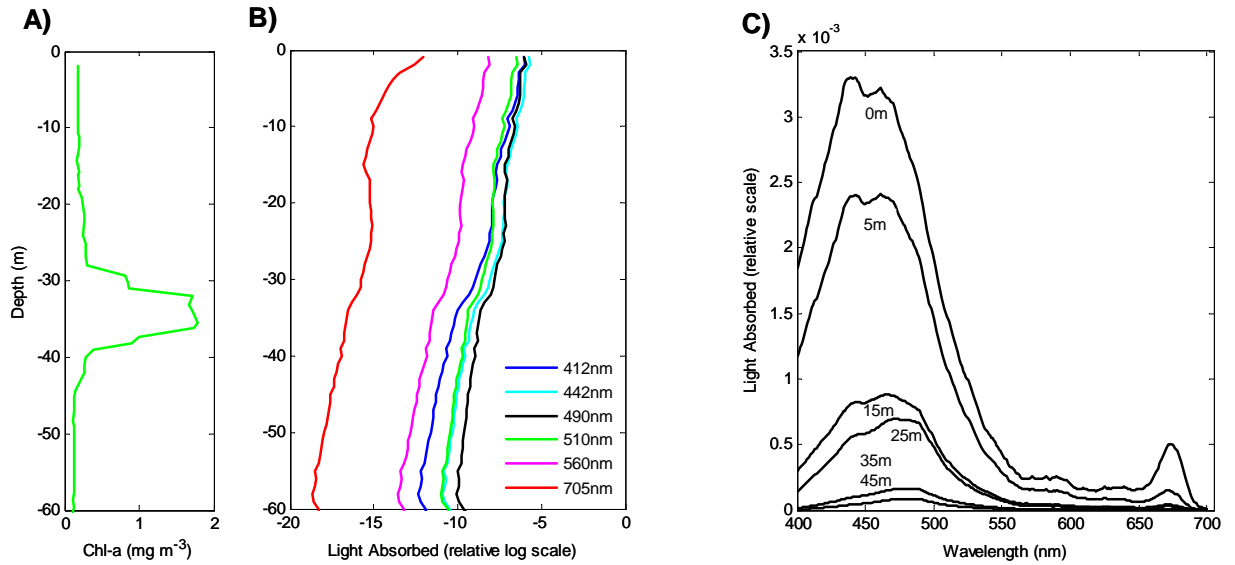


Figure 4.13. Determination of the light absorbed by phytoplankton during CS05 using chl-a and phytoplankton absorption data from CTD47, and an arbitrary (underwater) surface irradiance of  $100 \mu\text{E m}^{-2} \text{s}^{-1}$ . A) Chlorophyll-a profile (CTD47), B) magnitude of irradiance absorbed by phytoplankton through the water column at six wavelengths, C) magnitude of light absorbed by phytoplankton (relative scale) at example depths through the water column.

The combined effect of available light and phytoplankton absorption spectra leads to phytoplankton obtaining light increasing in the range 450-500 nm and decreasing in 400-442 nm relative to total light absorbed, with depth (details of the chromatic adaptation of phytoplankton can be found in Chapter 3).

#### 4.3.2 *In situ* Primary Production

Profiles of daily primary production *in situ* are shown in Figure 4.14 as obtained following the methods and assumptions outlined in Chapter 2. The ability to manipulate the incident irradiance allowed the potential range of PP at each location to be identified such that, for each location, PP is estimated for the cloudy and sunny conditions indicated in Figure 4.11. Profiles were principally constructed using measurements obtained from pre-dawn CTD casts and assumed constant throughout the day. One exception was CS2b where numerous chl-a profiles obtained over a 25 hour period showed that the pre-dawn cast did not adequately represent the typical

water-column structure at this site. Hereafter, daily PP estimates at CS2b are as calculated using all available chl-a profiles interpolated over the day.

During CS03 an additional set of measurements were obtained from daylight casts and profiles constructed from these are indicated by a sun symbol in Figure 4.14A. In general daytime measurements resulted in PP estimates greater in magnitude than those from pre-dawn casts presumably owing to the diel periodicity of physiological parameters (as outlined in Chapter 2) This illustrates the potential underestimate of PP using measurements from pre-dawn casts. However, sufficient data were not available to address this issue fully and subsequently only PP estimated from pre-dawn casts are included in the analysis that follows.

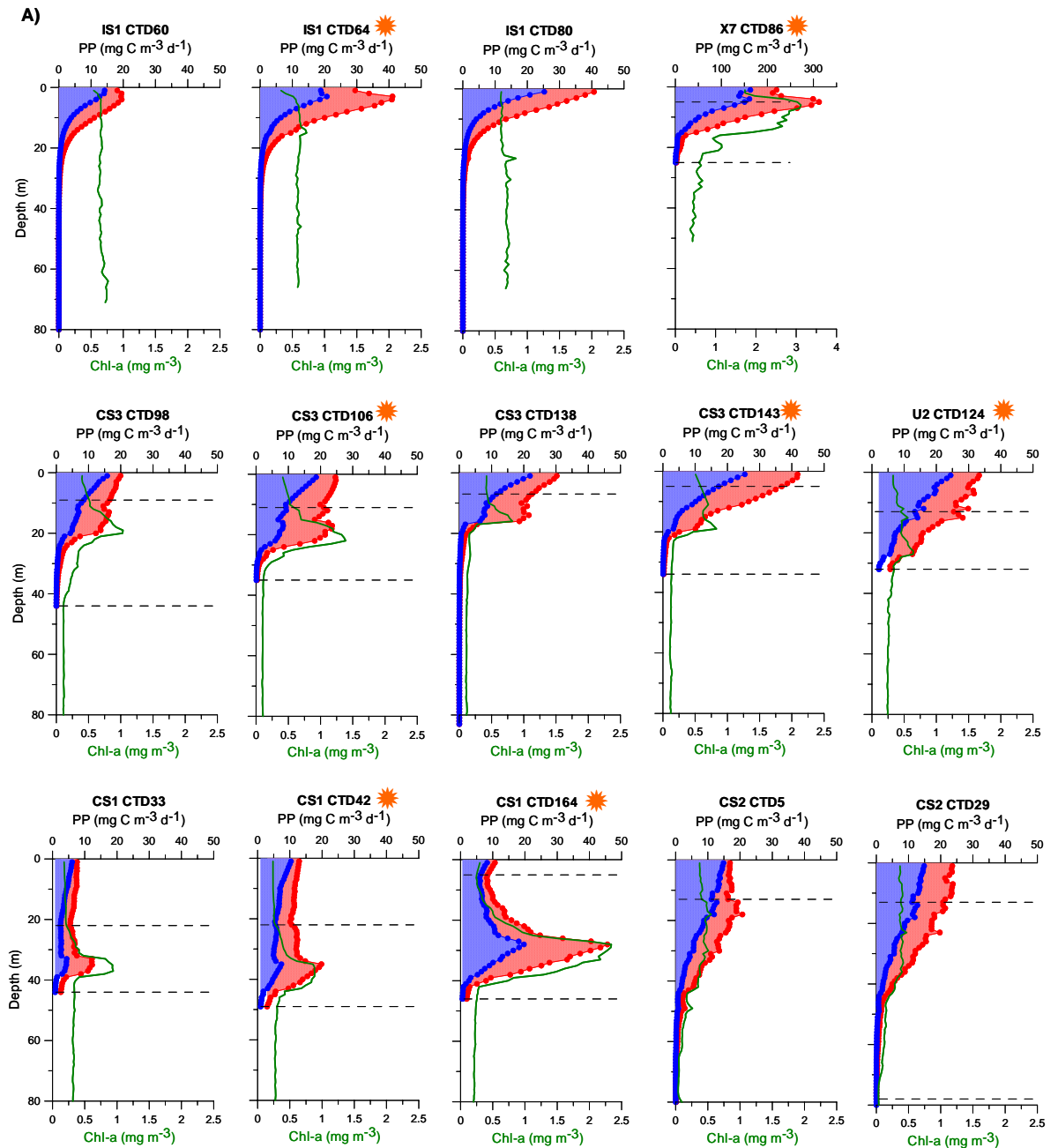


Figure 4.14. Chl-a and daily Primary Production (PP) through the water column at all available stations during A) CS03 and B) CS05. Primary Production was estimated for sunny (red line) and cloudy (blue line) day using irradiance as described in Figure 4.11. Primary production was estimated following methods described in Chapter 2. For each location the chl-a profile is shown for the cast corresponding to sample collection, with the chl-a profile assumed constant throughout the day. The only exception is CS2b (CS05) where daily PP was estimated using all available chl-a profiles obtained at this site over a 24hr sampling period, and the mean chl-a profile is shown. Dotted lines indicate the top and bottom thermocline boundaries defined by the density gradient, as described in the text. Sun symbols indicate that physiological parameters were collected during daytime CTD casts. Note the different scales for the frontal location X7.

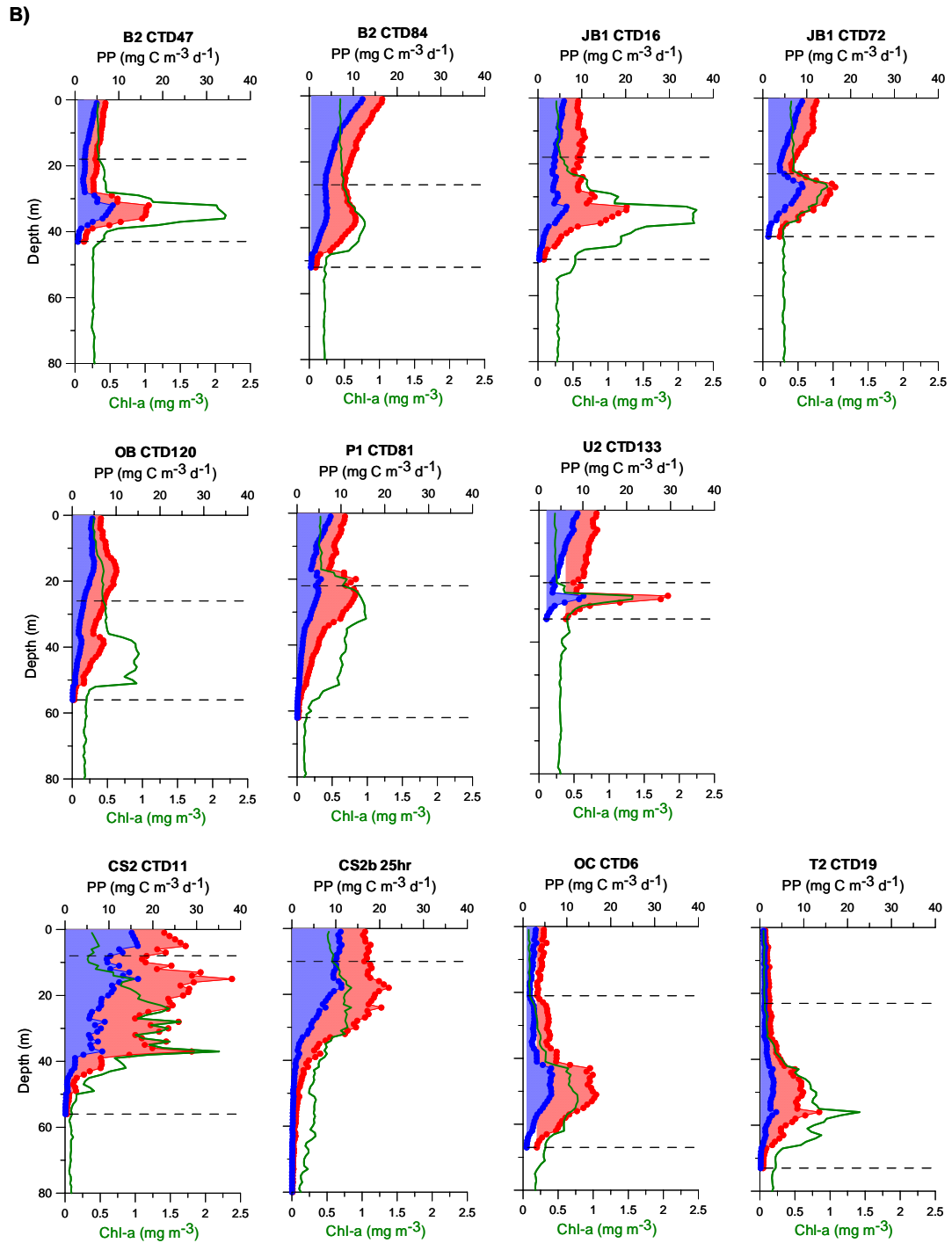


Figure 4.14. B) data from CS05. Refer to caption overleaf.

In general, profiles of PP were broadly similar within locations but distinct differences were apparent between stations. For each region, the estimated daily PP and the distribution of PP through the water column are briefly summarised in the following paragraphs.  $P_{\text{SURF}}$ ,  $P_{\text{THERM}}$  and  $P_{\text{WC}}$  for cloudy and sunny conditions obtained from each of the pre-dawn casts are provided in Table 4.2.

Table 4.2. Daily Primary Productivity integrated through the surface ( $P_{\text{SURF}}$ ), thermocline ( $P_{\text{THERM}}$ ) and water column ( $P_{\text{WC}}$ ) for pre-dawn casts.  $P_{\text{WC}}$  was estimated from  $P_{\text{SURF}} + P_{\text{THERM}}$ . Daily Primary Production was estimated following methods in Chapter 2. Cloudy and Sunny refer to the cloudiest and sunniest days recorded during each cruise with irradiances as in Figure 4.11. Thermocline boundaries were defined by the density gradient as described in the text. \*CS2b daily primary productivity estimates were calculated using multiple chl-a profiles over the 25 hour occupation. Divisions are between regions, i.e. shelf, shelf edge, oceanic.

		CLOUDY			SUNNY		
		$P_{\text{WC}}$ (mg C m <sup>-2</sup> d <sup>-1</sup> )	$P_{\text{SURF}}$ (mg C m <sup>-2</sup> d <sup>-1</sup> )	$P_{\text{THERM}}$ (mg C m <sup>-2</sup> d <sup>-1</sup> )	$P_{\text{WC}}$ (mg C m <sup>-2</sup> d <sup>-1</sup> )	$P_{\text{SURF}}$ (mg C m <sup>-2</sup> d <sup>-1</sup> )	$P_{\text{THERM}}$ (mg C m <sup>-2</sup> d <sup>-1</sup> )
<b>CS03</b>							
<b>IS1</b>	CTD60	110	-	-	225	-	-
<b>IS1</b>	CTD80	143	-	-	342	-	-
<b>X7</b>	CTD86	1355	-	-	2928	-	-
<b>CS1</b>	CTD33	148	89	59	303	144	158
<b>CS3a</b>	CTD98	185	98	87	363	147	216
<b>CS3b</b>	CTD138	198	103	95	397	162	235
<b>U2</b>	CTD124	372	227	145	667	359	308
<b>CS2a</b>	CTD5	364	161	203	623	201	422
<b>CS2b</b>	CTD29	300	59	241	645	100	544
<b>CS05</b>							
<b>B2a</b>	CTD47	147	60	87	291	101	190
<b>B2b</b>	CTD84	249	177	72	489	302	188
<b>JB1</b>	CTD16	185	84	101	466	164	303
<b>JB1</b>	CTD72	234	134	100	420	214	206
<b>OB</b>	CTD120	149	107	42	344	204	141
<b>P1</b>	CTD81	175	106	68	423	201	222
<b>U2</b>	CTD133	179	129	50	393	241	152
<b>CS2a</b>	CTD11	396	105	291	940	169	770
<b>CS2b*</b>	CTD28	254	202	52	594	408	187
<b>OC</b>	CTD6	203	44	159	500	83	417
<b>T2</b>	CTD19	108	24	84	290	38	253

In order to investigate the consequences of the choice of method used to determine the depth of the top and bottom of the thermocline on estimates of  $P_{\text{SURF}}$  and  $P_{\text{THERM}}$  a comparison was made between estimates in Table 4.2 and those where the top and bottom of the thermocline were defined by the 25.8 and 27.1  $\text{kg m}^{-3}$  density contour respectively. For the latter definition,  $P_{\text{SURF}}$  was on average 7 % greater and  $P_{\text{THERM}}$  was 11% less than estimates in Table 4.2 (for available data for CS05 only). The choice of method used to provide (realistic) thermocline boundary depths are therefore expected to lead to variations in layer-integrated PP of approximately +/- 10 %.

Overall, values of chl-a and PP were in agreement with those of previous studies (as mentioned in Chapter 1). Oceanic stations visited during CS05 exhibited a deep thermocline with very low surface chl-a ( $\sim 0.1 \text{ mg m}^{-3}$ ). The percentage irradiance of the DCM remained relatively high (9.2% +/- 18.4% of surface irradiance, Table 4.1A) such that maximal PP occurred in the DCM and was  $\sim 15 \text{ mg C m}^{-3} \text{ d}^{-1}$  during sunny days. The DCM was a PP maximum in both cloudy and sunny conditions.

The shelf edge was typically characterised by a broad productive region penetrating to  $\sim 50 \text{ m}$  with PP at the surface of  $15 - 25 \text{ mg C m}^{-3} \text{ d}^{-1}$ . The DCM occupied much of the euphotic zone and, although sometimes reached the surface, a narrow SML was typically present. The DCM was not always a productivity maximum at the shelf edge. Despite strong tidal influence caused by the continental slope topography (Pingree et al. 1981), the shape of the chl-a and PP profiles at the shelf edge remained relatively similar over both cruises. The absolute magnitude of PP, however, was variable with the  $P_{\text{WC}}$  ranging from  $254 - 939 \text{ mg C m}^{-2} \text{ d}^{-1}$  over both cruises (Table 4.2). This range is in agreement with  $400 - 1400 \text{ mg C m}^{-2} \text{ d}^{-1}$  recorded by Joint et al (2001) at a shelf edge station close by.

Across the stratified region of the Celtic Sea shelf the distribution of chl-a and PP through the water column varied widely. The DCM was never a productivity maximum at the weakly stratified site CS3, close to the Irish Sea front, where PP at the surface ( $15 - 40 \text{ mg C m}^{-3} \text{ d}^{-1}$ ) was higher than at the DCM ( $5 - 23 \text{ mg C m}^{-3} \text{ d}^{-1}$ ). In contrast, during CS05 the strongly stratified site U2 (characterised by a narrow thermocline) the DCM corresponded to a strong PP maxima (reaching  $\sim 29 \text{ mg C m}^{-3} \text{ d}^{-1}$  in sunny conditions) compared to  $< 15 \text{ mg C m}^{-3} \text{ d}^{-1}$  at the surface.

Accepting these two extreme cases, where the degree of stratification has clear implications for the distribution of chl-a and PP through the water column, across the remainder of the open shelf, the distribution of PP through the water column did not appear to vary coherently with location. For the majority of open shelf stations PP was typically maximal at the

DCM in sunny conditions. The most distinct peaks in PP within the thermocline were observed at CS1, JB1 and B2 when these stations were visited close to spring tides, and were less pronounced close to neap tides. Despite low light levels, PP was always enhanced within the thermocline due to the vertical gradients in chl-a and physiological characteristics. Across the stratified shelf,  $P_{\text{THERM}}$  ranged from 42 – 308 mg C m<sup>-2</sup> d<sup>-1</sup> between locations and irradiance conditions (Table 4.2).  $P_{\text{WC}}$  ranged from 147 – 667 mg C m<sup>-2</sup> d<sup>-1</sup>, comparing well to 316 – 540 mg C m<sup>-2</sup> d<sup>-1</sup> obtained in the stratified Celtic Sea by Joint et al. (1986) and 100 – 600 mg C m<sup>-2</sup> d<sup>-1</sup> by Holligan et al. (1984c).

In the frontal region (X7, CTD86 during CS03) where the thermocline reached the surface due to tidal mixing, productivity at the surface was estimated to exceed 100 - 200 mg C m<sup>-3</sup> d<sup>-1</sup> on a cloudy and sunny day respectively, although PP was limited to < ~20 m. On the mixed side of the front in the Irish Sea (IS1, CS03 only), chl-a and phytoplankton physiology were homogenous through the water column and resulted in PP at the surface of 15 – 40 mg C m<sup>-3</sup> d<sup>-1</sup> though restricted to < 20 m due to diminishing *in situ* irradiance.  $P_{\text{WC}}$  in the mixed region was therefore low compared to stratified waters.

Over the entire study region the potential ~3-fold increase in light conditions between the cloudy and sunny day caused a ~2-fold increase in  $P_{\text{WC}}$ .

### 4.3.3 Controls on Primary Production

This section deals with the factors contributing to the variability of estimated daily primary production. In particular, focus is on the significance of irradiance, firstly in terms of water column production, but also the relative importance of irradiance on production in the SML and thermocline.

Figure 4.15 shows the  $P_{\text{WC}}$  at all available stations (excluding the Irish Sea Front station) for both cruises under the sunny and cloudy conditions shown in Figure 4.11. Considering all stations, the mean  $P_{\text{WC}}$  was significantly different between cloudy and sunny days to the 95% confidence level (via student's T-test). The variability in  $P_{\text{WC}}$  due to the potential range in ambient irradiance was therefore greater than the difference in  $P_{\text{WC}}$  between all locations estimated under constant irradiance. Therefore the potential range in  $P_{\text{WC}}$  due to possible changes in incident irradiance is greater than the potential range in  $P_{\text{WC}}$  resulting from the other contributing factors such as chl-a concentration and physiological parameters.

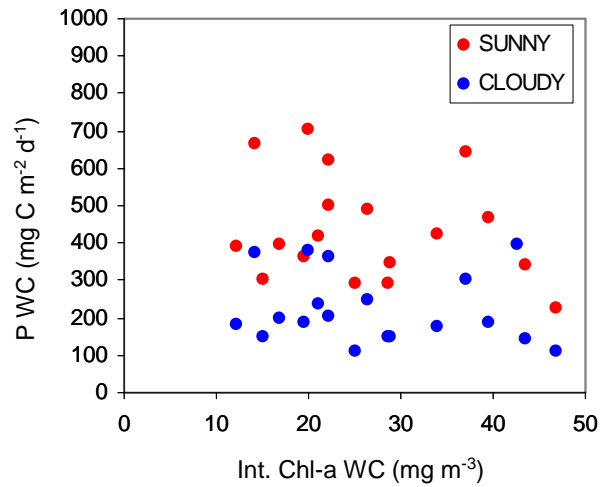


Figure 4.15. Relationship between  $P_{WC}$  and water column-integrated chl-a for the cloudy and sunny conditions shown in Figure. 4.11. Data are shown for all hydrographic regions visited during both cruises, with the exception of the Irish Sea front. Integrated primary production was estimated following methods in Chapter 2.

In order to investigate the effect of irradiance on productivity within the surface and thermocline, daily PP was estimated for the irradiance conditions recorded at each location on the actual day of sampling and shown in Figure 4.16. The water-column depth refers to the ‘productive’ region of the water column only (defined by SML thickness + thermocline thickness). Frontal, shelf edge and mixed sites were omitted in order to focus on the more typical stratified conditions of the oceanic and shelf regions. The statistics quoted on Figure 4.16 are the result of model II regression using combined data from both cruises.

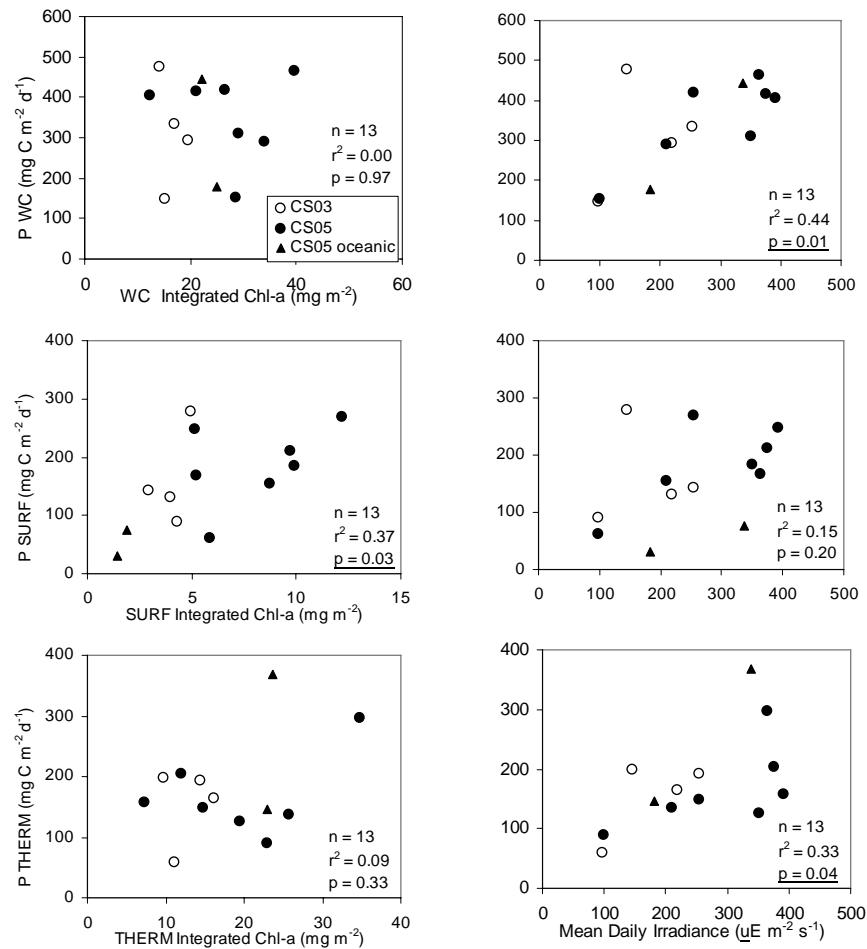


Figure 4.16. Integrated primary production in the water column (top panels), SML (middle panels) and thermocline (lower panels) against layer-integrated chl-a (left panels) and daily mean irradiance below the surface for the day of sampling (right panels). The water column is assumed to be only the ‘productive’ region above the BML represented by SML + thermocline. Data shown are from stratified shelf (circles) and oceanic regions (triangles) during both cruises, open symbols = CS03, closed symbols = CS05. Integrated primary production was estimated following methods in Chapter 2. Mean daily surface irradiance is the 24 hour mean PAR recorded from the ships meteorological package for the days of sample collection, and adjusted for the transmittance through the air-sea interface (see Chapter 2), therefore representing irradiance just below the surface. Statistics shown are the result of model II regression for combined data from both cruises. Relationships that are significant to the 95% confidence level are underlined.

Estimated daily primary production in the SML ( $P_{\text{SURF}}$ ) was not significantly correlated to surface irradiance with 55% of the variability in  $P_{\text{SURF}}$  attributable to SML-integrated chl-a. It

follows (from the relationship between layer-integrated chl-a and layer thickness (Fig. 4.5 above)) that  $P_{\text{SURF}}$  was also correlated to the thickness of the SML (not shown).

In contrast,  $P_{\text{THERM}}$  was not significantly correlated to integrated chl-a within the thermocline with 33% of the variability in  $P_{\text{THERM}}$  attributable to surface irradiance. Consequently, 44% of the variance in overall  $P_{\text{WC}}$  was due to surface irradiance with no relationship between  $P_{\text{WC}}$  and water column-integrated chl-a. The scatter around these relationships is likely to be partly due to the variability in physiological and absorption characteristics at each location. 51% of the variability in  $P_{\text{WC}}$  was due to  $P_{\text{THERM}}$  ( $n = 10$ ,  $r^2 = 0.51$ ,  $p = 0.020$ ) and 40% by  $P^*_m$  at the surface ( $\sim 2$  m) ( $n = 10$ ,  $r^2 = 0.416$ ,  $p = 0.044$ ) in agreement with Lorenzo et al. (2004).

These data show that the influence of irradiance was more significant in the thermocline than in the surface, likely due to the fact that phytoplankton in the thermocline were light limited compared to at the surface, and therefore sensitive to variability in light intensity (see Chapter 3).

#### 4.3.4 Temporal Variability in Primary Production

This section describes the effect of the observed temporal variability in water column structure on the estimated primary production at individual sites. Specifically, the influences of the semidiurnal and spring-neap tidal cycles are discussed.

As mentioned above, the daily PP estimated using all chl-a profiles obtained over 24 hours compared to PP estimated using only the pre-dawn chl-a profile (assumed constant over the day) were similar, such that temporal variability in chl-a structure over 24 hours at each location was not as significant as the difference in PP between locations. However, it is important to describe the potential temporal variability at each location, and quantify the influence on primary production.

##### *Temporal variability over a semidiurnal tidal cycle*

A limited number of stations were occupied for a 25 hour period, including CS2a, CS2b, CS1, CS3b, OB, B2a and B2b. Temporal variability at CS1 and B2a and B2b is provided in Figure 4.4.

Changes in water column structure over the semidiurnal tidal cycle were not consistent between sites. Factors such as local wind conditions, timing within the spring-neap cycle and local features such as water depth and seabed topography were likely to cause mixing conditions

unique to each location. However, in general, the fluctuation in tidal current speed over 25 hours caused changes in the depth and / or thickness of the thermocline (e.g. Fig. 4.4).

For all available 25 hour occupations, layer-integrated chl-a was significantly correlated to layer thickness (Fig. 4.5) and therefore changes in water column structure were accompanied by variable integrated chl-a over a tidal cycle. Over all available data, the thickness of the thermocline during a 24 hour period was determined primarily by the depth of the base of the thermocline rather than the depth of the SML (average standard deviation of the depth of the top of the thermocline was 4.1 m compared to 8.8 m for the base of the thermocline, for all 25 hour station data, Table 4.1).

In order to investigate the effect of the daily variability in water column structure on PP, estimates of hourly PP through the water column were obtained for each of 24 chl-a profiles available over the 25 hour sampling period at CS1. PP for each chl-a profile was estimated for a constant incident (above-surface) irradiance of  $500 \mu\text{E m}^{-2} \text{s}^{-1}$  (below surface irradiance was  $312 \mu\text{E m}^{-2} \text{s}^{-1}$  after adjustment for the transmittance through the sea surface (described in Chapter 2)). Chl-a profiles were linearly interpolated between any gaps in the hourly CTD sampling sequence.

Table 4.3. Values of  $r^2$  from model II regression analysis for the co-variance of layer-integrated chl-a, layer-integrated primary production and layer thickness for the surface, thermocline and water-column layers, at CS1. PP through the water column was estimated for each of 24 chl-a profiles obtained over a semidiurnal tidal cycle at CS1 under irradiance of  $500 \mu\text{E m}^{-2} \text{s}^{-1}$  incident at the sea surface. A linear interpolation of chl-a at each meter was applied to fill gaps in the hourly sampling sequence. Total water column (WC) thickness represents the productive region of the water column above the BML and was obtained from SML + thermocline thickness. All relationships were significant to the 95% confidence level, with the exception of those in italics.

<b>SURFACE</b>	Chl-a	PP	<b>THERM</b>	Chl-a	PP	<b>WC</b>	Chl-a	PP
Thickness	0.42	0.21	Thickness	0.80	0.63	Thickness	0.70	<i>0.16</i>
PP	0.94		PP	0.77		PP	0.67	

Hourly PP was significantly correlated to both integrated chl-a and layer thickness (Table 4.3). However, a greater proportion of the variability in layer-integrated PP was attributable to changes in chl-a rather than layer thickness (Table 4.3) such that  $P_{\text{WC}}$  was not significantly

correlated to layer thickness. For CS1,  $P_{\text{THERM}}$  was not significantly correlated to the percentage irradiance of the DCM, though a significant relationship was found at some locations (e.g. OB,  $n = 24$ ,  $r^2 = 0.363$ ,  $p = 0.002$ , OB shown in Figure 4.4).

A similar relationship between chl-a and PP was also found when each available chl-a profile from a given location was interpolated over a 25 hour period. Using this method it was possible to show that the variability in daily PP between a cloudy and sunny day was more significant than that potentially resulting from the daily variability in water column-integrated chl-a (e.g. for CS1, the mean of daily PP estimated from each chl-a profile for sunny conditions was significantly different to the mean of daily PP estimated from each chl-a profile for cloudy conditions, to the 95% confidence level).

It follows from the observations in this section that greatest *in situ* PP at any location would occur on a sunny day with the co-incident occurrence of increased chl-a within the thermocline (typically associated with a thermocline that is broad) and increased percent irradiance of the DCM (when the thermocline is shallow) as driven by the tidal cycle. Daily PP at a given location would therefore be maximal if the thermocline was broad and shallow at noon. In general, when the thermocline was broad, the peak of the DCM was deeper than when the thermocline was narrow, and subsequently a trade-off occurs between integrated chl-a and light availability in the amount of primary productivity at the DCM. Overall, however, the greatest degree of variability in estimated *in situ* primary production was due to the potential range of ambient irradiance, rather than the potential range in integrated chl-a, or water column structure, either between or within locations.

#### *Temporal variability over the spring - neap tidal cycle*

A limited number of locations (CS2, CS3, B2) were sampled for 25 hours on more than one occasion during a spring-neap cycle. At each of these locations the daily variability in temperature and chl-a structure was enhanced close to spring tides (e.g. B2, as shown in Fig. 4.4). At CS2 and CS3 the water column -integrated chl-a (and subsequently estimated PP) was greater close to neap tides (CS2a and CS3a) compared to springs (CS2b and CS3b) (Table 4.1 and 4.2). However, at B2 integrated chl-a and PP was greatest close to springs (B2a) compared to neaps (B2b) (Table 4.1 and 4.2).

The mixing of nitrate into, and chl-a out of, the thermocline mainly occur at times of increased mixing associated with spring tides (Sharples et al. 2001b). Changes in chl-a concentration over spring-neap timescales (order of days) are likely to result from variability in PP due to fluctuations in nitrate supply from the BML, combined with the losses due to mixing

of chl-a into the BML (as well as losses due to grazing). The interactions between mixing conditions and PP are complex with no consistent patterns occurring across the study region in these data. The effect of the spring-neap cycle on PP is discussed in more detail in Chapters 5 and 7.

#### 4.3.5 The Significance of Primary Production in the Thermocline

The contribution of primary production in the thermocline to water column production is given by the ratio of  $P_{\text{THERM}}/P_{\text{WC}}$  and is illustrated in Figure 4.17. The contribution is determined by PP as well as the relative thickness of the surface and thermocline layers.

The thermocline always contributed more significantly to water column productivity in sunny, compared to cloudy, conditions. As described above, this is due to the light-limited nature of phytoplankton within the thermocline compared to in the SML (see also Chapter 3).

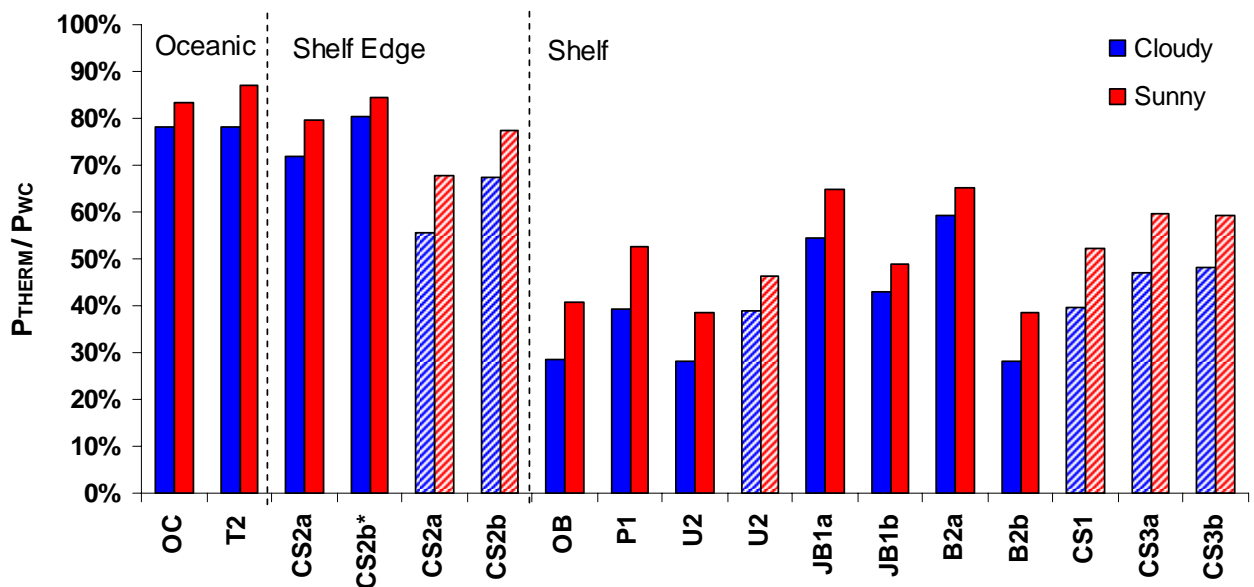


Figure 4.17. The percentage contribution of daily primary production in the thermocline ( $P_{\text{THERM}}$ ) to water column production ( $P_{\text{WC}}$ ) for cloudy and sunny conditions (shown in Fig. 4.11). Solid bars are data from CS05 and striped bars are data from CS03. Primary production was calculated following methods described in Chapter 2. \*CS2b daily primary productivity estimates are calculated using multiple chl-a profiles over the 25 hour occupation.

Primary production in the thermocline contributed more than 25% of water column primary production over the study region. The contribution was greatest in the oceanic region (~80%) where low chl-a in the surface waters allowed light to penetrate to the DCM despite the relatively deep SML depth.

At the shelf edge, the primary production was greater at the surface than at depth but the SML was relatively shallow compared to the broad thermocline. Subsequently, the thermocline was the location of > 75% of productivity in the water column. The contribution of PP in the thermocline at the shelf edge was greater during CS05 than during CS03 reflecting the greater integrated chl-a concentration at this site during CS05 (Fig. 4.14AB, Table 4.1).

Across the stratified shelf, the contribution of PP within the thermocline was consistently within the range from ~30 – 70%. Variability in  $P_{\text{THERM}}/P_{\text{WC}}$  was as significant between occupations of the same location as between sites. The difference in  $P_{\text{THERM}}/P_{\text{WC}}$  between cloudy and sunny conditions was not as great as between repeated occupations at the same site, or between sites.

Despite the relatively high PP in the surface at the weakly stratified site CS3 the thermocline was broad, leading to  $P_{\text{THERM}}$  contributing between 47 – 60% to  $P_{\text{WC}}$ . Similarly, despite the high PP within the narrow thermocline at U2, the thermocline was deep such that production in the SML was greater than that within the thermocline and  $P_{\text{THERM}}$  only contributed 28-46% to  $P_{\text{WC}}$ .

#### 4.4 Summary of Main Points

The major observations within this chapter were:

- A DCM was present within the thermocline across the entire Celtic Sea region with the exception of the mixed Irish Sea.
- The vertical structure of the water column (particularly regarding the depth and thickness of the thermocline) varied considerably across the shelf, and across diurnal and spring-neap tidal cycles.
- On the stratified shelf, the DCM was generally located at the base of the thermocline and was associated with the nitracline, which rarely reached the top of the thermocline.
- Phytoplankton community composition was mostly small cells (< 2  $\mu\text{m}$ ) and was slightly different between the SML and the thermocline. Vertical gradients in taxonomic

composition (particularly via AFC enumeration of small cells) were observed within the thermocline itself.

- Primary production in the thermocline accounted for ~30-70% of total water column production on the shelf, > 60% at the shelf edge and ~80% in the oceanic region just off the shelf.
- Primary production in the SML was most sensitive to chl-a concentration, while in the thermocline, PP was most sensitive to ambient irradiance.
- Physical water column structure appeared to have a minor influence on estimates of daily PP. The most significant variable affecting daily PP estimates was mean daily irradiance.

## CHAPTER 5: NEW PRODUCTION IN THE CELTIC SEA

In this chapter the biogeochemical processes occurring within the thermocline are investigated in order to establish the capacity for the thermocline to support new production. The chapter begins by introducing the vertical distribution of nitrate and dissolved oxygen compared to chl-a and estimated daily primary production (from carbon fixation) through the water column. The light response of nitrate uptake and oxygen evolution at the DCM is described and compared to estimates of carbon fixation at two contrasting locations. This is brought into the broader context by considering the nitrate flux into the thermocline estimated from turbulent mixing measurements (provided by J. Tweddle, *pers. comm.*). The larger scale implications of these biogeochemical processes are then illustrated over the entire study region by comparing measurements of dissolved oxygen and nitrate concentrations in the water column. The functioning of the thermocline is discussed with emphasis on mixing and the implications for new production.

### 5.1 Study Area

Data are presented from the Celtic Sea (CS03 and CS05) and stations are the same as those described in Chapter 4 (refer to the map, Figure 4.1). Hereafter, daily irradiance conditions referred to as ‘sunny’ and ‘cloudy’ represent the daily irradiance recorded on the sunniest and cloudiest days during each cruise, as shown in Figure 4.11.

#### 5.1.1 Vertical Distribution of $\text{NO}_3^-$ and Dissolved $\text{O}_2$

The concentration of nitrate and dissolved oxygen (as percent saturation, % $\text{O}_2$ ) are shown in Figure 5.1 alongside chl-a distribution and estimated daily primary production for three stratified locations. Nitrate concentration is below the limit of detection by standard colorimetric techniques ( $< 0.1 \mu\text{M}$ ) in the SML and as such the thermocline (as the location of the nitracline) is likely to be the main site of new production in the water column.

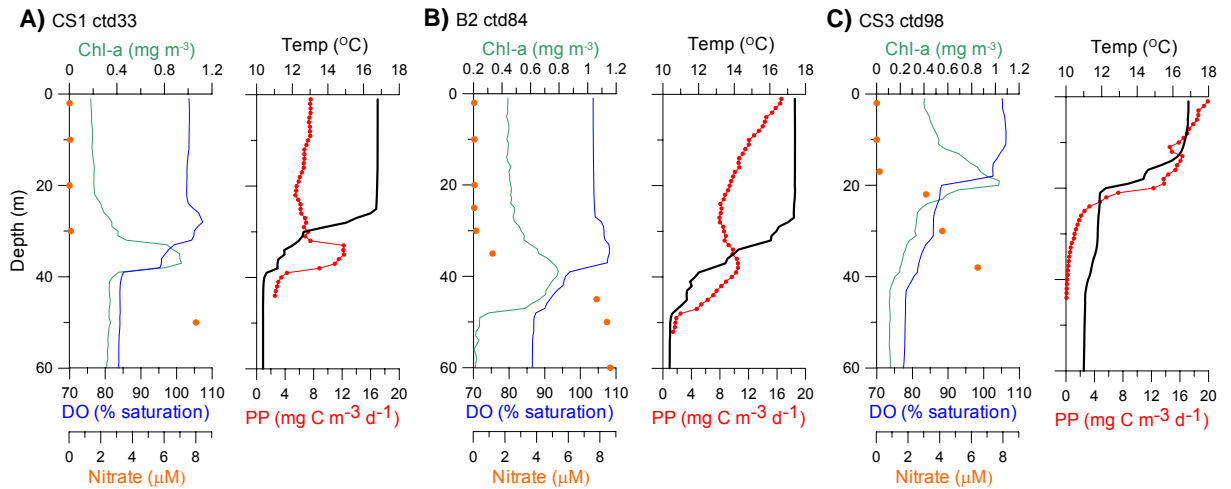


Figure 5.1. Vertical profiles of chl-a, DO (dissolved oxygen saturation (%O<sub>2</sub>)) and nitrate (left panel) and temperature and estimated daily Primary Production (right panel) for three selected stations during CS03 (for CS1 and CS3) and CS05 (for B2). Daily primary production is illustrated for sunny conditions following methods outlined in Chapter 2.

When expressed in terms of percent saturation, the effect of temperature on the seawater capacity for dissolved oxygen is accounted for. Figure 5.1 shows that %O<sub>2</sub> is close to saturation (100%) in the SML as a result of air-sea exchange and mixing. In contrast, in the BML %O<sub>2</sub> is sub-saturated, with the deficit representing the net losses due to respiration and remineralisation processes that have occurred in the BML (with no contact with the atmosphere) since the onset of stratification.

Figure 5.1 clearly shows the presence of a dissolved oxygen maximum, with %O<sub>2</sub> greater than 100% saturation in the upper part of the thermocline. Such a %O<sub>2</sub> maxima in the shelf sea thermocline has also been observed in the North Sea (Richardson et al. 2000) and was a persistent feature across the study region. Super-saturation of oxygen within the thermocline cannot be formed purely by physical mixing processes (Williams and Purdie 1991), though it could result from subsequent warming of surface water ‘trapped’ within the thermocline following stratification. If the cycling of dissolved oxygen and reduced forms of nitrogen by heterotrophic respiration and recycled (as opposed to new) primary production are balanced, there is no net gain or loss of either nitrate or oxygen in solution. Dissolved oxygen super-saturation therefore likely reflects net community oxygen evolution in response to an external source of nitrate fuelling new production (Reid and Shulenberger 1986, Craig and Hayward

1987). However, Figure 5.1 illustrates that the peak in %O<sub>2</sub> typically does not occur at the location of maximal estimated PP.

The concentrations of nitrogen and oxygen are generally exchanged in balance following the Redfield ratio (-138O<sub>2</sub>:106C:16N:1P by atoms) (Redfield et al. 1963). The Redfield ratio of -O<sub>2</sub>:N is therefore 8.625 (by atoms). However, -O<sub>2</sub>:N has since been reported as 9.375 for organic matter (Anderson 1995) and 10.625 for the stoichiometry of remineralisation in the deep ocean (Anderson and Sarmiento 1995).

First, the focus is to quantify the utilisation of NO<sub>3</sub><sup>-</sup> and evolution of O<sub>2</sub> at the peak of the DCM and investigate the light-response of these processes in comparison to carbon fixation.

## 5.2 Light-response of NO<sub>3</sub><sup>-</sup> uptake and O<sub>2</sub> evolution at the DCM

This section investigates the relative balance of nitrate uptake and carbon fixation with the evolution of oxygen by phytoplankton in a range of realistic light conditions at the DCM peak. The balance of these processes is discussed with reference to the Redfield ratio and in respect of new and total production at the DCM.

### 5.2.1 Nitrate Uptake at the DCM

In order to quantify the light response of nitrate utilisation and therefore new production directly, the uptake of <sup>15</sup>N-labelled nitrate was measured in P vs. E type incubation experiments following methods outlined in Chapter 2. The use of <sup>13</sup>C and <sup>15</sup>N uptake vs. irradiance curves in investigation of assimilation ratios is a relatively novel approach; only one example of its use has been found in published literature (Frenette et al. 1998). The use of P vs. E responses allows investigation of C:NO<sub>3</sub><sup>-</sup> uptake ratios across a range of realistic *in situ* irradiances.

Successful experiments were achieved at numerous sampling times at CS3 and CS1 (during CS03). For DCM samples, the irradiance response of carbon (<sup>13</sup>C and <sup>14</sup>C) and nitrate uptake at these two contrasting shelf stations (during CS03) is given in Fig 5.2. Nitrate uptake is strongly dependent on the ambient concentration. The maximal light-saturated nitrate uptake rate would increase with increased nitrate concentration if the ambient concentration is not saturating. However, nitrate is often considered saturating at concentrations ~1 μM (Eppley et al. 1969).

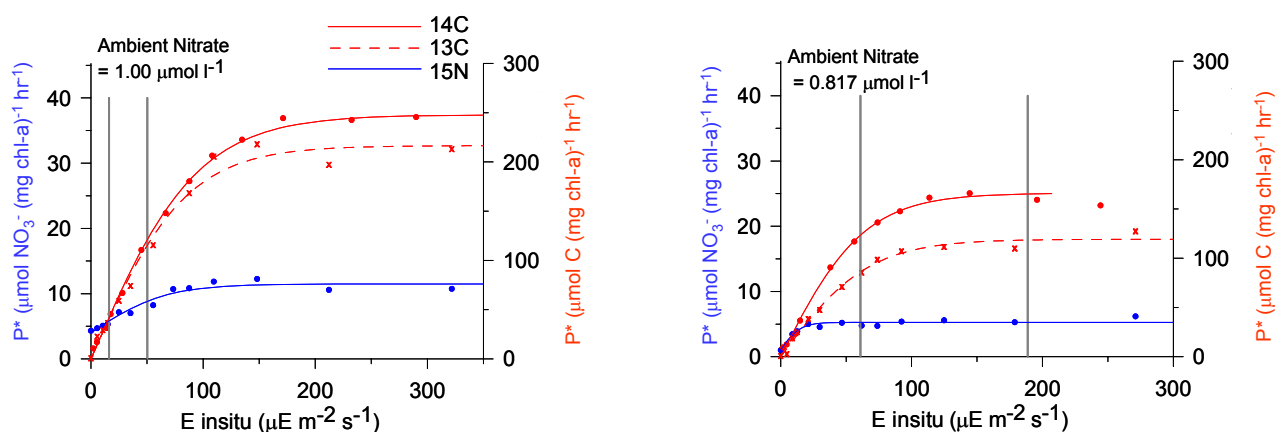


Figure 5.2. Hourly nitrate and carbon (<sup>14</sup>C, <sup>13</sup>C and <sup>15</sup>N) uptake per unit chl-a against irradiance for CS3 (CTD138, left panel) and CS1 (CTD 164, right panel) during CS03. <sup>13</sup>C and nitrate (by <sup>15</sup>N) uptake were estimated by dual labelling on same samples, following methods in Chapter 2. Axis lengths are relative to Redfield C:N (6.625) such that the curves cross at the irradiance at which the C:NO<sub>3</sub><sup>-</sup> uptake ratio is equal to 6.625. Irradiance is corrected for *in situ* spectral light field at each location. Vertical grey lines indicate peak irradiance experienced on a cloudy (JD = 212) and sunny (JD = 213) day using *in situ* optics characteristics and following methods in Chapter 2. Samples were collected close to midday at CS1 and at night at CS3. Ambient nitrate concentrations are as indicated. Chl-a concentrations at CS3 and CS1 were 0.92 and 2.34 mg chl-a m<sup>-3</sup> respectively.

There was good repeatability between experiments at CS3 (not shown), with no evidence to show diel periodicity in <sup>15</sup>NO<sub>3</sub><sup>-</sup>-uptake vs. irradiance response in samples taken throughout (3 times) the day. There was good agreement between <sup>13</sup>C and <sup>14</sup>C curve fitting parameters (e.g. Ek  $r^2 = 0.43$ , slope = 0.99,  $n = 4$ , all data CS03), giving confidence in the measurement. Due to methods used and practical issues regarding analysis of <sup>13</sup>C samples, the <sup>14</sup>C-uptake measurements were deemed more reliable and were used in the subsequent analysis.

Due to low chl-a concentration in the surface (and subsequent light attenuation) the *in situ* ambient irradiance was greater at the DCM at CS1 than CS3 (the DCM was at 7.6% and 5.5% surface irradiance for CS1 and CS3 respectively). The light-limited nature of the DCM was clearly evident at CS3, where peak irradiance on the sunny day remained sub-saturating for both carbon and nitrate assimilation. In contrast, at CS1 <sup>15</sup>NO<sub>3</sub><sup>-</sup>-uptake was saturated even during cloudy conditions. Ambient nitrate concentrations (for these representative samples) at CS3 and CS1 were 1.0 μmol l<sup>-1</sup> and 0.8 μmol l<sup>-1</sup> respectively.

<sup>15</sup>NO<sub>3</sub><sup>-</sup>-uptake was less sensitive to irradiance than <sup>14</sup>C-uptake, with a lower range in nitrate uptake over the range of incubation irradiances. Nitrate uptake was saturated at a lower

irradiance intensity ( $^{15}\text{NO}_3^-$ -uptake  $E_k < ^{14}\text{C}$ -uptake  $E_k$ ) and had a steeper initial slope of the uptake-irradiance curve than that for carbon fixation. It follows that the  $\text{C}:\text{NO}_3^-$  uptake ratio increased with irradiance as illustrated in (Fig. 5.3). During sunny conditions, at both CS3 and CS1, the  $\text{C}:\text{NO}_3^-$  uptake ratio at the DCM was greater than the Redfield ratio (6.625 by atoms) for a significant proportion of the daylight period.

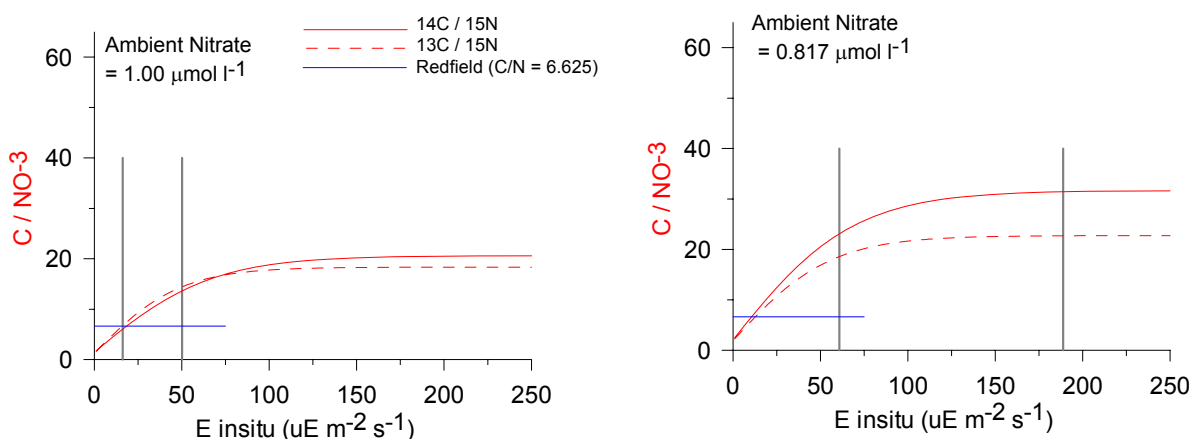


Figure 5.3. Carbon ( $^{14}\text{C}$  and  $^{13}\text{C}$ ) to nitrate uptake ratios against irradiance for CS3 (left panel) and CS1 (right panel) during CS03.  $^{13}\text{C}$  and nitrate (by  $^{15}\text{N}$ ) uptake were estimated by dual labelling on same samples, following methods in Chapter 2. Redfield  $\text{C}:\text{NO}_3^-$  ratio of 6.625 is indicated by the blue line. Irradiance was corrected for *in situ* spectral light fields at each location. Grey lines indicate the peak irradiance experienced on a cloudy (JD = 212) and sunny (JD = 213) day using *in situ* optics characteristics and following methods in Chapter 2. Samples were collected close to midday at CS1 and at night at CS3. Ambient nitrate concentrations are as indicated. Units of ratio are mol:mol.

In the following estimates of daily nitrate uptake (over 24 hours), the dark uptake of nitrate was estimated from the intercept of the  $\text{NO}_3^-$ -uptake vs. irradiance curve and was assumed to be representative of the night-time nitrate uptake, which was assumed to be constant. As with  $^{14}\text{C}$ -uptake, the diel periodicity of  $\text{NO}_3^-$  was not considered.

At CS3, estimated daily nitrate uptake at the DCM (20 m) was 19 - 25  $\mu\text{mol } ^{15}\text{NO}_3^-$  ( $\text{mg chl-a}^{-1} \text{d}^{-1}$ ) from cloudy to sunny conditions respectively (assuming the cloudiest and sunniest days experienced during CS03 represent the extremes of irradiance conditions). The corresponding  $^{14}\text{C}$ -uptake for the same conditions was 55 - 171  $\mu\text{mol } ^{14}\text{C}$  ( $\text{mg chl-a}^{-1} \text{d}^{-1}$ ). Therefore the mean daily  $\text{C}:\text{NO}_3^-$  uptake ratio for CS3 was 3.1 - 7.5. A duplicate dataset for another CTD cast at CS3 of similar ambient nitrate concentrations yielded nitrate uptake of 77 - 101  $\mu\text{mol } ^{15}\text{NO}_3^-$  ( $\text{mg chl-a}^{-1} \text{d}^{-1}$ ), carbon uptake of 291 - 889  $\mu\text{mol } ^{14}\text{C}$  ( $\text{mg chl-a}^{-1} \text{d}^{-1}$ ) and

therefore a similar C:NO<sub>3</sub><sup>-</sup> uptake ratio of 3.8 – 8.8 between cloudy and sunny conditions. At CS3 the uptake stoichiometry at the peak of the DCM was therefore close to Redfield over a 24 hour period for realistic light conditions, such that the nitrogen requirement of carbon fixation at the DCM was likely to be largely sustained by nitrate.

At CS1, estimated nitrate uptake at the DCM peak was 148 – 171 μmol <sup>15</sup>NO<sub>3</sub><sup>-</sup> (mg chl-a)<sup>-1</sup> d<sup>-1</sup> and carbon uptake was 1084 – 2830 μmol <sup>14</sup>C (mg chl-a)<sup>-1</sup> d<sup>-1</sup> between cloudy and sunny conditions, leading to a daily-mean C:NO<sub>3</sub><sup>-</sup> uptake ratio of 7.3 – 16.6. In this case, carbon fixation appears to not have been entirely supported by nitrate and carbon fixation must therefore have been partly sustained by other forms of nitrogen. The higher C:NO<sub>3</sub><sup>-</sup> uptake ratio at CS1 compared to CS3 may be due to greater *in situ* irradiance and/or lower ambient nitrate concentrations at the DCM peak as well as taxonomic and/or physiological differences in the phytoplankton present.

Accounting for chl-a concentration, the amounts of nitrate uptake at CS3 were close to those observed at the thermocline in the Western English Channel of 0.02 mg NO<sub>3</sub><sup>-</sup> m<sup>-3</sup> h<sup>-1</sup> (Le Corre et al. 1993) (i.e. 19 - 25 μmol <sup>15</sup>NO<sub>3</sub><sup>-</sup> (mg chl-a)<sup>-1</sup> d<sup>-1</sup> converted to mg by multiplying by 14/1000, multiplying by 0.92 mg chl-a m<sup>-3</sup> and dividing by 16 h).

These analyses indicate that the light-response of carbon and nitrate uptake yield a C:NO<sub>3</sub><sup>-</sup> uptake ratio that varies over the day with ambient irradiance, in agreement with Frenette et al. (1998). This indicates a distinct diel periodicity of the C:NO<sub>3</sub><sup>-</sup> ratio (Cochlan et al. 1991, Tremblay et al. 2000). Further, nitrate (rather than regenerated sources of nitrogen) fuels a greater proportion of carbon fixation at low irradiances than at midday and during sunny conditions (when regenerated sources are more important). In the dark and at low irradiance, nitrate uptake was greater than carbon fixation thus implying the potential for cellular luxury uptake of nitrate. Phytoplankton may benefit from nitrate storage (known to be possible in, typically larger, cells (Falkowski and Raven 1997)) at times of higher irradiance and, presumably, reduced nitrate flux. The benefit of nitrate storage would only be available for the timescale of the lifespan of the cell (or a few divisions (Pedersen and Borum 1996)), and this analysis suggests that this mechanism may act to balance the irradiance variability in C:NO<sub>3</sub><sup>-</sup> uptake over the day.

Potential sources of error in the estimation of daily C:NO<sub>3</sub><sup>-</sup> uptake ratio result largely from the assumptions used in extrapolation of available data over a 24 hour period. The physiology of nitrate and carbon uptake are representative only of the time of the 2-6 hour period at the time of sampling and do not acknowledge diel variability in these processes (e.g. Cochlan et al. 1991). Similarly, assumption that dark uptake of nitrate is constant throughout the

night is likely to not be the case in the field, although dark uptake of nitrate is poorly understood (Falkowski and Raven 1997). Other potential errors include the estimates of *in situ* irradiance or experimental considerations including the different incubation procedures between the  $^{15}\text{N}$  and  $^{14}\text{C}$  techniques (Le Bouteiller 1993).

### 5.2.2 Oxygen Evolution at the DCM

$\text{O}_2$ -evolution vs. irradiance experiments were successful only at a limited number of locations owing to low biomass and the relatively small change in dissolved oxygen over the period of incubation (Williams et al. 1983). However, successful results were achieved at CS1 and at the frontal location X7 (Fig. 5.4). This frontal region was close in proximity to CS3, with maximum chl-a concentration just below the surface of  $2.31 \text{ mg m}^{-3}$ . Both samples were obtained close to midday. No optical data were available for the frontal region and so optical properties for the mixed region of the Irish Sea were assumed.

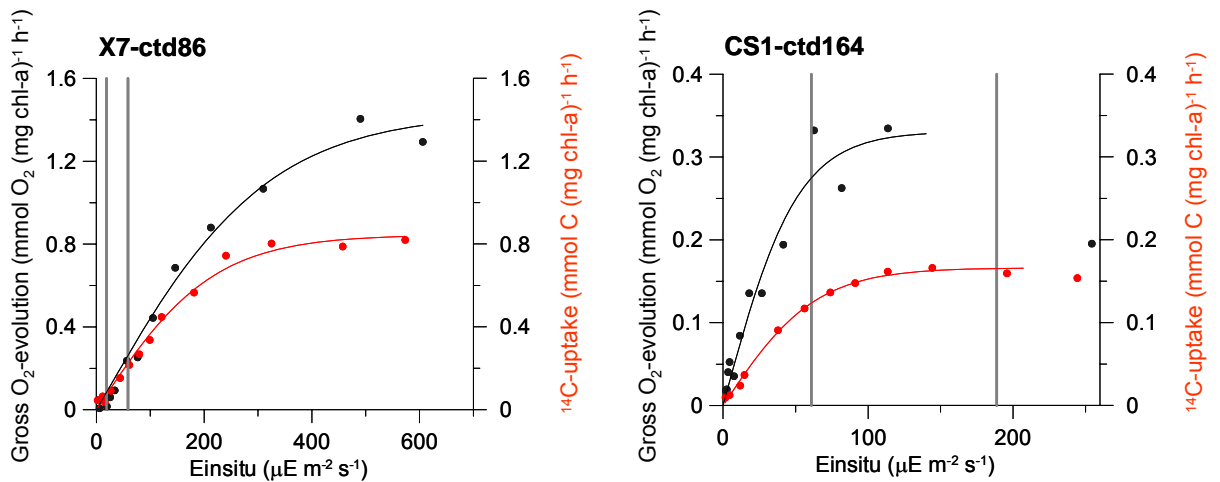


Figure 5.4.  $^{14}\text{C}$ -uptake and  $\text{O}_2$ -evolution vs. irradiance curves for DCM samples at a frontal location (X7) (CTD86, left panel) and CS1 (CTD164, right panel) during CS03. Irradiance was corrected for *in situ* spectral light fields at each location. Vertical grey lines indicate the peak irradiance experienced on a cloudy (JD = 212) and sunny (JD = 213) day using *in situ* optical characteristics and following methods in Chapter 2. Optical characteristics from the mixed region were assumed for the front. Note the difference in the irradiance scale between the two plots. Both sets of samples were obtained close to midday. Chl-a concentration at CS1 and X7 was  $2.34 \text{ mg m}^{-3}$  and  $2.31 \text{ mg m}^{-3}$  respectively.

At CS1, the irradiance at which  $O_2$ -evolution and  $^{14}C$ -uptake were saturated ( $Ek_{14C}$ ) were similar ( $\sim 65 \mu E m^{-2} s^{-1}$  for  $^{14}C$ -uptake compared to  $\sim 50 \mu E m^{-2} s^{-1}$  for  $O_2$ -evolution). This was also the case at X7 ( $\sim 200 \mu E m^{-2} s^{-1}$  for  $^{14}C$ -uptake compared to  $\sim 300 \mu E m^{-2} s^{-1}$  for  $O_2$ -evolution) and reflects the similarity of processes governing carbon fixation and oxygen evolution.

Estimated daily oxygen evolution at CS1 ranged from 2.64 – 6.32 mmol  $O_2$  (mg chl-a) $^{-1} d^{-1}$  compared to carbon fixation which ranged from 1.08 – 2.83 mmol  $^{14}C$  (mg chl-a) $^{-1} d^{-1}$  between cloudy and sunny conditions. At X7,  $O_2$ -evolution was 1.41 – 4.64 mmol  $O_2$  (mg chl-a) $^{-1} d^{-1}$  between cloudy and sunny conditions, compared to carbon fixation of 1.16 – 3.78 mmol  $^{14}C$  (mg chl-a) $^{-1} d^{-1}$ . The photosynthetic quotient was therefore  $\sim 2$  in both sunny and cloudy conditions at CS1 compared to  $\sim 1.2$  in both light regimes at X7. These values are similar to the photosynthetic quotient obtained by Holligan et al. (1984c) of 2 for the stratified Celtic Sea and 1.5 at the Ushant Front in the Western English Channel. The value of the photosynthetic quotient at the DCM at CS1 was also close to that for new production of 1.8 (Laws 1991).

The similarity in the irradiance response of carbon uptake and oxygen evolution means that the light response of  $O_2:NO_3^-$  was similar to that of  $C:NO_3^-$  (not shown). At CS1 where comparable samples were available, the ratio of oxygen evolved to nitrate utilised was 17.8 – 36.9 (mol:mol) between cloudy and sunny conditions. This was greater than the stoichiometry of  $-O_2:N$  of 8.625 of Redfield (Redfield et al. 1963) suggesting that the requirement for nitrogen by photosynthesis at this site was not entirely supported by nitrate, particularly at high irradiance (as was found by comparison with carbon uptake).

Uncertainties surrounding comparison of oxygen evolution and carbon uptake measurements include many of those already mentioned for the nitrate and carbon uptake techniques. Particularly significant are the assumptions regarding extrapolation of short-term (< 2-6 h) incubation measurements over a 24 hour period. Additional considerations include the difference in rates of photosynthesis measured by the carbon and oxygen methods (as described in Chapter 2). Specifically, in contrast to  $O_2$ -evolution, the  $^{14}C$ -uptake method is likely to measure closer to gross photosynthesis at low, compared to high, irradiances due to the potential difference in isotopic dilution between samples of different carbon fixation rates (Marra 2002). This discrepancy is a likely cause of the slight difference in coupling between the light response of  $^{14}C$ -uptake and  $O_2$ -evolution with irradiance (e.g. slightly different  $Ek$  between the two methods). Such de-coupling causes an apparent change in photosynthetic quotient with irradiance but is likely to result from experimental (or curve fitting) artefacts rather than representing, for example, a change in the nitrogen source with irradiance.

A potential source of error in the estimation of the photosynthetic quotient at location X7 is the possibility that light-saturation was not achieved during the incubation, i.e. the plateau of maximal oxygen evolution may not have been reached (Fig. 5.4). This would subsequently result in underestimation of  $E_k$  due to curve fitting and therefore subsequent underestimation of the photosynthetic quotient at high irradiance. Further uncertainties at X7 lie in the estimation of *in situ* irradiance, since optical properties of the mixed water were assumed. Chl-a in the surface at X7 was higher than that of the mixed side of the front, leading to a potential underestimation of  $K_d(\lambda)$  and subsequent overestimation of *in situ* irradiance at the DCM peak (see Chapter 2).

In general, measurements of the light response of nitrate and carbon uptake and oxygen evolution compared well (both in terms of light responses and absolute magnitudes), despite the different laboratory and incubation techniques used and the limited number of comparable experiments. The irradiance responses illustrated the physiological mechanisms involved in photosynthesis within the phytoplankton community at the time of sampling. The data indicated that despite the variability with irradiance, uptake stoichiometry may be close to Redfield proportions over a period of a day such that primary production may be sustained by nitrate at the DCM peak and is therefore 'new' production. However, this is not necessarily the case at all locations (e.g. CS1) such that recycled forms of nitrogen are likely to be important in some irradiance conditions or when nitrate flux is low.

### 5.3 Nitrate Flux into the Thermocline

Estimates of the upward flux of  $\text{NO}_3^-$  across the base of the thermocline were calculated for a limited number of locations over two cruises (data provided by J. Tweddle, *pers. comm.*). Nitrate flux at each location was estimated from physical turbulence measurements (FLY profiler) over a 25 hour period, combined with the nitrate gradient (Sharples et al. 2001a,b). Nitrate gradients obtained from a profiling instrument (SUV-6) attached to the CTD frame (during CS03) were used where discrete samples of nitrate were not of sufficient resolution. Alternatively, in absence of suitable SUV-6 measurements (for example during CS05) nitrate gradients were reconstructed using relationship between nitrate concentrations and temperature or density profiles where appropriate relationships were found. During CS03, and for shelf stations (away from the shelf edge) during CS05, turbulence measurements were obtained from aboard a second ship (the *RV Prince Madog*) which remained in the vicinity of the main vessel (< 100 m).

Estimated nitrate fluxes for the available stations are illustrated in Table 5.1. Also shown are the estimated thermocline-integrated daily primary production estimates for cloudy and sunny conditions, obtained following methods in Chapter 2. For each primary production estimate a total nitrogen requirement was calculated assuming the Redfield C:N uptake ratio (6.625 by atoms).

Table 5.1. Estimated thermocline-integrated daily primary production (PP) and associated nitrogen requirement for available stations, along with nitrate flux from the BML. Nitrate flux was calculated from physical processes (provided by J. Tweddle, *pers. comm.*, methods as described in text). PP was calculated from  $^{14}\text{C}$  P vs. E and *in situ* optics information, following methods described in Chapter 2. Daily PP estimates are as calculated for one chl-a profile assumed constant throughout the day, but estimates were not significantly different when all chl-a profiles were used (see Chapter 4). Values are given for the cloudiest and sunniest days experienced during each cruise (CS03 cloudy day = JD212, sunny day = JD213; CS05 cloudy day = JD204, sunny day = JD197) as shown in Figure. 4.11. The associated nitrogen requirement was assumed from the Redfield C:N uptake ratio (6.625). Thermocline boundaries were determined by density gradient. \* CS2b PP estimate was calculated using all available chl-a profiles for the 25 hour occupation. Percentage errors associated with the nitrate flux estimates are shown.

	Estimated PP Within Thermocline ( $\text{mg C m}^{-2} \text{d}^{-1}$ )	Nitrogen Requirement (assuming Redfield) ( $\text{mg N m}^{-2} \text{d}^{-1}$ )	Estimated Nitrate Flux ( $\text{mg N m}^{-2} \text{d}^{-1}$ )
<b>CS03</b>			
CS1	59 - 158	10 - 28	-
CS3a	87 - 216	15 - 38	53 +/- 51%
CS3b	95 - 235	17 - 41	39 +/- 60%
U2	145 - 308	26 - 54	-
<b>CS05</b>			
B2a	87 - 190	15 - 33	220 +/- 170%
B2b	69 - 188	12 - 33	41 +/- 61%
JB1	101 - 303	18 - 53	-
JB1	100 - 206	18 - 36	-
OB	42 - 141	7 - 25	15 +/- 87%
P1	68 - 222	12 - 39	-
U2	50 - 152	9 - 27	-
CS2a	291 - 770	51 - 136	25 +/- 50%
CS2b*	52 - 187	9 - 33	55 +/- 51%
OC	159 - 417	28 - 73	-
T2	84 - 253	15 - 44	-

In general, the nitrate fluxes into the thermocline measured from the independent physical processes compare reasonably well to estimated production rates in the thermocline. Fluxes estimated at different occupations of the same station reflect changes in mixing conditions during the spring – neap tidal cycle. In summary, fluxes were higher closer to spring tides when tidal current speeds over the seabed (and therefore bed friction and turbulence at the thermocline) were greater (Sharples et al. 2001b). Estimates of nitrate flux are sensitive to isolated mixing events, potentially explaining the high flux value at B2b (Table 5.1). The associated errors in this estimate suggest this value should be considered with some caution.

Nitrate flux (at available stations) ranged from 15 – 220 mg N m<sup>-2</sup> d<sup>-1</sup> across all stratified shelf locations, though excluding the very high flux estimated at B2b the range was 15 – 55 mg N m<sup>-2</sup> d<sup>-1</sup>. The range in the nitrogen requirement for primary production in the thermocline for all locations visited during both cruises was 7 - 54 mg N m<sup>-2</sup> d<sup>-1</sup>. For all stations, nitrate flux would have been capable of supporting a greater proportion of carbon fixation at low irradiance. At CS3 the estimated flux of nitrate from the BML was largely in balance with the assumed nitrogen requirement estimated from the thermocline-integrated primary production.

CS3a was visited two days prior to neap tide, whilst CS3b was occupied three days after neaps, leading up to spring tides. Estimated PP was similar for both occupations. The apparently greater flux closer to neap tides may reflect the mixing conditions preceding sampling, as greater mixing conditions may be experienced in the period following spring tides (and leading up to neaps) than in the period following neap tides (and leading up to springs). However, the difference between the estimates for CS3a and CS3b was less than the associated errors.

The shelf location B2 was visited between spring and neap tide (B2a) and at neap tide (B2b), with lower nitrate flux observed at neap tide. The difference in the estimated nitrogen requirement was not different between the two occupations and as such nitrate flux was likely to exceed the nitrogen requirement during B2a and be closer to the nitrate requirement during B2b. At another shelf site, OB, the estimated nitrogen requirement was similar to the nitrate flux from the BML.

The shelf edge station, CS2, was visited between neap to spring tides (CS2a) and at spring tides (CS2b). The nitrate flux from below the thermocline was greatest at spring tides, in contrast to the primary production which was lowest at spring tides (see also Sharples et al. *submitted*). Since mixing at this station occasionally causes the top of the thermocline to reach the surface, nitrate could be used to support growth in the entire water column. However, nitrate input from below the thermocline was also in excess of the nitrogen demand throughout the entire euphotic zone at this site during spring tides (not shown). It is possible that excess nitrate

at springs may support the primary production at times of weaker nitrate flux, for example at neap tides, when nitrate flux does not appear to satisfy the nitrogen requirement.

The imbalance between nitrate supply and uptake by primary production at CS2 suggest a potential time lag between nitrate supply and utilisation, such that nitrate supplied in excess of demand could be utilised at times when the opposite occurs. A potential time lag in nitrate supply and utilisation would explain the relative difference in these processes at any instantaneous sampling time.

These data illustrate that nitrate may not necessarily satisfy the nitrogen demand for photosynthesis at times of low nitrate flux (usually neap tides (Sharples et al. 2001b)) and / or high irradiance. During such conditions, other sources of nitrogen could be used to support growth. In contrast, during periods of high nitrate flux and / or low irradiance, nitrate supply may be in excess of demand by phytoplankton. During such periods nitrate may either build up in the thermocline, or alternatively, be mixed into the SML. The latter is not expected due to the fact that nitrate concentration for most stratified sites was diminished well below the top of the thermocline (see Chapter 4) and also that nitrate was never observed in the SML at measurable concentrations ( $> 0.1 \mu\text{M}$ ). However, this does not explicitly rule out this possibility since small amounts of nitrate would likely be used almost instantaneously by phytoplankton in the SML. Nitrate build up in the thermocline could subsequently be available for use by phytoplankton at times when nitrate demand exceeded supply (see also Banse 1987, Letelier et al. 2004) for example at neap tides. This is notable in the case of CS2 where photosynthetic rates were greatest when nitrate flux was low, potentially fuelled by the excess nitrate supplied during spring tides.

As described above, the physiological mechanisms regulating the light response of the relative uptake of carbon and nitrate suggest that processes of carbon and nitrate uptake may balance over a period of a day. Importantly, the data indicate that nitrate may be assimilated in excess of demand for photosynthesis at low irradiance, suggesting that luxury uptake of nitrate may be another mechanism for phytoplankton to balance the supply vs. demand problem. Luxury uptake may be an investment for individual phytoplankton cells as well as the nitrate 'stores' potentially incorporated into daughter cells during division, leading to longer term gain, however, details of this processes and its ecological significance in the field setting are poorly understood (e.g. Falkowski and Raven 1997, Pedersen and Borum 1996).

Due to the limited number of nitrate flux estimates at each location, it is unlikely that the sampling captured the extremes in the flux estimates (or primary productivity) that potentially occurs over the spring-neap cycle. In order to observe the relative time lag between

nitrate supply and utilisation measurements would need to be made over a full spring- neap cycle at a given location.

Acknowledging the relative errors and sampling limitations associated with these techniques (see Sharples et al. 2001a,b for discussion on errors associated with nitrate flux estimates), these data suggests that nitrate flux from the BML may sustain most, if not all, of the production in the thermocline, with the supply and demand of nitrate possibly in balance over the timescale of a complete spring - neap cycle (14 days).

#### **5.4 Distributions of Chl-a, $\text{NO}_3^-$ , $\text{O}_2$ and PP within the Thermocline**

The distribution of nitrate and dissolved oxygen saturation through the water column for three example sites is shown in Figure 5.1. The data in the sections above illustrate the dynamic nature of the physical processes determining nitrate flux and the complex physiological mechanisms governing nitrate utilisation. This section illustrates that, despite this complex variability, largely repeatable trends in nitrate and dissolved oxygen concentration are evident between locations and within locations over time. These repeatable trends provide important insights into the functioning of the thermocline both physically and biologically, and provide a further means to investigate new production.

##### **5.4.1 Distributions of Chl-a and Dissolved $\text{O}_2$ on the Nitracline**

As illustrated in Chapter 4 the distribution of chl-a on the nitracline was repeatable between and within stations. The chl-a distribution against nitrate for all available locations is shown in Figure 5.5. The data presented in Figure 5.5 are data points from repeat CTD casts at each location, thereby increasing the sampling resolution through the nitracline. The distribution of dissolved oxygen (as Apparent Oxygen Utilisation, AOU) on the nitracline is also shown. AOU (as calculated from Eqn. 2.6 and 2.7) provides a measure of the amount that dissolved oxygen is above or below saturation ( $\text{mg l}^{-1}$ ), i.e. AOU is zero when dissolved oxygen saturation ( $\%\text{O}_2$ ) is 100% and negative when a water mass is super-saturated. Despite variability in the position of the nitracline within the thermocline (refer to Fig. 4.7), the distributions of chl-a and dissolved oxygen saturation (as AOU) were strongly coupled to the nitrate concentration, regardless of the density structure (Fig. 5.5).

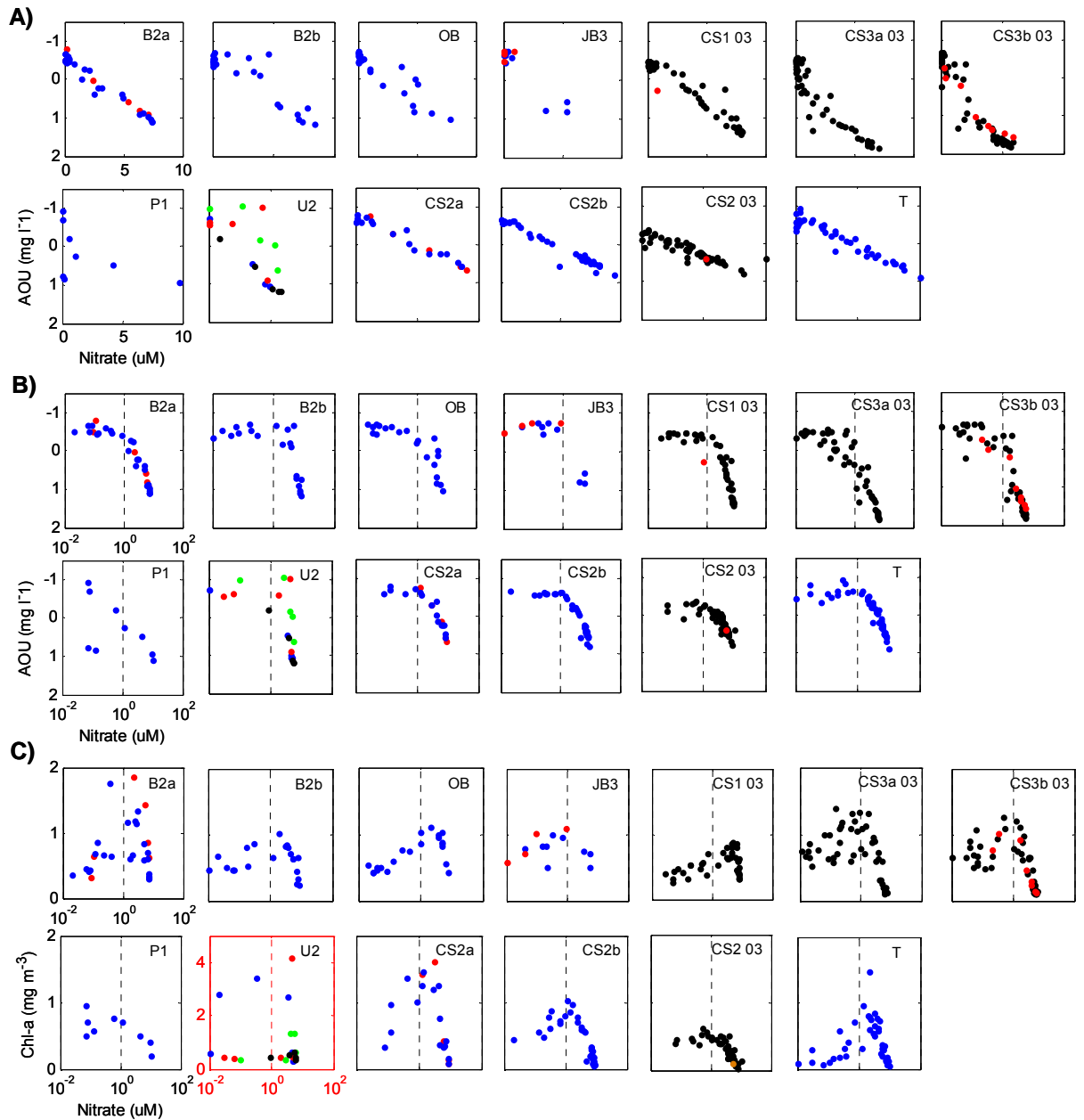


Figure 5.5. Distribution of dissolved oxygen (as Apparent Oxygen Utilisation, AOU,  $\text{mg l}^{-1}$ ) and chl-a on the nitracline. A) AOU against  $\text{NO}_3^-$  ( $\mu\text{M}$ ) (linear scale), B) AOU against  $\text{NO}_3^-$  (log scale), C) chl-a against  $\text{NO}_3^-$  (log scale) for repeat CTD casts at example stations (CS05 only). Nitrate is from discrete samples. AOU and chl-a is as measured from the calibrated instruments on the CTD, at depths corresponding to the nitrate measurements. Note that AOU is negative when dissolved oxygen is super-saturated. Panels with blue symbols indicate data from CS05, and those with black symbols are data from CS03. Red and green symbols indicate repeat visits where a single CTD cast was carried out. Data collected during different 25 hour occupations are in separate panels.

Figure 5.5 illustrates that the maximal chl-a concentration typically occurred at a nitrate concentration of  $\sim 1\text{-}2\ \mu\text{M}$  and the point on the nitracline at which  $\%O_2$  was roughly super-saturated (AOU  $\sim 0$ ).  $\%O_2$  super-saturation was maximal (minimal AOU) in the upper thermocline where  $NO_3^- < \sim 1\ \mu\text{M}$  (Fig. 5.5B) whilst in the lower thermocline ( $NO_3^- > \sim 1\ \mu\text{M}$ ) the relationship between  $NO_3^-$  and AOU was close to linear (Fig. 5.5A). It follows that there appears to be a shift in thermocline characteristics from low nitrate, low chl-a and super-saturated dissolved oxygen at the top of the thermocline, through to high chl-a, high nitrate and sub-saturated dissolved oxygen at the base of the thermocline. The regime apparently shifts at  $NO_3^-$  concentration of around  $\sim 1\ \mu\text{M}$  across the entire shelf sea region.

Referring to Figures 4.7 and 4.8 (Chapter 4), the distribution of chl-a through the density gradient at CS2 was more symmetrical than on the shelf and nitrate penetrated the entire thermocline. This meant that the distribution of chl-a and dissolved oxygen on the nitracline was consistent with other locations. However, there are some inconsistencies with the general trend, notably at CS3, P1 and U2.

At CS3 the chl-a distribution on the nitracline was consistent with the general trend but dissolved oxygen saturation and nitrate did not appear to vary linearly at the base of the thermocline (Fig. 5.5A). At P1 dissolved oxygen saturation was variable between visits and chl-a was maximal at a lower nitrate concentration than other sites, however, the limited number of data points restricted further investigation into the cause of this variability. At U2 the relationships between nitrate dissolved oxygen saturation and chl-a was variable between occupations. For two of the three visits to U2,  $\%O_2$  was lower (greater AOU) than at other sites and chl-a was maximal at higher nitrate concentrations.

The cause of scatter around the relationships (e.g. at OB and B2b) is difficult to determine due to the limited number of data points obtained from each individual CTD cast. Some scatter may arise from offset in CTD sensors and niskin bottle inlets, although this is thought to be minimal.

Figure 5.6 shows the relationship between AOU and  $NO_3^-$  for all locations visited during CS05. The relationship was highly consistent between the oceanic and shelf edge sites, with ratio of AOU: $NO_3^-$  for the near-linear part of the trend (assumed  $NO_3^- > 1\ \mu\text{M}$ ) of 5.15 by atoms ( $n = 73$ ,  $r^2 = 0.926$ ,  $p < 0.001$ ). On the shelf the relationship was more variable. The ratio of AOU: $NO_3^-$  for locations conforming to the linear trend (i.e. excluding U2, P1) was 8.09 (mol:mol) ( $n = 44$ ,  $r^2 = 0.699$ ,  $p < 0.001$ ).

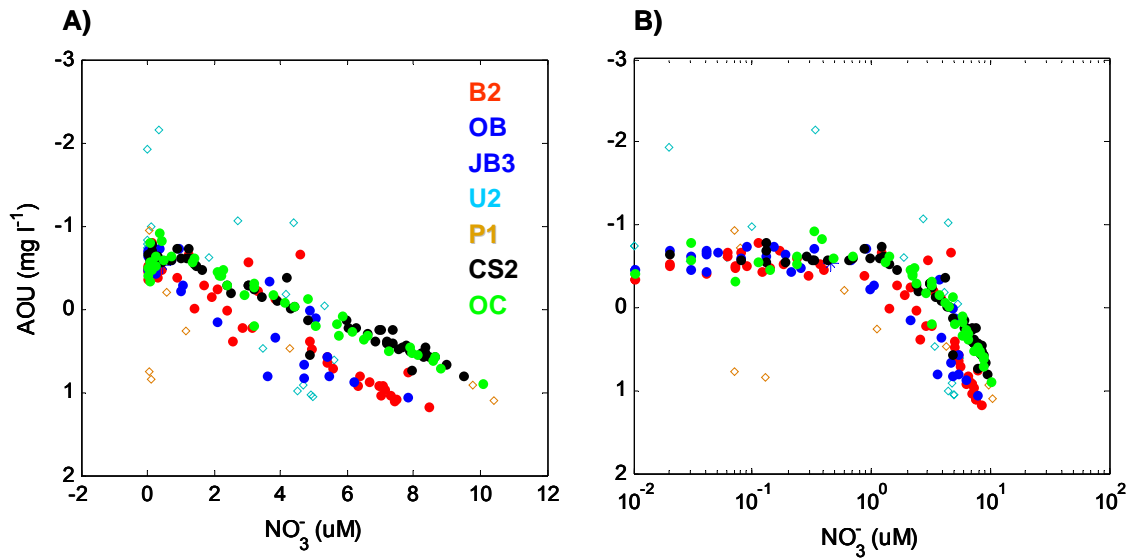


Figure 5.6. Dissolved oxygen saturation (as AOU,  $\text{mg l}^{-1}$ ) against nitrate concentration ( $\mu\text{M}$ ) for example stations (CS05 only). A) linear nitrate scale, B) logarithmic nitrate scale.

For the shelf stations, the ratio of  $\text{AOU}:\text{NO}_3^-$  was close to the Redfield  $-\text{O}_2:\text{N}$  ratio (8.625), but at the shelf edge the ratio was lower, possibly indicating that processes may not have been conforming to “Redfield” exchange. Similarly, the occurrence of scatter around the general trend across the shelf suggests that at some instance, or locations, deviation from the mean ratio occurs frequently. Figure 5.6 also indicates that for shelf stations the slope of  $\text{AOU}:\text{NO}_3^-$  at nitrate concentrations  $>1 \mu\text{M}$  may be less variable and closer to that of the oceanic and shelf sites at higher nitrate concentrations ( $> \sim 4 \mu\text{M}$ ) compared to at lower concentrations ( $1 - 4 \mu\text{M}$ ). The slope of the linear  $\text{AOU}:\text{NO}_3^-$  relationship may also reflect changes in the end-member conditions. The reasons for the relationships between dissolved oxygen saturation and nitrate, and their implications, are discussed in detail below.

One important outcome of a relatively robust and repeatable relationship between dissolved oxygen saturation and nitrate is that high-resolution nitrate profiles may be estimated from the dissolved oxygen measurements obtained from the oxygen probe on the CTD. Using just the simple linear relationships between  $\text{AOU}:\text{NO}_3^-$  for the region  $\text{NO}_3^- > \sim 1 \mu\text{M}$  for both the shelf edge and oceanic and the stratified shelf regions, vertical profiles of nitrate were constructed from those of oxygen saturation as measured by the oxygen probe on the CTD. The modelled nitrate profiles were well correlated to those measured from bottle samples for  $\text{NO}_3^- > 1 \mu\text{M}$  ( $n = 303$ ,  $r^2 = 0.750$ ,  $p < 0.001$ ) thus illustrating the potential for obtaining high resolution

nitrate profiles suitable for use in, for example, estimating nitrate flux in the future. Complete profiles (i.e. whole water column, not just  $\text{NO}_3^- > 1 \mu\text{M}$ ) may be reproduced following a more sophisticated model fit to the  $\text{AOU}:\text{NO}_3^-$  relationship.

#### *Maximum %O<sub>2</sub> super-saturation and maximum chl-a*

Figure 5.7 indicates that the maximum oxygen saturation (as minimum AOU) was correlated to the maximum chl-a concentration at the DCM, despite the different depths of these two maxima in the water column (Fig. 5.1).

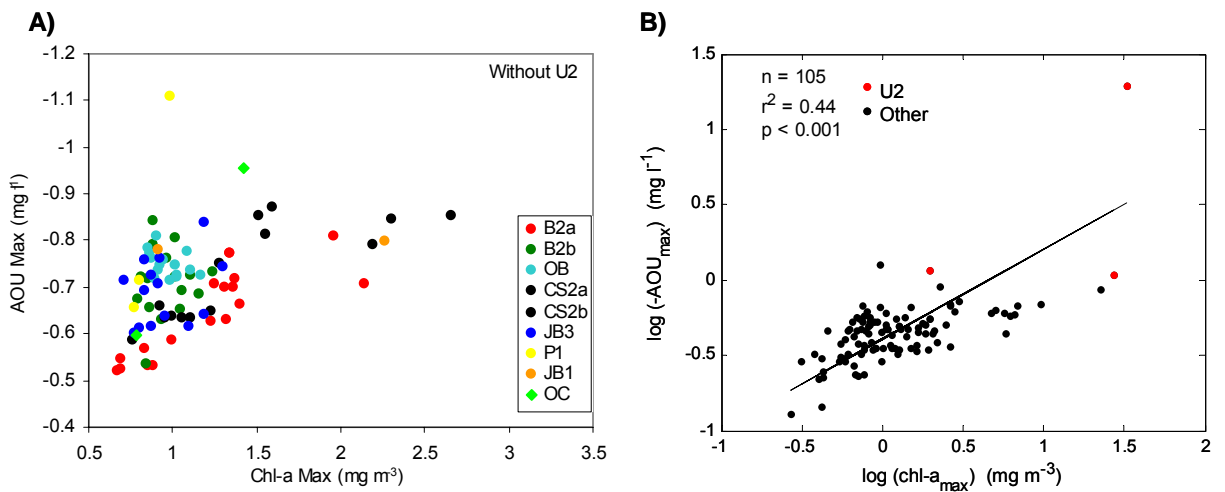


Figure 5.7. A) Maximum chl-a concentration ( $\text{mg m}^{-3}$ ) against maximum dissolved oxygen super-saturation (expressed as AOU,  $\text{mg l}^{-1}$ ) for all CTD casts except U2 during CS05, and B) maximum chl-a concentration against maximum oxygen super-saturation (as  $\log(-\text{AOU})$ ) during CS05 including U2 on log-log axis. Statistics shown are the results of model II regression analysis for all data. -AOU and chl-a are both from calibrated CTD sensors. Note that maximum dissolved oxygen saturation did not occur at the same depth as maximum chl-a concentration.

No relationship was found between the %O<sub>2</sub> maximum and the BML nitrate concentration (data not shown). These results imply that the peak magnitude of %O<sub>2</sub> is the result of current (recent) processes within the thermocline rather than those associated with the spring bloom or cumulatively responsible for %O<sub>2</sub> reduction (or nitrate remineralisation) in the BML since the onset of stratification. The correlation implies that the %O<sub>2</sub> maximum is derived, at least in part, from biological processes such that purely physical mechanisms (e.g. warming of trapped SML

water in the thermocline since stratification) are not solely responsible for this phenomenon. The implication of this relationship is discussed in more detail below.

#### 5.4.2 Physical-Biological Interaction and Implications for New Production in the Thermocline

The change in coupling between dissolved oxygen saturation and nitrate concentration that appears to occur around  $\text{NO}_3^- = \sim 1 \mu\text{M}$  suggests that different biogeochemical processes occur within the upper and lower thermocline in relation to the nitrate gradient. The following section explores relationship between oxygen and nitrate and the implications for new production.

Within the upper thermocline, where chl-a concentration was generally below the DCM value and nitrate was typically  $< \sim 1 \mu\text{M}$ , dissolved oxygen was super-saturated (negative AOU) despite low nitrate concentrations (approaching or equal to zero). The correlation between AOU and chl-a peak magnitude (Fig. 5.7) suggests that the oxygen super-saturation has (at least partly) biological origin (Craig and Hayward 1987) and therefore it is likely that new production fuelled by nitrate flux from the BML occurs in this region. Alternatively, the super-saturation of dissolved oxygen may represent the cumulative new production occurring between the base of the thermocline and the depth of maximal %O<sub>2</sub> (minimal AOU) (this is synonymous with the nitrate gradient reflecting the cumulative net utilisation of nitrate through the thermocline). This is also reflected in fact that the magnitudes of the %O<sub>2</sub> maximum and the DCM peak are correlated despite their different depths.

In the lower part of the thermocline (nitrate  $> \sim 1 \mu\text{M}$ ) dissolved oxygen saturation increased from the BML concentration as nitrate concentration decreased, presumably through a combination of mixing and biological processes. New production in this region could result in a net increase in dissolved oxygen despite sub-saturating concentrations. The location of the chl-a maximum is in this region of the thermocline and persists despite the physical mixing. This suggests that biological processes are a significant factor in the increase in O<sub>2</sub> and decrease in NO<sub>3</sub><sup>-</sup> in this region.

In order to identify the possible contribution of biological and physical processes at work, a simple linear mixing model was considered. Figure 5.8A is a schematic representation of the oxygen and nitrate profiles that would result assuming only linear mixing between the SML and BML, which is assumed to be established if there was no biological activity following the collapse of the spring bloom. Fig 5.8B depicts a schematic distribution of a typical shelf dissolved oxygen saturation profile, compared to the simple linear mixing scenario.

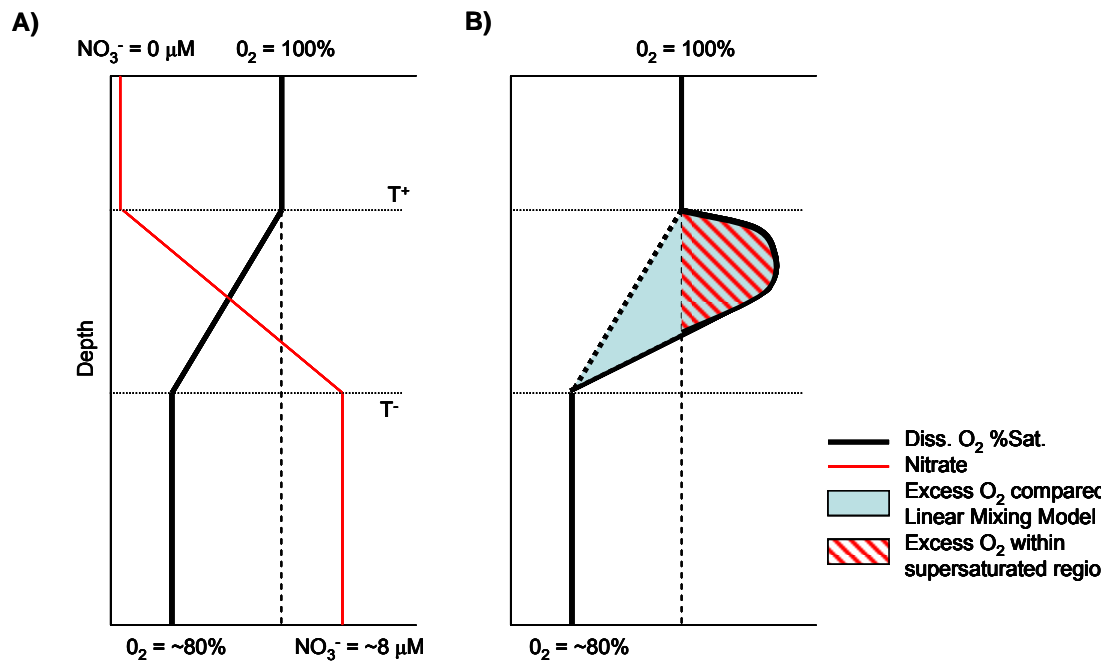


Figure 5.8 A) Schematic representation of post-spring bloom stratified shelf scenario assuming linear mixing of nitrate and dissolved oxygen between the surface mixed layer (SML) and bottom mixed layer (BML).  $T^+$  and  $T^-$  indicate that the region of linear mixing represents the thermocline. Hypothetical SML and BML nitrate and oxygen saturation values are given. B) Schematic representation of deviation from the linear mixing scenario due to biological activity that results in a net increase in dissolved oxygen throughout the thermocline. It is assumed such a scenario results from net oxygen evolution from phytoplankton growth fuelled by nitrate flux from the BML due to the nitrate gradient. The dissolved oxygen saturation increases above that which would occur from mixing alone and super-saturation is achieved within the thermocline. The upper bound for net oxygen excess due to new production is given by the area between the resulting oxygen saturation curve and the linear mixing line. The supersaturated region could only result from biological processes (Williams and Purdie 1991) and therefore provides the minimum bound for the excess oxygen resulting from new production. Details are provided in the text.

In the presence of biological activity, where some fraction of phytoplankton production is fuelled by nitrate flux from the BML, %O<sub>2</sub> would increase relative to the linear mixing scenario. This net increase would occur regardless of whether or not the %O<sub>2</sub> is saturated (a decrease in nitrate concentration may or may not be observed depending on the relative balance between phytoplankton production and nitrate flux). It is therefore suggested that the deviation of %O<sub>2</sub> from the simple mixing model represents the amount of new production that has taken place

over some timescale. By comparison, the area of the super-saturated region represents the amount of dissolved oxygen that can *only* have resulted from biological activity (Craig and Hayward 1987, Williams and Purdie 1991) and can therefore be considered a minimum bound for the amount of new production that has taken place in the thermocline over some timescale (Richardson et al. 2000). It should be noted that in both cases the excess %O<sub>2</sub> will yield an underestimate of total new production because of the mixing at the top and bottom of the thermocline mixing out the excess %O<sub>2</sub>.

Table 5.2 shows the excess %O<sub>2</sub> as estimated from the two hypotheses from AOU profiles from the CTD averaged over selected 25 hour occupations.

Table 5.2. Excess dissolved oxygen (as –AOU, i.e. positive values represent dissolved oxygen generation) estimated from comparison to the linear mixing model (“Linear Mixing”) and by the area of the super-saturated region (“Supersaturation”) for selected locations occupied for 25 hours during CS05. See text for details. The associated nitrogen requirement for the evolved oxygen is estimated assuming a value of 8.625 for the -O<sub>2</sub>:NO<sub>3</sub><sup>-</sup> assimilation ratio (Redfield et al. 1963). The NO<sub>3</sub><sup>-</sup> flux from the BML is provided as estimated from physical processes (J. Tweddle, *pers. comm.*). The timescale for the excess O<sub>2</sub> accumulation is calculated as described in the text.

	Mean O <sub>2</sub> excess (mg O <sub>2</sub> m <sup>-2</sup> d <sup>-1</sup> )	N Requirement (mg N m <sup>-2</sup> d <sup>-1</sup> )	NO <sub>3</sub> <sup>-</sup> Flux (mg N m <sup>-2</sup> d <sup>-1</sup> )	O <sub>2</sub> Accumulation Time (days)
<b>Excess: Linear Mixing</b>				
B2a	12256	622	220	3
B2b	7196	365	41	9
OB	8529	433	15	28
CS2a	2332	118	25	5
CS2b	-375	-19	55	0
<b>Excess: Supersaturation</b>				
B2a	10540	535	220	2
B2b	8022	407	41	10
OB	9307	472	15	31
CS2a	15953	809	25	32
CS2b	12567	637	55	12

Also included in Table 5.2 are estimates of the timescale (in days) over which the oxygen excess may have evolved, as estimated following equation 5.1.

$$t(\text{days}) = \frac{O_2 \text{ excess}}{8.625 \cdot \text{daily} \text{NO}_3^- \text{ flux}} \quad (5.1)$$

Where  $O_2 \text{ excess}$  is the oxygen excess estimated by each of the two hypothesis (in  $\text{mol l}^{-1}$ ), 8.625 is the  $-\text{O}_2:\text{N}$  of (Redfield et al. 1963), and daily  $\text{NO}_3^-$  flux (in  $\text{mol l}^{-1}$ ) is that estimated by physical methods (J. Tweddle, *pers. comm.*, Table 5.1).

The relative difference between the oxygen excess derived from the two methods is discussed below. First, consideration is given to the estimated timescales for new production.

Given the rates of nitrate flux into the thermocline, the oxygen excess (estimated by either method) for the stratified shelf stations would have built up over timescales of 2 – 31 days (OB and B2). The timescale for the build up of excess dissolved oxygen appears to vary with location with lower values (2 - 10 days) at B2 and longer timescales (~30 days) at OB, which reflects variability in the flux estimates, rather than estimates of oxygen excess. If the ratio of Anderson and Sarmiento (1995) were assumed for the uptake stoichiometry (10.625), the timescales for OB and B2 range from 2 – 25 days.

An independent estimate of timescales for complete ventilation of the thermocline can be calculated via turbulent diffusion using  $t = L^2 / 2K_z$  (Denman and Gargett 1983), where  $L^2$  the turbulent length-scale for mixing over the length-scale (m), representing the nitrate or oxygen gradient, and  $K_z$  the vertical eddy diffusivity ( $\text{m}^{-1} \text{s}^{-1}$ ). Measurements of  $K_z$  (averaged over the nitracline) were made during CS03 and CS05 and the average of all available shelf sites during these cruises was  $5.4 \times 10^{-4} \text{ m}^{-1} \text{ s}^{-1}$  ( $n = 4$ ) (T. Rippeth, *pers. comm.*). Length-scales were obtained from the both the distance between the base of the thermocline and the  $\%O_2$  maximum, and the base of the thermocline and  $\text{NO}_3^- = 1 \mu\text{M}$  (estimated from the conversion of AOU profiles as described above) for all shelf sites visited during CS05 and ranged from 16.7 - 21.4 m. The estimated timescales for ventilation of the shelf thermocline therefore ranged from 30 – 49 days. Given the assumptions and errors associated with all measurements, and the fact that that the estimation of mixing timescales from measurements of eddy diffusivity is considered “very approximate” (Denman and Gargett 1983), the estimated timescales from measurements of eddy diffusivity and those in Table 5.2 compared fairly well.

The potential time-lag between nitrate supply by flux from the BML and utilisation in new production (as described in Section 5.3 above) could equally explain the variability in

estimated timescales for new production. The average timescale for accumulation of dissolved oxygen in the thermocline (for available shelf stations) was 23 days. Accepting the limitations and errors involved with the measurements, the range of values suggests that nitrate supply and utilisation could be balanced over spring – neap timescales.

With the exception of CS2, the magnitudes of the oxygen excess measured following the two hypotheses described above (Table 5.2) were similar at all stratified shelf stations (+/- 14%). This has important implications for identifying the location of new production in the thermocline, as it implies that excess oxygen evolution at the base of the thermocline (below the onset of super-saturation) is not important. It is suggested that the shelf sea thermocline can be described as a 3-layer system.

In the lower thermocline mixing processes dominate the system such that any oxygen evolution by new production is mixed to the BML and there is no ‘net’ oxygen accumulation over time. This would also mean that chl-a is mixed to the BML. The ratio of  $-O_2:NO_3^-$  in the water column is dominated by mixing processes and likely reflects the BML concentration or something between BML and upper thermocline concentration depending on the strength of mixing compared to biological activity.

In a mid-thermocline region the effect of mixing with the BML becomes less dominant and a net increase in dissolved oxygen due to new production may be observable over the losses due to mixing. This may or may not be associated with a depletion of  $NO_3^-$  concentration (in Redfield proportions) in the water column because a proportion of the new production is fuelled by  $NO_3^-$  flux rather than utilisation of the  $NO_3^-$  pool. The new production based on nitrate flux may lead to an increase in the  $-O_2:NO_3^-$  in the water column. An increase in the  $-O_2:NO_3^-$  may or may not occur when dissolved oxygen saturation is  $> 100\%$ , and these data suggest that the change in  $-O_2:NO_3^-$  in the water column occurs slightly deeper on the nitracline than the point at which dissolved  $O_2$  exceeds 100% saturation at a nitrate concentration of around  $\sim 1 \mu M$  on the shelf ( $\sim 3 \mu M$  at the shelf edge and oceanic regions). This regime of net new production (in excess of losses due to mixing) may continue up the thermocline until the point at which  $\%O_2$  is maximal at the top of the nitracline (nitrate potentially  $< 0.1 \mu M$ ) such that new production is fuelled by the nitrate flux and utilised almost instantaneously. This region includes the upslope of the DCM and the DCM peak which was typically located at or above the depth at which  $\%O_2$  was  $\sim 100\%$  (for examples see Fig. 5.1, CS1 was an exception). Further, daily PP estimates showed that most of the carbon fixation in the thermocline occurred at or above the depth at which  $\%O_2 = 100\%$  (e.g. Fig. 5.1).

At the top of the thermocline nitrate in the water column is depleted. With no  $\text{NO}_3^-$  pool and no nitrate gradient to incur an upward nitrate flux, phytoplankton are likely nitrate-limited. Primary production may continue, though fuelled by other sources of nitrogen. A net decrease of dissolved oxygen occurs due to mixing across the top of the SML and (possibly) net utilisation by biological processes (respiration and remineralisation). A schematic representation of this system is shown in Figure 5.9A.

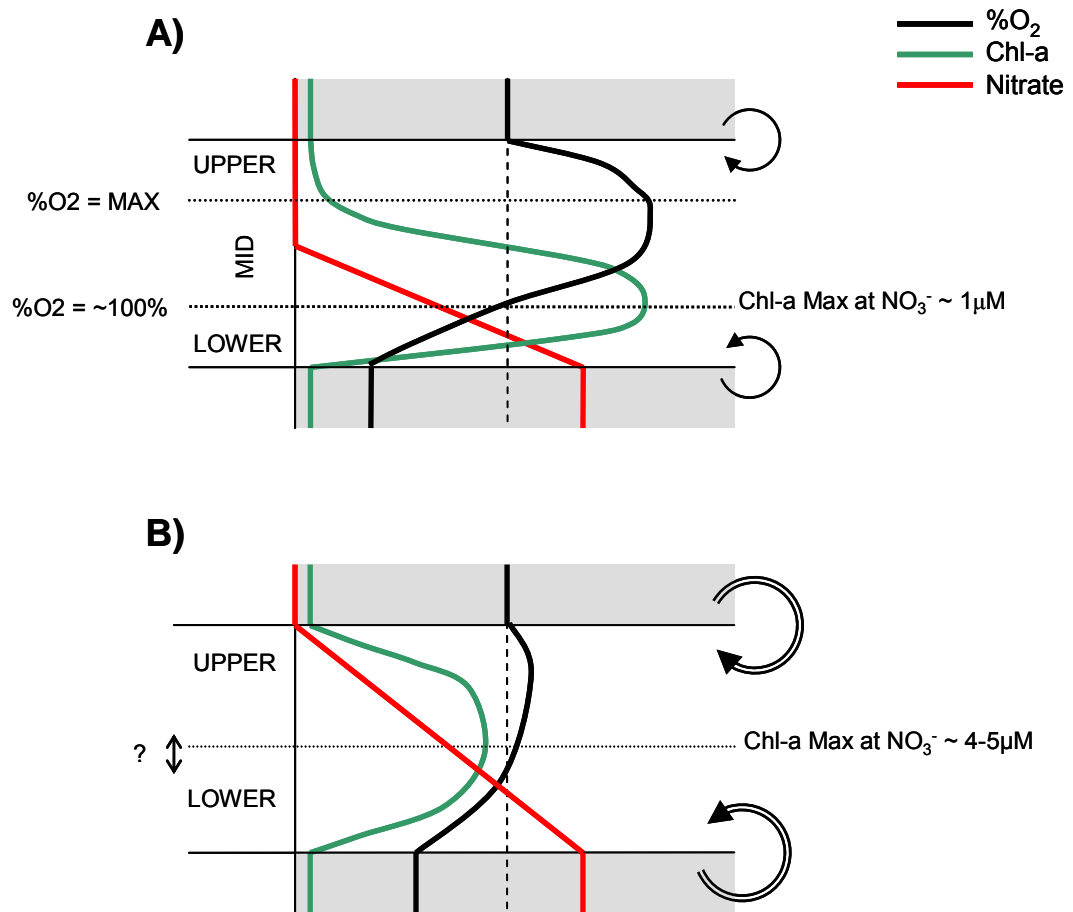


Figure 5.9. Schematic representations of 'Three-Layer' and 'Two-Layer' thermocline scenarios. A) A 'Three-layer' thermocline representing typical stratified shelf stations. Details are given in text. Briefly, 'Upper' and 'Lower' thermocline regions are susceptible to mixing such that biological exchanges of oxygen, nutrients and chl-a are mixed between SML and BML respectively. In the 'Mid' region relatively low mixing means that oxygen and chl-a can build up, fuelled either by nitrate in the water column or by nitrate flux from the BML B) A 'Two-layer' thermocline such as could be expected in regions of strong vertical mixing, for example, at the shelf edge. Mixing from above and below is such that no stable 'mid' section is set up. Signals of biological exchange are rapidly mixed away. Increased chl-a may prevail if growth rates are fast enough and chl-a is likely to be maximal in the most stable region.

The mid-section of the thermocline, where biological processes and net oxygen evolution appear to dominate over mixing processes, is likely to be more marked in locations that are strongly stratified thus providing a region of relative stability within the mid-thermocline region. This appears to be the case for the majority of shelf sites (e.g. B2, Figure 5.10A), with temporal variability in the mixing regime potentially responsible for the scatter in the  $-O_2:NO_3^-$  relationships (Fig 5.5 and Fig 5.6). In contrast, in weakly stratified sites such as at the shelf edge (and possible at some instance at U2), a stable region in the thermocline is unlikely to occur such that the effect of biological processes may not be noticeable over the physical mixing. A two-layer model is suggested for such regions (Fig. 5.9B) and is discussed below.

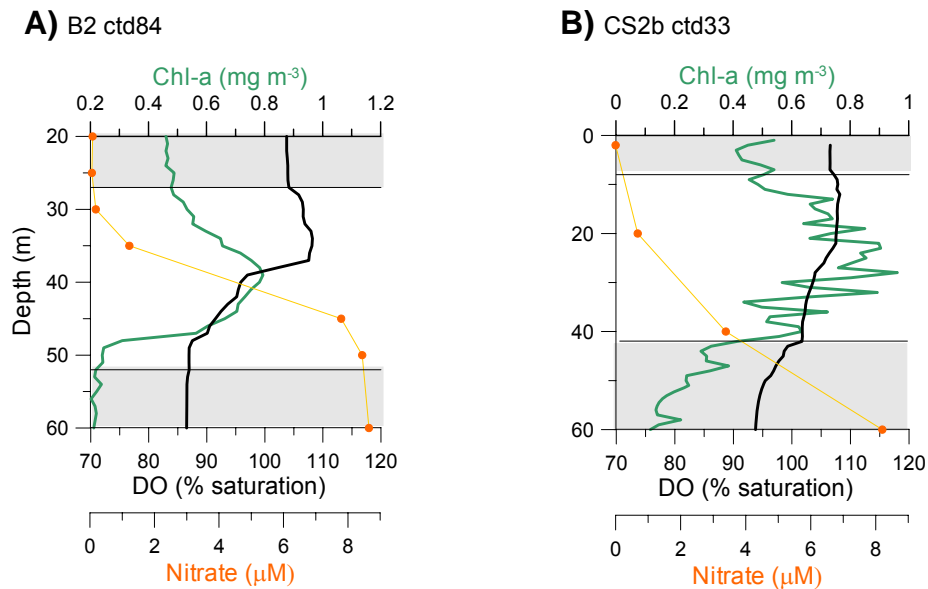


Figure 5.10. Profiles of chl-a, dissolved oxygen saturation ( $\%O_2$ ) and nitrate for selected stations, A) example cast from shelf station B2b, similar to the three-layer structure, and B) example cast from the shelf edge (CS2a) representing the two-layer structure. two-layer and three-layer thermocline structures are described in the text and Figure 5.9.

At the shelf edge (CS2) the dissolved oxygen excess estimated from the region of supersaturation was well in excess of that estimated from comparison with the linear mixing model (Table 5.2). This may partly result from the difficulty in identifying the thermocline boundaries at this site where the density gradient was poorly defined, as well as relatively high  $\%O_2$  in the SML, making interpolation problematic. However, the low net dissolved oxygen build up

estimated from the linear mixing model may indicate that mixing dominates throughout the entire thermocline region, such that net oxygen evolution due to biological processes above the mixing processes are minimal (Fig. 5.9B). The position of the chl-a maximum in the centre of the density gradient (rather than towards the base of the thermocline as at most shelf sites (Fig. 4.7, Fig. 5.10B)) is a further indication that mixing from below and above the thermocline is acting through the entire thermocline.

In the two-layer scenario, the ratio of  $-O_2:NO_3^-$  in the water column would remain constant through much of the thermocline (since no net build up of oxygen alter this ratio) until nitrate is depleted at the top of the thermocline and mixing with the SML occurs. However, these data indicate that super-saturation occurs at the top of the thermocline at CS2 such that some fraction of production must be new and observable above mixing processes (e.g. Fig. 5.10B). The supersaturated region was greater at neaps than spring tides (Table 5.2) and is further indication that net new production may increase between spring to neap tides.

The data presented provide a useful insight into the biological-physical interactions at work in the shelf sea thermocline. The three-layer and two-layer models represent end-member scenarios and are based on the general trends observed across the study region. Locations where variations from the general trends were observed (e.g. U2 and P1) may or may not conform to the suggested models. Data were not available to investigate each specific case. This is discussed further in Chapter 7.

Some potential limitations of the methods used should be considered and these principally regard the estimates of net oxygen evolution within the thermocline. The estimates of net oxygen evolution in Table 5.2 are likely underestimates of total net oxygen evolved for a number of reasons. The main cause of underestimation of the estimated oxygen excess results from mixing between the thermocline and the SML and BML, as mixing at both boundaries reduces the amount of excess dissolved oxygen in the thermocline. Underestimation was worse for the oxygen excess calculated from the linear mixing hypothesis because the SML was slightly super-saturated (mean = 105%), particularly at CS2, which caused some of the oxygen in the super-saturated region to be excluded from the calculated excess. Although oxygen super-saturation in the SML is likely to originate, at least in part, from within the thermocline the potential exchange at the sea surface (e.g. bubble entrainment) is also a source of dissolved oxygen to the SML (e.g. Reid and Shulenberger 1986) and subsequently the relative contribution of biological and physical processes to dissolved oxygen saturation in the SML is largely unknown.

Estimates of excess oxygen evolution also represent net community production. The effects of respiration and remineralisation have not been considered. Underestimation of the excess dissolved oxygen leads to underestimates of the nitrogen requirement and also subsequently the timescales for dissolved oxygen accumulation.

A further potential source of error on the estimates of the timescales of excess dissolved oxygen build-up is the fact that estimates were based on a limited number of nitrate flux measurements at each location. To gather a thorough representation of the range and offset in the nitrate flux and utilisation, a full spring-neap cycle would need to be observed at each location.

High resolution vertical nitrate profiles and nitrate gradients are potentially obtained from CTD %O<sub>2</sub> profiles combined with the robust relationship observed between dissolved oxygen and nitrate concentration. Such profiles may provide further clues as to the location of the greatest nitrate gradient, and subsequently the location of greatest nitrate flux, within the thermocline.

A true estimation of the amount and location of new production cannot be achieved without de-convolution of the relative biological and physical processes occurring in the thermocline. Despite the useful information contained in these data it is suggested that the biological and physical processes occurring within the thermocline cannot fully be separated without application of numerical modelling.

## 5.5 Summary of Main Points

The major observations within this chapter were:

- Regardless of their locations in the density gradient, the distribution of chl-a on the nitracline was often the same across the study region.
- A maximum in dissolved oxygen super-saturation was observed at the top of the thermocline which correlated to the chl-a concentration at the DCM.
- The light response of NO<sub>3</sub><sup>-</sup> and <sup>14</sup>C showed that relative uptake may be in Redfield proportions over a period of a day, but that variability in C:NO<sub>3</sub><sup>-</sup> occurs due to irradiance.
- A photosynthetic quotient ~2 for the shelf sea DCM was obtained at one location on the shelf, compared to 1.5 at the Irish Sea Front.

- A de-coupling of physical nitrate supply and biological utilisation is likely to exist, although on average the nitrate flux from the BML (estimated by physical methods) may roughly balance the estimated requirement for carbon fixation in the thermocline.
- The repeatable trends in the distribution of  $\text{NO}_3^-$ ,  $\% \text{O}_2$  and chl-a within the thermocline provided a means to characterise the thermocline as a three-layer system.
- The location of new production in the thermocline is suggested to be in the region where oxygen is supersaturated at the top of the nitracline, with mixing dominating below the depth of the chl-a maximum.
- The timescale for the observed build-up of oxygen given the measure nitrate flux was estimated to be of the order of 10 days.

## CHAPTER 6: PHYTOPLANKTON PHOTOPHYSIOLOGY AND PRIMARY PRODUCTION IN THE ATLANTIC OCEAN

The aim of this chapter is to expand the investigation of the DCM, previously focussed on the Celtic Sea shelf, to the open ocean. Data from AMT15, a north to south transect through the Atlantic Ocean, were analysed in a similar manner to those from the Celtic Sea in order to highlight the similarities and differences between the continental shelf and open ocean environments.

An overview section precedes the main data analysis briefly summarising the hydrographic setting, chl-a distribution and phytoplankton taxonomic composition. The results are then divided into two sections. The first section deals with the photophysiology of the phytoplankton, using phytoplankton absorption, FRRF and  $^{14}\text{C}$  P vs. E measurements. The second part describes the distribution of chl-a and primary production through the water column, paying particular attention to the DCM. The main factors driving variability in the distribution of primary production through the water column are investigated.

### 6.1 Study Area

The AMT15 cruise departed from the UK on 17<sup>th</sup> September and reached South Africa on 29<sup>th</sup> October 2004 and included an upwelling region off NW Africa (Fig. 6.1). The majority of biological samples (including for FRRF measurements) were collected at pre-dawn stations as marked in Figure 6.1. In addition to the biological samples,  $^{14}\text{C}$  P vs. E experiments were carried out at the locations highlighted in red in Figure 6.1 including one station on the edge of the NW African upwelling.

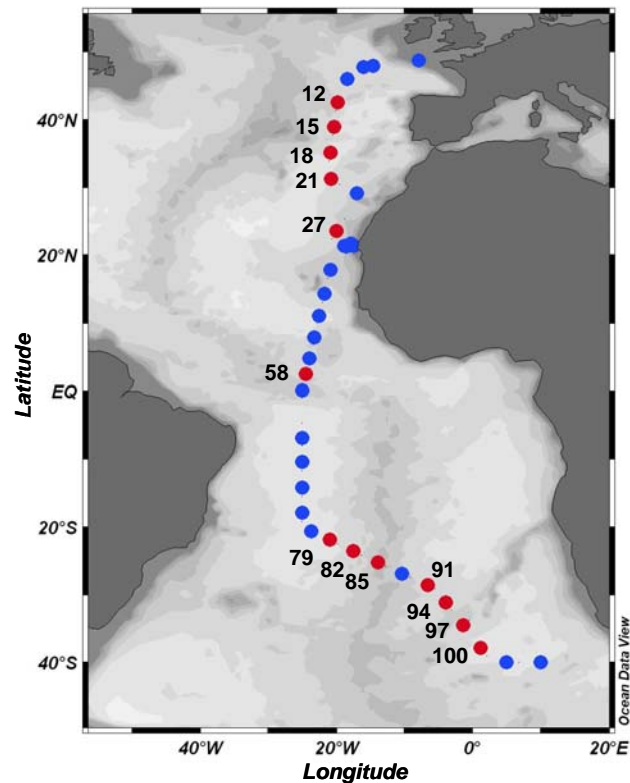


Figure 6.1. The AMT15 cruise track from the UK to South Africa. Blue dots indicate pre-dawn biological sampling stations where FRRF measurements were made. Red dots are also pre-dawn biological (and FRRF) sampling stations but where  $^{14}\text{C}$  P vs. E experiments were also carried out. CTD cast numbers at these stations are shown. The cruise entered the NW African upwelling between  $22.24^{\circ}\text{N}$  and  $20.70^{\circ}\text{N}$ , and reached the South Subtropical Convergence (SSTC) at latitude  $\sim 35^{\circ}\text{S}$ .

In general FRRF and other biological measurements were made at 6 depths, including one at the peak of the DCM. P vs. E and particle absorbance measurements were carried out at two depths, one in the upper surface mixed layer (SML) and one at the peak of the DCM. The SML sample was obtained from between 5 to 30 meters reflecting the depth of the DCM (i.e. the surface sample was deep where the DCM was deep).

## 6.2 Hydrography and Phytoplankton Distribution

The temperature structure and chl-a distribution in the upper water column during AMT15 followed those of previous AMT transects (Robinson et al. 2006) (Fig. 6.2).

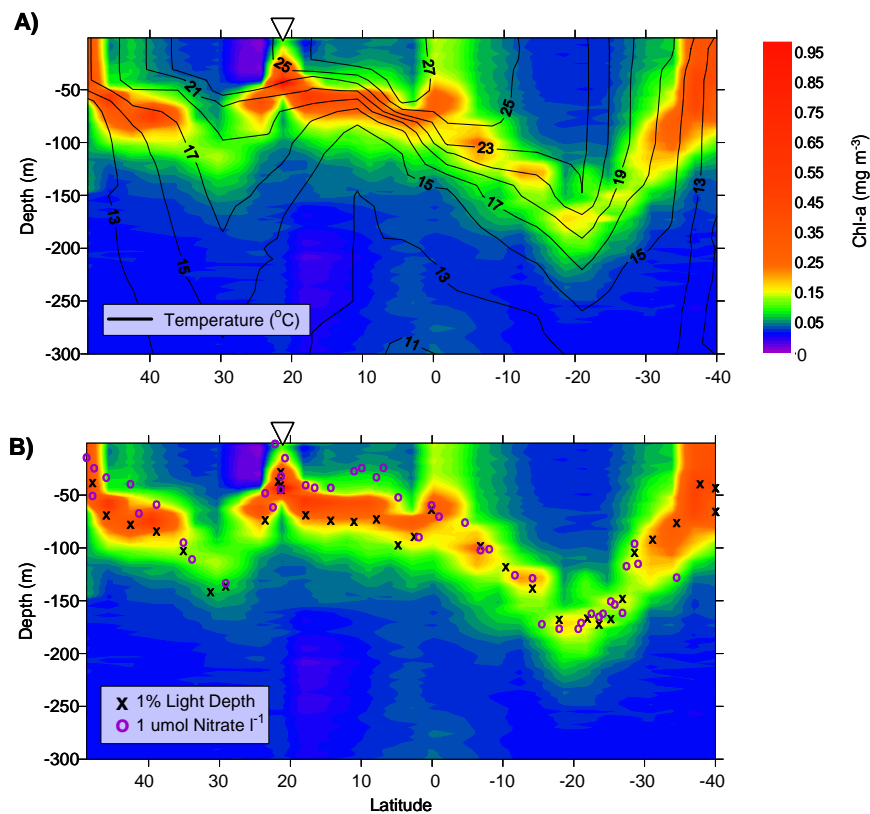


Fig 6.2. Variability in Chl-a concentration against depth along with A) temperature contours, and B) depths of the 1% surface irradiance and 1  $\mu\text{M}$  nitrate concentration marked as determined from linear interpolation between sample depths for each CTD. Sections are from North (left of panel) to South (right of panel) following cruise track in Fig 6.1. Chl-a was obtained from calibrated CTD fluorescence profiles (see Chapter 2). The open triangle indicates the location of the NW African Upwelling. Depth of 1% surface irradiance was obtained from reconstructed *in situ* light fields following methods in Chapter 2. Chl-a concentration exceeded  $0.95 \text{ mg m}^{-3}$  in the NW African upwelling region where maximal chl-a was  $7.67 \text{ mg m}^{-3}$ .

It is clear that a distinct DCM was present along the transect, but that it was not consistently positioned within the thermocline (Fig. 6.2A). Figure 6.2B illustrates that the DCM was closely linked to the 1% surface irradiance contour and strongly correlated to the nitracline, with maximal chl-a positioned close to the 1  $\mu\text{M}$  nitrate concentration along much of the transect.

The northern end of the transect (sampled during local autumn) was characterised by a seasonal thermocline at  $\sim 50 \text{ m}$ . The DCM was close to the depth of the thermocline with chl-a at the DCM of  $\sim 0.4 \text{ mg m}^{-3}$  compared to  $< 0.1 \text{ mg m}^{-3}$  at the surface. Towards the northern gyre the DCM deepened below the thermocline reaching a maximum depth of  $\sim 125 \text{ m}$  (see also Fig 6.3A), the magnitude of the DCM decreased to  $0.1 \text{ mg m}^{-3}$  with surface chl-a around  $0.02 \text{ mg m}^{-3}$ .

<sup>3</sup> in this oligotrophic region. An example profile from the northern gyre is shown in Figure 6.3A and shows that the depth of the DCM and nitracline occur below the depth of the main temperature gradient.

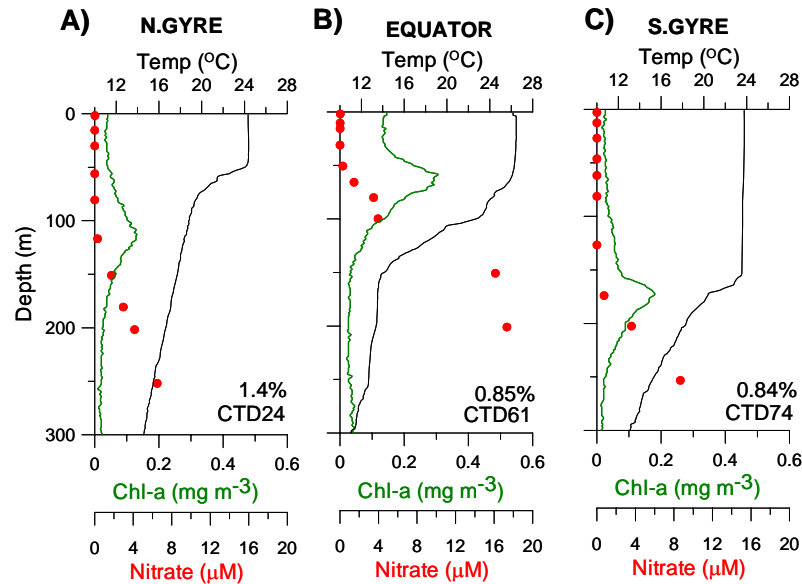


Figure 6.3. Temperature, Chl-a and nitrate concentration with depth for three locations representing A) the North Gyre, B) the Equator and C) the South Gyre. The percentage of surface irradiance present at the depth of the DCM (i.e. the percentage irradiance at the DCM) is also shown. Chl-a and temperature are from the calibrated CTD fluorometer and temperature sensor respectively. Nitrate is as measured from discrete samples.

Chl-a concentration was  $> 7 \text{ mg m}^{-3}$  in the surface in the NW African upwelling. The DCM and thermocline shoaled with proximity to the upwelling region and remained relatively shallow between the upwelling region and the equator. Similar shoaling of the isotherms and DCM were observed at the equatorial upwelling region (Fig. 6.3B). The DCM was located within the thermocline at the equator and was coincident with the nitracline. Chl-a concentration at the DCM at the equator was  $\sim 0.3 \text{ mg m}^{-3}$  compared to  $\sim 0.1 \text{ mg m}^{-3}$  at the surface.

The thermocline and DCM were deepest within the southern oligotrophic gyre where the DCM occurred close to the thermocline at a depth of  $\sim 175 \text{ m}$  (Fig. 6.2A, Fig. 6.3C). The chl-a concentration at the DCM in the southern gyre was  $\sim 0.2 \text{ mg m}^{-3}$  and  $\sim 0.02 \text{ mg m}^{-3}$  at the surface.

The southern end of the transect was sampled in local spring and extended into the south subtropical convergence (SSTC), characterised by relatively weakly stratified to mixed waters with high nitrate and chl-a at the surface (Fig. 6.2A) suggesting early spring bloom conditions.

### Phytoplankton Taxonomy

This section provides a brief overview of the taxonomic composition of the phytoplankton along the transect. In general the pattern of phytoplankton community composition agreed with those of previous AMT transects (Maranon et al. 2000, Barlow et al. 2002, Perez et al. 2006, Poulton et al. 2006a).

With the exception of the NW African upwelling and SSTC region, the Atlantic Ocean was dominated by small phytoplankton (more than 75% of chl-a was in the  $< 2.0 \mu\text{m}$  size fraction). Figure 6.4 shows the concentrations of cyanobacteria (*Synechococcus* and *Prochlorococcus*) and picoeukaryotes, as measured by Analytical Flow Cytometry (AFC).

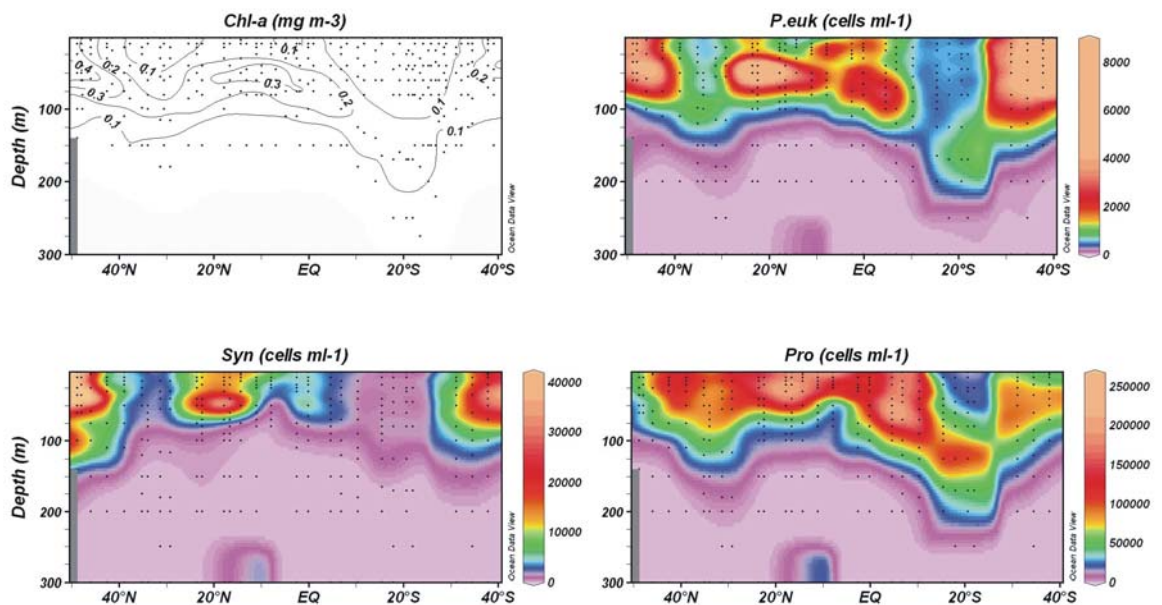


Figure 6.4. Concentrations of phytoplankton groups identified by Analytical Flow Cytometry along the AMT15 transect. Chl-a concentration is also shown. The transect location is shown in Figure 6.1. The NW African upwelling was between 22.24°N and 20.70°N, but the detour of the cruise track into the upwelling region is not included. Chl-a is from CTD bottle samples, scaled to HPLC-derived chl-a. Black dots indicate sample locations. Syn = *Synechococcus*, Pro = *Prochlorococcus*, P.euk = picoeukaryotes.

Picoeukaryotes were most numerous in the mesotrophic high-latitude regions, in the NW African and equatorial upwelling regions, and within the DCM. *Prochlorococcus* was the most abundant phytoplankton group, and concentrations of *Prochlorococcus* were greater in the SML compared the DCM along the transect, with the exception of the southern gyre. *Synechococcus* concentrations were greatest in the high latitude regions and within the NW African and

equatorial upwelling regions. The picoeukaryote concentration was lowest in the surface of the oligotrophic regions. Concentrations of all three phytoplankton types were low in the surface of the southern oligotrophic gyre.

The distribution of cyanobacteria and picoeukaryotes observed by AFC was supported by the distribution of marker pigments measured by HPLC. Figure 6.5 shows the ratios of the key marker pigments to chl-a (composed of chl-a + divinyl chl-a), which illustrate the dominance of certain phytoplankton species within the total population.

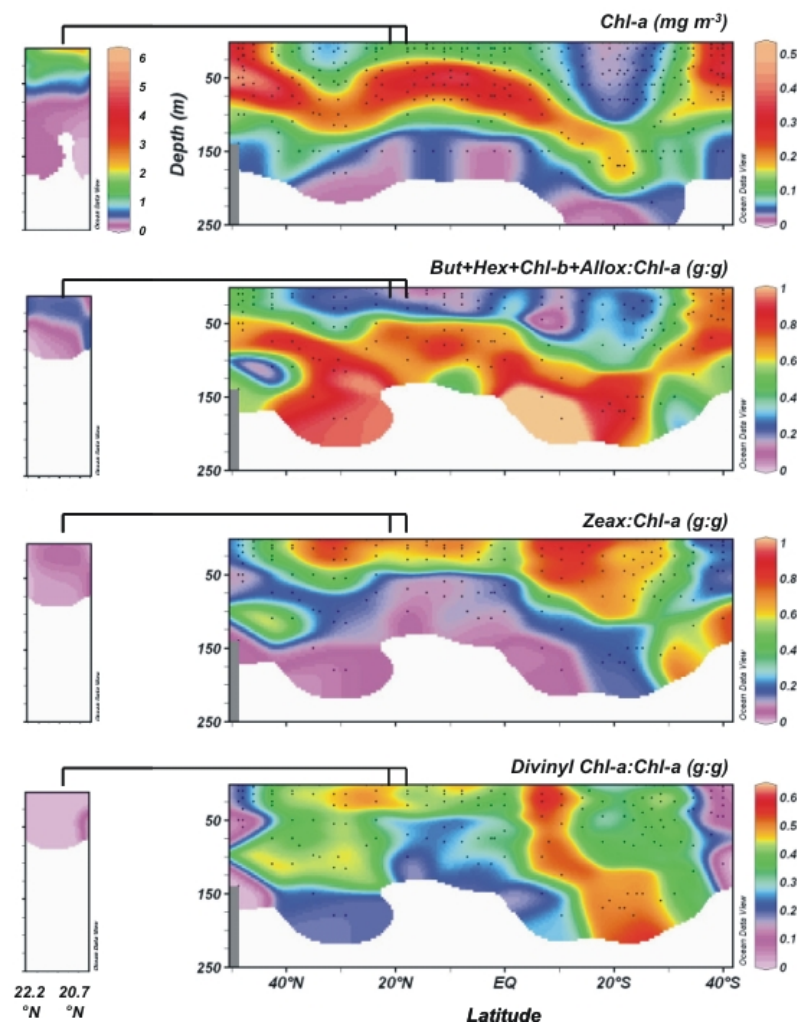


Figure 6.5. Concentrations of phytoplankton pigments compared to Chl-a with depth along the transect. Pigment ratios are compared to chl-a obtained from HPLC which represents divinyl chl-a + chl-a. The NW African upwelling (between 22.24°N and 20.70°N) is shown in the left hand panels. A colour scale bar is shown for the upwelling region if different from the scale used for the main transect. Chl-a concentration is also shown and is from bottle samples measured by the on board fluorometer, weighted to the HPLC-derived chl-a. Black dots indicate sample locations.

Figure 6.5 shows the marker pigment for cyanobacteria (zeaxanthin, contained in both *Synechococcus* and *Prochlorococcus*) was highest (with respect to chl-a) in the surface of the oligotrophic regions. The ratio of divinyl chl-a (present in *Prochlorococcus* only) to chl-a was higher in the DCM than the SML throughout the transect, particularly in the oligotrophic gyres. The presence of *Prochlorococcus* in the DCM of the oligotrophic gyres was also likely to be the reason for increased Chl-b:chl-a in the DCM in the gyre regions (Fig. 6.5) (e.g. MacManus et al. 1994).

The ratios of pigment biomarkers typical of picoeukaryote species shown in Figure 6.5 are 19'-butanoyloxyfucoxanthin (But) (present in pelagophytes), 19'-hexanoyloxyfucoxanthin (Hex) (indicative of prymnesiophytes), alloxanthin (Allox) (present in cryptophytes) and chl-b (present in green flagellates) compared to chl-a (marker pigments as described by Jeffrey et al. (1997)). The taxonomic groups represented by these marker pigments were dominant in the DCM throughout the whole transect as well as in the surface of the NW African and equatorial upwelling regions and the high latitudes. Peridinin (indicative of dinoflagellates) and fucoxanthin (Fuc) (contained in many eukaryotes including prymnesiophytes and diatoms) compared to chl-a was also high in the NW African upwelling and high latitude regions.

Distributions of non-photosynthetic carotenoids (NPC) and photosynthetic carotenoids (PSC) (as defined in Chapter 2) compared to chl-a are shown in Figure 6.6.

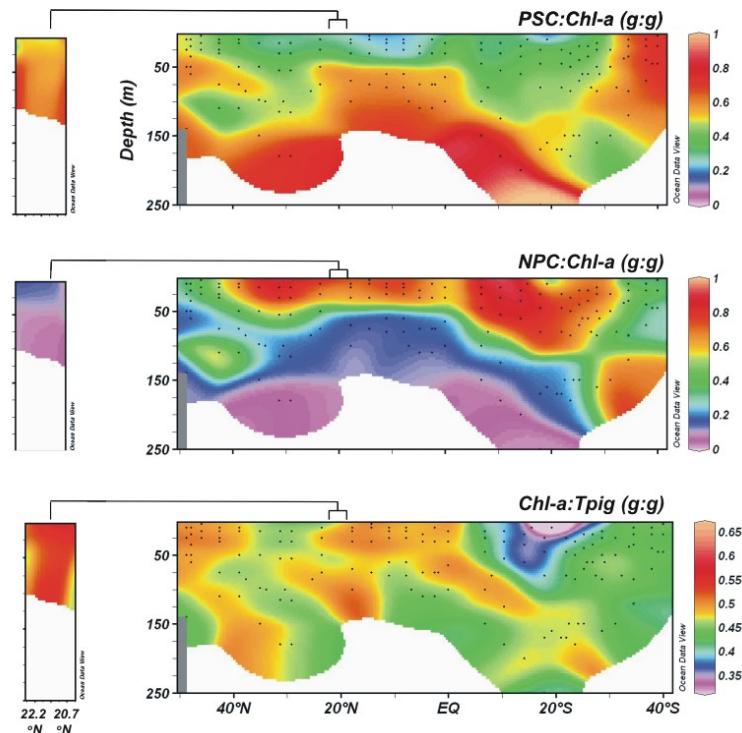


Figure 6.6. Concentrations of photosynthetic carotenoids (PSC), non-photosynthetic carotenoids (NPC) and total pigments (Tpig) compared to Chl-a with depth along the transect. The NW African upwelling (between 22.24°N and 20.70°N) is shown in additional panels, using the same colour scale as used for the main transect. Pigment concentrations are compared to chl-a obtained from HPLC which represents divinyl chl-a + chl-a. PSC and NPC pigment groups are as defined Chapter 2. Tpig is the sum of all pigments measured by HPLC. The open triangle indicates the location of the NW African upwelling. Black dots indicate sample locations.

NPC:chl-a was highest in the SML with PSC:chl-a greatest at depth. 98% of the variance of NPC:chl-a was accounted for by Zeax:Chl-a ( $n = 185$ ,  $r^2 = 0.978$ ,  $p < 0.001$ ), and 98% of the variance in PSC:chl-a could be explained by the ratio of (But + Hex + Fuc):chl-a ( $n = 190$ ,  $r^2 = 0.982$ ,  $p < 0.001$ ). It follows that the distribution of NPC:chl-a and PSC:chl-a reflect changes in the species composition of the phytoplankton population. Chl-a:Tpig (where Tpig is the sum of all pigments identified by HPLC) was generally higher in the mesotrophic waters of the equatorial and NW African upwelling regions and northern high latitudes, and lowest in the oligotrophic gyres (Fig. 6.6). With the exception of the region between the NW African upwelling and the equator, Chl-a:Tpig generally decreased with depth. This parameter may vary with phytoplankton physiology, as phytoplankton may be expected to synthesise more chl-a compared to other pigments in favourable growth conditions (Aiken et al. 2004). Chl-a:Tpig was

not correlated to NPC:chl-a or PSC:chl-a and therefore, on basin scales, was not related to phytoplankton taxonomic composition (Fig 6.6).

It is likely that the phytoplankton composition reflects the phytoplankton adaptation to both the light and nutrient environment, with small cyanobacteria (with high NPC content) dominating the low nutrient, high light environments oligotrophic regions and picoeukaryotes (rich in PSC) within the low light, relatively high nitrate environment of the DCM and mesotrophic waters (Chisholm 1992). The low-light adapted ecotype of *Prochlorococcus* may out-compete picoeukaryotes in the deep DCM of the oligotrophic gyres due to the likely relatively low nitrate flux into the DCM (compared to the equatorial, upwelling or high latitude regions where the nitrate gradient is steeper than in the gyres (Planas et al. 1999, Fig. 6.3, see also Fig. 6.10)) and their suitability to low nitrate environments (Chisholm 1992, Moore et al. 2002). A further example is the low abundance of cryptophytes across the study region (as inferred from the relatively low concentration of alloxanthin a NPC) which may be due to these phytoplankton being out completed in the SML by low nutrient suited cyanobacteria, and out competed in the DCM by prymnesiophytes and pelagophytes which contain higher proportion of PSC:chl-a.

Distinct taxonomic differences were observed between the SML and the DCM possibly resulting from the fact that the open ocean thermocline is relatively stable physical environment which allows time for phytoplankton composition to adapt to the physical environment.

### 6.3 Phytoplankton Photophysiology

This section summarises the evidence for chromatic adaptation and photoacclimation of phytoplankton at the DCM as inferred from phytoplankton absorbance characteristics and parameters obtained by FRRF and  $^{14}\text{C}$  P vs. E experiments.

#### 6.3.1 Optical Properties of Phytoplankton

Across all data, the difference between the chl-a normalised absorption coefficient,  $a^*_{\text{meas}}$ , in the SML and that at the DCM was not significant to the 95% confidence level (according to a T-test). However, the shape of the absorption spectra changed with depth (Fig. 6.7). The differences in the shape of the absorbance spectra ( $a(\lambda)^*_{\text{meas}}$ ) between the SML and DCM are the result of both the change in taxonomic composition (and hence the change in pigment complement) as well as pigment packaging (refer to Chapter 4). However, the dominance of

picophytoplankton, including cyanobacteria, across much of the study region meant that the change in shape of the measured absorption spectra ( $a(\lambda)^*_{\text{meas}}$ ) due to the package effect was likely to be small (Bricaud et al. 2004, Suggett et al. 2004).

The difference in the shape of the absorption spectra (with absorption by NPC removed) between the surface and DCM sample (normalised to the total PAR, i.e. normalised to the area between 400-700 nm) is shown in Figure 6.7. The difference in the shape of the *in situ* irradiance spectra at the SML sample depth and the DCM is also shown (Fig. 6.7A).

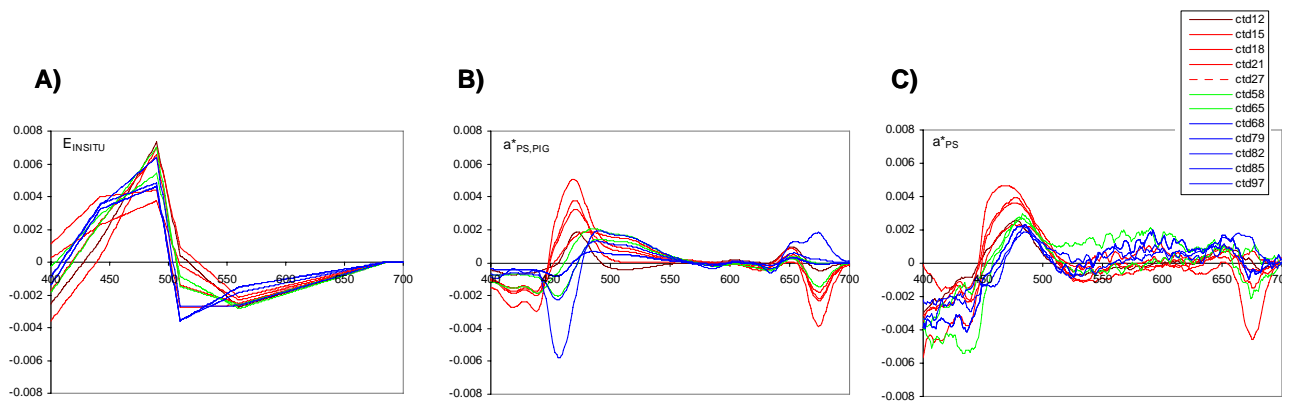


Figure 6.7. The difference in normalised spectral composition between the DCM peak and the SML sample for A) *in situ* irradiance spectra, B) absorption spectra measured by the pigment reconstruction technique with absorption by non-photosynthetic carotenoids (NPC) removed ( $a(\lambda)_{\text{pspig}}$ ), and C) absorption spectra of intact cells measured by the filter technique with absorption by non-photosynthetic carotenoids (NPC) removed ( $a(\lambda)_{\text{ps}}$ ). Spectra were normalised to the sum over the range 400-700 nm and then the normalised spectra at the DCM were subtracted from that in the SML. These figures therefore illustrate the *difference* in the wavelength composition between the surface and DCM. Positive values indicate an increase at the DCM, while negative values indicate a decrease. Coloured lines represent different locations. Data are to a relative scale with the area under each curve equal to zero.

The contribution to irradiance between wavelengths  $\sim 420$ - $450$  nm was greater at the DCM than at the surface. In contrast, irradiance at wavelengths  $< 420$  nm and  $> 500$  nm formed less of a proportion of *in situ* PAR at the DCM compared to the surface. The changes in shape of the phytoplankton absorption spectra reconstructed from pigment concentrations in solution ( $a(\lambda)^*_{\text{pspig}}$ ) broadly followed the changes in wavelength contribution of irradiance. The absorption (relative to total absorption between 400-700 nm) was reduced at wavelengths  $< 450$  nm at the DCM compared to at the surface, with increased absorption between  $\sim 450$  –  $\sim 550$  nm.

The difference in absorption spectra derived from the filter technique (i.e. representing the absorption of intact cells) largely followed the same patterns as those derived from the reconstruction method, and therefore also irradiance.

An exception to the general trend described above occurred in the southern gyre. In contrast to the change in *in situ* irradiance, the contribution of phytoplankton absorption between 450-475 nm to total light absorbed was lower in the DCM than in the SML. This phenomenon was apparent in absorption spectra measured by both the reconstruction method and filter technique (Fig. 6.7), and is possibly the result of the deep population of *Prochlorococcus* present in the DCM within the oligotrophic gyres as the subsequent presence of zeaxanthin, a non-photosynthetic carotenoid, in the DCM may cause the reduced contribution of absorption at these wavelengths compared to the DCM of other regions.

These data show that, in general, the difference in pigment composition between the SML and DCM followed the changes in wavelength composition of *in situ* irradiance. Further, the difference in pigment composition between the phytoplankton in the SML and the DCM led to absorption spectra suited to the wavelength composition of *in situ* irradiance. The coupling between phytoplankton absorption and light availability is a combination of both phytoplankton adaptation to the light environment and the change in irradiance spectra at depth due to absorption by phytoplankton at the surface (Kirk 1994). There was no clear evidence to suggest that phytoplankton taxonomic composition at the DCM varied in response to the species present (and therefore light absorbed) in the surface at different locations along the transect.

The similarity in absorption spectra between the pigment reconstruction and filter methods also indicated that the package effect had a minimal influence on the shape of the absorption spectra. It should be noted that the absorption by the filter technique is not entirely independent of the pigment reconstructions since the latter is used in removal of absorption of NPC (see Chapter 2).

### 6.3.2 Directly Measured Physiological Parameters

In the following sections, a brief summary of the measured physiological parameters by the FRRF and  $^{14}\text{C}$  P vs. E experiments is given initially, followed by a detailed analysis of the physiological parameters separated into those related to light harvesting ( $\sigma_{\text{PSII}}$ ,  $\alpha^*$  and  $\Phi_m$ ) and rates of electron transfer ( $1/\tau_{\text{Qa}}$ ,  $1/\tau_{\text{PSII}}$ ,  $P_m^*$ ). An overall account of variability in the light saturation parameter,  $E_k$ , is then provided.

The physiological parameters measured by FRRF and  $^{14}\text{C}$  P vs. E curves are illustrated in Figure 6.8. In general the magnitudes of the physiological parameters were similar to those of previous studies (e.g. Suggett et al. 2006, Maranon and Holligan 1999); full comparison is given in Chapter 7. A gap in P vs. E experiments between  $20^\circ\text{N}$  and the equator was due to technical problems with facilities on board, and a gap between the equator and  $20^\circ\text{S}$  at the surface was due to light conditions in the P vs. E incubator not achieving saturated rates of carbon fixation. This latter problem meant that for 5 P vs. E experiments (corresponding to CTD79 - CTD94, latitude  $-21.92^\circ\text{S}$  to  $-31.13^\circ\text{S}$ ) surface experiments were carried out using a slide projector with a fluorescent bulb, instead of the normal tungsten halogen lamp. The regression between  $\alpha^*_{14\text{C}}:\alpha^*_{478}$  and  $\alpha^*_{14\text{C}}:\Phi_m$  for these experiments were significantly different to other samples (to the 95% confidence level, according to a T-test) indicating that the difference in the spectral shapes between the two bulb types had a significant effect on the value of  $\alpha^*_{14\text{C}}$ . For the following analysis the spectrally-adjusted values of  $\alpha^*_{478}$  (and  $\text{Ek}_{478}$ ) are used to overcome this discrepancy. Over all data  $\alpha^*_{14\text{C}}$  and  $\alpha^*_{478}$  were significantly correlated, with  $\alpha^*_{478}$  3-times the magnitude of  $\alpha^*$  ( $n = 31$ ,  $r^2 = 0.983$ ,  $p < 0.001$ ).

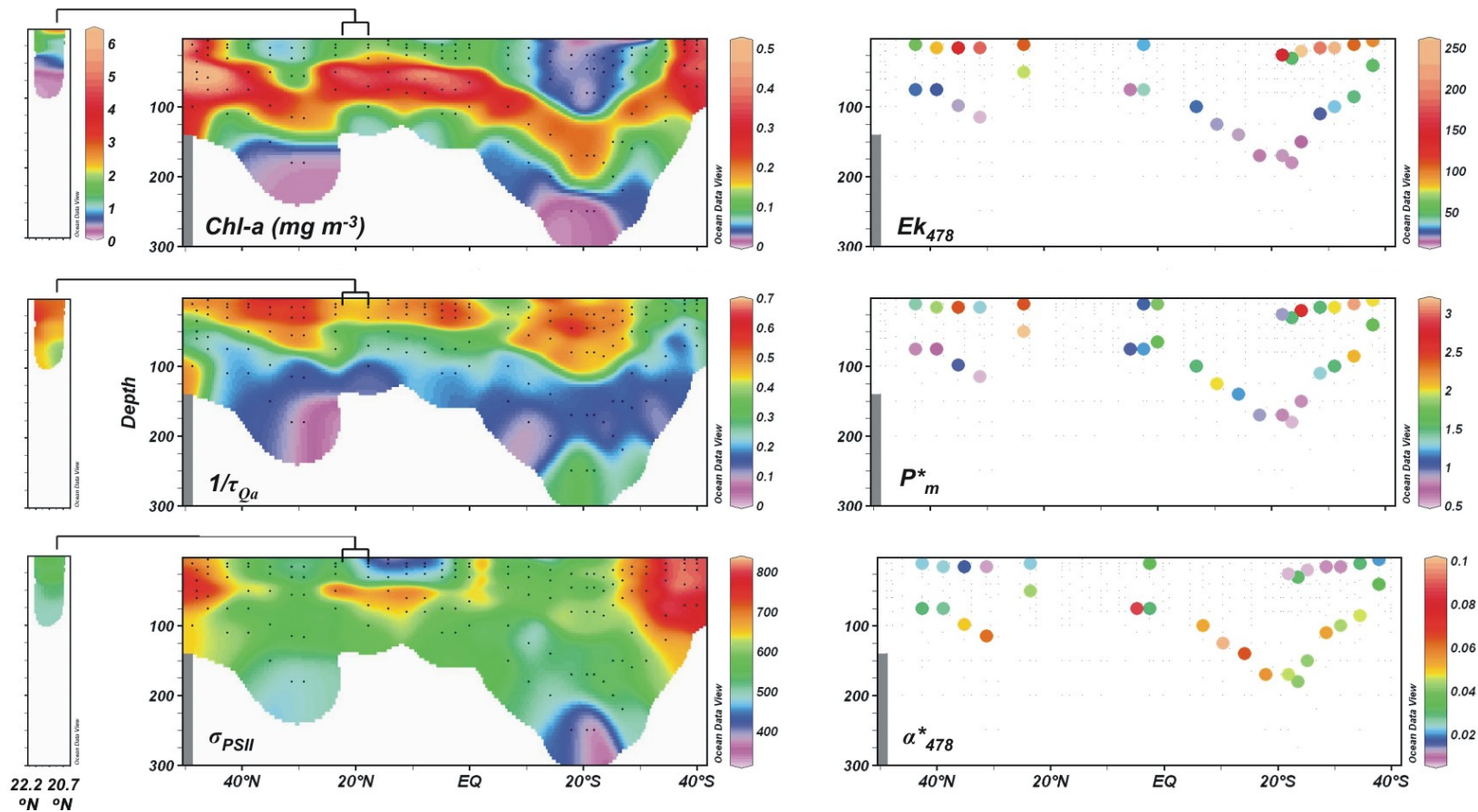


Figure 6.8. Changes in the magnitudes of physiological parameters measured by FRRF and  $^{14}\text{C}$  P vs. E curves with depth along the transect. Chl-a concentration is also shown (top left panel) obtained from bottle samples measured by the on board fluorometer, scaled to HPLC-derived chl-a. Samples collected within the NW African upwelling (22.24–22.70°N), where available, are shown in additional panels. Scale bars for the upwelling region are shown where different scaling was used to that of the main transect. Physiological parameters measured by FRRF (left hand panels) are  $1/\tau_{Qa}$  the electron turnover rate from Qa to PQ ( $\text{s}^{-1}$ ), and  $\sigma_{PSII}$  the effective absorption cross section of PSII ( $\times 10^{-20} \text{ m}^2 \text{ quanta}^{-1}$ ).  $^{14}\text{C}$  P vs. E parameters (right hand panels) include the light saturation parameter corrected for an excitation spectra centered on 478 nm ( $E_{k_{478}}$ ) ( $\mu\text{E m}^{-2} \text{ s}^{-1}$ ), the light-saturated photosynthetic rate normalised to chl-a ( $P^*_m$ ) ( $\text{mg C (mg chl-a)}^{-1} \text{ h}^{-1}$ ) and the maximum light utilisation coefficient scaled for excitation spectrum centered on 478 nm ( $\alpha^*_{478}$ ), ( $\text{mg C (mg chl-a)}^{-1} \text{ h}^{-1} (\mu\text{E m}^{-2} \text{ s}^{-1})^{-1}$ ). Coloured dots represent values for individual samples shaded according to the associated colour scale.

In general, the physiological parameters (with the exception of  $\sigma_{PSII}$ ) were distinctly different between the SML and DCM across the majority of the transect. Both horizontal and vertical variability was evident in  $P^*_{m}$ ,  $Ek_{478}$  and  $1/\tau_{O_a}$  and these parameters were significantly lower in the DCM than in the SML for all available data (to 95% confidence, via a T-test).  $\alpha^*_{478}$  was generally higher in the DCM than at depth with the exception of the equatorial upwelling region.  $\sigma_{PSII}$  varied both horizontally across the transect with vertical variability most evident in the region between the NW African upwelling and the equator.

$^{14}C$ -derived  $Ek_{478}$  was significantly lower at the DCM across the whole transect (to 95% confidence, via a T-test), with 44% of the variability in  $Ek_{478}$  attributable to variability in  $\alpha^*_{478}$  ( $n = 31$ ,  $r^2 = 0.442$ ,  $p < 0.001$ ), and 24% attributable to  $P^*_{m}$  ( $n = 31$ ,  $r^2 = 0.238$ ,  $p < 0.001$ ). Due to the resolution of sampling (particularly of  $^{14}C$ -derived parameters) the investigation of changes in physiology through the SML and within the DCM was limited.

### 6.3.3 Light Harvesting Parameters

$\sigma_{PSII}$

61% of the variability in  $\sigma_{PSII}$  was explained by the variability in pigment ratio But+Hex+Allox:chl-a ( $n = 60$ ,  $r^2 = 0.609$ ,  $p < 0.001$ ). Figure 6.9 illustrates the relationship between  $\sigma_{PSII}$  and But+Hex:chl-a with other major pigment concentrations (with respect to chl-a) highlighted in order to illustrate the influence of pigment composition on  $\sigma_{PSII}$ .

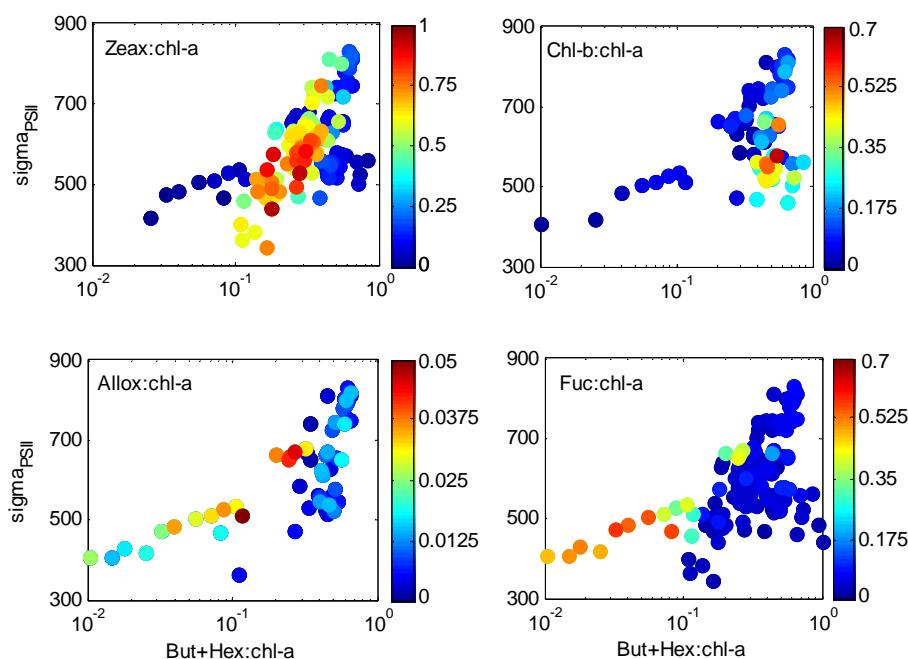


Figure 6.9. Relationship between the effective absorption cross section,  $\sigma_{\text{PSII}}$  ( $\times 10^{-20} \text{ m}^2 \text{ quanta}^{-1}$ ) and the But+Hex:chl-a pigment ratio (g:g). Colours of the symbols represent the pigment ratios as annotated on each panel, with reference to the associated colour scale. Pigment ratios are in g:g. Differences in the number of data points between panels reflect the HPLC limit of detection for the minor pigments.

The low values of  $\sigma_{\text{PSII}}$  was associated with low But+Hex:chl-a coincident with high Zeax:chl-a and Fuc:chl-a ratios. In contrast,  $\sigma_{\text{PSII}}$  was maximal when the dominant pigments were But+Hex:chl-a. To the first order, this may reflect an increase in  $\sigma_{\text{PSII}}$  from the cyanobacteria-dominated surface waters to the picoeukaryote-dominated DCM, which would imply an increase in effective absorption cross section at depth compared to at the surface. However, the concentration of other key pigment types (compared to chl-a) clearly influenced the value of  $\sigma_{\text{PSII}}$ , and suggested that this parameter was driven by phytoplankton community structure in the first instance and therefore was only indirectly as a response to the light environment. For example, Chl-b:chl-a was highest at the deepest DCM in the oligotrophic gyres and was associated with mid-range values of  $\sigma_{\text{PSII}}$ . Subsequently,  $\sigma_{\text{PSII}}$  decreased with depth in the southern gyre (Fig. 6.8). Similarly, maximal Fuc:chl-a and Allox:chl-a were associated with the NW African upwelling region where  $\sigma_{\text{PSII}}$  varied with pigment ratio but decreased with optical depth (not shown).

$\sigma_{\text{PSII}}$  was not significantly correlated to the phytoplankton absorption parameter  $a^*_{\text{meas}}$  or that corrected for the FRRF excitation spectra  $a^*_{\text{meas},478}$ . There was a significant relationship

between  $\sigma_{\text{PSII}}$  and cell size (by the percentage of chl-a in the  $< 2 \mu\text{m}$  size fraction,  $n = 38$ ,  $r^2 = 0.300$ ,  $p < 0.001$ ). However, it was not possible to identify any changes in  $\sigma_{\text{PSII}}$  that could not be explained by pigment composition.

The relationship between  $\sigma_{\text{PSII}}$  and the variable fluorescence yield (Fv/Fm) was also observed to be related to the dominant pigment concentrations compared to chl-a (Fig. 6.10). The linear co-variance of Fv/Fm and  $\sigma_{\text{PSII}}$ , and the deviations from the linear trend, can be ascribed to the types of dominant pigments present. This is the first time that FRRF parameters  $\sigma_{\text{PSII}}$  and Fv/Fm have been related to the pigment content of phytoplankton populations in the field over such a wide range of hydrographic (and taxonomic) regimes.

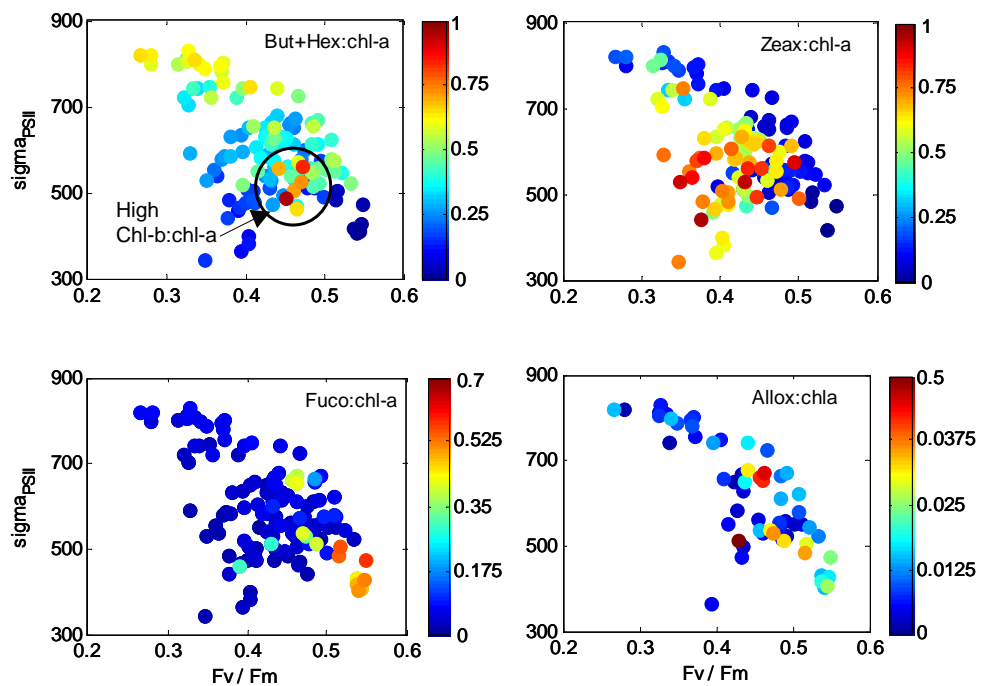


Figure 6.10. Relationship between the effective absorption cross section,  $\sigma_{\text{PSII}}$ , ( $\times 10^{-20} \text{ m}^2 \text{ quanta}^{-1}$ ) and the quantum efficiency of photochemistry (Fv/Fm). Colours of the symbols represent pigment ratios as annotated on each panel, with reference to the associated colour scale. Pigment ratios are in g:g. The circled symbols in the top left panel indicates high ratio of Chl-b:chl-a. Differences in the number of data points between panels reflect the HPLC limit of detection for the minor pigments.

It is suggested that taxonomic groups (as identified by their pigment signatures) are associated with a particular absorption cross section ( $\sigma_{\text{PSII}}$ ) and quantum efficiency of photochemistry (Fv/Fm) in the first instance. The relationships shown in Figure 6.10 would therefore represent

the overall  $\sigma_{\text{PSII}}$  and Fv/Fm signatures of the phytoplankton species constituting the mixed assemblage (accepting the diel variability in both parameters, and second order variability due to changes in environmental conditions (Falkowski and Raven 1997)). This hypothesis is supported by the Fv/Fm and  $\sigma_{\text{PSII}}$  signatures of phytoplankton species in culture (D. Suggett, *pers. comm.*) and potentially means that the FRRF could become a tool for identifying community structure of field populations in the future. An important outcome of the pigment-dependence of  $\sigma_{\text{PSII}}$  and Fv/Fm is that interpretation of field measurements of these parameters must account for taxonomic variability in the first instance.

### $\alpha^*$ and $\Phi_m$

The light utilisation coefficient (corrected to excitation spectrum centred on 478 nm,  $\alpha^*_{478}$ ) and that corrected for the amount of light absorbed, the maximum quantum yield ( $\Phi_m$ ) were significantly correlated ( $n = 31$ ,  $r^2 = 0.937$ ,  $p < 0.001$ ).  $\Phi_m$  varied between 0.015 – 0.001 mol C (mol photons)<sup>-1</sup> in the SML, and was highest in the surface of the high latitude regions, and lowest in the surface of the oligotrophic gyres. At the DCM,  $\Phi_m$  varied between 0.035 – 0.009 mol C (mol photons)<sup>-1</sup> and was lowest at the DCM at high latitudes and highest at the DCM at the edges of the oligotrophic gyres. Along the transect,  $\alpha^*_{478}$  largely followed the patterns described for previous AMT cruises by Maranon and Holligan (1999). The magnitudes of  $\Phi_m$  were on average lower, but in the range of, those obtained in oligotrophic regions by other authors (Babin et al. 1996, Marra et al. 2000).

$\alpha^*$  adjusted to the *in situ* irradiance spectra at the sample depth ( $\alpha^*_{\text{insitu}}$ ) was 95% the magnitude of  $\alpha^*_{478}$  ( $n = 31$ ,  $r^2 = 0.969$ ,  $p < 0.001$ ). For the following analysis, trends within the data are described for  $\Phi_m$  as well as  $\alpha^*_{478}$  (spectrally adjusted where appropriate), but illustrations are for  $\Phi_m$  only.

Values of  $\alpha^*_{478}$  and  $\Phi_m$  were significantly greater at the DCM than at the surface (to 95% confidence, via a T-test), suggesting a higher photosynthetic yield at the DCM. The only exception was at the equator, where (contrary to previous AMT transects (Maranon and Holligan 1999)  $\alpha^*_{478}$  and  $\Phi_m$  were greater in the SML. Neither  $\alpha^*_{478}$  nor  $\Phi_m$  were correlated to  $\sigma_{\text{PSII}}$ , or to the phytoplankton absorption coefficients ( $a^*_{\text{meas}}$  or  $a^*_{\text{ps}}$ ). Variability in  $\alpha^*_{478}$  and  $\Phi_m$  with depth was significantly correlated to chl-a:POC which was a factor of 4 greater at the DCM compared to at the surface ( $\Phi_m$   $n = 22$ ,  $r^2 = 0.361$ ,  $p = 0.003$ ).  $\alpha^*_{478}$  and  $\Phi_m$  were significantly correlated to other factors (for example, chl-a and nitrate concentration (not shown)) however, these factors could not be identified as causative.

There was no significant relationship between  $\alpha^*_{478}$  or  $\Phi_m$  and the major pigment ratios in the SML or DCM, but  $\Phi_m$  and  $\alpha^*_{478}$  were significantly (inversely) correlated to NPS:PSC over the whole region ( $\Phi_m$   $n = 26$ ,  $r^2 = 0.250$ ,  $p = 0.009$ ). Further, the relationship between  $\Phi_m$  estimated using the absorption coefficient with NPC removed ( $\Phi_{m,ps}$ ) and NPS:PSC was not significant. These results indicate either taxonomic variability of  $\Phi_m$  or, more likely, a reduction in  $\Phi_m$  due to the presence of NPC in the SML (MacIntyre et al. 2002).

Variability in neither  $\alpha^*_{478}$  nor  $\Phi_m$  in the SML was significantly correlated to that at the DCM. In order to investigate horizontal gradients in  $\alpha^*_{478}$  and  $\Phi_m$  consideration was given to the SML and DCM separately.

The depth and optical depth of the DCM appeared to influence the value of  $\alpha^*$  and  $\Phi_m$  in the SML and at the DCM respectively (Fig. 6.11) although these relationships were not significant at the 95% confidence level.

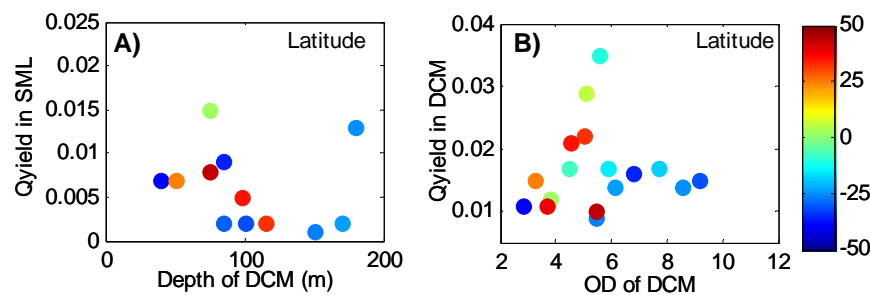


Figure 6.11. A) Relationships between the quantum yield of photosynthesis ( $\Phi_m$ ) ( $\text{mol C (mol photons)}^{-1}$ ) in the SML and depth of the peak of the DCM, B)  $\Phi_m$  at the DCM against the optical depth of the DCM peak. Optical depth is calculated from the sample depth  $\times$   $K_d(\text{PAR})$ .

Figure 6.11B indicates that at the DCM,  $\Phi_m$ , was correlated to optical depth (OD), suggesting that the light environment may influence the value of  $\Phi_m$ . However,  $\Phi_m$  appears reduced relative to OD in the southern gyre (Fig. 6.11B), which cannot be explained by pigment concentrations (phytoplankton taxonomy).

With the exception of one southern gyre location (CTD82)  $\alpha^*_{478}$  and  $\Phi_m$  in the SML appear weakly correlated to the depth of the DCM ( $\Phi_m$   $n = 11$ ,  $r^2 = 0.354$ ,  $p = 0.054$  excluding CTD82, Fig. 6.11A). The depth of the DCM peak (and consequently the nitracline) is often used as a proxy for nutrient flux since a shallow DCM is associated with upwelling or mesotrophic regions in contrast to the deep DCM in the oligotrophic gyres (Herbland and Voituriez 1979,

Malone et al. 1993, Maranon and Holligan 1999). The relationship between  $\Phi_m$  and  $\alpha_{478}^*$  in the SML and depth of the DCM peak therefore suggests that these parameters may vary in response to the nutrient availability.

#### 6.3.4 Electron Transfer Parameters

##### $P_m^*$

The maximum photosynthetic rate,  $P_m^*$ , varied horizontally as well as with depth along the transect (Fig. 6.8). With the exception of the equator and NW African upwelling,  $P_m^*$  was always lower at the DCM than in the SML. Within the SML  $P_m^*$  was variable (range 0.9 – 3.1 mg C (mg chl-a)<sup>-1</sup> h<sup>-1</sup>) and was often relatively high (> 2 mg C (mg chl-a)<sup>-1</sup> h<sup>-1</sup>) in the oligotrophic gyres. Within the DCM values of  $P_m^*$  varied between 0.5 – 3.2 mg C (mg chl-a)<sup>-1</sup> h<sup>-1</sup> and were greatest at the edge of the NW African upwelling, just south of the equator and within the south subtropical convergence (SSTC). The magnitudes and range of  $P_m^*$  were lower than those obtained by Maranon and Holligan (1999) who observed  $P_m^*$  in the range of 0.3 – 14 mg C (mg chl-a)<sup>-1</sup> h<sup>-1</sup>. However, Maranon and Holligan (1999) showed data from two cruises, with the magnitude of  $P_m^*$  for AMT2 only reaching < 6 mg C (mg chl-a)<sup>-1</sup> h<sup>-1</sup> which is more similar to the range in these data. Further, since Maranon and Holligan (1999) sampled at ~10:30am and incubated over 2.5 h, diel variability could also contribute to the higher  $P_m^*$  observed by these authors compared to this study. This issue is discussed further in Chapter 7.

Along the transect, horizontal variability in  $P_m^*$  in the SML was not correlated to that at the DCM to within 95% confidence ( $n = 12$ ,  $r^2 = 0.251$ ,  $p = 0.097$ ), indicating that different factors determine the magnitude of this parameter in the SML compared to the DCM. Horizontal variability in  $P_m^*$  in the DCM was significantly correlated to the depth of the DCM ( $n = 18$ ,  $r^2 = 0.281$ ,  $p = 0.024$ ) but not optical depth of the DCM.  $P_m^*$  at the DCM was also significantly correlated to the pigment ratio But+Hex+Allox:chl-a at the DCM ( $n = 14$ ,  $r^2 = 0.561$ ,  $p = 0.002$ ), although no relationship with pigment ratios could be found with  $P_m^*$  in the SML.  $P_m^*$  in the SML was not significantly correlated to either the depth of the DCM, or the optical depth of the DCM.

These data are in agreement with Maranon and Holligan (1999) who showed  $P_m^*$  was higher in the southern gyre than the northern gyre, but Maranon and Holligan (1999) also reported that horizontal gradients in  $P_m^*$  in the SML were correlated to the depth of the nitracline, which was not observed in these data.

*1/τ<sub>Qa</sub> and 1/τ<sub>PSII</sub>*

As in the case of  $P^*_m$ , both horizontal and vertical gradients were evident in the electron transfer rates from Qa to the PQ pool ( $1/\tau_{Qa}$ ) and across the entire electron transport chain ( $1/\tau_{PSII}$ , as estimated from  $\sigma_{PSII}$  and  $^{14}C$ -derived  $Ek_{478}$ ). Both  $1/\tau_{Qa}$  and  $1/\tau_{PSII}$  were significantly different between the SML and at the DCM (to 95% confidence, via a T-test). There was no significant difference in the magnitudes of electron transfer rates between samples from the upper (~2 m) and lower SML indicating that these parameters remained relatively constant with depth in the SML (according to a T-test).

Horizontal gradients in  $1/\tau_{Qa}$  within the SML were not correlated to those at the DCM. At the DCM,  $1/\tau_{Qa}$  was significantly correlated to both the depth ( $n = 32$ ,  $r^2 = 0.4625$ ,  $p < 0.001$ ) and optical depth of the DCM ( $n = 32$ ,  $r^2 = 0.127$ ,  $p = 0.046$ ). Within the SML horizontal gradients in  $1/\tau_{Qa}$  were not significantly correlated to the depth of the DCM, or the mean growth irradiance of the previous 24 hours. For all data, Figure 6.12 shows the relationship between  $1/\tau_{Qa}$  and the pigment ratio But+Hex:chl-a.

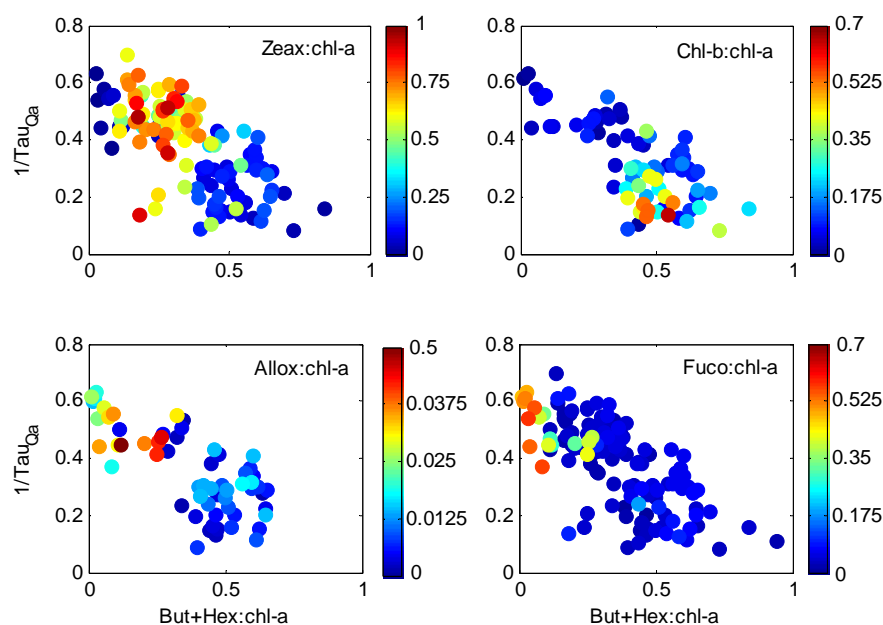


Figure 6.12. Relationship between the rate of electron transport from Qa – PQ pool,  $1/\tau_{Qa}$ , and the But+Hex:chl-a pigment ratio (g:g). Colours of the symbols represent pigment ratios as annotated on each panel, with reference to the associated colour scale. Pigment ratios are in g:g. Differences in the number of data points between panels reflect the HPLC limit of detection for the minor pigments.

The relationship between  $1/\tau_{Qa}$  and But+Hex:chl-a was linear regardless of the concentrations of other pigments compared to chl-a (Zeax:chl-a, Fuc:chl-a, Chl-b:chl-a), suggesting that (unlike

$\sigma_{\text{PSII}}$ )  $1/\tau_{\text{Qa}}$  was correlated to these pigment ratios due to their vertical gradients, rather than as a consequence of pigment concentrations directly. For example,  $1/\tau_{\text{Qa}}$  was lowest where But+Hex:chl-a was greatest (i.e. at the DCM) and also coincident with the high Chl-b:chl-a in the DCM of the central gyres.  $1/\tau_{\text{Qa}}$  was highest in the surface, associated with low But+Hex:chl-a, and high Zeax:chl-a, and despite the pigment ratios of Allox:chl-a and Fuc:chl-a in the NW African upwelling region.

The relationships between  $1/\tau_{\text{Qa}}$ ,  $1/\tau_{\text{PSII}}$  and  $P^*_m$  are shown in Figure 6.13.  $P^*_m$  was significantly correlated to  $1/\tau_{\text{Qa}}$  ( $n = 33$ ,  $r^2 = 0.151$ ,  $p = 0.026$ ) and  $1/\tau_{\text{PSII}}$  ( $n = 31$ ,  $r^2 = 0.282$ ,  $p = 0.002$ ).  $1/\tau_{\text{Qa}}$  was also significantly correlated to  $1/\tau_{\text{PSII}}$  ( $n = 31$ ,  $r^2 = 0.2242$ ,  $p = 0.007$ ). Despite these linear trends, the gradients between  $P^*_m$  and the electron transfer rates varied along the transect (Fig. 6.13B and C). Figure 6.13D shows that the change in slope of the relationship between  $1/\tau_{\text{Qa}}$  and  $P^*_m$  (expressed as the ratio  $1/\tau_{\text{Qa}} : P^*_m$ ) appears to be related to the ratio of picoeukaryotes to cyanobacteria (log-log relation  $P.\text{euk}:\text{Syn}+\text{Pros}$  (cells  $\text{ml}^{-1}$ )  $n = 25$ ,  $r^2 = 0.422$ ,  $p < 0.001$ ) and the ratio of But+Hex:chl-a ( $n = 27$ ,  $r^2 = 0.453$ ,  $p < 0.001$ , not shown).

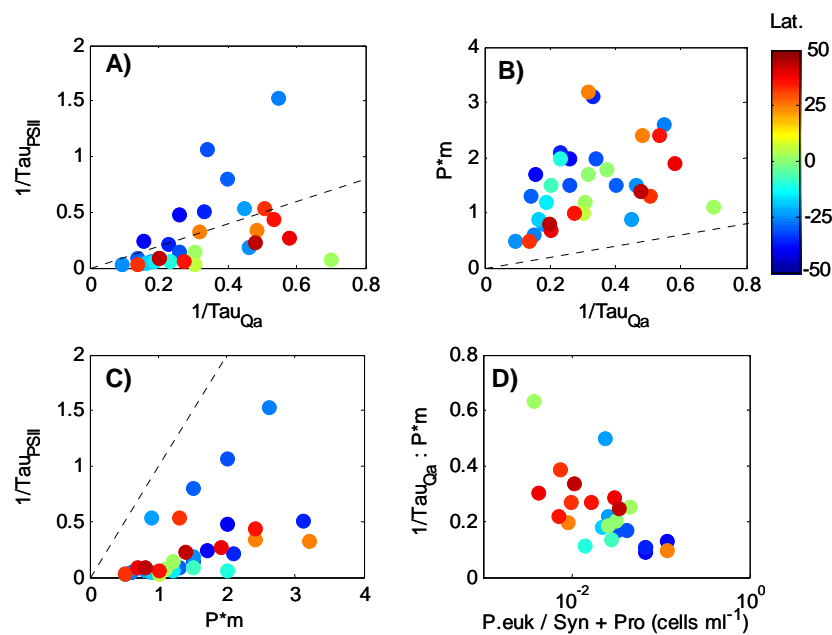


Figure 6.13. A) Relationship between electron transport rates from Qa-PQ,  $1/\tau_{\text{Qa}}$ , ( $\text{s}^{-1}$ ) and through the whole-chain,  $1/\tau_{\text{PSII}}$ , estimated from  $166030 \times (\sigma_{\text{PSII}} / \text{Ek}_{478})$ . B) Relationship between  $1/\tau_{\text{Qa}}$  and the light-saturated photosynthetic rate,  $P^*_m$ , ( $\text{mg C} (\text{mg chl-a})^{-1} \text{h}^{-1}$ ). C) Relationship between  $1/\tau_{\text{PSII}}$  and  $P^*_m$ . D) Relationship between the ratio of  $1/\tau_{\text{Qa}} : P^*_m$  to the ratio of the cellular abundance (cells  $\text{ml}^{-1}$ ) of picoeukaryotes to that of cyanobacteria (*Synechococcus* + *Prochlorococcus*) as measured by AFC. Colour of symbols represents latitude with reference to the colour scale. Dotted lines indicate 1:1 relationship.

The linear relationship between  $1/\tau_{Qa}$  and  $1/\tau_{PSII}$  indicates that the rate of electron transport from Qa to PQ, and that across the entire chain are limited by the same process, likely the downstream processes of carbon fixation (Sukenik et al. 1987, Moore et al. 2006). The magnitude of  $1/\tau_{Qa}$  was greater than  $1/\tau_{PSII}$  for most stations, with the exception of 7 samples in the southern gyre. This is in contradiction of the general theory, which states that the whole chain transfer should always be slower than that from Qa to PQ due to the relatively slow rate of electron transport through the PQ pool compared to the re-oxidation rate of  $Qa^-$  (Falkowski and Raven 1997). On two occasions, both on the boundary of the southern gyre,  $1/\tau_{PSII}$  was in excess of the theoretical maximum of  $1 \text{ (s}^{-1}\text{)}$  (Falkowski and Raven 1997).

The phenomenon of  $1/\tau_{PSII}$  exceeding  $1/\tau_{Qa}$ , has been observed during previous AMT transects (Suggett et al. 2006) although the reasons for it are not well understood. No previous occurrence  $1/\tau_{PSII}$  exceeding the theoretical maxima has been reported. The variance of  $1/\tau_{PSII}$  may partly be explained by the de-coupling of FRRF and  $^{14}\text{C}$ -derived parameters, since  $1/\tau_{PSII}$  is estimated by combining  $\sigma_{PSII}$  and  $^{14}\text{C}$ -derived  $Ek_{478}$ . The importance of pigment concentrations, and therefore taxonomic variability, in the decoupling FRRF and  $^{14}\text{C}$ -derived parameters is clearly evident in the change in the variance between  $P^*_m$  and  $1/\tau_{Qa}$  with the ratio of picoeukaryotes to cyanobacteria (Fig. 6.13D). This is discussed in more detail below.

### 6.3.5 Light Saturation Index, $Ek$

#### *$^{14}\text{C}$ vs. FRRF-derived $Ek$*

Values of FRRF-derived  $Ek$  ( $Ek_{ETR,478}$ ) were significantly different between the SML and DCM (to 95% confidence according to a T-test). The difference in  $Ek_{ETR,478}$  between the top (~2 m) and base of the SML were not significant to 95% confidence (via T-test) indicating that this parameter was relatively constant with depth within the SML. The relationship between  $^{14}\text{C}$  and FRRF-derived  $Ek$  is shown in Figure 6.14, where  $^{14}\text{C}$ -derived  $Ek$  is corrected to refer to the spectra of the FRRF.

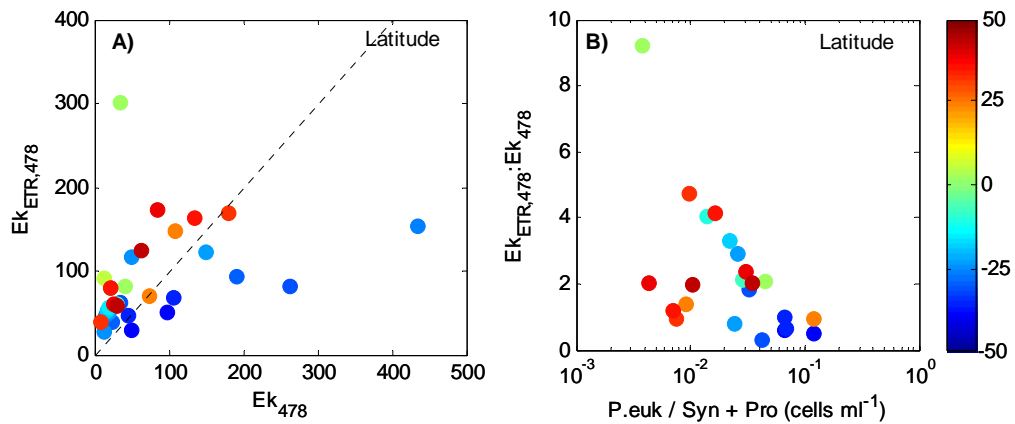


Figure 6.14. A) Relationship between light saturation parameter derived by  $^{14}\text{C}$  corrected to the excitation spectra of the FRRF ( $Ek_{478}$ ) and that as measured by FRRF parameters ( $Ek_{ETR,478}$ ) ( $\mu\text{E m}^{-2} \text{s}^{-1}$ ). B) Relationship between the ratio of  $^{14}\text{C}$  derived  $Ek_{478}$  and FRRF derived  $Ek_{ETR,478}$  to the ratio of the cellular abundance (cells  $\text{ml}^{-1}$ ) of picoeukaryotes to that of cyanobacteria (*Synechococcus* + *Prochlorococcus*) as measured by AFC. Colour of symbols represents latitude with reference to the colour scale. Dotted lines indicate 1:1 relationship.

Figure 6.14 illustrates horizontal variability in the relationship between  $^{14}\text{C}$ -derived  $Ek_{478}$  and  $Ek_{ETR,478}$ . Within the southern, equatorial and northern regions, the values of  $Ek$  derived by the two techniques were approximately linearly correlated. Figure 6.14B illustrates that the decoupling of  $Ek$  measured by the two methods may be due to horizontal taxonomic gradients along the transect, specifically the proportion of cyanobacteria compared to picoeukaryotes.

There is a distinct similarity in the relationships between  $1/\tau_{Qa}$  and  $1/\tau_{PSII}$  and that between  $Ek_{478}$  and  $Ek_{ETR,478}$  (Fig. 6.14 and 6.13C). A common factor in  $Ek_{ETR,478}$  and  $1/\tau_{PSII}$  (but not  $Ek_{478}$  and  $1/\tau_{Qa}$ ) is  $\sigma_{PSII}$ . It is therefore suggested that taxonomic variability, affecting  $\sigma_{PSII}$ , plays a part in changing the coupling between PSII photochemistry and carbon fixation along the transect.  $\sigma_{PSII}$  was also correlated to the Euk:Syn+Pro ratio, particularly in the SML (Fig. 6.15) where latitudinal variability in the Euk:Syn+Pro ratio and subsequently  $\sigma_{PSII}$  is clear.

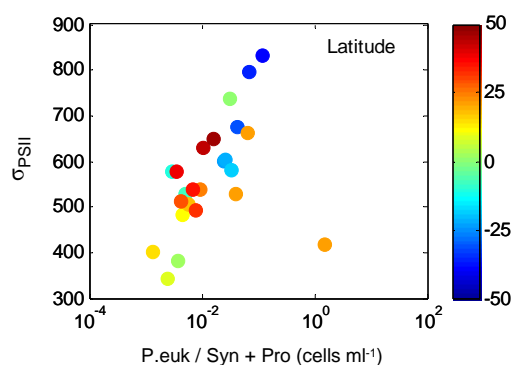


Figure 6.15. Relationship between the effective absorption cross section,  $\sigma_{\text{PSII}}$ , ( $\times 10^{-20} \text{ m}^2 \text{ quanta}^{-1}$ ) and the ratio of the cellular abundance ( $\text{cells ml}^{-1}$ ) of picoeukaryotes to that of cyanobacteria (*Synechococcus* + *Prochlorococcus*) as measured by AFC for mid-depth SML samples only (collected at the depth at which irradiance was 55% of that at the surface). Colour of symbols represents latitude with reference to the colour scale. Data are shown for the SML samples only.

#### *Ek and in situ irradiance*

The <sup>14</sup>C-derived light saturation parameter (adjusted to excitation spectrum centred on 478 nm),  $Ek_{478}$ , was significantly different between the SML and DCM to 95% confidence level (T-test), with values in the DCM on average 5-fold lower than in the SML. Correlation analysis revealed that horizontal gradients in  $Ek_{478}$  in the SML were not related to those in the DCM.

With the exception of two southern gyre stations (CTD79 and CTD82) where  $Ek_{478}$  in the SML was relatively low (due to low  $P^*_m$  and high  $\alpha^*_{478}$ ), horizontal gradients in  $Ek_{478}$  within the SML were correlated to the depth of the SML sample ( $n = 10$ ,  $r^2 = 0.645$ ,  $p = 0.005$ ). In contrast, at the DCM horizontal gradients in  $Ek_{478}$  were significantly correlated to the depth of the DCM ( $n = 18$ ,  $r^2 = 0.470$ ,  $p = 0.002$ ) but were not significantly correlated to the optical depth of the DCM. However, horizontal gradients of  $Ek_{\text{insitu}}$  at the DCM were significantly correlated to the optical depth of the DCM ( $n = 17$ ,  $r^2 = 0.239$ ,  $p = 0.046$ ). These data therefore indicate that the light environment was a major factor determining  $Ek$  in both the SML and the DCM.

A greater variability in  $\alpha^*_{478}$  between the SML and the DCM was observed compared to  $P^*_m$ , with  $\alpha^*_{478}$  responsible for a greater proportion of the variability in  $Ek_{478}$  (as mentioned above). The magnitudes of  $P^*_m$  and  $\alpha^*_{\text{insitu}}$  led to magnitudes of  $Ek_{\text{insitu}}$  that corresponded to the *in situ* mean growth irradiance for the previous 24 hours (Fig. 6.16). The growth irradiance of the SML was estimated from the mean irradiance throughout the SML, and assumed a full overturning of the SML in the 24 hour period. The base of the SML was assumed to be the depth at which chl-a increased in association with the DCM.

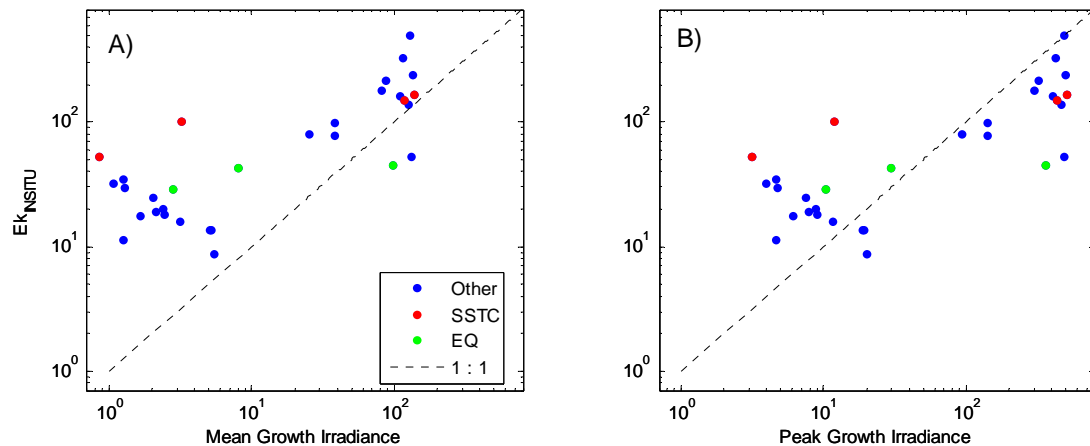


Figure 6.16. Relationship between the  $^{14}\text{C}$ -derived light saturation parameter corrected for the spectrum of *in situ* irradiance,  $E_{k_{\text{insitu}}}$  ( $\mu\text{E m}^{-2} \text{s}^{-1}$ ) and A) mean growth irradiance and, B) peak *in situ* irradiance ( $\mu\text{E m}^{-2} \text{s}^{-1}$ ). The mean growth irradiance was calculated from the mean irradiance experienced over the 24 hours prior to sampling, with spectral composition modelled following methods in Chapter 2. For surface samples irradiance was averaged through the depth of the surface mixed layer (SML) determined by the onset of increase in chl-a associated with the DCM. Peak *in situ* irradiance was estimated from mean growth irradiance  $\times 3.7$  (the mean difference between the maximum daily irradiance and the mean daily irradiance).

In general, phytoplankton within the SML were associated with  $E_{k_{\text{insitu}}}$  close to the magnitude of mean growth irradiance. In contrast, at the DCM  $E_{k_{\text{insitu}}}$  remained greater than *in situ* irradiance even during midday conditions of maximal irradiance such that the rate of photosynthesis of the phytoplankton was less than optimal (as indicated by the (instantaneous) P vs. E curve) (Geider et al. 1998, Moore et al. 2006). The similarity in magnitudes of  $E_{k_{\text{insitu}}}$  between the SML and at the DCM in the equatorial and SSTC regions likely reflects the mixing conditions of these regions.

### 6.3.6 Adaptation and Photoacclimation

As described above, the taxonomic composition of phytoplankton across the transect likely results from the horizontal and vertical gradients in light and nutrient availability across the study region. In this section, the evidence for photoacclimation of phytoplankton in addition to the community composition (reflecting genotypic traits resulting from adaptation) is assessed.

The variability of *Synechococcus*, *Prochlorococcus* and picoeukaryote fluorescence per cellular biomass (as inferred from the ratio of fluorescence per cell to side scatter, F:SS,

measured by Analytical Flow Cytometry) are provided for a representative location in the southern gyre (CTD 74, Fig. 6.17).

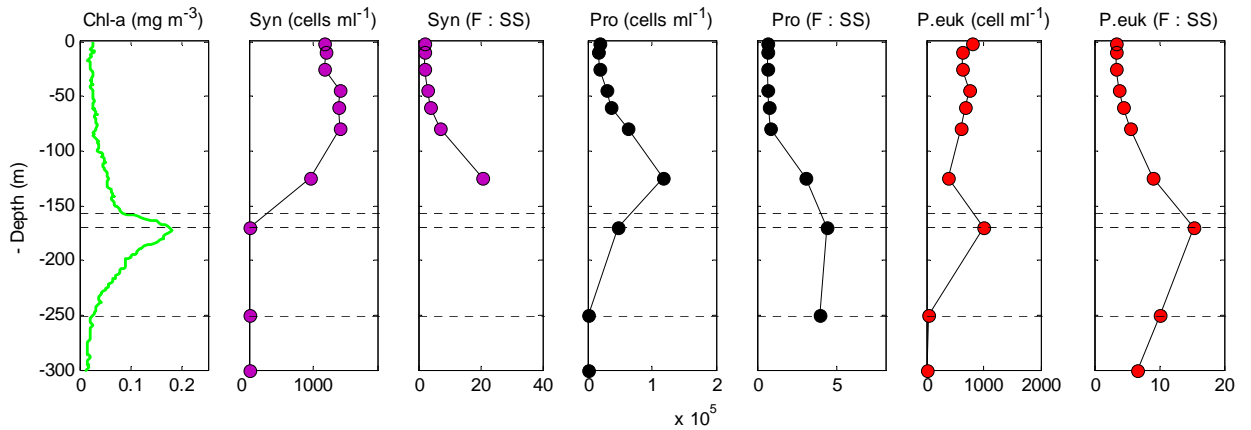


Figure 6.17. Vertical profiles of chlorophyll-a (left hand panel) and characteristics of *Synechococcus* (Syn), *Prochlorococcus* (Pro) and picoeukaryotes (P.euk) obtained from Analytical Flow Cytometry (AFC) against depth, for an example station in the southern gyre (CTD74). For each phytoplankton group, profiles are of cell concentrations ( $\text{cells ml}^{-1}$ ) and the ratio of cellular fluorescence to cell side scatter (F : SS) which is an indication of the ratio of cellular chl-a:C. Correction factors have not been applied to obtain absolute values of chl-a:C, so values are given to an arbitrary scale. Dashed lines in all panels indicate the top and bottom of the DCM (as determined by the increase in chl-a associated with the DCM) and the depth of the peak of the DCM.

In the southern gyre (CTD74, Fig.6.17), fluorescence per cell size (F:SS) was greater at the DCM than in the SML for all phytoplankton types (accepting missing data for *Synechococcus*). Picoeukaryote F:SS increased by a factor of  $\sim 4$  between the SML and DCM, and *Prochlorococcus*, by a factor of  $\sim 7$ . Using available data for CTD74 (Fig. 6.17), *Synechococcus* F:SS increased by a factor of  $\sim 10$  between the top and bottom of the SML. In the case of picoeukaryotes, cell numbers were also higher at the DCM than the SML. Although the picoeukaryotes group does not distinguish between species, these data imply that chl-a:C varies with depth and potentially within species as in the case of *Synechococcus* and *Prochlorococcus*. However, in the case of *Prochlorococcus* this may also reflect transition from high-light to low-light adapted ecotypes (Moore et al. 1998). For *Synechococcus* and *Prochlorococcus* Figure 6.17 indicates that the depth of maximum cell density was shallower than that of F:SS.

The ratio of chl-a:POC also increased by a factor of 3 between the SML and the DCM (not shown). The magnitude of the difference in the indicators of chl-a:C (i.e. F:SS and chl-

a:POC) between the SML and DCM would closely balance the 4.5 – fold decrease in  $E_{k_{478}}$ , suggesting that cellular pigment synthesis was related to photoacclimation (Geider 1987).

Since the absorption cross section of PSII ( $\sigma_{PSII}$ ) varied with phytoplankton pigment and taxonomic composition, rather than with optical depth, the apparent photoadaptation inferred from chromatic adaptation did not act to always increase  $\sigma_{PSII}$  at the DCM. In contrast,  $E_{k_{478}}$  was always reduced at the DCM. Given the lack of consistent increase in  $\sigma_{PSII}$  at the DCM it is unlikely that the mechanism of photoacclimation was by altering the ‘size’ of PSII antennae. Further, the reduction in electron transfer rates *could* result from the increase in numbers of PSII reaction centres with depth. It is suggested that reaction centre numbers are subsequently increased by a proportion necessary to achieve  $E_k$ , given the phytoplankton taxonomy (and subsequently  $\sigma_{PSII}$ ).

The mechanisms of photoacclimation are discussed in Chapter 7, along with further discussion on the variability in coupling between the FRRF and  $^{14}\text{C}$ -derived parameters.

#### 6.4 Chl-a and Primary Productivity through the Water Column

This section first quantifies the distribution of chl-a through the water column in the main hydrographic regimes visited along the transect. The daily primary production (PP) through the water column is then illustrated for available locations (as estimated following methods outlined in Chapter 2). The water column is divided into two layers, the SML and DCML. The abbreviation DCML refers to the Deep Chlorophyll Maximum Layer defined as the region in the water column where chl-a is increased (relative to SML concentrations) in association with the deep chlorophyll maximum. The main factors controlling primary production in the SML and within the DCML are explored, and the contribution of primary production within the DCML to total water-column (WC) production at each location along the transect is illustrated.

Estimates of daily PP for a range of hypothetical light conditions were not obtained due to differences in the potential range of ambient irradiance along the transect. No data regarding this variability was collected during the cruise, although such data could be found in incident irradiance records from satellite remote sensing or optical models and used in future analysis.

##### 6.4.1 Chl-a Distribution

The SML and DCML thickness and the integrated-chl-a for representative CTD casts for the main hydrographic regimes visited during the cruise are shown in Table 6.1.

Table 6.1. Layer-integrated chl-a concentration and DCML boundary depths at representative stations for each of the hydrographic regimes visited. Integrated chl-a concentration is taken from calibrated CTD profiles. The percentage irradiance (i.e. the irradiance as % of that at the surface) at the peak of the DCM was calculated from the  $K_d(\lambda)$  vs. chl-a relationships as described in Chapter 2. DCML boundary depths were defined by the chl-a profile as described in the text. Note that the northern hemisphere was sampled during autumn and the southern hemisphere was sampled during local spring. Region definitions ‘North’ and ‘South’ refer to the northern and southern high latitudes, with ‘South’ located between the southern gyre and the SSTC.

		SML Integrated Chl-a (mg m <sup>-2</sup> )	DCM Integrated Chl-a (mg m <sup>-2</sup> )	Top of DCM (m)	Base of DCM (m)	DCM Thickness (m)	DCM Peak Depth (m)	Max chl-a (mg m <sup>-3</sup> )	Percentage Irradiance at the DCM (% surface irradiance)
<b>North</b>	CTD12	3.3	15.4	42	129	87	75	0.42	1.20
<b>N.Gyre</b>	CTD21	1.4	9.4	53	195	142	115	0.22	2.49
<b>nr. UW</b>	CTD27	2.2	14.2	37	100	63	50	0.41	8.71
<b>EQ</b>	CTD58	2.4	13.1	48	140	92	75	0.45	3.49
<b>S.Gyre</b>	CTD82	5.2	8.8	139	220	81	180	0.17	0.36
<b>South</b>	CTD94	5.0	15.5	62	165	103	100	0.20	0.47

The DCML was deepest and broadest within the oligotrophic gyres, but integrated chl-a in the DCML was low (< 10 mg m<sup>-2</sup>). The DCML was deepest in the southern gyre, and integrated chl-a within the SML was higher in the southern gyre than in other regimes (5.2 mg m<sup>-2</sup>). This is in contrast to the northern gyre, where the DCML was shallower than in the southern gyre and integrated chl-a in the SML was low (< 2 mg m<sup>-2</sup>). The DCML was narrower and integrated chl-a within the DCML was lower (8.8 mg m<sup>-2</sup>) in the southern gyre compared to in the northern gyre (9.4 mg m<sup>-2</sup>).

In the high latitude regions, the DCML depth shoaled but the percentage irradiance at the DCM (i.e. the % of irradiance just below the surface) remained relatively low (< 1.2 % surface irradiance) due to the chl-a present in the surface (> 3 mg m<sup>-2</sup>). However, integrated chl-a in the DCML was high (> 15 mg m<sup>-2</sup>).

In the upwelling regions of the equator and close to the NW African upwelling, the shoaling of the DCML also caused an increase in the percentage irradiance at the DCM (to > 3% surface irradiance). Despite the broad DCML at the equator compared to the narrow DCML close to the NW African upwelling, the integrated chl-a in the DCML towards the NW African

upwelling was greater than that at the equator. SML and DCML thickness and integrated chl-a were similar to those of the high latitude regions, although chl-a in the SML remained low ( $< 3 \text{ mg m}^{-2}$ ).

The integrated-chl-a within the productive region of the water column (WC), SML and DCML was not significantly correlated to the layer-thickness (not shown). For these analyses the ‘WC thickness’ represents the productive region of the water column, as defined by SML thickness + DCML thickness. A significant, inverse relationship was evident between integrated chl-a in the DCML and WC and the depth of the DCM peak (Fig. 6.18A and C), which reflects the reduced chl-a in the oligotrophic regions (with deep DCM), compared to the increased chl-a in the mesotrophic and upwelling regions associated (with shallower DCM).

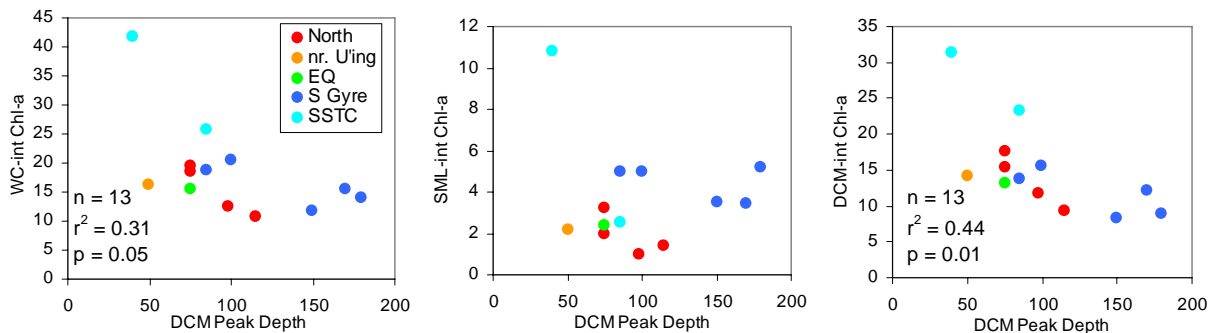


Figure 6.18. Layer-integrated chl-a ( $\text{mg m}^{-2}$ ) through the ‘productive’ water column (WC), surface (SML) and deep chlorophyll maximum (DCML) layers against the depth of the DCM peak (m). WC-integrated chl-a was obtained from the sum of chl-a in the SML and DCML. DCML boundaries were defined from the chl-a profile as described in the text. Statistics are shown where the relationship was significant and are the result of model II regression. Colours represent stations in the hydrographic regimes including the northern high latitudes and northern gyre (North), close to the NW African upwelling (nr. U’ing), equatorial (EQ), southern gyre (S.Gyre) and south subtropical convergence (SSTC).

#### 6.4.2 *In situ* Primary Production

Profiles of daily primary production (PP) as estimated for the incident irradiance recorded on the day of sampling are shown in Figure 6.19. The nitrate concentrations are also included where available.

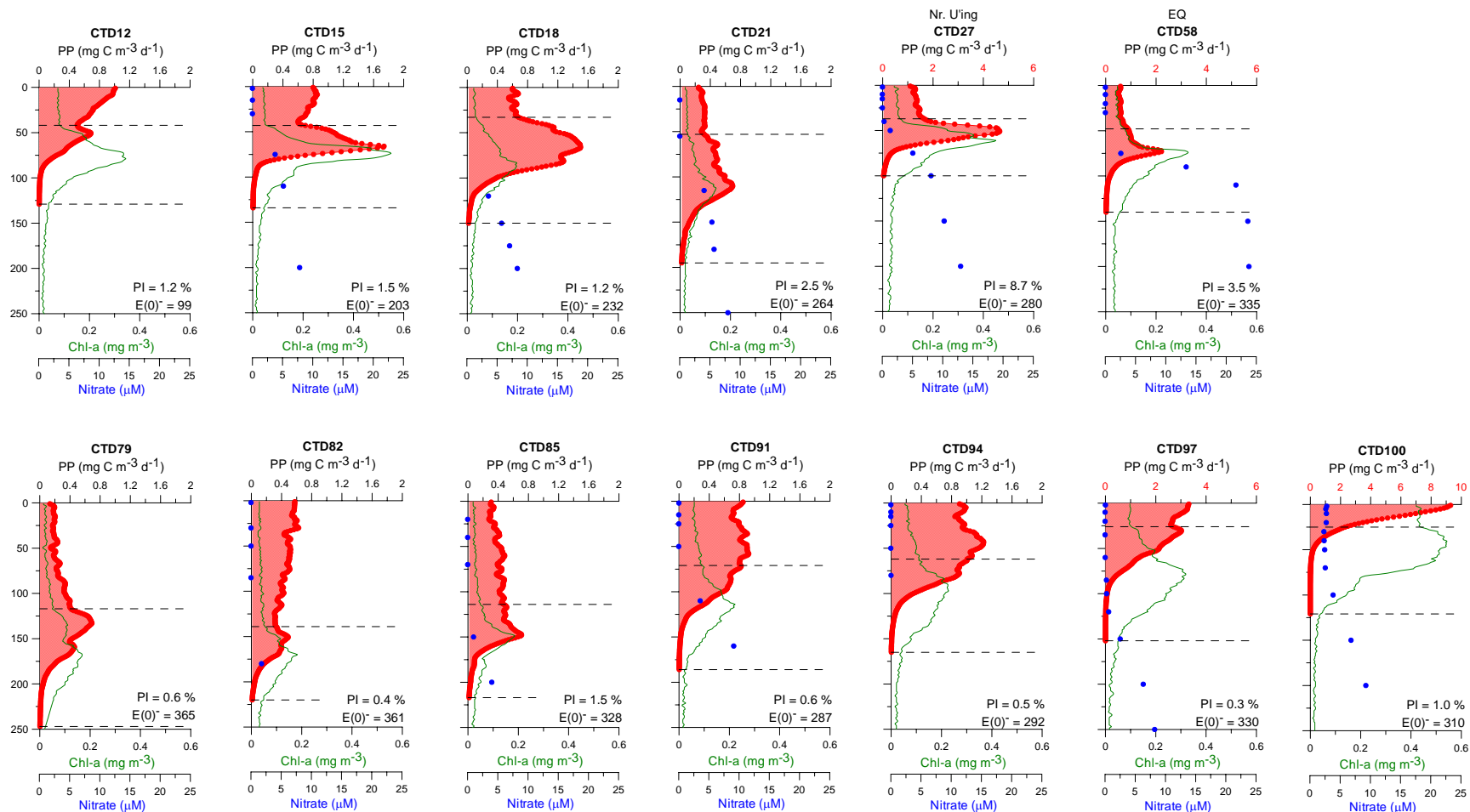


Figure 6.19. Profiles of chl-a (green line) and daily Primary Production (PP) (red line) through the water column at all available stations. Primary production was estimated following methods described in Chapter 2. For each location the chl-a profile is shown for the cast corresponding to sample collection, with the chl-a profile assumed constant throughout the day. At each location PP was estimated for the incident irradiance recorded on the day of sampling. Nitrate sample values are provided where available. Dotted lines indicate the location of the top and bottom of the DCML boundaries as defined by the chl-a gradient, as described in the text. Additional information for each profile includes the percent irradiance at the peak of the DCM (PI, the irradiance as % of that at the surface) and the mean irradiance just below the surface (E(0)<sup>-</sup>) (averaged over 24 hours) recorded for the day of sampling (μE m<sup>-2</sup> s<sup>-1</sup>).

Overall magnitudes of estimated daily PP were somewhat lower (sometimes by ~50%) than literature values based on Simulated-In-Situ experiments (SIS) (e.g. Maranon and Holligan 1999, Maranon et al. 2000, Poulton et al. 2006a, Perez et al. 2006) and were also lower than SIS experiments carried out alongside PP estimates in these data (see Chapter 2). The most likely cause of this discrepancy is diel variability in phytoplankton physiology that is not captured in the PP estimates from P vs. E curves. Behrenfeld et al. (1998) observed diel periodicity in phytoplankton physiology that caused  $P_m^*$  to increase by between 1.4 – 3 times the dawn value in the surface as well as at the DCM at two locations in the tropical south Pacific (the range was between locations). Diel variability of such magnitude could account for the underestimation of PP when assuming a constant value of  $P_m^*$  collected at dawn. No data were available to correct for this problem in these data. For the purposes of this study, diel variability was ignored and emphasis is placed on the relative variability in PP across the transect, rather than the absolute magnitudes. The considerations surrounding this assumption and implications for the observed trends are further discussed in Chapter 7.

In general, the magnitude of PP through the water column was lowest in the oligotrophic gyre regions and increased towards the high latitudes and the equatorial regions. The integrated PP within the SML ( $P_{SURF}$ ), DCML ( $P_{DCML}$ ) and WC ( $P_{WC}$ ) is shown in Table 6.2.

Table 6.2. Estimated daily Primary Production (PP) integrated through the SML ( $P_{SURF}$ ), deep chlorophyll maximum layer ( $P_{DCML}$ ) and water column ( $P_{WC}$ ) for pre-dawn casts.  $P_{WC}$  was estimated from  $P_{SURF} + P_{DCML}$ . Daily PP was estimated following methods in Chapter 2. DCML boundaries were defined from the chl-a gradient as described in the text. Region definitions ‘North’ and ‘South’ refer to the northern and southern high latitudes, with ‘South’ located between the southern gyre and the SSTC.

		$P_{WC}$ (mg C m <sup>-2</sup> d <sup>-1</sup> )	$P_{SURF}$ (mg C m <sup>-2</sup> d <sup>-1</sup> )	$P_{DCML}$ (mg C m <sup>-2</sup> d <sup>-1</sup> )
<b>North</b>	CTD12	50.2	31.7	18.5
<b>N.Gyre</b>	CTD21	61.4	15.9	45.5
<b>nr. UW</b>	CTD27	152.0	48.8	103.2
<b>EQ</b>	CTD58	82.7	28.4	54.3
<b>S.Gyre</b>	CTD82	81.1	63.6	17.4
<b>South</b>	CTD94	95.8	63.2	32.6

In both the north and south high latitude regions the DCM was not a primary production maximum, with maximal PP occurring at the surface. This was particularly evident in the SSTC (e.g. CTD100) where PP was close to zero at the DCM peak. In the northern subtropical region (CTD15 and CTD18) PP at the peak of the DCM was 2-fold greater than at the surface, and nitrate concentration at the DCM peak was  $3.8 \mu\text{M}$  (CTD15).  $P_{\text{WC}}$  was lowest in the northern high latitudes, likely due to the relatively shallow WC thickness compared to the southern high latitudes where  $P_{\text{WC}}$  was high (CTD94).

$P_{\text{WC}}$  was low in both oligotrophic gyre regions. In both gyres the change in phytoplankton physiology between the SML and DCML led to PP remaining relatively constant throughout the entire euphotic zone. In the southern gyre the nitracline was gradual and nitrate at the peak of the DCM was  $1.8 \mu\text{M}$  (CTD82), compared to  $4.0 \mu\text{M}$  in the northern gyre (CTD21).  $P_{\text{DCML}}$  in the northern gyre was  $\sim 2$  times greater than that in the southern gyre, whilst  $P_{\text{SURF}}$  was greater in the southern gyre.

At the edge of the NW African upwelling region and the equator the shoaling of the DCM was associated with PP at the peak of the DCM that was  $\sim 4$  times greater than at the surface. Nitrate at the DCM peak was  $1.3 \mu\text{M}$  and  $2.6 \mu\text{M}$  at the NW African and equatorial upwelling respectively. Despite the increased nitrate at the DCM at the equator,  $P_{\text{DCML}}$  was  $\sim 2$  times greater close to the NW African upwelling than at the equator. Both the increase in nitrate availability and the increased percentage irradiance at the DCM are likely causes of increased PP at the DCM in these regions.

In contrast to the NW African and equatorial upwelling regions, the gradual shoaling of the DCM towards the edges of the gyre regions (shown here particularly for CTD91 - CTD97) was not associated with an increase in the percentage irradiance at the DCM, due to the associated increase in chl-a in the SML. It is suggested that increased nitrate concentration and steeper nitrate gradient (observed in Figure 6.19) contribute to the higher PP at the DCM at the edges of the gyres.

In all profiles the effect of increased light attenuation within the DCML is clearly evident as the primary production maximum is located on the upslope of the DCM (Fig. 6.19). Variability in ambient irradiance would affect the distribution of PP through the water column, particularly in the DCML where phytoplankton were light limited and therefore sensitive to ambient irradiance (Fig. 6.16). However, through much of the transect (including northern and southern oligotrophic gyre regions) ambient irradiance may not be expected to change considerably from one day to the next. Greater variability may be expected in equatorial and coastal upwelling regions and the higher latitudes particularly during autumn.

### 6.4.3 Controls on Primary Production

$P_{\text{SURF}}$ ,  $P_{\text{DCML}}$ ,  $P_{\text{WC}}$  were not significantly correlated to incident irradiance at the time of sampling (not shown). The ambient irradiance was therefore not a significant cause of variability in estimated PP along the transect compared to other factors, although the effect of the full potential range in ambient irradiance was not investigated.

In general, the variance in  $P_{\text{SURF}}$  and  $P_{\text{DCM}}$  were not significantly correlated to individual hydrographic variables measured during the cruise. However, some trends were observable in the data and are shown in Figure 6.20.

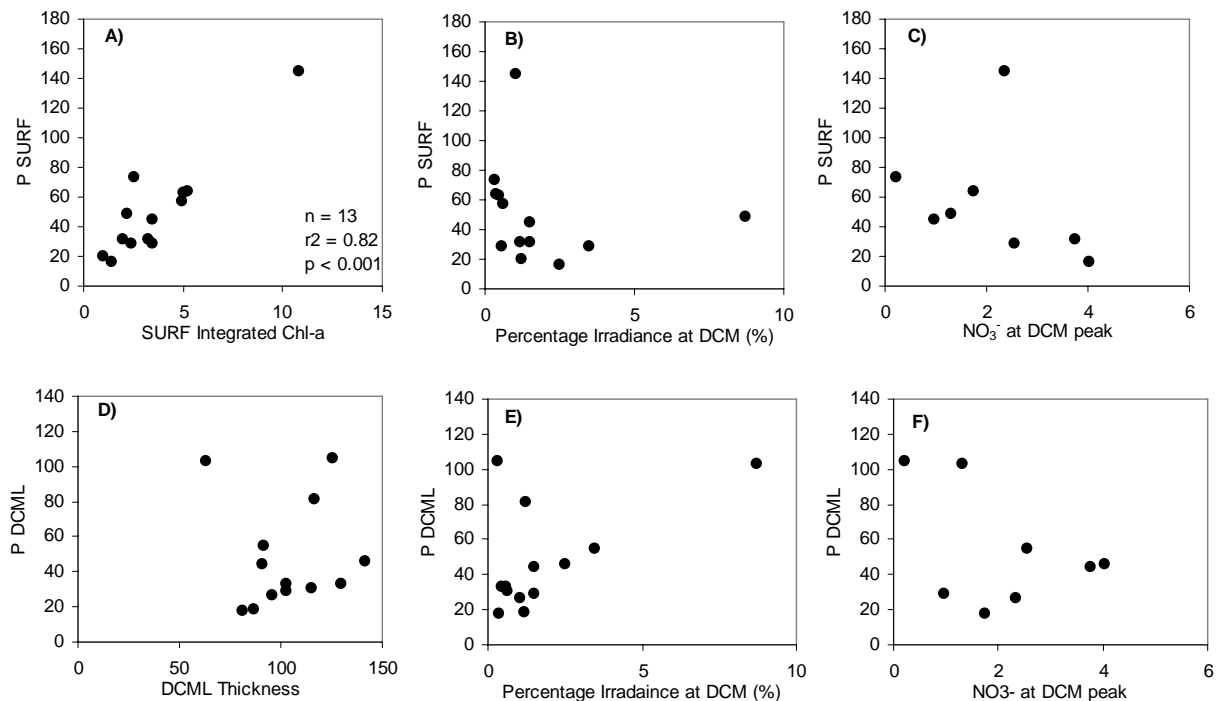


Figure 6.20. Relationships between integrated primary production in the SML ( $P_{\text{SURF}}$ ) ( $\text{mg C m}^{-2} \text{ d}^{-1}$ ) (A,B,C) and in the DCML (D,E,F) and selected environmental variables. A)  $P_{\text{SURF}}$  against integrated chl-a in the SML ( $\text{mg m}^{-2}$ ), B)  $P_{\text{SURF}}$  against the percentage irradiance at the DCM (% of irradiance just below the surface), C)  $P_{\text{SURF}}$  against nitrate concentration at the DCM ( $\mu\text{M}$ ), D)  $P_{\text{DCML}}$  against the thickness of the DCML (m), E)  $P_{\text{DCML}}$  against the percentage irradiance at the DCM peak, F)  $P_{\text{DCML}}$  against nitrate concentration at the DCM ( $\mu\text{M}$ ). Integrated primary production was estimated following methods in Chapter 2. Statistics shown are the results of model II regression where significant to the 95% confidence level. DCML boundaries were defined from the chl-a gradient as described in the text.

82 % of the variability in  $P_{\text{SURF}}$  was explained by the integrated chl-a in the SML (Fig. 6.20A), but the integrated chl-a in the SML was not determined by SML depth (e.g. Fig. 6.18).  $P_{\text{SURF}}$  was inversely correlated to the nitrate concentration at the DCM, likely because nitrate tended to be high at the DCM in the northern hemisphere where the percentage irradiance at the DCM was also high, and integrated chl-a in the SML and  $P_{\text{SURF}}$  was relatively low. At one location in the SSTC (CTD100),  $P_{\text{SURF}}$  and SML-integrated chl-a were exceptionally high ( $P_{\text{SURF}} > 140 \text{ mg C m}^{-2} \text{ d}^{-1}$ ) considering the relatively low nitrate concentration and low percentage irradiance at the DCM. However, nitrate concentration was  $> 2 \text{ } \mu\text{M}$  at the surface at this site, likely fuelling the high PP in the surface. The influence of integrated chl-a in the SML (and therefore  $P_{\text{SURF}}$ ) on the percentage irradiance at the DCM is observed in Figure 6.20B; decreased light availability at the DCM occurred where surface chl-a (and therefore  $P_{\text{SURF}}$ ) was high.

In contrast to  $P_{\text{SURF}}$ ,  $P_{\text{DCML}}$  was not correlated to integrated chl-a in the DCML, but instead was correlated to the thickness of the DCML (Fig. 6.20D).  $P_{\text{DCML}}$  was also correlated to the percentage irradiance at the DCM (Fig. 6.20E). It follows that the combination of the percentage irradiance of the DCM and the DCML thickness explained much of the variability in  $P_{\text{DCML}}$ . Figure 6.20F indicates that nitrate concentration at the peak of the DCM could be an important factor influencing  $P_{\text{DCML}}$ , although the relationship is weak. This would contrast with the findings of Poulton et al. (2006a) who observed that nitrate concentrations exceeded the requirement for carbon fixation at the DCM such that production at the DCM is likely to be light, rather than nutrient limited.

37% of the variability in  $P_{\text{WC}}$  could be explained by  $P_{\text{DCML}}$  ( $n = 13$ ,  $r^2 = 0.371$ ,  $p = 0.027$ ) and 45% by  $P^*_m$  in the SML ( $n = 13$ ,  $r^2 = 0.457$ ,  $p = 0.011$ ), in agreement with Maranon and Holligan (1999), thus indicating the importance of the physiological parameters and primary production in the DCML to overall  $P_{\text{WC}}$ . In order to investigate the combined factors in controlling PP through the water column, more detailed multiple component analysis could be carried out.

#### 6.4.4 The Significance of Primary Production in the DCML

The contribution of primary production in the DCML and SML to total water column production along the transect is shown in Figure 6.21. The relative contributions of  $P_{\text{SURF}}$  and  $P_{\text{DCML}}$  to  $P_{\text{WC}}$  are sensitive to the definition of the layer-boundaries (is apparent in Figure 6.19).

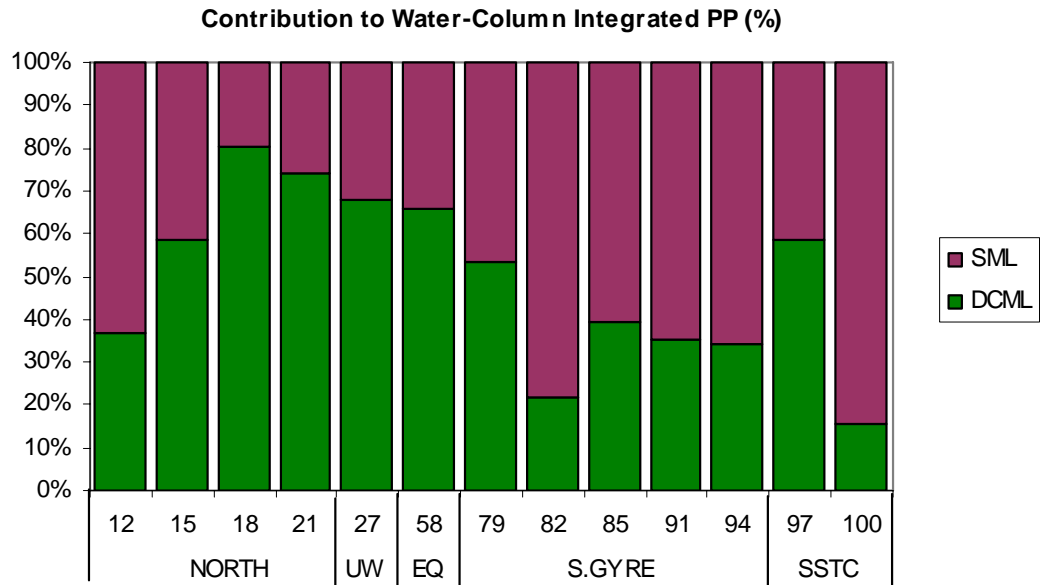


Figure 6.21. The percentage contribution of daily primary production (PP) in the deep chlorophyll maximum layer ( $P_{DCML}$ ) and surface ( $P_{SURF}$ ) for available locations. PP was estimated for the irradiance recorded during the day of sampling, following methods in Chapter 2. Locations are grouped into hydrographic regimes including the northern high latitude and northern gyre (North), close to the NW African upwelling (UW), equatorial (EQ), southern gyre (S.Gyre) and south subtropical convergence (SSTC). DCML boundaries were defined from the chl-a gradient as described in the text.

The DCML contributed 37 – 80 % to water-column production in the northern region (CTD12-CTD21), the highest contribution occurring in the northern oligotrophic gyre. The percentage irradiance at the DCM and the nitrate concentration at the DCM were both relatively high in this region, where the DCM was shallow and chl-a concentration in the SML was low. In contrast, the DCML accounted for only 22 – 54 % of water-column production in the southern gyre. Despite the shoaling of the DCML at the southern edge of the southern gyre (CTD91 and CTD94), the DCM remained optically deep such that PP remained low compared to at the SML.

The DCML contributed 66 % and 68 % to water column production in the at the edge of the NW African upwelling region and at the equator respectively, as the percentage irradiance and nitrate concentration at the peak of the DCM were elevated in these regions.

$P_{DCML}$  was least significant compared to  $P_{SURF}$  in the SSTC (CTD100) where the DCML only accounted for 15% of water column-integrated production. The water column at this location was weakly stratified (a temperature difference of only 0.3°C at a shallow thermocline

associated with the shallow DCM) and the nitrate concentration at the surface was  $> 2 \mu\text{M}$ . Thus the high surface nitrate concentration (in excess of  $8 \text{ mg C m}^{-3} \text{ d}^{-1}$ ) probably fuelled the PP at the surface and led to high light attenuation and low PP at the DCML. This was in contrast to CTD97 where the water column was stratified, nitrate at the surface was  $< 0.001 \mu\text{M}$  and  $P_{\text{DCML}}$  contributed 59 % to water column-integrated production.

## 6.5 Summary of Main Points

The major observations within this chapter were:

- The DCM did not necessarily follow the density gradient, but was associated with the 1% surface irradiance isolume and, normally, the nitracline.
- Distinct taxonomic differences (from HPLC and AFC data) were observed between the SML and DCM for most of the transect.
- Evidence of chromatic adaptation was identified by the co-variability of phytoplankton absorption and *in situ* irradiance spectra with depth. The effect of pigment packaging appeared to be minor.
- Relationships between  $\sigma_{\text{PSII}}$ ,  $F_v/F_m$  and pigment ratios indicated that these parameters varied with phytoplankton taxonomy.
- The parameters  $\alpha^*_{478}$  and  $\Phi_m$  generally increased at the DCM but the cause of the variability in these parameters could not be assigned to one particular environmental variable.
- $E_{\text{insitu}}$  and  $E_{k_{\text{insitu}}}$  were correlated and phytoplankton in the SML were likely to be light saturated but those at the DCM were not.
- Vertical gradients in  $P^*_m$  and electron transfer rates suggested that the same processes were limiting electron transfer as carbon fixation, and that the mechanism for photoacclimation could be by synthesis of PSII reaction centres, but significant vertical gradients in taxonomy (and hence  $\sigma_{\text{PSII}}$ ) made this difficult to establish.
- Horizontal gradients in the degree of coupling between P vs. E and FRRF parameters were difficult to determine but appeared to be associated with the proportion of cyanobacteria compared to picoeukaryotes.

- Primary production within the DCML accounted for 20-80% of the water-column primary production along the transect. Lower contributions were seen in the southern gyre compared to the northern gyre.
- The DCM was a primary production maximum in the northern high latitudes, equator and close to the NW African upwelling, but not in the central oligotrophic gyres.
- Primary production in the SML was determined largely by integrated chl-a while within the DCML, the percentage irradiance at the DCM and / or the thickness of the DCML peak were important.

## CHAPTER 7: SYNTHESIS AND DISCUSSION

This chapter provides a synthesis and discussion of results describing the key principles responsible for the primary production of phytoplankton within the deep chlorophyll maximum (DCM). The chapter and is divided into five sections. The first section deals with the phytoplankton taxonomic and physiological characteristics that determine phytoplankton growth in the DCM. The second section concentrates on the Celtic Sea shelf DCM, as the main focus of this thesis. The physical controls on primary productivity in the shelf sea DCM are summarised and the biological-physical interactions are discussed in detail. The third section briefly summarises the characteristics of the DCM observed in other hydrographic regimes visited in the Atlantic Ocean, drawing attention to the similarities and differences with the shelf sea system. The regional and global significance of primary production of the DCM is quantified in section four. Finally, consideration is given to the methods used and the chapter concludes with a reflection on the achievements of the thesis. Suggestions for further work are provided in the relevant sections.

### 7.1 Phytoplankton Physiology in the DCM

As described in Chapter 1, a DCM is a general characteristic of stratified systems. The form of the DCM depends largely on the physical environment and the relative balance of biological and physical (including chemical) processes. A range of hydrographic regimes were investigated during this study. The physical structure of the water column, including the presence, magnitude and location of the DCM were largely consistent with expectations (described in Chapter 1).

The tidally active, temperate Celtic Sea shelf in summer represents an extreme case where physical processes dominate the water column structure and hence largely dictate the environment for phytoplankton growth. The low chl-a concentration in the SML, with phytoplankton apparently limited by lack of nutrient inputs, coupled with the physical mixing processes, caused the thermocline to be above the critical depth for phytoplankton growth (~1% – 16% of surface irradiance) (Sverdrup 1953). *In situ* irradiance within the thermocline often decreased as much between the top and bottom of the thermocline as from the top and bottom of the SML, with the nutrients ranging from virtually zero to BML concentrations. The stripping of chl-a from the base of the thermocline means that physical mixing processes provide the lower-limit on the depth of phytoplankton growth, whilst these mixing processes also provide a source of nitrate to the thermocline (Sharples et al. 2001b).

In contrast to the Celtic Sea shelf, the oceanic gyres represent an environment where physical mixing processes are relatively weak. The DCM was often decoupled from the thermocline at irradiance often < 1% surface irradiance. This section summarises the similarities and differences in physiological characteristics of phytoplankton in the DCM in the two environments. The relative contributions of taxonomic variability (i.e. adaptation) and phenotypic response (acclimation) to the overall physiological function of the phytoplankton are discussed. The combination of simultaneous FRRF and  $^{14}\text{C}$  P vs. E measurements provided important insights into the mechanisms of photoacclimation and highlighted areas in which to focus future investigation.

### 7.1.1 Adaptation

Phytoplankton community composition varied both horizontally and vertically. Small cells and cyanobacteria dominated low nutrient environments and larger cells occurred in regions richer in nutrients and regions of pulsed nutrient supply (Chisholm 1992). In both the Celtic Sea and Atlantic Ocean, taxonomic differences were observed between SML and DCM (Holligan et al. 1984c, Maranon et al. 2000, Perez et al. 2006) although less vertical variability was observed during CS03 (Moore et al. 2006), perhaps due to poorer sampling resolution during this cruise.

The evidence for chromatic adaptation in both the Celtic Sea (Fig. 3.7) and Atlantic Ocean (Fig. 6.7) community structure provided evidence for *photoadaptation* to the light environment. Similarities between phytoplankton absorption and *in situ* light spectra through the water column have been recorded previously either by using measurements of particulate absorption (Takahashi et al. 1989, Markager and Vincent 2001, Sosik et al. 2001) or by construction of absorption spectra from chromatographically-derived pigment concentrations (Bidigare et al. 1990a, Majchrowski and Ostrowska 2000, Barlow et al. 2002). Only on one occasion have absorption by both methods been compared simultaneously (Lutz et al. 2003) and in that study no data were provided for the *in situ* light environment. Data from the Celtic Sea and AMT15 were in support of Lutz et al. (2003) who illustrated that cyanobacteria (absorbing a broad spectral range) were observed in the clear water environments such as oligotrophic gyres whilst eukaryotes occurred in the greener waters off NW Africa, in the open ocean DCM, and in the surface of the (relatively turbid) shelf and shelf edge (Lutz et al. 2001, 2003). Culture experiments also showed the potential for manipulation of pigment composition as a phenotypic response to changing spectral light quality within phytoplankton taxa (e.g. Mouget et al. 2004, Johnsen et al. 1997).

The comparison of absorption by HPLC-reconstruction and by the filter technique gave insight into the effects of pigment packaging (Berner et al. 1989). Pigment packaging appeared to dominate the vertical gradients in the amount of light absorbed by phytoplankton ( $a^*_{\text{meas}}$ ) in the Celtic Sea but it was difficult to quantify (Bricaud et al. 2004). In contrast, in the open ocean setting where small phytoplankton dominated the community, less vertical change in  $a^*_{\text{meas}}$  presumably reflected the reduced susceptibility of small cells to the package effect (Ciotti et al. 2002). In the Celtic Sea the package effect also appeared to reduce the similarities between the wavelength composition of *in situ* irradiance and the absorption by intact cells (given by  $a^*(\lambda)_{\text{ps}}$ ) even though the changes in wavelength composition of irradiance and the absorption inferred from the pigment complement ( $a^*(\lambda)_{\text{pspig}}$ ) were similar (Fig. 3.7 and 3.8). The effect of pigment packaging in this regard was also less pronounced in the open Atlantic Ocean than the Celtic Sea (Fig. 6.7).

The vertical gradients in pigment composition, absorption and taxonomy did not necessarily result in an increase in the photochemical efficiency of PSII (given by  $\sigma_{\text{PSII}}$ ) with depth. This was again particularly notable in the Celtic Sea rather than the Atlantic open ocean, potentially reflecting the relative importance of pigment packaging on reducing  $\sigma_{\text{PSII}}$  (Suggett et al. 2004, Moore et al. 2005). However an increase in the quantum yield for carbon fixation ( $\Phi_m$ ) was often observed in both the shelf and open ocean settings.

### $\sigma_{\text{PSII}}$

Interspecific variability in the effective absorption cross section,  $\sigma_{\text{PSII}}$ , has been previously reported in laboratory cultures (see Suggett, 2004 and references therein) as well as suggested in field data (Moore et al. 2005, Suggett et al. 2006). However, this is one of the first assessments to have been made over a large taxonomic range (Fig. 6.9, also Suggett et al. 2004). Possible intraspecific changes in  $\sigma_{\text{PSII}}$  (or Fv/Fm) due to, for example, photoacclimation (Babin et al. 1996), state transitions (Falkowski and Raven 1997) or loss of PSII function due to nutrient stress (e.g. Greene et al. 1992, Berges et al. 1996) were not observable over the large-scale co-variability in  $\sigma_{\text{PSII}}$  (and Fv/Fm) with the marker pigment ratios in either the Celtic Sea or Atlantic Ocean. To detect such intraspecific variability in field data enough measurements would have to be made within taxonomic regimes and data analysis must first rule out taxonomic variability in the first instance.

The data presented indicated that  $\sigma_{\text{PSII}}$  does not vary *in response* to the light gradient as  $\sigma_{\text{PSII}}$  did not *always* increase with depth. Rather, the effective absorption cross section ( $\sigma_{\text{PSII}}$ ) appears to be a taxonomic trait and is therefore one of the many factors governing the success of

a particular species in any given environment. The inverse relationship between  $\sigma_{\text{PSII}}$  and Fv/Fm (Fig. 3.15 and 6.10) suggests that the variable fluorescence yield (Fv/Fm) is also a predominantly taxonomic trait of phytoplankton species. The fact that  $\sigma_{\text{PSII}}$  did not always increase with depth may either represent the relative importance of the PSI cross section or the significance of other environmental factors and ecological traits in determining the dominant phytoplankton groups.

Great care must be taken in interpreting field measurements of  $\sigma_{\text{PSII}}$  and Fv/Fm with reference to, for example, nutrient stress. Investigations using  $\sigma_{\text{PSII}}$  or Fv/Fm to identify nutrient limitation (for example) must first acknowledge and identify taxonomic gradients (either spatial or temporal) that may contribute to the variability in these parameters. This is particularly important in studies spanning a wide range of hydrographic regimes although the effects of taxonomy on these parameters has also been shown to be important within bottle incubations (Moore et al. *Submitted*).

Following the discussions above, the layering of phytoplankton taxonomy in the thermocline of the Celtic Sea (Fig. 3.22 and 4.10) could be explained as the result of adaptation to different environmental conditions. Specifically, *Synechococcus* cell numbers were maximal in the upper thermocline where nitrate availability was low and light levels were relatively high, thus suiting an ability to survive in low nutrient conditions (Chisholm 1992). In addition, the associated NPC content and low PSII cross sections of this species may contribute to their preference for high-light environments. In contrast, picoeukaryote cell numbers were maximal below that of *Synechococcus* and lower on the nitracline, possibly out-competing the cyanobacteria in this dimly lit region due to their PSC content and ‘larger’ PSII cross sections. A similar pattern was seen in the Atlantic Ocean gyres where cyanobacteria dominated in the SML and picoeukaryotes occurred in the DCM. The signature of the vertical gradients in  $\sigma_{\text{PSII}}$  through the thermocline in the Celtic Sea were likely not observed in these data due to the sampling resolution of FRRF compared to AFC measurements and the mixed nature of the total phytoplankton assemblage.

It appears that shifts in the taxonomic composition of the phytoplankton community to the environmental conditions, including light and nutrient availability, sets the framework for further acclimation given the light harvesting credentials of the dominant phytoplankton. Susceptibility to the package effect and photoinhibition are also species specific traits that influence the competitive advantages of a particular phytoplankton.

$\Phi_m$ 

It proved difficult to explain the variability in  $\alpha^*$  and  $\Phi_m$  in both the Celtic Sea and Atlantic Ocean. The environmental factors determining variability in the quantum yield remain poorly understood, with nutrient availability (Vaillancourt et al. 2003), pigment composition (Babin et al. 1996, Sorensen and Siegel 2001) and light (Marra et al. 2000) all suggested as the dominant factor, while other studies have failed to relate variability in  $\Phi_m$  to any measured environmental variable (Schofield et al. 1993). Culture experiments have shown that variability in  $\Phi_m$  and  $\alpha^*$  due to acclimation to low light is not significant (Geider et al. 1985) and that variability in  $\Phi_m$  due to nutrient limitation is only seen under extreme starvation (MacIntyre et al. 2002), although though some variability is observed between species (Langdon 1988). The correlation between  $\Phi_m$  and NPS:PSC during CS05 and AMT15 (Fig. 3.16, Section 6.3.3) and between  $\alpha^*$  and POC:PON during CS05 (Fig. 3.16) therefore support the conclusions of Babin et al. (1996) who showed that that NPC:PSC may contribute to the variability in  $\Phi_m$  (also MacIntyre et al. 2002), and (in the Celtic Sea) support Cleveland and Perry (1987) and Marra et al. (2000) who showed that nutrient availability was important. The vertical trends in  $\Phi_m$  were similar when this parameter was estimated from the absorption spectra for photosynthetic carotenoids only, which would indicate that the presence of NPC were not the only factor causing variability in  $\Phi_m$ .

The lack of correspondence between  $\sigma_{\text{PSII}}$  and  $\alpha^*$  indicates a de-coupling between the factors driving variability in the light limited photosynthetic efficiency of PSII compared to carbon fixation (Kolber et al. 1988).

### 7.1.2 Photoacclimation

The covariance of the electron transfer rates and  $^{14}\text{C}$ -derived maximal rates of carbon fixation ( $P^*_m$ ) suggested that the same processes were limiting electron transfer as carbon fixation, likely the rate of the dark reactions (Sukenic et al. 1987, Kolber and Falkowski 1993, Cleland 1998, Kana et al. 2002) (Fig. 3.18 and 6.13). The ability of phytoplankton to acclimate to low light by synthesis of photosynthetic pigments leading to increases in chl-a:C is well established (Geider 1987, Falkowski and LaRoche 1991, Falkowski and Raven 1997). The lack of consistent vertical gradients in the effective absorption cross section  $\sigma_{\text{PSII}}$  in the Celtic Sea indicated that the mechanism of photoacclimation was not by increasing of the 'size' of the light harvesting antennae associated with each PSII (Moore et al. 2006). Co-variance of  $E_k$ , chl-a:C, electron transfer rates and  $P^*_m$  suggested that the response to low light was an increase in the number of PSII reaction centres (thereby increasing chl-a:C), with each reaction centre therefore sharing a

smaller proportion of the cellular capacity for carbon fixation (represented by  $P^C$ ) and subsequently reducing the rates of electron turnover through each PSII (Moore et al. 2006) (Fig. 3.18 and 3.23).

Other possible explanations for variability in electron transfer rates through PSII include variability in the inherent transfer rates downstream of Qa reoxidation (Cleland 1998), cyclic electron flow (Prasil et al. 1996) and variability in the channelling of electrons to different downstream metabolic pathways of reductant use (Behrenfeld et al. 2004). However, the balance of vertical changes in  $E_k$ ,  $P^*_m$  and electron transfer rates with those of chl-a:C suggests that other causes of variability in the rates of electron transport were not significant (Moore et al. 2006). In addition to the data presented in Moore et al. (2006) the vertical gradients of  $P^*_m$  and chl-a:C (using data from Celtic Sea 2005, Fig. 3.24) confirmed that the cellular capacity for carbon fixation rates ( $P^C_m$ ) were largely constant with depth, consistent with previous studies (Geider et al. 1998, MacIntyre et al. 2002).

In contrast to the Celtic Sea, in the Atlantic Ocean a greater vertical variability was observed in the parameters  $\Phi_m$  and  $\sigma_{PSII}$  which contributed to the variance in  $E_k$ . However, adjustment of the number of reaction centres remains a possible mechanism for ‘fine-tuning’ the light harvesting apparatus (Suggett et al. 2006). Given the potential variability in the form of the photochemical apparatus between taxonomic groups it is suggested that the number of reaction centres required to achieve  $E_k$  in a given light environment varies between species. This means that the regression between chl-a:C and  $E_k$  would vary depending on the dominant phytoplankton type in any given environment. For example, species with a low PSII cross section and high susceptibility to packaging (e.g. diatoms) may require synthesis of more PSII to achieve  $E_k$  than a species with high PSII cross section and low susceptibility to packaging (e.g. picoeukaryotes). This may be a reason for the relative difference in *Synechococcus*, *Prochlorococcus* and picoeukaryote chl-a:C (inferred from F:SS) between the SML and DCM observed in the southern gyre of the Atlantic Ocean (Fig. 6.17).

In many instances it was shown that the factors governing the variability in the  $^{14}C$ -derived parameters were not the same as those affecting those derived from FRRF. Most obvious was the taxonomic control on  $\sigma_{PSII}$  compared to  $\Phi_m$  but this was also evident in the  $E_k$ -independent variability in  $^{14}C$  but not FRRF parameters in the Celtic Sea during 2005 (Fig. 3.20), the change in coupling between  $P^*_m$  and  $1/\tau_{Qa}$  in the SML and DCM in the Celtic Sea (Fig. 3.21) and the change in coupling between  $P^*_m$  and  $1/\tau_{Qa}$  and between  $E_{k14C}$  and  $E_{kETR,478}$  with latitude along the AMT (Fig. 6.13 and 6.14).

Following Equations 1.11 and 1.12 the de-coupling of FRRF and  $^{14}\text{C}$  parameters may result from variance in the unresolved variables in these equations, including the ratio PSII:chl-a, the quantum efficiency of electron transport through PSII (typically assumed  $0.25 \text{ mol O}_2 (\text{mol photons})^{-1}$ ), the photosynthetic quotient and the fraction of functional reaction centres ( $f$ , normally assumed  $(F_v/F_m)/0.65$ ) (Kolber and Falkowski 1993, Falkowski and Raven 1997).

The fraction of functional PSII reaction centres ( $f$ ) is known to vary both between and within species (Kolber and Falkowski 1993, Behrenfeld et al. 1998). As pointed out by Babin et al. (1996), since all electrons involved in carbon fixation originated at the charge separation within PSII it may be expected that anything affecting changes in  $f$  (the quantum efficiency of PSII) must also influence  $\Phi_m$ . Variability in the photosynthetic quotient is known to exist across a wide range of environmental regimes (Laws 1991). Over basin-scales, or between SML and DCM populations, the photosynthetic quotient may vary and contribute to the decoupling of FRRF and  $^{14}\text{C}$  derived parameters (Laws 1991, Suggett et al. 2001).

The parameter PSII:chl-a represents the ratio of PSII per unit chl-a, in which chl-a is the *total* chl-a (i.e. the chl-a associated with both PSI and PSII). It does not represent the amount of chl-a associated with *each* PSII. The total chl-a can therefore be considered as the sum of  $(n_{\text{PSII}} \times \text{chl-a}_{\text{PSII}}) + (n_{\text{PSI}} \times \text{chl-a}_{\text{PSI}})$  where  $\text{chl-a}_{\text{PSII}}$  and  $\text{chl-a}_{\text{PSI}}$  are the amount of chl-a associated with PSII and PSI respectively, and  $n_{\text{PSII}}$  and  $n_{\text{PSI}}$  are the number of the reaction centres. It follows that any change in the numbers of PSI or PSII, in the amount of chl-a associated with each photosystem, or in the relative amounts of the two photosystem (i.e. PSII:PSI) can all potentially influence PSII:chl-a.

Direct measurement of PSII:chl-a, as well as the measurement of the numbers of reaction centres and their associated chl-a, is inherently difficult to achieve in the field (Falkowski et al. 1981, Falkowski and Kolber 1995, Suggett et al. 2004, Moore et al. 2006). Culture experiments indicate a variability in PSII:chl-a with growth irradiance (e.g. Dubinsky et al. 1986) and nitrate limitation (e.g. Berges et al. 1996). Variability in PSI:PSII with growth irradiance is also observed (Falkowski et al. 1981). However, PSII:chl-a is also seen to vary between phytoplankton taxa; values of chl-a:PSII (i.e.  $\text{mol chl-a} (\text{mol PSII})^{-1}$ ) ranging between 280 – 830 in eukaryotes (Dubinsky et al. 1986) compared to 133 – 384 in *Synechococcus* (Barlow and Alberte 1985).

In the Atlantic Ocean the coupling between FRRF and  $^{14}\text{C}$  measurements appeared to be correlated to the relative abundance of eukaryotes compared to *Prochlorococcus* and *Synechococcus* in the phytoplankton community (e.g. Fig. 6.13, 6.14 and 6.15). This could also be important in the observed Ek-independent variability in the Celtic Sea (Behrenfeld et al.

2004) (Fig. 3.20). Both *Prochlorococcus* and *Synechococcus* are observed to have a low chl-a:PSII (i.e. lower chl-a:PSII, as above) and high PSI:PSII compared to eukaryotes (Barlow and Alberte 1985, Kolber and Falkowski 1993, Bibby et al. 2003) although for *Prochlorococcus* the ratios are somewhat uncertain and likely differ between ecotypes (Moore et al. 1998, Bibby et al. 2003). Further, *Synechococcus*, in contrast to eukaryotes (accepting cryptophytes) contain phycobillins associated with PSII which give these species their characteristically broad spectral range of light absorption (e.g. Suggett et al. 2004). Overall, differences in the photochemical apparatus of prokaryotes compared to eukaryotes includes the fact that the former do not have chloroplasts, rather their light harvesting apparatus is arranged in the outer membrane (Falkowski and Raven 1997). One potential implication of this is less susceptibility to the package effect (Suggett et al. 2004). However, the fact that *Prochlorococcus* and *Synechococcus* have lower chl-a:PSII compared to eukaryotes would not explain the variation in coupling of  $P^*_m$  and  $1/\tau_{Qa}$  (Fig. 6.13), as the opposite relationship would be expected (refer to Eqn. 1.11).

Another possible source of offset in the  $^{14}\text{C}$  and FRRF measurement, relating to the relative abundance of eukaryotes and phycobillin-containing cyanobacteria (e.g. *Synechococcus*) is in the excitation spectrum of the FRRF compared to the P vs. E incubator. The FRRF excitation spectra is in a narrow band centred on 478 nm whilst the  $^{14}\text{C}$  incubator was fitted with a halogen bulb rich in light at high wavelengths (Fig. 2.6). Subsequently there is potential for PSI of phycobillin-containing cyanobacteria to become light saturated in the P vs. E incubator at irradiances that PSII remains sub-saturated. This could potentially lead to lower  $^{14}\text{C}$ -derived  $Ek_{478}$  compared to  $Ek_{\text{ETR},478}$  for cyanobacteria-dominated communities than for eukaryotes regardless of spectral correction (Fig. 6.14).

Overall, the precise reasons for the de-coupling of  $^{14}\text{C}$  and FRRF derived parameters remain unresolved, but may reflect variance of processes within PSII as well as those between PSII and carbon fixation. These problems are precisely those which currently limit the use of FRRF as an independent tool for measuring carbon fixation in the field (e.g. Suggett et al. 2004). Further work to investigate the coupling between carbon fixation and PSII photochemistry is clearly desirable, as are advances in the understanding of the function of PSI. The fact that these data suggest a significant difference between the photochemical processes of prokaryotic and eukaryotic phytoplankton mean that further investigation is critical if the photochemical processes of field populations are to be fully understood.

It follows from the above discussions that the mechanisms available and efficiency with which cells can adjust their photochemical apparatus are additional species specific-traits that

contribute to the adaptive response determining the dominant phytoplankton groups in any given hydrographic environment.

The combined effect of adaptation and photoacclimation led to photophysiology of the phytoplankton community in which the irradiance at which phytoplankton became light saturated ( $E_{k_{in situ}}$ ) was roughly equal to the mean *in situ* irradiance to which they are exposed over a 24 hour period (Fig. 3.19 and 6.16) (Geider et al. 1998, Moore et al. 2006). The fact that in both the stratified Celtic Sea and Atlantic Ocean phytoplankton in the surface were, on average, light saturated over the mean daily irradiance whereas in the DCM the phytoplankton remain light limited in all but the highest (midday) irradiances is consistent with recent models (Geider et al. 1998) and field observations (see review by MacIntyre et al. 2002). The reasons for the phytoplankton to remain light limited at the DCM are not well understood, but may reflect the requirement for the phytoplankton to avoid photo-damage (MacIntyre et al. 2002). In these data the photoacclimation of phytoplankton did not lead to higher maximal carbon-specific growth rates ( $P_m^C$ ) at the DCM (MacIntyre et al. 2002).

The combination of taxonomic and physiological gradients in the Celtic Sea thermocline were such that the cellular chl-a (from AFC measurements) increased progressively with depth in both *Synechococcus* and picoeukaryotes, presumably in response to the light gradient, whilst the dominance shifted from *Synechococcus* to picoeukaryotes in terms of cell numbers (Fig. 3.22). The latter likely reflects the competition between species in both the light and nutrient gradient (as described above). In terms of cell biomass, for both phytoplankton groups the cells were smallest where they were most numerous (on the upslope of the DCM) with the increase in cell size possibly related to the synthesis of pigment in photoacclimation. The DCM was subsequently observed to be both a pigment and biomass maximum with the pigment maximum generally below the depth of the DCM peak and the cell density highest on the upslope of the DCM, with precise depths depending on the species. This is consistent with the model investigation of Fennel and Boss (2003) who illustrated that the biomass maximum in stable environments was generated due to the balance of growth and loss terms (i.e. phytoplankton growth rate balanced by respiration, grazing and sinking) whereas the pigment maximum was generated as a result of photoacclimation, and often located significantly below the particle maximum. In addition, Fennel and Boss (2003) showed that the layering of taxonomic groups occurs since each species occurs at the highest abundance (in the vertical) where the species-specific growth and loss rates balance. The comparisons of Fennel and Boss (2003) were with data from oligotrophic systems but they may be equally valid in a stratified shelf sea.

Similar investigation of the layering of phytoplankton abundance and pigment maxima (and the contribution to the location of the DCM) in the Atlantic Ocean was limited due to the low sample resolution through the DCM (multiple flow cytometry measurements could be made through the DCM to investigate this further). However, as described above, vertical patterns of taxonomy between the SML and DCM were similar to those of the Celtic Sea thermocline thus indicating a similarity between the two contrasting environments. Taxonomic differences between SML and DCM in the Atlantic Ocean compared to the shelf sea likely reflect, at least in part, the relative difference in the light environment. However, in addition, the vertical gradients in taxonomic composition in the open ocean could be exaggerated compared to the shelf sea due to the relative stability of the physical environment and therefore the timescales over which phytoplankton adaptation can take place (e.g. McManus and Dawson 1994, Moore et al. 1998).

The overall photophysiology of phytoplankton field populations is fundamental to the primary productivity of a given hydrographic environment.

## 7.2 The DCM of the Celtic Sea Shelf

### 7.2.1 Primary Production in the Thermocline

In the stratified shelf of the Celtic Sea, photo-acclimated phytoplankton in the thermocline of the stratified shelf accounted for between ~20-60% of total water column production (Fig. 4.16). The combination of  $^{14}\text{C}$ -derived P vs. E parameters, phytoplankton absorption measurements and an empirically modelled *in situ* light field provided a means to test the influence of irradiance on the primary productivity of the phytoplankton. The mean water column primary production (PP) across the entire Celtic Sea region was significantly different when estimated for a realistic cloudy and sunny day. Thus, spatial variability in phytoplankton physiology and hydrographic gradients were less important than temporal variability in irradiance conditions to primary production (Fig. 4.15).

In addition, estimated PP for the irradiance obtained at each location on the day of sampling, showed that thermocline phytoplankton were responsible for most of the variability in PP due to irradiance (Fig. 4.16). By contrast, the variability of PP in the SML was explained by chl-a concentration. This difference reflects the conditions of sub-saturating irradiance in the thermocline and light saturation in the SML (Fig. 3.19). Irradiance was still important to water-column integrated PP, as supported by modelling studies for example, variability in irradiance

has been shown to account for ~60% of the variability in net production in a modelled tidally active shelf sea system (after the removal of seasonal trends) (Allen et al. 2004).

When incident irradiance was held constant across all locations the estimated integrated PP was not significantly correlated to integrated chl-a (Fig. 4.15) reflecting the importance of the physiological parameters in contributing to the overall primary production.

When both the incident surface irradiance and phytoplankton physiological characteristics were held constant, for example during analysis of the effect of semi-diurnal variability in water column structure (Table 4.3), over 60% of the variance in hourly PP within the surface, thermocline and water-column was explained by changes in the chl-a concentration within each layer. The percentage of surface irradiance available at the DCM was correlated to thermocline productivity in some locations, for example, OB where the depth of the chlorophyll maximum varied by 13 m over a semi-diurnal tidal cycle. Similarly, daily integrated PP was similar when estimated with the chl-a distribution assumed constant throughout the day compared to when a full 25 hour suite of chl-a profiles were used thus implying that the variability in chl-a during the day had a minor influence on overall daily PP compared to the variability between locations or mean daily irradiance.

These data suggest that, among physical and biological properties, mean daily irradiance was the principle factor governing primary production in the water column followed by phytoplankton photophysiology and chl-a concentration. However, quantifying the relative contribution of each of these factors was not achieved in this study. A more thorough analysis of the contribution of these factors to primary production might be possible by the application of, for example, multiple component analysis.

An important implication of the sensitivity to irradiance is that a large proportion of the range in primary production estimated from traditional incubation experiments, where incubation takes place under (screened) ambient sunlight, arises from the irradiance conditions on the day of incubation.

### 7.2.2 The Physical and Biological Structure of the Thermocline

At any location the thermocline varied in depth and thickness within the water column over periods of 10's minutes, partly due to advection of water past the ship but also due to physical mixing processes. The effects of mixing processes on the thermocline depend on local tidal current speeds and wind stress with factors such as water depth and sea-bed topography likely to be important (Simpson and Bowers 1981, Sharples et al. 2001b). At some locations (e.g. CS1,

Fig. 4.4) the thickness of the thermocline was influenced primarily from below whereas at others (e.g. B2b, Fig 4.4) the tidally generated turbulence appeared to dominate variance in depth of both the top and bottom of the thermocline. The importance of wind generated turbulence in ventilating the thermocline from above varies over time in a relatively unpredictable manner, in contrast to that of tidally induced mixing at the base.

Within the density gradient, the distribution of chl-a and nitrate varied both within and between locations leading to variability in the light environment and nitrate flux (Fig. 4.7) (Sharples et al. 2001b). However, the distribution of chl-a on the nitracline remained relatively constant across the entire shelf region (Fig 5.5) implying that, despite the dynamic mixing environment, the interactions between physical and biological processes were relatively consistent. Further, the nitrate gradient was of fundamental importance in determining the chl-a distribution. A dissolved oxygen super-saturation maxima at the top of the thermocline has been previously observed in a similar shelf sea system (e.g. Richardson et al. 2000) but has generally not received much attention in studies to date (e.g. Kemp et al. 1994, Revelante and Gilmartin 1995, Richardson et al. 2000). Correlation between the magnitudes of maximal dissolved oxygen saturation and chl-a concentration, despite the offset in their relative depths, indicates that the mechanisms involved in their formation are linked.

The three-layer structure of the thermocline, proposed in Chapter 5, implies that a relatively stable region exists in the mid-portion of the density gradient. The relative depth and size of this stable region will depend on the strength of mixing at the top and bottom of the thermocline. In steady state, the phytoplankton growth induced by the nitrate flux would balance loss terms (including sinking, grazing and remineralisation). Any deviation from steady state may be manifest as fluctuations in the chl-a concentration and dissolved oxygen saturation and/or changes in the depth of the nitracline (and therefore the DCM peak) with respect to the density gradient.

#### *The thermocline in steady state*

On the shelf, the chl-a concentration averaged through the thermocline was  $0.63 \pm 0.09 \text{ mg m}^{-3}$  (range 0.43 – 0.96); thus there was little variability in the mean chl-a concentration within the thermocline. On average, the nitrate flux measured from physical processes and estimated daily primary production within the Celtic Sea thermocline compared well (considering the uncertainties and errors associated with the methods) and indicated that the nitrate flux from the BML supports almost all the carbon fixation within the thermocline (Table 5.1). Further, the assumed total magnitudes of new production (based on the net oxygen evolution within the

thermocline (Table 5.2)) were also well correlated to the nitrate flux estimates in that they yielded realistic timescales for the build up and maintenance of dissolved oxygen saturation (and therefore chl-a concentration).

There is some evidence in the literature to support steady state dynamics in stratified water columns. For example, in a region of weak tidal forcing, Kemp et al. (1994) showed that realistic magnitudes of oxygen super-saturation were observed when oxygen production and BML and benthic oxygen consumption were in balance. Further, the magnitude of eddy diffusion was more important to achieving observed oxygen profiles than the relative balance between oxygen generation and consumption by biological processes (Kemp et al. 1994).

The overall physical and biological structure within the thermocline depends on both physical and biological processes. Strong mixing regimes are characterised by a 'weak' thermocline and the DCM in the middle of the density gradient (e.g. two-layer case such as at the shelf edge) and stable locations are characterised by a 'strong' thermocline and the DCM towards the base of the density gradient (e.g. three-layer case such as the mid-summer stratified shelf). The mid thermocline region, where biological processes are visible above mixing, will allow development of vertical physiological and taxonomic gradients if the period of stability is prolonged for long enough, and this was observed to be the case in the Celtic Sea (see above). However, in a temperate, tidally active shelf seas such as the Celtic Sea a truly steady state is unlikely ever to be reached due to temporal variability in mixing (including semidiurnal and spring-neap tidal cycles, and wind mixing) and irradiance. The significance of these processes is discussed in the following sections.

### *Spring – neap periodicity*

At locations on the stratified shelf, nitrate flux from the BML was greatest at spring tides compared to neaps, while primary production remained relatively similar over the spring – neap tidal cycle (Table 5.1). In contrast, at the shelf edge PP was reduced at spring tides compared to neaps reflecting lower chl-a concentrations at spring tides. This may reflect the difference in the mixing conditions at the shelf edge compared to on the shelf as the mixing conditions may lead to more chl-a being mixed out of the euphotic zone at spring tides at the shelf edge compared to on the shelf where the three-layer thermocline allows chl-a in the 'mid' thermocline region to be maintained. Despite the limited sampling resolution of the measurements made it is clear that the pulsing of nitrate into the thermocline was not matched by an instantaneous increase in PP, rather, the mixing of chl-a out of the euphotic zone is likely to lead to an instantaneous reduction of PP.

A time lag in the utilisation of excess nitrate supplied at springs requires the capacity for nitrate storage either in the water column or (possibly to some degree) in the phytoplankton following luxury  $\text{NO}_3^-$  uptake. The latter was suggested to occur over short time periods by the comparison of  $^{14}\text{C}$  and  $^{15}\text{NO}_3^-$  uptake vs. irradiance curves but its ecological significance over longer timescales is poorly understood (Falkowski and Raven 1997). Storage of nitrate in the water column would lead to shoaling of the nitracline which would have implications for nitrate flux (this is discussed below). The extent to which excess nitrate supplied at springs can be used over time (and the timescale of offset between nitrate supply and utilisation) is likely to vary with location, at least partly due to the relative strength of tidal mixing.

The indication of a time lag between nitrate supply and the response of phytoplankton is observed in modelling studies. For example, Allen et al. (2004) observed that in the absence of fluctuating surface irradiance phytoplankton biomass was maximal at neap tides and followed a rising of the nitracline at springs. Allen et al. (2004) also observed a further 3-4 day lag in the response of zooplankton abundance.

It is worth noting that chl-a concentration in the thermocline reflects changes in both phytoplankton biomass as well as photoacclimation (changing chl-a:C) and that (as discussed again below) the timescale for the response of photoacclimation, biomass and potentially species succession are likely to differ.

#### *Other sources of temporal variability*

Periodically high chl-a concentrations at the DCM were observed at CS1 ( $2.34 \text{ mg m}^{-3}$ ) compared to the typical  $\sim 1 \text{ mg m}^{-3}$ , and have been recorded as high as  $80 \text{ mg m}^{-3}$  during previous studies in the region (site U2) (Sharples et al. 2001). Such periodic pulses of chl-a presumably result from changes in the balance of biological (phytoplankton gains and losses) and physical processes. A significant factor is likely to be incident irradiance.

In contrast to nutrient supply, a time lag is not observed in the phytoplankton growth response to changes in irradiance (Allen et al. 2004) and, in combination, the effects of variations in irradiance and mixing conditions on phytoplankton in the shelf sea thermocline are complex. From this study (Section 4.3.4) it was observed that favourable light conditions for growth were likely to occur when the thermocline was shallow coincident with high irradiance (e.g. at midday). Allen et al. (2004) also reported that phytoplankton biomass was greatest if a mixing event was followed by a period of high irradiance. In addition, prolonged periods of high irradiance may also be associated with increased heat input at the surface and possibly reduced

wind mixing, which would act to increase the strength of stratification (Simpson and Bowers 1981).

Changes in the ambient irradiance superimposed on the variability in mixing conditions could also add to the potential variability in nitrate flux (Banse 1987). For example, during periods of high irradiance increased phytoplankton photosynthesis may erode the nitracline thereby increasing the nitrate gradient and subsequently nitrate flux. In contrast, in periods of low irradiance the reduced nitrate requirement may cause the nitracline (and hence chl-a max) to shoal. The location of the DCM would then be in a slightly more favourable light environment and enhanced PP may subsequently begin eroding the nitracline. These feedback mechanisms are superimposed on dynamic semi-diurnal and spring – neap tidal cycles so may be more significant in a stable open ocean environment (Banse 1987) than a tidally-dominated shelf sea.

Whatever the cause, shoaling of the nitracline could provide an opportunity for nitrate to be mixed into the SML, which is therefore more likely at times of increase nitrate flux and/or periods of low irradiance (Banse 1987). In these data, the nitrate gradient rarely reached the top of the thermocline on the stratified shelf (Fig. 4.7), although the periodic input of nitrate to the SML at some locations should not be ruled out. Any amount of nitrate leaked into the SML is likely to be small and may be used up quickly such that concentrations at the base of the SML may remain below limit of detection ( $< 0.1 \mu\text{M}$  by the techniques used in this study).

Phytoplankton photoacclimation could act to compensate for irradiance changes over periods of days (Falkowski and Raven 1997) and may partly affect chl-a concentrations at the DCM. The correct combination of high irradiance coupled with the timing of strong (or weak) mixing for extended periods may then lead to conditions favourable for phytoplankton growth and further influence the magnitude of chl-a due to generation of phytoplankton biomass. The effect may last until conditions reverse or until grazing or other losses act to counterbalance growth. Persistent conditions favourable to a particular species may be the trigger for mono-specific blooms, as have been observed in the DCM in the region during previous studies (e.g. the coccolithophore *Calyptrorphaera oblonga* (Sharpley et al. 2001b)).

Despite the complex interaction of temporal and spatial changes in the balance of biological and physical processes (including nitrate supply) the variability in irradiance and mixing conditions did not generally cause deviations in the location of the DCM on the nitracline (Fig. 5.5). Deviation from the otherwise repeatable  $-\text{O}_2:\text{NO}_3^-$  relationship included stations at P1 and (periodically) U2. A specific cause of these deviations from the general trend is unknown, although at both of these stations large subsurface ammonium maxima were

observed in the thermocline compared to other shelf sites (E. Achterberg, *pers. comm.*) potentially indicating differences in nitrogen cycling at these sites (Holligan et al. 1984a).

In order to investigate the variability in physical and biological processes over spring neap cycles a particular location would need to be repeatedly sampled for an entire tidal cycle. Ideally a water parcel could be followed in order to account for horizontal advection, though this would be logistically problematic in such dynamic conditions.

### 7.3 The DCM of the Atlantic Ocean

For the hydrographic regimes visited in the Atlantic Ocean, the form of the DCM and its relation to the density, nitrate and light gradients agreed with previous descriptions (e.g. Barlow et al. 2002, Poulton 2002, Perez et al. 2006, Robinson et al. 2006). Following original hypotheses of Cullen and Eppley (1981) and Cullen (1982) and recent model studies (e.g. Varela et al. 1994, Fennel and Boss 2003) the form of the DCM reflected physical and biological processes acting in each region. For example, in the oligotrophic gyres weak vertical mixing allowed phytoplankton acclimation, adaptation and growth below the thermocline and led to the DCM being located at < 1% surface irradiance (as dictated by biomass in the SML) and the top of the nitrate gradient. The DCM in this case is typically a pigment, rather than biomass maximum and the DCM was not observed to be a production maximum (Perez et al. 2006, Poulton et al. 2006a). The lack of physical mixing processes meant the DCM was normally symmetrical in profile (Fig. 6.19). In contrast, in upwelling regions physical processes act to shoal the density gradient, nitracline and hence DCM, such that the light level at the DCM was increased. The favourable light and nutrient conditions leads to a DCM that is typically observed to be a production and biomass maximum as well as a pigment maximum (Longhurst and Harrison 1989, Perez et al. 2006). The upwelling meant that the DCM was asymmetric (Fig. 6.19) and it was observed that the PP maximum was located on the upslope of the DCM, due to the increased chl-a and therefore light attenuation associated with the DCM. In these data, the gradual progression from the southern oligotrophic gyre to the seasonal SSTC (where spring bloom conditions were observed) displayed a shoaling of the density gradient and DCM but the DCM did not experience increasing light availability due to the increased biomass in the SML (Fig. 6.19). This was in contrast to the upwelling regions and Northern high latitudes. The latter were sampled in autumn and exhibited relatively high light and nutrient conditions at the DCM. The contribution of PP in the DCML ranged from ~20 - 80 %, with ~70% in the northern gyre

compared to 22 – 54 % in the southern gyre (Fig. 6.21). These estimates were similar to the 45% found by Perez et al. (2006) for the average contribution of PP in the DCML in the gyres, averaged over seasonal cycles. However, estimates are sensitive to the definition of the DCML boundaries, which generally yielded a slightly wider DCML in this study compared to Perez et al. (2006).

Nutrient and light conditions at the DCM were more favourable in the northern gyre (sampled in autumn) compared to the southern gyre (sampled in spring) which likely led to the higher PP estimated in the DCML in the northern compared to southern gyre (also observed by Perez et al. (2006) and Poulton et al. (2006a)). This is in contrast to the seasonal variability observed by Letelier et al. (2004) who, at the HOTS site, observed a relative shoaling of the nitracline and deepening of the 1% surface irradiance isolume during winter months suggesting that nitrate and light availability at the DCM were likely to be favourable in spring compared to autumn in oligotrophic regions.

As mentioned above, the key differences between the environment for growth at the DCM between the shelf sea and open ocean lie primarily in the light environment (nutrient limitation in the SML and mixing in the shelf sea causes the DCM to be maintained at a higher irradiance than in much of the open ocean), nutrient availability (nitrate flux into the euphotic zone is much less in the open ocean than the shelf sea, e.g. Planas et al. (1999), Sharples et al. (2001b)) and physical stability (the relative stability of the open ocean allows time for phytoplankton adaptation compared to the shelf sea). Despite the relatively low nitrate flux from deep waters in the open ocean Poulton et al. (2006a) showed that phytoplankton were likely to be light rather than nutrient limited at the DCM. Thus, the transition from light to nutrient limitation upwards from the base of the DCM in the open ocean may be similar to that of the shelf seas. The variability of phytoplankton taxonomy and physiology in response to such gradients has been described above. Overall, despite the different physical regimes, it appears that the form and functioning of the DCM in the shelf seas and open ocean followed the same basic principles (e.g. Varela et al. 1994, Fennel and Boss 2003).

The variability in physiological parameters was similar to those previously documented for AMT transects (e.g. Maranon and Holligan 1999, Suggett et al. 2006). The range in magnitudes of  $P^*_m$  in this study was more similar to AMT2 (range  $< \sim 6 \text{ mg C (mg chl-a)}^{-1} \text{ h}^{-1}$  for tropical and subtropical regions) than AMT3 (range  $< 14 \text{ mg C (mg chl-a)}^{-1} \text{ h}^{-1}$  for tropical and subtropical regions) as reported by Maranon and Holligan (1999). Despite the fact that AMT3 was more similar to AMT15 in terms of season, the study by Maranon and Holligan (1999) indicates large potential inter-cruise variability in  $P^*_m$  exists which could explain the

difference between magnitudes in Maranon and Holligan (1999) compared to this study. High degree of variability in PP in the Atlantic Ocean has also been reported by Maranon et al. (2003), Tiera et al. (2005). Further, diel variability may have also contributed to the higher  $P^*_m$  observed by Maranon and Holligan (1999) as their samples were collected during the day.

In this study, latitudinal variability in  $^{14}\text{C}$ -derived  $P^*_m$  and FRRF-derived electron transfer rates could not be attributed to horizontal gradients in nitracline depth or growth irradiance as in Maranon and Holligan (1999) and Suggett et al. (2006). Similarly, horizontal variability in estimated daily primary production in the SML and DCML could not easily be attributed to these environmental variables despite the fact that the relative variability in PP estimates were consistent with previous studies (Perez et al. 2006, Poulton et al. 2006a). The inability to establish significant correlations between horizontal gradients in P vs. E parameters and PP estimates likely reflects the relatively small dataset (1 cruise and 33 P vs. E curves) and the incorporation of all hydrographic regimes in the analysis (as well as the methodological issues described below). Perez et al. (2006), Poulton et al. (2006a) and Suggett et al. (2006) included data from 4 - 10 cruises, whilst Maranon and Holligan (1999) presented data from 150 P vs. E curves. Further, the limited sampling in the northern hemisphere coupled with the incorporation of NW African upwelling and SSTC meant that basin scale trends may have been obscured by a few extreme cases. Despite the lack of statistically significant correlations in these data, nutrient and light availability were observed to be important in the variability of both the physiological parameters and PP estimates in agreement with Maranon and Holligan (1999), Perez et al. (2006) and Suggett et al. (2006).

Overall the data presented from AMT15 complemented the published literature on the form and functioning of the DCM in response to the physical environment. The most successful aspect of the Atlantic Ocean study was in the physiological analysis described above. Physiological and chromatic adaptation data provided additional information to that reported by Suggett et al. (2006).

The relationships between physiological parameters, environmental variables and PP estimates could be investigated further using statistical methods. For example, multiple regression analysis or multi-component analysis may highlight the relative importance of measured variables to primary production. In addition, the relationships between nitrate concentration and dissolved oxygen saturation (as for the Celtic Sea) may provide additional information on the functioning of the DCM in the different hydrographic regimes, although calibrated oxygen probe data were not available in time for this study.

## 7.4 Temporal and Regional Significance of the DCM

### 7.4.1 Total and New Production in the Celtic Sea

The mean primary production within the thermocline across all stratified shelf sea stations (for both Celtic Sea cruises) under cruise-mean incident irradiance was  $169 \text{ mg C m}^{-2} \text{ d}^{-1}$ , which equates to a nitrogen requirement of  $30 \text{ mg N m}^{-2} \text{ d}^{-1}$  (assuming Redfield stoichiometry). The average nitrate flux from the BML across the stratified shelf sea regions (over both cruises) as measured by physical methods (J. Tweddle, *pers. comm.*) was  $74 \text{ mg N m}^{-2} \text{ d}^{-1}$ . The values of nitrate flux are estimated from a limited number of sites and strongly skewed by a high estimate of nitrate flux at B2 (Table 5.1). Excluding this high value at B2 leads to a shelf-mean flux of  $37 \text{ mg N m}^{-2} \text{ d}^{-1}$ . Consequently, on average, all the primary production within the thermocline across the stratified shelf sea can potentially be fuelled by nitrate flux from the BML and can therefore be considered 'new' production.

Within the SML, the average primary production across the study region was  $176 \text{ g C m}^{-2} \text{ d}^{-1}$  such that as much primary production occurred in the surface as in the thermocline, resulting in a water-column average f-ratio of 0.5. This compares with the range of f-ratio estimations of Weston et al. (2005) in the North Sea, although they found the f-ratio in the DCM to be 0.3.

In the North Sea, Weston et al. (2005) estimated the daily primary production within the thermocline (following similar methods) to be  $385 \text{ mg C m}^{-2} \text{ d}^{-1}$  of which  $116 \text{ mg C m}^{-2} \text{ d}^{-1}$  was new production and Richardson et al. (2000) estimated total primary production in the DCM of  $295 \text{ mg m}^{-2} \text{ d}^{-1}$  of which  $106 - 320 \text{ mg C m}^{-2} \text{ d}^{-1}$  was new production. Also in the North Sea, Richardson and Pedersen (1998) estimated daily new production in frontal and stratified DCM regions to be  $\sim 50 \text{ mg C m}^{-2} \text{ d}^{-1}$  (based on their  $40 \text{ g C m}^{-2} \text{ y}^{-1}$ , of which 80% was due to the spring bloom and coastal regions, and assuming a stratified period of 150 days). Accounting for their relative areas (see below) a corresponding estimate of new production in frontal and stratified regions in the Celtic Sea was  $304 \text{ mg C m}^{-2} \text{ d}^{-1}$  although these comparisons would presumably differ by the relative contributions of frontal and/or stratified regions in each case.

At the shelf edge, the mean daily primary production in the thermocline (for both cruises, estimated for cruise-mean daily irradiance) was  $398 \text{ mg C m}^{-2} \text{ d}^{-1}$ , corresponding to a nitrogen requirement of  $70 \text{ mg N m}^{-2} \text{ d}^{-1}$  (assuming Redfield stoichiometry). The mean daily nitrate flux from below the thermocline was  $46 \text{ mg N m}^{-1} \text{ d}^{-1}$  such that not all the production in the thermocline could be sustained by nitrate. Including PP in the surface, at the shelf edge the

upward nitrate flux would support 60 % of the mean total water column production ( $620 \text{ mg C m}^{-1} \text{ d}^{-1}$ ), such that the f-ratio at the shelf edge was 0.6. The estimate of mean daily water-column production at the shelf edge, and the estimate of the f-ratio, compared well to those of Joint et al. (2001).

The surface areas of the hydrographic regimes in the Celtic Sea regions were estimated as follows: the stratified region on the shelf ( $132,000 \text{ km}^2$ ), the shelf edge ( $21,500 \text{ km}^2$ ), the mixed region of the Irish Sea (defined as the mixed water north of the Irish Sea front, away from the coast and latitude  $< 53^\circ\text{N}$ ) ( $8,400 \text{ km}^2$ ) and the frontal region ( $8,400 \text{ km}^2$ ). The frontal region consists of the Irish Sea front ( $3,700 \text{ km}^2$ ) and the Ushant front ( $4,700 \text{ km}^2$ ). Considering the relative areas of the hydrographic regions, the thermally stratified shelf (SML and thermocline) contributed 56% of daily regional water-column PP during the summer, with the shelf edge, mixed and frontal regions accounting for 17%, 2% and 25% respectively. Primary production in the thermocline of the stratified shelf region attributed 27% of all daily PP in the Celtic Sea.

Scaling-up by the regional areas leads to daily new production estimated for the summer Celtic Sea of  $33 \times 10^3 \text{ tonnes C d}^{-1}$ , of which 51% occurred in the stratified thermocline ( $22 \times 10^3 \text{ tonnes C d}^{-1}$ ), 20% at the shelf edge (based on new production of 60% of total production) and 30% at the frontal regions. Frontal estimates of new production were based on only one measurement of daily primary production at the Irish Sea front (X7) and this was assumed to represent both the Irish Sea and Ushant front. Frontal productivity may be underestimated due to this assumption as Holligan et al. (1984c) measured daily primary production at the Ushant front in excess of that estimated for the Irish Sea front in this study. Since no nitrate flux estimates were obtained at the Irish Sea front it was assumed that all primary production within the thermocline at the front (as was the case on the open shelf) was new production.

Assuming that the mean BML shelf sea nitrate concentration represents the winter nitrate concentration ( $\sim 8 \mu\text{M}$ ), a stratified SML depth of 30 m and Redfield stoichiometry, the annual new production associated with the spring bloom may be estimated as  $19 \text{ g C m}^{-2} \text{ y}^{-1}$ . This compares to  $20 \text{ g C m}^{-2} \text{ y}^{-1}$  for the summer new production in the shelf sea thermocline (by assuming a stratified summer period of 120 days). The summer new production within the thermocline was also seen to be similar to that of the spring bloom in the North Sea (Richardson and Pedersen 1998, Richardson et al. 2000, Weston et al. 2005).

Table 7.1 provides estimates of annual total and new production scaled over the regional areas in the Celtic Sea.

Table 7.1. Estimates of annual new and total primary production in the Celtic Sea region during summer, spring and winter, by hydrographic regimes. Regional estimates are based on average daily primary production (PP) estimated through the water column using information from  $^{14}\text{C}$  P vs. E curves and the *in situ* light field, using cruise-mean daily irradiance. Daily PP is scaled by the regional areas described in the text. The stratified summer period was assumed to be 120 days. New production was estimated from nitrate flux (measured by physical methods as described in the text, data were supplied by (J. Tweddle, *pers. comm.*)) compared to total PP estimates. Estimates of spring bloom production in the shelf and stratified regions were based on data of the BML nitrate concentration and the SML depth, as described in the text. \* indicates literature values: estimates of spring bloom PP at the shelf edge are from Rees et al. (1999), and winter PP is from the stratified Celtic Sea according to Joint et al. (1986).

	<b>Annual New Primary Production</b> ( $\times 10^6$ tonnes C $\text{y}^{-1}$ )	<b>Annual Total Primary Production</b> ( $\times 10^6$ tonnes C $\text{y}^{-1}$ )
Summer Mixed	-	0.2
Summer Frontal (Irish Sea + Ushant)	1.5	2.4
Summer Stratified Shelf	2.7	5.5
Summer Shelf Edge	1.0	1.6
Spring Bloom (Shelf + Frontal region)	2.7	2.7
Spring Bloom* (Shelf Edge region)	0.4	0.4
Winter* (all regions)	-	2.0
<b>TOTAL (spring + summer)</b>	<b>8.3</b>	<b>12.9</b>

The total new production over the shelf and frontal region was  $7.9 \times 10^6$  tonnes C  $\text{y}^{-1}$  of which 34% was due to the spring bloom and 34% due to summer PP in the thermocline of the stratified shelf. Including the shelf edge (based on measurements by Rees et al. (1999)), this becomes an annual new production for the Celtic Sea region of  $8.3 \times 10^6$  tonnes C  $\text{y}^{-1}$  of which the thermocline contributed 32%.

These data imply that of the annual primary production in the Celtic Sea region ( $12.9 \times 10^6$  tonnes C  $\text{y}^{-1}$ ) 64% is 'new' production, therefore leading to a seasonal f-ratio for the entire shelf sea region of 0.6.

The overall amount of PP across the region for any given season would be strongly dependent on the irradiance conditions. For example, in a warm, sunny season the spring bloom may occur earlier, leading to a longer stratified period potentially with a warmer and more stable

SML. The favourable light conditions could fuel more growth in the thermocline (the depth of which would not be significantly altered as it is largely determined by tidal mixing processes from below). New production could be increased during particularly sunny summers if strong stratification and PP in the thermocline were to sharpen the nitrate gradient, and hence increase the nitrate flux from the BML. In contrast, a relatively cool, cloudy summer could lead to reduced PP across the region, particularly in the thermocline.

These rough calculations of total and new production highlight the significance of primary production in the thermocline in the Celtic Sea both temporally and regionally. Potentially large sources of error in these estimates lie in the frontal productivity (as outlined above) and also in the limited number of nitrate flux estimates. This leads to poorly-constrained estimates of the proportions of primary production that is 'new'. However, these estimates provide a valuable context for the significance of the thermocline in the shelf sea setting.

#### 7.4.2 Total Production in the Atlantic Ocean

In the following analysis, estimates of daily primary production (for the irradiance experienced on the day of sampling) in the Atlantic Ocean are scaled by the relative sizes of the hydrographic regimes. Accepting the uncertainties of the magnitude of PP derived by the empirical modelling technique (discussed below), emphasis is on the relative significance of PP in the DCM between the hydrographic regimes. It is also acknowledged that extrapolation of limited data coverage over large areas is of questionable accuracy, particularly in the northern oligotrophic gyre where sampling coverage and penetration into the gyre was poor. However, such extrapolation is necessary if the productivity of hydrographic regimes of such different sizes is to be compared.

In the Atlantic Ocean the surface area of the hydrographic provinces visited during the cruise (except the NW African upwelling) were as follows: Northern high latitudes (625,000 km<sup>2</sup>), North Atlantic Gyre (16,200,000 km<sup>2</sup>), Equatorial Upwelling (6,400,00 km<sup>2</sup>), South Atlantic Gyre (13,700,000 km<sup>2</sup>) and Southern High Latitudes (7,833,700 km<sup>2</sup>). Scaled by the area of the hydrographic provinces, estimated daily water-column primary production is shown as the right-hand values in Figure 7.1. PP estimated for the northern high latitudes also includes oceanic stations occupied during Celtic Sea cruise 2005. AMT15 departed prior to the breakdown of seasonal stratification in the northern Atlantic and therefore oceanic conditions are likely to have been comparable during the two cruises.

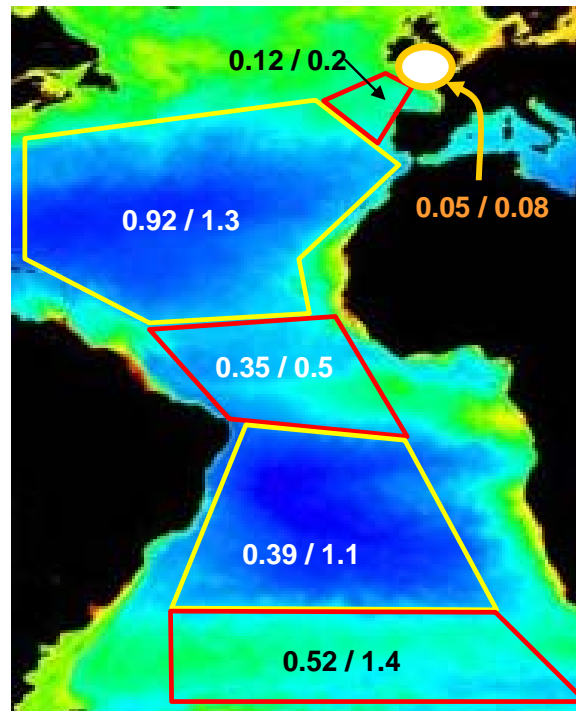


Figure 7.1. Estimated daily primary production ( $\times 10^6$  tonnes  $C d^{-1}$ ) within the DCML (left hand values) and water-column (right hand values) in each of the hydrographic regimes (from north to south: Celtic Sea shelf, northern high latitudes, northern gyre, equatorial upwelling, southern gyre, SSTC). The mean primary production is as estimated from measured values extrapolated over the surface area of each region as stated in text. Mean primary production estimates for the northern high latitudes include oceanic stations occupied during the Celtic Sea cruise (CS05). The background is a yearly (2003) composite of chl-a concentration on an arbitrary scale and for contextual reference only (source: [www.research.plymouth.ac.uk/geomatics/amt/images.html](http://www.research.plymouth.ac.uk/geomatics/amt/images.html)).

Despite the relatively low productivity of the gyre regions, the northern and southern oligotrophic gyres contributed  $> 50\%$  of daily primary production across the considered regions of the Atlantic Ocean due to their large surface area. This value is in agreement with Longhurst et al. (1995) who stated that the ocean gyres contributed  $> 30\%$  of total marine primary productivity, an estimation which included many of the oceanic regions not considered here including coastal regions and regions affected by river outflows. The equatorial upwelling contributed only 12% of daily primary production in the Atlantic Ocean despite relatively high local productivity. The contribution to the total Atlantic Ocean daily primary production was greatest in the SSTC (31%).

Estimated daily primary production in the DCML is given by the left hand values in Figure 7.1. Combining all regions, the DCML contributed 52% of total daily primary production in the Atlantic Ocean. Daily primary production in the DCML of the northern and southern oligotrophic gyre regions was  $1.3 \times 10^6$  tonnes C d<sup>-1</sup>. The DCML in the gyre regions alone accounted for 29% of total primary production in the Atlantic Ocean region.

It is clear that primary production in the DCML contributes significantly to oceanic primary productivity, even in the gyre regions where the DCML was deep.

## 7.5 Methodological Considerations

As identified in the relevant chapters, the directly measured parameters generally compared well to the published literature. Some differences in the measured parameters occurred between the two Celtic Sea cruises, but the potential for discrepancies in calibration (e.g. of the FRRF) and methodological differences meant that the differences could not be assumed to represent true differences in field conditions without a significant degree of uncertainty. However, trends within datasets for each cruise were robust and repeatable. The sampling strategy for CS05 was much improved compared to CS03 providing a dataset which corroborated and expanded on that obtained in the earlier cruise (and published by Moore et al. 2006).

The improved sampling strategy during CS05 was particularly important for the viability of the empirical modelling approach used to estimate daily PP from <sup>14</sup>C P vs. E parameters and *in situ* light fields, which was considered to be most reliable for CS05 compared to CS03 or AMT15. For CS05 this approach provided a useful tool for investigating the effects of irradiance and chl-a concentration on PP through the water column.

The weaknesses of this technique (described in Chapter 2) were most acute for AMT15. The linear interpolation of physiological characteristics between the SML and DCM sample was almost certainly not a realistic representation of true vertical variability but <sup>14</sup>C P vs. E measurements were not available to investigate this fully. Particularly in the gyres, FRRF-parameters remained homogenous with depth well below the depth of the SML sample but did appear to change before the top of the DCML as a result of the mixing conditions (Maranon and Holligan 1999). At least one additional <sup>14</sup>C P vs. E curve from the base of the SML would have largely overcome this problem. A minimum of three sample depths is suggested (at the top and bottom of the SML and the peak of the DCM) for future application of this technique.

The fact that the empirical model did not incorporate diel periodicity of phytoplankton physiology was also likely to be more problematic in the Atlantic Ocean than the Celtic Sea (see

Chapter 2). This is due to the high degree of diel periodicity known to exist in the photophysiology of cyanobacteria (e.g. Bruyant et al. 2005) and variability in the degree of diel periodicity across basin-scales (Behrenfeld et al. 2006).

Overall, estimates of daily PP for AMT15 were up to 50% lower than literature observations using traditional SIS methods (Maranon et al. (2000), Perez et al. (2006), Poulton et al. 2006a). The agreement between estimated PP and SIS measurements in these data were strongest in the DCM along the entire transect, and throughout the southern hemisphere, whilst the greatest underestimation occurred in the surface of the northern hemisphere (not shown). Underestimation of PP in the SML in the northern hemisphere may partly explain the relatively high contribution of  $P_{DCML}$  compared to  $P_{SURF}$  in this region of the transect (Fig. 6.20) and possibly contributed to the difficulties in finding correlations between horizontal gradients in PP and environmental variables.

Further potential errors in estimates of daily PP in the Atlantic Ocean study may arise from calibration of CTD chl-a profiles. The variability in the overall calibration factor (from the regression between nominal CTD chl-a and HPLC weighted chl-a) used for the calibration was 1.16 (see Chapter 2). Considering only the northern hemisphere the regression would have been 1.33 and for the southern hemisphere 0.98. It follows that CTD chl-a (and hence PP) may have been overestimated by a factor of ~15% in the southern hemisphere, and underestimated (by ~15%) in the northern hemisphere due to this issue. The calibration of CTD chl-a may therefore have contributed to the latitudinal variability in the discrepancy between modelled and SIS PP estimates. It is subsequently noted that regional (and potentially vertical) variability in the correlation between chl-a samples and the CTD fluorometer must be thoroughly addressed in any studies where absolute magnitudes of chl-a are obtained from the CTD fluorometer.

The influence of diel variability in daily PP estimates could be investigated further by including a model for diel variability in  $P^*_m$  (and/or  $\Phi_m$ ); possibly by using a simple sinusoid of realistic amplitude to scale each parameter over the day. It is clear that diel variability must be considered in future application of similar empirical models and indeed in any extrapolation of instantaneous measurements of phytoplankton physiology to estimate daily primary production.

## 7.6 Concluding Remarks

This thesis provides a thorough investigation into the functioning and significance of the DCM in a seasonally stratified shelf sea. The data presented provide insight into the biological and physical processes acting within the thermocline as well as investigating the phenotypic and

taxonomic changes that occur within the phytoplankton community in response to the physical conditions.

The physiological investigation was successful in providing useful information on phytoplankton physiological characteristics and the mechanisms of photoacclimation in both the shelf and open ocean environments. Comparison of  $^{14}\text{C}$  and FRRF parameters provided significant information on the mechanism of photoacclimation in the shelf sea DCM that could not have been achieved using one or other method independently (Moore et al. 2006). Along the AMT transect, and with depth in the Celtic Sea, the change in the degree of coupling between photochemistry and carbon fixation was unexpected (Suggett et al. 2006). The data presented provide a possible link between these changes and the proportion of cyanobacteria and picoeukaryotes within the population. It is subsequently suggested that further investigation should be targeted on the photochemical apparatus and processes of these taxonomic groups.

Estimates of PP by the (relatively novel) empirical modelling approach were most successful in the Celtic Sea where the significance of primary production in the thermocline was quantified for a range of hydrographic conditions. The approach was particularly useful in highlighting the importance of irradiance on primary production, particularly at the DCM. The repeated sampling at a range of locations illustrated the robust distribution of chl-a (and dissolved oxygen) on the nitracline that has not previously been reported. This clearly illustrated the importance of the nitracline in determining the structure of the DCM and contributed to the suggestion that the thermocline is a three-layer system. The description of the shelf sea thermocline as a three-layer system provides a hypothesis for further investigation and discussion.

## CHAPTER 8: REFERENCES

- Aiken, J., J. Fishwick, G. Moore, and K. Pemberton. 2004. The annual cycle of phytoplankton photosynthetic quantum efficiency, pigment composition and optical properties in the western English Channel. *Journal of the Marine Biological Association of the United Kingdom* 84: 301-313.
- Allali, K., A. Bricaud, and H. Claustre. 1997. Spatial variations in the chlorophyll-specific absorption coefficients of phytoplankton and photosynthetically active pigments in the equatorial Pacific. *Journal of Geophysical Research. C. Oceans* 102: 12,413-12,423.
- Allen, J. I., J. R. Siddorn, J. C. Blackford, and F. J. Gilbert. 2004. Turbulence as a control on the microbial loop in a temperate seasonally stratified marine systems model. *Journal of Sea Research* 52: 1-20.
- Anderson, L. A. 1995. On the Hydrogen and Oxygen-Content of Marine-Phytoplankton. *Deep-Sea Research Part I-Oceanographic Research Papers* 42: 1675-1680.
- Anderson, L. A., and J. L. Sarmiento. 1995. Global Ocean Phosphate and Oxygen Simulations. *Global Biogeochemical Cycles* 9: 621-636.
- Arbones, B., F. G. Figueiras, and R. Varela. 2000. Action spectrum and maximum quantum yield of carbon fixation in natural phytoplankton populations: implications for primary production estimates in the ocean. *Journal of Marine Systems* 26: 97-114.
- Azam, F., T. Fenchel, J. G. Field, J. S. Gray, L. A. Meyerreil, and F. Thingstad. 1983. The Ecological Role of Water-Column Microbes in the Sea. *Marine Ecology-Progress Series* 10: 257-263.
- Babin, M., A. Morel, H. Claustre, A. Bricaud, Z. Kolber, and P. G. Falkowski. 1996. Nitrogen- and irradiance-dependent variations of the maximum quantum yield of carbon fixation in eutrophic, mesotrophic and oligotrophic marine systems. *Deep-Sea Research Part I-Oceanographic Research Papers* 43: 1241-1272.
- Babin, M., J. C. Therriault, L. Legendre, and A. Condal. 1993. Variations in the specific absorption coefficient for natural phytoplankton assemblages: Impact on estimates of primary production. *Limnology and Oceanography* 38: 154-177.
- Banse, K. 1987. Clouds, Deep Chlorophyll Maxima and the Nutrient Supply to the Mixed Layer of Stratified Water Bodies. *Journal of Plankton Research* 9: 1031-1036.
- . 1994a. Commentary: an unpleasant note about the carbon-14 method of estimating plankton photosynthesis. Pages 3,6. *US JGOFS News*.
- . 1994b. Uptake of Inorganic Carbon and Nitrate by Marine Plankton and the Redfield Ratio. *Global Biogeochemical Cycles* 8: 81-84.
- Barlow, R. G., J. Aiken, P. M. Holligan, D. G. Cummings, S. Maritorea, and S. Hooker. 2002. Phytoplankton pigment and absorption characteristics along meridional transects in the Atlantic Ocean. *Deep-Sea Research Part I-Oceanographic Research Papers* 49: 637-660.
- Barlow, R. G., and R. S. Alberte. 1985. Photosynthetic Characteristics of Phycoerythrin-Containing Marine *Synechococcus* Spp .1. Responses to Growth Photon Flux-Density. *Marine Biology* 86: 63-74.
- Barlow, R. G., D. G. Cummings, and S. W. Gibb. 1997. Improved resolution of mono- and divinyl chlorophylls *a* and *b* and zeaxanthin and lutein in phytoplankton extracts using reverse phase C-8 HPLC. *Marine Ecology Progress Series* 161: 303-307.
- Barlow, R. G., R. F. C. Mantoura, D. G. Cummings, and T. W. Fileman. 1997. Pigment chemotaxonomic distribution of phytoplankton during summer in the western Mediterranean. *Deep-Sea Research Part II-Topical Studies in Oceanography* 44: 833-850.
- Behrenfeld, M. J., O. Prasil, M. Babin, and F. Bruyant. 2004. In search of a physiological basis for covariations in light-limited and light-saturated photosynthesis. *Journal of Phycology* 40: 4-25.
- Behrenfeld, M. J., O. Prasil, Z. S. Kolber, M. Babin, and P. G. Falkowski. 1998. Compensatory changes in Photosystem II electron turnover rates protect photosynthesis from photoinhibition. *Photosynthesis Research* 58: 259-268.
- Behrenfeld, M. J., K. Worthington, R. M. Sherrell, F. P. Chavez, P. Strutton, M. McPhaden, and D. M. Shea. 2006. Controls on tropical Pacific Ocean productivity revealed through nutrient stress diagnostics. *Nature* 442: 1025-1028.
- Bender, M., K. Grande, K. Johnson, J. Marra, P. J. L. Williams, J. Sieburth, M. Pilson, C. Langdon, G. Hitchcock, J. Orchardo, C. Hunt, P. Donaghay, and K. Heinemann. 1987. A comparison of four

- methods for determining planktonic community production. *Limnology and Oceanography* 32: 1085-1098.
- Berges, J. A., D. O. Charlebois, D. C. Mauzerall, and P. G. Falkowski. 1996. Differential effects of nitrogen limitation on photosynthetic efficiency of photosystems I and II in microalgae. *Plant Physiology* 110: 689-696.
- Berner, T., Z. Dubinsky, K. Wyman, and P. G. Falkowski. 1989. Photoadaptation and the Package Effect in *Dunaliella-Tertiolecta* (Chlorophyceae). *Journal of Phycology* 25: 70-78.
- Bertilsson, S., O. Bergland, D. M. Karl, and S. W. Chisholm. 2003. Elemental composition of marine *Prochlorococcus* and *Synechococcus*: Implications for the ecological stoichiometry of the sea. *Limnology and Oceanography* 48: 1721-1731.
- Bibby, T. S., I. Mary, I. Nield, F. Partensky, and J. Barber. 2003. Low-light-adapted *Prochlorococcus* species possess specific antennae for each photosystem. *Nature* 424: 1051-1054.
- Bidigare, R. R., J. Marra, T. D. Dickey, R. Iturriaga, K. S. Bakers, R. C. Smith, and H. Pak. 1990a. Evidence for phytoplankton succession and chromatic adaptation in the Sargasso Sea during spring 1985. *Marine Ecology Progress Series* 60: 113-122.
- Bidigare, R. R., M. E. Ondrusek, J. H. Morrow, and D. A. Kiefer. 1990b. In vivo absorption properties of algal pigments. *SPIE* 1302 (Ocean Optics X): 290-302.
- Bouman, H. A., T. Platt, S. Sathyendranath, B. D. Irwin, M. R. Wernand, and G. W. Kraay. 2000. Bio-optical properties of the subtropical North Atlantic. II. Relevance to models of primary production. *Marine Ecology-Progress Series* 200: 19-34.
- Boyer, T., M. E. Conkright, and S. Levitus. 1999. Seasonal variability of dissolved oxygen, percent oxygen saturation, and apparent oxygen utilization in the Atlantic and Pacific Oceans. *Deep-Sea Research Part I-Oceanographic Research Papers* 46: 1593-1613.
- Brewer, P. G., and J. P. Riley. 1965. The automatic determination of nitrate in seawater. *Deep Sea Research* 12: 765-772.
- Bricaud, A., M. Babin, A. Morel, and H. Claustre. 1995. Variability in the Chlorophyll-Specific Absorption-Coefficients of Natural Phytoplankton - Analysis and Parameterization. *Journal of Geophysical Research-Oceans* 100: 13321-13332.
- Bricaud, A., H. Claustre, J. Ras, and K. Oubelkheir. 2004. Natural variability of phytoplanktonic absorption in oceanic waters: Influence of the size structure of algal populations. *Journal of Geophysical Research-Oceans* 109, doi:10.1029/2004JC002419.
- Bricaud, A., A. Morel, and L. Prieur. 1983. Optical-Efficiency Factors of Some Phytoplankters. *Limnology and Oceanography* 28: 816-832.
- Bricaud, A., and D. Stramski. 1990. Spectral Absorption-Coefficients of Living Phytoplankton and Nonalgal Biogenous Matter - a Comparison between the Peru Upwelling Area and the Sargasso Sea. *Limnology and Oceanography* 35: 562-582.
- Bruyant, F., M. Babin, B. Genty, O. Prasil, M. J. Behrenfeld, H. Claustre, A. Bricaud, L. Garczarek, J. Holtzendorff, M. Koblizek, H. Dousova, and F. Partensky. 2005. Diel variations in the photosynthetic parameters of *Prochlorococcus* strain PCC 9511: Combined effects of light and cell cycle. *Limnology and Oceanography* 50: 850-863.
- Butler, W. L. 1962. Absorption of light by turbid samples. *Journal of the Optics Society of America* 52: 292-299.
- Chavez, F. P., K. R. Buck, S. K. Service, J. Newton, and R. T. Barber. 1996. Phytoplankton variability in the central and eastern tropical Pacific. *Deep-Sea Research Part II-Topical Studies in Oceanography* 43: 835-870.
- Chisholm, S. W. 1992. Phytoplankton size. Pages 213-237 in P. G. Falkowski and A. D. Woodhead, eds. *Primary Productivity and Biogeochemical Cycles in the Sea*. Plenum Press, New York.
- Ciotti, A. M., M. R. Lewis, and J. J. Cullen. 2002. Assessment of the relationships between dominant cell size in natural phytoplankton communities and the spectral shape of the absorption coefficient. *Limnology and Oceanography* 47: 404-417.
- Cleland, R. E. 1998. Voltammetric measurement of the plastoquinone redox state in isolated thylakoids. *Photosynthesis Research* 58: 183-192.
- Cleveland, J. S., and M. J. Perry. 1987. Quantum Yield, Relative Specific Absorption and Fluorescence in Nitrogen-Limited *Chaetoceros-Gracilis*. *Marine Biology* 94: 489-497.
- Cochlan, W. P., P. J. Harrison, and K. L. Denman. 1991. Diel Periodicity of Nitrogen Uptake by Marine-Phytoplankton in Nitrate-Rich Environments. *Limnology and Oceanography* 36: 1689-1700.

- Cote, B., and T. Platt. 1983. Day-to-Day Variations in the Spring-Summer Photosynthetic Parameters of Coastal Marine-Phytoplankton. *Limnology and Oceanography* 28: 320-344.
- Cottrell, M. T., and C. A. Suttle. 1995. Dynamics of a lytic virus infecting the photosynthetic marine picoflagellate *Micromonas pusilla*. *Limnology and Oceanography* 40: 730-739.
- Craig, H., and T. Hayward. 1987. Oxygen supersaturation in the ocean: biological versus physical contributions. *Science* 235: 199-202.
- Crofts, A. R., I. Baroli, D. Kramer, and S. Taoka. 1993. Kinetics of Electron-Transfer between Q(a) and Q(B) in Wild-Type and Herbicide-Resistant Mutants of *Chlamydomonas-Reinhardtii*. *Zeitschrift Fur Naturforschung C-a Journal of Biosciences* 48: 259-266.
- Crofts, A. R., and C. A. Wraight. 1983. The Electrochemical Domain of Photosynthesis. *Biochimica Et Biophysica Acta* 726: 149-185.
- Cullen, J. J. 1982. The Deep Chlorophyll Maximum - Comparing Vertical Profiles of Chlorophyll-A. *Canadian Journal of Fisheries and Aquatic Sciences* 39: 791-803.
- Cullen, J. J., and R. F. Davis. 2003. The blank can make a big difference in oceanographic measurements. *Limnology and Oceanography Bulletin* 12: 29-35.
- Cullen, J. J., and R. W. Eppley. 1981. Chlorophyll Maximum Layers of the Southern-California Bight and Possible Mechanisms of Their Formation and Maintenance. *Oceanologica Acta* 4: 23-32.
- Cullen, J. J., and M. R. Lewis. 1988. The Kinetics of Algal Photoadaptation in the Context of Vertical Mixing. *Journal of Plankton Research* 10: 1039-1063.
- Cullen, J. J., M. R. Lewis, C. O. Davis, and R. T. Barber. 1992. Photosynthetic Characteristics and Estimated Growth-Rates Indicate Grazing Is the Proximate Control of Primary Production in the Equatorial Pacific. *Journal of Geophysical Research-Oceans* 97: 639-654.
- Cullen, J. J., F. M. H. Reid, and E. Stewart. 1982. Phytoplankton in the Surface and Chlorophyll Maximum Off Southern-California in August, 1978. *Journal of Plankton Research* 4: 665-694.
- Davison, I. R. 1991. Environmental effects on algal photosynthesis: Temperature. *Journal of Phycology* 27: 2-8.
- Denman, K. L., and A. E. Gargett. 1983. Time and Space Scales of Vertical Mixing and Advection of Phytoplankton in the Upper Ocean. *Limnology and Oceanography* 28: 801-815.
- Dubinsky, Z., P. G. Falkowski, and K. Wyman. 1986. Light Harvesting and Utilization by Phytoplankton. *Plant and Cell Physiology* 27: 1335-1349.
- Dugdale, R. C. 1967. Nutrient limitation in the sea: dynamics, identification and significance. *Limnology and Oceanography* 12: 685-695.
- Dugdale, R. C., and J. J. Goering. 1967. Uptake of new and regenerated forms of nitrogen in primary productivity. *Limnology and Oceanography* 12: 196-206.
- Dugdale, R. C., and F. Wilkerson. 1986. The use of  $^{15}\text{N}$  to measure nitrogen uptake in eutrophic oceans; experimental considerations. *Limnology and Oceanography* 31: 673-689.
- . 1992. Nutrient limitation of new production in the sea. Pages 107-122 in P. G. Falkowski, ed. *Primary productivity and biogeochemical cycles in the sea*. Plenum, New York.
- Duysens, L. N. M. 1956. The flattening of the absorption spectrum of suspensions as compared to that of solutions. *Biochimica Et Biophysica Acta* 19: 1-12.
- Eppley, R. W. 1972. Temperature and Phytoplankton Growth in Sea. *Fishery Bulletin* 70: 1063-1085.
- . 1980. Estimating phytoplankton growth rates in the oligotrophic oceans. Pages 231-242 in P. G. Falkowski, ed. *Primary productivity in the sea*. Plenum, New York.
- Eppley, R. W., J. N. Rogers, and J. J. McCarthy. 1969. Half-saturation constants for uptake and ammonium by marine phytoplankton. *Limnology and Oceanography* 14: 912-920.
- Escoubas, J. M., M. Lomas, J. Laroche, and P. G. Falkowski. 1995. Light-Intensity Regulation of Cab Gene-Transcription Is Signaled by the Redox State of the Plastoquinone Pool. *Proceedings of the National Academy of Sciences of the United States of America* 92: 10237-10241.
- Falkowski, P. G. 1980. Light-shade adaptation in marine phytoplankton. Pages 99-117 in P. G. Falkowski, ed. *Primary productivity in the sea*. Plenum, New York.
- Falkowski, P. G., Z. Dubinsky, and K. Wyman. 1985. Growth-Irradiance Relationships in Phytoplankton. *Limnology and Oceanography* 30: 311-321.
- Falkowski, P. G., and Z. Kolber. 1995. Variations in Chlorophyll Fluorescence Yields in Phytoplankton in the World Oceans. *Australian Journal of Plant Physiology* 22: 341-355.
- Falkowski, P. G., and J. LaRoche. 1991. Acclimation to Spectral Irradiance in Algae. *Journal of Phycology* 27: 8-14.

- Falkowski, P. G., and T. G. Owens. 1980. Light-Shade Adaptation - 2 Strategies in Marine-Phytoplankton. *Plant Physiology* 66: 592-595.
- Falkowski, P. G., T. G. Owens, A. C. Ley, and D. C. Mauzerall. 1981. Effects of Growth Irradiance Levels on the Ratio of Reaction Centers in 2 Species of Marine-Phytoplankton. *Plant Physiology* 68: 969-973.
- Falkowski, P. G., and J. A. Raven. 1997. *Aquatic Photosynthesis*. Blackwell Science, UK.
- Falkowski, P. G., K. Wyman, A. C. Ley, and D. C. Mauzerall. 1986. Relationship of Steady-State Photosynthesis to Fluorescence in Eukaryotic Algae. *Biochimica Et Biophysica Acta* 849: 183-192.
- Fennel, K., and E. Boss. 2003. Subsurface maxima of phytoplankton and chlorophyll: Steady-state solutions from a simple model. *Limnology and Oceanography* 48: 1521-1534.
- Fiedler, R., and G. Proksch. 1975. The determination of nitrogen-15 by emission and mass spectrometry in biochemical analysis: A review. *Analytica Chimica Acta* 78: 1-62.
- Frenette, J. J., W. F. Vincent, and L. Legendre. 1998. Size-dependent C : N uptake by phytoplankton as a function of irradiance: Ecological implications. *Limnology and Oceanography* 43: 1362-1368.
- Furuya, K. 1990. Subsurface Chlorophyll Maximum in the Tropical and Subtropical Western Pacific-Ocean - Vertical Profiles of Phytoplankton Biomass and Its Relationship with Chlorophyll-a and Particulate Organic-Carbon. *Marine Biology* 107: 529-539.
- Geider, R. J. 1987. Light and Temperature-Dependence of the Carbon to Chlorophyll-a Ratio in Microalgae and Cyanobacteria - Implications for Physiology and Growth of Phytoplankton. *New Phytologist* 106: 1-34.
- . 1992. Respiration: Taxation without representation. Pages 333-360 in P. G. Falkowski and A. Woodhead, eds. *Primary Productivity and Biogeochemical Cycles in the Sea*. Platinum Press, New York.
- Geider, R. J., R. M. Greene, Z. Kolber, H. L. Macintyre, and P. G. Falkowski. 1993a. Fluorescence Assessment of the Maximum Quantum Efficiency of Photosynthesis in the Western North-Atlantic. *Deep-Sea Research Part I-Oceanographic Research Papers* 40: 1205-1224.
- Geider, R. J., and J. La Roche. 2002. Redfield revisited: variability of C : N : P in marine microalgae and its biochemical basis. *European Journal of Phycology* 37: 1-17.
- Geider, R. J., J. La Roche, R. M. Greene, and M. Olaizola. 199b. Response of the Photosynthetic Apparatus of *Phaeodactylum-Tricornutum* (Bacillariophyceae) to Nitrate, Phosphate, or Iron Starvation. *Journal of Phycology* 29: 755-766.
- Geider, R. J., and H. L. MacIntyre. 2002. Physiology and biochemistry of photosynthesis and algal carbon acquisition. Pages 44-77 in P. J. B. Williams, D. N. Thomas, and C. S. Reynolds, eds. *Phytoplankton Productivity: carbon assimilation in marine and freshwater ecosystems*. Blackwell Science, Oxford.
- Geider, R. J., H. L. MacIntyre, and T. M. Kana. 1998. A dynamic regulatory model of phytoplanktonic acclimation to light, nutrients, and temperature. *Limnology and Oceanography* 43: 679-694.
- Geider, R. J., B. A. Osborne, and J. A. Raven. 1985. Light Dependence of Growth and Photosynthesis in *Phaeodactylum-Tricornutum* (Bacillariophyceae). *Journal of Phycology* 21: 609-619.
- Gieskes, W. W. C., G. W. Kraay, and M. A. Baars. 1979. Current <sup>14</sup>C methods for measuring primary production: Gross underestimates in oceanic waters. *Netherlands Journal of Sea Research* 13: 58-78.
- Goering, J. J., D. D. Wallen, and R. M. Nauman. 1970. Nitrogen Uptake by Phytoplankton in Discontinuity Layer of Eastern Subtropical Pacific-Ocean. *Limnology and Oceanography* 15: 789-796.
- Greene, R. M., R. J. Geider, and P. G. Falkowski. 1991. Effect of Iron Limitation on Photosynthesis in a Marine Diatom. *Limnology and Oceanography* 36: 1772-1782.
- Greene, R. M., R. J. Geider, Z. Kolber, and P. G. Falkowski. 1992. Iron-Induced Changes in Light Harvesting and Photochemical Energy-Conversion Processes in Eukaryotic Marine-Algae. *Plant Physiology* 100: 565-575.
- Harrison, W. G., T. Platt, and M. R. Lewis. 1987. F-Ratio and Its Relationship to Ambient Nitrate Concentration in Coastal Waters. *Journal of Plankton Research* 9: 235-248.
- Heldal, M., D. J. Scanlan, S. Norland, F. Thingstad, and N. H. Mann. 2003. Elemental composition of single cells of various strains of marine *Prochlorococcus* and *Synechococcus* using X-ray microanalysis. *Limnology and Oceanography* 48: 1732-1743.

- Herbland, A., and B. Voituriez. 1979. Hydrological Structure-Analysis for Estimating the Primary Production in the Tropical Atlantic Ocean. *Journal of Marine Research* 37: 87-101.
- Heywood, J. L., M. V. Zubkov, G. A. Tarran, B. M. Fuchs, and P. M. Holligan. 2006. Prokaryoplankton standing stocks in oligotrophic gyre and equatorial provinces of the Atlantic Ocean: Evaluation of inter-annual variability. *Deep-Sea Research Part II-Topical Studies in Oceanography* 53: 1530-1547.
- Holligan, P. M., W. M. Balch, and C. M. Yentsch. 1984a. The Significance of Subsurface Chlorophyll, Nitrite and Ammonium Maxima in Relation to Nitrogen for Phytoplankton Growth in Stratified Waters of the Gulf of Maine. *Journal of Marine Research* 42: 1051-1073.
- Holligan, P. M., and D. S. Harbour. 1977. Vertical Distribution and Succession of Phytoplankton in Western English-Channel in 1975 and 1976. *Journal of the Marine Biological Association of the United Kingdom* 57: 1075-1093.
- Holligan, P. M., R. P. Harris, R. C. Newell, D. S. Harbour, R. N. Head, E. A. S. Linley, M. I. Lucas, P. R. G. Tranter, and C. M. Weekley. 1984b. Vertical-Distribution and Partitioning of Organic-Carbon in Mixed, Frontal and Stratified Waters of the English-Channel. *Marine Ecology-Progress Series* 14: 111-127.
- Holligan, P. M., R. D. Pingree, and G. T. Mardell. 1985. Oceanic Solitons, Nutrient Pulses and Phytoplankton Growth. *Nature* 314: 348-350.
- Holligan, P. M., P. J. L. Williams, D. Purdie, and R. P. Harris. 1984c. Photosynthesis, respiration and nitrogen supply of plankton populations in stratified, frontal and tidally mixed shelf waters. *Marine Ecology-Progress Series* 17: 201-213.
- Horne, E. P. W., J. W. Loder, C. E. Namie, and N. S. Oakey. 1996. Turbulent dissipation rates and nitrate supply in the upper water column on Georges Bank. *Deep-Sea Research Part II-Topical Studies in Oceanography* 43: 1683-1712.
- Huisman, J., P. van Oostveen, and F. J. Weissing. 1999. Critical depth and critical turbulence: Two different mechanisms for the development of phytoplankton blooms. *Limnology and Oceanography* 44: 1781-1787.
- Huthnance, J. M. 1989. Internal Tides and Waves near the Continental-Shelf Edge. *Geophysical and Astrophysical Fluid Dynamics* 48: 81-106.
- Jassby, A. D., and T. Platt. 1976. Mathematical Formulation of Relationship between Photosynthesis and Light for Phytoplankton. *Limnology and Oceanography* 21: 540-547.
- Jeffrey, S. W., and G. Humphrey. 1975. New spectrophotometric equations for determining chlorophylls a, b, c1 and c2 in higher plants, algae and natural phytoplankton. *Biochemical Physiology Pflanzen* 167: 191-194.
- Jeffrey, S. W., R. F. C. Mantoura, and S. W. Wright. 1997. *Phytoplankton Pigments in Oceanography*. UNESCO, Paris.
- Johnsen, G., N. B. Nelson, R. V. M. Jovine, and B. B. Prezelin. 1994. Chromoprotein-Dependent and Pigment-Dependent Modeling of Spectral Light-Absorption in 2 Dinoflagellates, *Prorocentrum-Minimum* and *Heterocapsa-Pygmaea*. *Marine Ecology-Progress Series* 114: 245-258.
- Johnsen, G., B. B. Prezelin, and R. V. M. Jovine. 1997. Fluorescence excitation spectra and light utilization in two red tide dinoflagellates. *Limnology and Oceanography* 42: 1166-1177.
- Joint, I., R. Wollast, L. Chou, S. Batten, M. Elskens, E. Edwards, A. Hirst, P. Burkill, S. Groom, S. Gibb, A. Miller, D. Hydes, F. Dehairs, A. Antia, R. Barlow, A. Rees, A. Pomroy, U. Brockmann, D. Cummings, R. Lampitt, M. Loijens, F. Mantoura, P. Miller, T. Raabe, X. Alvarez-Salgado, C. Stelfox, and J. Woolfenden. 2001. Pelagic production at the Celtic Sea shelf break. *Deep-Sea Research Part II-Topical Studies in Oceanography* 48: 3049-3081.
- Joint, I. R., N. J. P. Owens, and A. J. Pomroy. 1986. Seasonal production of photosynthetic picoplankton and nanoplankton in the Celtic Sea. *Marine Ecology-Progress Series* 28: 251-258.
- Joint, I. R., and A. J. Pomroy. 1986. Photosynthetic Characteristics of Nanoplankton and Picoplankton from the Surface Mixed Layer. *Marine Biology* 92: 465-474.
- Kana, R., D. Lazar, O. Prasil, and J. Naus. 2002. Experimental and theoretical studies on the excess capacity of Photosystem II. *Photosynthesis Research* 72: 271-284.
- Kana, T. M., and P. M. Glibert. 1987. Effect of irradiances up to 2000  $\mu\text{E m}^{-2} \text{s}^{-1}$  on marine *Synechococcus* WH7803. I. Growth, pigmentation, and cell composition. *Deep Sea Research* 34: 479-495.
- Kemp, P. F., P. G. Falkowski, C. N. Flagg, W. C. Phoel, S. L. Smith, D. W. R. Wallace, and C. D. Wirrick. 1994. Modeling Vertical Oxygen and Carbon Flux During Stratified Spring and Summer

- Conditions on the Continental-Shelf, Middle Atlantic Bight, Eastern USA. *Deep-Sea Research Part II-Topical Studies in Oceanography* 41: 629-655.
- Kirk, J. T. O. 1994. *Light and photosynthesis in aquatic ecosystems*. Cambridge University Press.
- Klausmeier, C. A., E. Litchman, T. Daufresne, S. A. Levin. 2004. Optimal nitrogen-to-phosphorous stoichiometry of phytoplankton. *Nature* 429: 171-174.
- Kok, B. 1948. A critical consideration of the quantum yield of *Chlorella*-photosynthesis. *Enzymologia* 13: 1-56.
- Kolber, Z., and P. G. Falkowski. 1993. Use of active fluorescence to estimate phytoplankton photosynthesis *in-situ*. *Limnology and Oceanography* 38: 1646-1665.
- Kolber, Z., K. D. Wyman, and P. G. Falkowski. 1990. Natural variability in photosynthetic energy-conversion efficiency - a field-study in the Gulf of Maine. *Limnology and Oceanography* 35: 72-79.
- Kolber, Z., J. Zehr, and P. Falkowski. 1988. Effects of Growth Irradiance and Nitrogen Limitation on Photosynthetic Energy-Conversion in Photosystem-II. *Plant Physiology* 88: 923-929.
- Kolber, Z. S., O. Prasil, and P. G. Falkowski. 1998. Measurements of variable chlorophyll fluorescence using fast repetition rate techniques: defining methodology and experimental protocols. *Biochimica Et Biophysica Acta-Bioenergetics* 1367: 88-106.
- Kononen, K., S. Hallfors, M. Kokkonen, H. Kuosa, J. Laanemets, J. Pavelson, and R. Autio. 1998. Development of a subsurface chlorophyll maximum at the entrance to the Gulf of Finland, Baltic Sea. *Limnology and Oceanography* 43: 1089-1106.
- Krause, G. H., and E. Weis. 1991. Chlorophyll Fluorescence and Photosynthesis - the Basics. *Annual Review of Plant Physiology and Plant Molecular Biology* 42: 313-349.
- Kywalyanga, M., T. Platt, and S. Sathyendranath. 1992. Ocean Primary Production Calculated by Spectral and Broad-Band Models. *Marine Ecology-Progress Series* 85: 171-185.
- Laney, S. R. 2003. Assessing the error in photosynthetic properties determined by fast repetition rate fluorometry. *Limnology and Oceanography* 48: 2234-2242.
- Langdon, C. 1988. On the Causes of Interspecific Differences in the Growth Irradiance Relationship for Phytoplankton .2. a General-Review. *Journal of Plankton Research* 10: 1291-1312.
- Lavin, A. M., L. Valdes, F. Sanchez, P. Abaunza, A. Forest, J. Boucher, P. Lazure, and A.-M. Jegou. 2006. The Bay of Biscay: the Encountering of the Ocean and Shelf. Pages 935-1002 in A. R. Robinson and K. Brink, eds. *The Sea, Volume 14B, The Global Coastal Ocean: Interdisciplinary Regional Studies and Syntheses*.
- Laws, E. A. 1984. Improved estimates of phytoplankton carbon based on super(14)C incorporation into chlorophyll a. *Journal of Theoretical Biology* 110: 425-434.
- . 1991. Photosynthetic Quotients, New Production and Net Community Production in the Open Ocean. *Deep-Sea Research Part I-Oceanographic Research Papers* 38: 143-167.
- Laws, E. A., G. R. DiTullio, and D. G. Redalje. 1987. High phytoplankton growth and production rates in the North Pacific subtropical gyre. *Limnology and Oceanography* 32: 905-918.
- Laws, E. A., E. Sakshaug, M. Babin, Y. Dandonneau, P. Falkowski, R. Geider, L. Legendre, A. Morel, M. Sondergaard, M. Takahashi, and W. P. leB. 2002. Photosynthesis and primary productivity in marine ecosystems: Practical aspects and application of techniques. Pages 93pp. *JGOFS Report No. 36*, Bergen, Norway.
- Lazzara, L., A. Bricaud, and H. Claustre. 1996. Spectral absorption and fluorescence excitation properties of phytoplanktonic populations at a mesotrophic and an oligotrophic site in the tropical North Atlantic (EUMELI program). *Deep-Sea Research Part I-Oceanographic Research Papers* 43: 1215-1240.
- Le Bouteiller, A. 1993. Comparison of in-bottle measurements using 15N and 14C. *ICES Marine Science Symposium* 197: 121-131.
- Le Corre, P., S. L'Helguen, and M. Wafar. 1993. Nitrogen-Source for Uptake by Gyrodinium Cf Aureolum in a Tidal Front. *Limnology and Oceanography* 38: 446-451.
- Legendre, L., S. Demers, C. M. Yentsch, and C. S. Yentsch. 1983. The 14C method: Patterns of dark CO2 fixation and DCMU correction to replace the dark bottle. *Limnology and Oceanography* 28: 996-1003.
- Letelier, R. M., D. M. Karl, M. R. Abbott, and R. R. Bidigare. 2004. Light driven seasonal patterns of chlorophyll and nitrate in the lower euphotic zone of the North Pacific Subtropical Gyre. *Limnology and Oceanography* 49: 508-519.

- Lewis, M. R., W. G. Harrison, N. S. Oakey, D. Hebert, and T. Platt. 1986. Vertical Nitrate Fluxes in the Oligotrophic Ocean. *Science* 234: 870-873.
- Li, W. K. W., B. D. Irwin, and P. M. Dickie. 1993. Dark fixation of  $^{14}\text{C}$ : Variations related to biomass and productivity of phytoplankton and bacteria. *Limnology and Oceanography* 38: 483-494.
- Longhurst, A. 1998. *Ecological geography of the sea*. Academic Press, London.
- Longhurst, A., S. Sathyendranath, T. Platt, and C. Caverhill. 1995. An Estimate of Global Primary Production in the Ocean from Satellite Radiometer Data. *Journal of Plankton Research* 17: 1245-1271.
- Longhurst, A. R., and W. G. Harrison. 1989. The Biological Pump - Profiles of Plankton Production and Consumption in the Upper Ocean. *Progress in Oceanography* 22: 47-123.
- Lorenzo, L. M., B. Arbones, F. G. Figueiras, G. H. Tilstone, and F. L. Figueroa. 2002. Photosynthesis, primary production and phytoplankton growth rates in Gerlache and Bransfield Straits during Austral summer: cruise FRUELA 95. *Deep-Sea Research Part II-Topical Studies in Oceanography* 49: 707-721.
- Lorenzo, L. M., F. G. Figueiras, G. H. Tilstone, B. Arbones, and L. Miron. 2004. Photosynthesis and light regime in the Azores Front region during summer: are light-saturated computations of primary production sufficient? *Deep-Sea Research Part I-Oceanographic Research Papers* 51: 1229-1244.
- Lutz, V. A., S. Sathyendranath, E. J. H. Head, and W. K. W. Li. 2001. Changes in the in vivo absorption and fluorescence excitation spectra with growth irradiance in three species of phytoplankton. *Journal of Plankton Research* 23: 555-569.
- Lutz, V. A., S. Sathyendranath, E. J. H. Head, and W. K. W. Li. 2003. Variability in pigment composition and optical characteristics of phytoplankton in the Labrador Sea and the Central North Atlantic. *Marine Ecology-Progress Series* 260: 1-18.
- MacIntyre, H. L., T. M. Kana, T. Anning, and R. J. Geider. 2002. Photoacclimation of photosynthesis irradiance response curves and photosynthetic pigments in microalgae and cyanobacteria. *Journal of Phycology* 38: 17-38.
- Maguer, J. F., S. L'Helguen, C. Madec, and P. Le Corre. 1999. Seasonal patterns of ammonium regeneration from size-fractionated microheterotrophs. *Continental Shelf Research* 19: 1755-1770.
- Majchrowski, R., and M. Ostrowska. 2000. Influence of photo- and chromatic acclimation on pigment composition in the sea. *Oceanologica* 42: 157-175.
- Malone, T. C., S. E. Pike, and D. J. Conley. 1993. Transient Variations in Phytoplankton Productivity at the JGOFS Bermuda Time-Series Station. *Deep-Sea Research Part I-Oceanographic Research Papers* 40: 903-924.
- Maranon, E., M. J. Behrenfeld, N. Gonzalez, B. Mourino, and M. V. Zubkov. 2003. High variability of primary production in oligotrophic waters of the Atlantic Ocean: uncoupling from phytoplankton biomass and size structure. *Marine Ecology-Progress Series* 257: 1-11.
- Maranon, E., P. Carmeno, and V. Perez. 2006. Continuity in the photosynthetic production of dissolved organic carbon from eutrophic to oligotrophic waters. *Marine Ecology Progress Series* 299: 7-17.
- Maranon, E., P. Carmeno, E. Fernandez, J. Rodriguez, and L. Zabala. 2004. Significance and mechanisms of photosynthetic production of dissolved organic carbon in a coastal eutrophic ecosystem. *Limnology and Oceanography* 49: 1652-1666.
- Maranon, E., and P. M. Holligan. 1999. Photosynthetic parameters of phytoplankton from 50 degrees N to 50 degrees S in the Atlantic Ocean. *Marine Ecology-Progress Series* 176: 191-203.
- Maranon, E., P. M. Holligan, R. Barciela, N. Gonzalez, B. Mourino, M. J. Pazo, and M. Varela. 2001. Patterns of phytoplankton size structure and productivity in contrasting open-ocean environments. *Marine Ecology-Progress Series* 216: 43-56.
- Maranon, E., P. M. Holligan, M. Varela, B. Mourino, and A. J. Bale. 2000. Basin-scale variability of phytoplankton biomass, production and growth in the Atlantic Ocean. *Deep-Sea Research Part I-Oceanographic Research Papers* 47: 825-857.
- Markager, S., and W. F. Vincent. 2001. Light absorption by phytoplankton: development of a matching parameter for algal photosynthesis under different spectral regimes. *Journal of Plankton Research* 23: 1373-1384.

- Marra, J. 2002. Approaches to the measurement of plankton production. Pages 78-108 in P. J. B. Williams, D. N. Thomas, and C. S. Reynolds, eds. *Phytoplankton Productivity: carbon assimilation in marine and freshwater ecosystems*. Blackwell Science, Oxford.
- Marra, J., C. C. Trees, R. R. Bidigare, and R. T. Barber. 2000. Pigment absorption and quantum yields in the Arabian Sea. *Deep-Sea Research Part II-Topical Studies in Oceanography* 47: 1279-1299.
- Mauzerall, D., and H. A. Herron. 1970. Light Saturation Curve of Photosynthesis. *Biochimica Et Biophysica Acta* 205: 312-314.
- McManus, G. B., and R. Dawson. 1994. Phytoplankton Pigments in the Deep Chlorophyll Maximum of the Caribbean Sea and the Western Tropical Atlantic-Ocean. *Marine Ecology-Progress Series* 113: 199-206.
- Mobley, C. D. 1999. Estimation of the remote-sensing reflectance from above-surface measurements. *Applied Optics* 38: 7442-7455.
- Moore, C. M., A. E. Hickman, J. T. Allen, M. I. Lucas, H. Planquette, R. T. Pollard, and A. J. Poulton. Submitted. Iron-light interactions during the CROZet natural iron bloom and EXport experiment (CROZEX) II: taxonomic responses and elemental stoichiometry. *Deep-Sea Research Part I-Oceanographic Research Papers*.
- Moore, C. M., M. I. Lucas, R. Sanders, and R. Davidson. 2005. Basin-scale variability of phytoplankton bio-optical characteristics in relation to bloom state and community structure in the Northeast Atlantic. *Deep-Sea Research Part I-Oceanographic Research Papers* 52: 401-419.
- Moore, C. M., D. Suggett, P. M. Holligan, J. Sharples, E. R. Abraham, M. I. Lucas, T. P. Rippeth, N. R. Fisher, J. H. Simpson, and D. J. Hydes. 2003. Physical controls on phytoplankton physiology and production at a shelf sea front: a fast repetition-rate fluorometer based field study. *Marine Ecology-Progress Series* 259: 29-45.
- Moore, C. M., D. J. Suggett, A. E. Hickman, Y. N. Kim, J. F. Tweddle, J. Sharples, R. J. Geider, and P. M. Holligan. 2006. Phytoplankton photoacclimation and photoadaptation in response to environmental gradients in a shelf sea. *Limnology and Oceanography* 51: 936-949.
- Moore, L. R., A. F. Post, G. Rocab, and S. W. Chisholm. 2002. Utilization of different nitrogen sources by the marine cyanobacteria *Prochlorococcus* and *Synechococcus*. *Limnology and Oceanography* 47: 989-996.
- Moore, L. R., G. Rocab, and S. W. Chisholm. 1998. Physiology and molecular phylogeny of coexisting *Prochlorococcus* ecotypes. *Nature* 393: 464-467.
- Morel, A., and D. Antoine. 1994. Heating Rate within the Upper Ocean in Relation to Its Biooptical State. *Journal of Physical Oceanography* 24: 1652-1665.
- Morel, A., D. Antoine, M. Babin, and Y. Dandonneau. 1996. Measured and modeled primary production in the northeast Atlantic (EUMELI JGOFS program): The impact of natural variations in photosynthetic parameters on model predictive skill. *Deep-Sea Research Part I-Oceanographic Research Papers* 43: 1273-1304.
- Morel, A., and A. Bricaud. 1981. Theoretical Results Concerning Light-Absorption in a Discrete Medium, and Application to Specific Absorption of Phytoplankton. *Deep-Sea Research Part I-Oceanographic Research Papers* 28: 1375-1393.
- Mouget, J. L., P. Rosa, and G. Tremblin. 2004. Acclimation of *Haslea ostrearia* to light of different spectral qualities - confirmation of 'chromatic adaptation' in diatoms. *Journal of Photochemistry and Photobiology B-Biology* 75: 1-11.
- Nelson, N. B., B. B. Prezelin, and R. R. Bidigare. 1993. Phytoplankton Light-Absorption and the Package Effect in California Coastal Waters. *Marine Ecology-Progress Series* 94: 217-227.
- Parsons, T. R., Y. Maita, and C. M. Lalli. 1984. *A manual of chemical and biological methods of seawater analysis*. Pergamon Press.
- Pedersen, M. F., and J. Borum. 1996. Nutrient control of algal growth in estuarine waters. Nutrient limitation and the importance of nitrogen requirements and nitrogen storage among phytoplankton and species of macroalgae. *Marine Ecology-Progress Series* 142: 261-272.
- Pemberton, K., A. P. Rees, P. I. Miller, R. Raine, and I. Joint. 2004. The influence of water body characteristics on phytoplankton diversity and production in the Celtic Sea. *Continental Shelf Research* 24: 2011-2028.
- Perez, V., E. Fernandez, E. Maranon, X. A. G. Moran, and M. V. Zubkov. 2006. Vertical distribution of phytoplankton biomass, production and growth in the Atlantic subtropical gyres. *Deep-Sea Research Part I-Oceanographic Research Papers* 53: 1616-1634.

- Perry, M. J., M. C. Talbot, and R. S. Alberte. 1981. Photoadaptation in Marine-Phytoplankton - Response of the Photosynthetic Unit. *Marine Biology* 62: 91-101.
- Peterson, B. J. 1980. Aquatic primary productivity and the <sup>14</sup>C-CO<sub>2</sub> method: A history of the productivity problem. *Annual Review of Ecological Systems* 11: 359-385.
- Pingree, R. D., P. M. Holligan, G. T. Mardell, and R. N. Head. 1976. Influence of Physical Stability on Spring, Summer and Autumn Phytoplankton Blooms in Celtic Sea. *Journal of the Marine Biological Association of the United Kingdom* 56: 845-873.
- Pingree, R. D., L. Maddock, and E. I. Butler. 1977. The influence of biological activity and physical stability in determining the chemical distributions of inorganic phosphate, silicate and nitrate. *Journal of the Marine Biological Society of the U.K.* 57: 1065-1073.
- Pingree, R. D., and G. T. Mardell. 1981. Slope Turbulence, Internal Waves and Phytoplankton Growth at the Celtic Sea Shelf-Break. *Philosophical Transactions of the Royal Society of London Series a-Mathematical Physical and Engineering Sciences* 302: 663-&.
- Pingree, R. D., G. T. Mardell, P. M. Holligan, D. K. Griffiths, and J. Smithers. 1982. Celtic Sea and Armorican current structure and the vertical distributions of temperature and chlorophyll. *Continental Shelf Research* 1: 99-116.
- Pingree, R. D., and L. Pennycuik. 1975. Transfer of Heat, Fresh-Water and Nutrients through Seasonal Thermocline. *Journal of the Marine Biological Association of the United Kingdom* 55: 261-274.
- Pingree, R. D., P. R. Pugh, P. M. Holligan, and G. R. Forster. 1975. Summer Phytoplankton Blooms and Red Tides Along Tidal Fronts in Approaches to English-Channel. *Nature* 258: 672-677.
- Planas, D., S. Agusti, C. M. Duarte, T. C. Granata, and M. Merino. 1999. Nitrate uptake and diffusive nitrate supply in the Central Atlantic. *Limnology and Oceanography* 44: 116-126.
- Poulton, A. J. 2002. Spatial and temporal variability of phytoplankton community composition in the tropical and subtropical Atlantic Ocean. Pages 203. *School of Ocean and Earth Science*. University of Southampton, UK.
- Poulton, A. J., P. M. Holligan, A. Hickman, Y. N. Kim, T. R. Adey, M. C. Stinchcombe, C. Holeton, S. Root, and E. M. S. Woodward. 2006a. Phytoplankton carbon fixation, chlorophyll-biomass and diagnostic pigments in the Atlantic Ocean. *Deep-Sea Research Part II-Topical Studies in Oceanography* 53: 1593-1610.
- Poulton, A. J., C. M. Moore, S. Seeyave, M. I. Lucas, S. Fielding, and P. Ward. Submitted. Phytoplankton community composition around the Crozex Palteau, with emphasis on diatoms and *Phaeocystis*. *Deep-Sea Research Part II-Topical Studies in Oceanography*.
- Poulton, A. J., R. Sanders, P. M. Holligan, M. C. Stinchcombe, T. R. Adey, L. Brown, and K. Chamberlain. 2006b. Phytoplankton mineralization in the tropical and subtropical Atlantic Ocean. *Global Biogeochemical Cycles* 20: GB4002, doi:10.1029/2006GB002712.
- Prasil, O., Z. Kolber, J. A. Berry, and P. G. Falkowski. 1996. Cyclic electron flow around photosystem II in vivo. *Photosynthesis Research* 48: 395-410.
- Prezelin, B. B. 1981. Light Reactions in Photosynthesis. *Canadian Bulletin of Fisheries and Aquatic Sciences*: 1-43.
- Raateoja, M., J. Seppala, and H. Kuosa. 2004. Bio-optical modeling of primary production in the SW Finnish coastal zone, Baltic Sea: fast repetition rate fluorometry in Case 2 waters. *Marine Ecology-Progress Series* 267: 9-26.
- Raven, J. A. 1993. Carbon: A phycocentric view. Pages 123-152 in G. T. Evans and M. J. R. Fasham, eds. *Towards a Model of Ocean Biogeochemical Processes*. Springer-Verlag, Berlin.
- Redfield, A. C. 1934. On the proportions of organic derivatives in sea water and their relation to the composition of plankton. Pages 179-192 in R. J. Daniel, ed. *James Johnston Memorial Volume*. University Press of Liverpool.
- Redfield, A. C., B. H. Ketchum, and F. A. Richards. 1963. The influence of organisms on the chemical composition of sea-water. Pages 26-77 in M. N. Hill, ed. *The Sea*. Interscience, New York.
- Rees, A. P., I. Joint, and K. M. Donald. 1999. Early spring bloom phytoplankton-nutrient dynamics at the Celtic Sea Shelf Edge. *Deep-Sea Research Part I-Oceanographic Research Papers* 46: 483-510.
- Rees, A. P., E. M. S. Woodward, and I. Joint. 2006. Concentrations and uptake of nitrate and ammonium in the Atlantic Ocean between 60 degrees N and 50 degrees S. *Deep-Sea Research Part II-Topical Studies in Oceanography* 53: 1649-1665.
- Reid, J. L., and E. Shulenberger. 1986. Oxygen-Saturation and Carbon Uptake near 28-Degrees-N, 155-Degrees-W. *Deep-Sea Research Part a-Oceanographic Research Papers* 33: 267-271.

- Revelante, N., and M. Gilmartin. 1995. The Relative Increase of Larger Phytoplankton in a Subsurface Chlorophyll Maximum of the Northern Adriatic Sea. *Journal of Plankton Research* 17: 1535-1562.
- Richardson, K., M. F. Lavin-Peregrina, E. G. Mitchelson, and J. H. Simpson. 1985. Seasonal distribution of chlorophyll *a* in relation to physical structure in the western Irish Sea. *Oceanologica Acta* 8: 77-86.
- Richardson, K., T. G. Nielsen, F. B. Pedersen, J. P. Heilmann, B. Lokkegaard, and H. Kaas. 1998. Spatial heterogeneity in the structure of the planktonic food web in the North Sea. *Marine Ecology-Progress Series* 168: 197-211.
- Richardson, K., and F. B. Pedersen. 1998. Estimation of new production in the North Sea: consequences for temporal and spatial variability of phytoplankton. *Ices Journal of Marine Science* 55: 574-580.
- Richardson, K., A. W. Visser, and F. B. Pedersen. 2000. Subsurface phytoplankton blooms fuel pelagic production in the North Sea. *Journal of Plankton Research* 22: 1663-1671.
- Robinson, C., A. J. Poulton, P. M. Holligan, A. R. Baker, G. Forster, N. Gist, T. D. Jickells, G. Malin, R. Upstill-Goddard, R. G. Williams, E. M. S. Woodward, and M. V. Zubkov. 2006. The Atlantic Meridional Transect (AMT) Programme: A contextual view 1995-2005. *Deep-Sea Research Part II-Topical Studies in Oceanography* 53: 1485-1515.
- Rodhe, J., P. Tett, and F. Wulff. 2006. The Baltic and North Seas: A Regional Review of Some Important Physical-Chemical-Biological Interaction Processes. Pages 1033-1075 in A. R. Robinson and K. Brink, eds. *The Sea, Volume 14B, The Global Coastal Ocean: Interdisciplinary Regional Studies and Syntheses*.
- Roy, S., R. P. Harris, and S. A. Poulet. 1989. Inefficient feeding by *Calanus helgolandicus* and *Temora longicornis* on *Coscinodiscus wailesii* : Quantitative estimation using chlorophyll-type pigments and effects on dissolved free amino acids. *Marine ecology progress series. Oldendorf* 52: 145-153.
- Sakshaug, E., A. Bricaud, Y. Dandonneau, P. G. Falkowski, D. A. Kiefer, L. Legendre, A. Morel, J. Parslow, and M. Takahashi. 1997. Parameters of photosynthesis: definitions, theory and interpretation of results. *Journal of Plankton Research* 19: 1637-1670.
- Sambrotto, R. N., G. Savidge, C. Robinson, P. Boyd, T. Takahashi, D. M. Karl, C. Langdon, D. Chipman, J. Marra, and L. Codispoti. 1993. Elevated Consumption of Carbon Relative to Nitrogen in the Surface Ocean. *Nature* 363: 248-250.
- Schofield, O., B. B. Prezelin, R. R. Bidigare, and R. C. Smith. 1993. In situ Photosynthetic Quantum Yield - Correspondence to Hydrographic and Optical Variability within the Southern California Bight. *Marine Ecology-Progress Series* 93: 25-37.
- Schlitzer, R. 2004. Ocean Data View. <http://odv.awi-bremerhaven.de>.
- Sharples, J., and P. M. Holligan. 2006. Interdisciplinary studies in the Celtic Sea. Pages 1003-1031 in A. R. Robinson and K. Brink, eds. *The Sea, Volume 14B, The Global Coastal Ocean: Interdisciplinary Regional Studies and Syntheses*.
- Sharples, J., C. M. Moore, and E. R. Abraham. 2001a. Internal tide dissipation, mixing, and vertical nitrate flux at the shelf edge of NE New Zealand. *Journal of Geophysical Research* 106: 14069-14081.
- Sharples, J., C. M. Moore, T. P. Rippeth, P. M. Holligan, D. J. Hydes, N. R. Fisher, and J. H. Simpson. 2001b. Phytoplankton distribution and survival in the thermocline. *Limnology and Oceanography* 46: 486-496.
- Sharples, J., and P. Tett. 1994. Modelling the Effect of Physical Variability on the Midwater Chlorophyll Maximum. *Journal of Marine Research* 52: 219-238.
- Sharples, J., J. F. Tweddle, M. J. A. Green, M. R. Palmer, Y.-N. Kim, A. E. Hickman, P. M. Holligan, C. M. Moore, T. P. Rippeth, and J. H. Simpson. *submitted*. Spring-neap modulation of internal tide mixing and vertical nutrient fluxes at a shelf edge in summer. *Limnology and Oceanography*.
- Simpson, J. H. 1998. Tidal Processes in Shelf Seas. Pages 113-150 in A. R. Robinson and K. Brink, eds. *The Sea, Volume 10, The Global Coastal Ocean: Processes and Methods*.
- Simpson, J. H., and D. Bowers. 1981. Models of Stratification and Frontal Movement in Shelf Seas. *Deep-Sea Research Part I-Oceanographic Research Papers* 28: 727-738.
- Simpson, J. H., and J. R. Hunter. 1974. Fronts in Irish Sea. *Nature* 250: 404-406.
- Simpson, J. H., T. P. Rippeth, and A. R. Campbell. 2000. The phase lag of turbulent dissipation in tidal flow in T. Yanagi, ed. *Interaction between estuaries, coastal seas and shelf seas*. Terra Scientific.

- Simpson, J. H., and J. Sharples. 1994. Does the Earth's Rotation Influence the Location of the Shelf Sea Fronts. *Journal of Geophysical Research-Oceans* 99: 3315-3319.
- Smetacek, V., and U. Passow. 1990. Spring Bloom Initiation and Sverdrup Critical-Depth Model. *Limnology and Oceanography* 35: 228-234.
- Sorensen, J. C., and D. A. Siegel. 2001. Variability of the effective quantum yield for carbon assimilation in the Sargasso Sea. *Deep-Sea Research Part II-Topical Studies in Oceanography* 48: 2005-2035.
- Sosik, H. M., R. E. Green, W. S. Pegau, and C. S. Roesler. 2001. Temporal and vertical variability in optical properties of New England shelf waters during late summer and spring. *Journal of Geophysical Research-Oceans* 106: 9455-9472.
- Steele, J. 1964. A study of phytoplankton in the Gulf of Mexico. *Journal of Marine Research* 3: 211-222.
- Steele, J., and C. S. Yentsch. 1960. The vertical distribution of chlorophyll. *Journal of the Marine Biological Association of the United Kingdom* 39: 217-226.
- Steeman-Nielsen, E. 1952. The use of radio-active carbon (C14) for measuring organic production in the sea. *Journal du Conseil Permanent International pour l'Exploration de la Mer* 18: 117-140.
- Strickland, J. D. H., and T. R. Parsons. 1968. *A practical handbook of seawater analysis*. Fisheries Research Board of Canada, Ottawa.
- Suggett, D., G. Kraay, P. M. Holligan, M. Davey, J. Aiken, and R. Geider. 2001. Assessment of photosynthesis in a spring cyanobacterial bloom by use of fast repetition rate fluorometry. *Limnology and Oceanography* 46: 802-810.
- Suggett, D. J., H. L. MacIntyre, and R. J. Geider. 2004. Evaluation of biophysical and optical determinations of light absorption by photosystem II in phytoplankton. *Limnology and Oceanography-Methods* 2: 316-332.
- Suggett, D. J., C. M. Moore, E. Maranon, C. Omachi, R. A. Varela, J. Aiken, and P. M. Holligan. 2006. Photosynthetic electron turnover in the tropical and subtropical Atlantic Ocean. *Deep-Sea Research Part II-Topical Studies in Oceanography* 53: 1573-1592.
- Sukenik, A., J. Bennett, and P. Falkowski. 1987. Light-Saturated Photosynthesis - Limitation by Electron-Transport or Carbon Fixation. *Biochimica Et Biophysica Acta* 891: 205-215.
- Sverdrup, H. U. 1953. On the conditions for the vernal blooming of phytoplankton. *Journal du Conseil Permanent International pour l'Exploration de la Mer* 18: 287-295.
- Takahashi, M., S. Ichimura, M. Kishino, and N. Okami. 1989. Shade and Chromatic Adaptation of Phytoplankton Photosynthesis in a Thermally Stratified Sea. *Marine Biology* 100: 401-409.
- Talling, J. F. 1957. Photosynthetic characteristics of some freshwater plankton diatoms in relation to underwater radiation. *New Phytology* 56: 26-50.
- Tassan, S., and G. M. Ferrari. 1995. An alternative approach to absorption measurements of aquatic particles retained on filters. *Limnology and Oceanography* 40: 1358-1368.
- Teira, E., B. Mourino, E. Maranon, V. Perez, M. J. Pazo, P. Serret, D. de Armas, J. Escanez, E. M. S. Woodward, and E. Fernandez. 2005. Variability of chlorophyll and primary production in the Eastern North Atlantic Subtropical Gyre: potential factors affecting phytoplankton activity. *Deep-Sea Research Part I-Oceanographic Research Papers* 52: 569-588.
- Tilstone, G. H., F. G. Figueiras, E. G. Fermin, and B. Arbones. 1999. Significance of nanophytoplankton photosynthesis and primary production in a coastal upwelling system (Ria de Vigo, NW Spain). *Marine Ecology-Progress Series* 183: 13-27.
- Tilstone, G. H., F. G. Figueiras, L. M. Lorenzo, and B. Arbones. 2003. Phytoplankton composition, photosynthesis and primary production during different hydrographic conditions at the Northwest Iberian upwelling system. *Marine Ecology-Progress Series* 252: 89-104.
- Trees, C. C., D. K. Clark, R. R. Bidigare, M. E. Ondrusek, and J. L. Mueller. 2000. Accessory pigments versus chlorophyll a concentrations within the euphotic zone: A ubiquitous relationship. *Limnology and Oceanography* 45: 1130-1143.
- Trees, C. C., M. C. Kennicutt, and J. M. Brooks. 1985. Errors Associated with the Standard Fluorimetric Determination of Chlorophylls and Phaeopigments. *Marine Chemistry* 17: 1-12.
- Tremblay, J. E., L. Legendre, B. Klein, and J. C. Therriault. 2000. Size-differential uptake of nitrogen and carbon in a marginal sea (Gulf of St. Lawrence, Canada): Significance of diel periodicity and urea uptake. *Deep-Sea Research Part II-Topical Studies in Oceanography* 47: 489-518.
- Trimmer, M., R. J. Gowen, B. M. Stewart, and D. B. Nedwell. 1999. The spring bloom and its impact on benthic mineralisation rates in western Irish Sea sediments. *Marine Ecology-Progress Series* 185: 37-46.

- Vaillancourt, R. D., J. Marra, R. T. Barber, and W. O. Smith. 2003. Primary productivity and *in situ* quantum yields in the Ross Sea and Pacific Sector of the Antarctic Circumpolar Current. *Deep-Sea Research Part II-Topical Studies in Oceanography* 50: 559-578.
- van Boekel, W. H. M., F. C. Hansen, R. Riegman, and R. P. M. Bak. 1992. Lysis-induced decline of a *Phaeocystis* spring bloom and coupling with the microbial foodweb. *Marine Ecology Progress Series. Oldendorf* 81: 269-276.
- Varela, R. A., A. Cruzado, and J. Tintore. 1994. A Simulation Analysis of Various Biological and Physical Factors Influencing the Deep-Chlorophyll Maximum Structure in Oligotrophic Areas. *Journal of Marine Systems* 5: 143-157.
- Varela, R. A., F. G. Figueiras, B. Arbones, and S. Agusti. 1998. Determining the Contribution of Pigments and the Nonalgal Fractions to Total Absorption: Toward an Improved Algorithm. *Limnology and Oceanography* 43: 449-457.
- Veldhuis, M. J. W., and G. W. Kraay. 1993. Cell Abundance and Fluorescence of Picoplankton in Relation to Growth Irradiance and Nitrogen Availability in the Red-Sea. *Netherlands Journal of Sea Research* 31: 135-145.
- Venrick, E. L. 1978. Systematic Sampling in a Planktonic Ecosystem. *Fishery Bulletin* 76: 617-627.
- . 1983. Percent Similarity - the Prediction of Bias. *Fishery Bulletin* 81: 375-387.
- von Liebig, J. 1840. *Organic Chemistry and its Application to Agriculture and Physiology*. Taylor and Walton, London.
- Weiss, R. F. 1970. Solubility of Nitrogen, Oxygen and Argon in Water and Seawater. *Deep-Sea Research* 17: 721-735.
- Welschmeyer, N. A. 1994. Fluorometric Analysis of Chlorophyll-a in the Presence of Chlorophyll-B and Pheopigments. *Limnology and Oceanography* 39: 1985-1992.
- Welschmeyer, N. A., and C. J. Lorenzen. 1981. Chlorophyll-Specific Photosynthesis and Quantum Efficiency at Sub-Saturating Light Intensities. *Journal of Phycology* 17: 283-293.
- Weston, K., L. Fernand, D. K. Mills, R. Delahunty, and J. Brown. 2005. Primary production in the deep chlorophyll maximum of the central North Sea. *Journal of Plankton Research* 27: 909-922.
- Williams, P. J. B., and D. A. Purdie. 1991. *Invitro* and *Insitu* Derived Rates of Gross Production, Net Community Production and Respiration of Oxygen in the Oligotrophic Subtropical Gyre of the North Pacific-Ocean. *Deep-Sea Research Part I-Oceanographic Research Papers* 38: 891-910.
- Williams, P. J. I. 1993. On the definition of primary production terms. *ICES Marine Science Symposia* 197: 9-19.
- Williams, P. J. L., K. R. Heinemann, J. Marra, and D. A. Purdie. 1983. Comparison of C-14 and O-2 Measurements of Phytoplankton Production in Oligotrophic Waters. *Nature* 305: 49-50.
- Williams, P. J. I., and N. W. Jenkinson. 1982. A transportable microprocessor-controlled precise Winkler titration suitable for field station and shipboard use. *Limnology and Oceanography* 27: 576-585.
- Williams, P. J. L. B., R. C. T. Raine, and J. R. Bryan. 1979. Agreement between the 14C and oxygen methods of measuring phytoplankton production: reassessment of the photosynthetic quotient. *Oceanologica Acta* 2: 411-416.
- Woodward, E. M. S., and N. J. P. Owens. 1990. Nutrient depletion studies in offshore North Sea areas. *Netherlands Journal of Sea Research* 25: 57-63.
- Yool, A., A. P. Martin, C. Fernandez, D. R. Clark. 2007. The significance of nitrification for ocean new production. *Nature* 447: 999-1002.
- Zubkov, M. V., M. A. Sleigh, P. H. Burkill, and R. J. G. Leakey. 2000. Picoplankton community structure on the Atlantic Meridional Transect: a comparison between seasons. *Progress in Oceanography* 45: 369-386.
- Zubkov, M. V., M. A. Sleigh, G. A. Tarran, P. H. Burkill, and R. J. G. Leakey. 1998. Picoplanktonic community structure on an Atlantic transect from 50 degrees N to 50 degrees S. *Deep-Sea Research Part I-Oceanographic Research Papers* 45: 1339-1355.